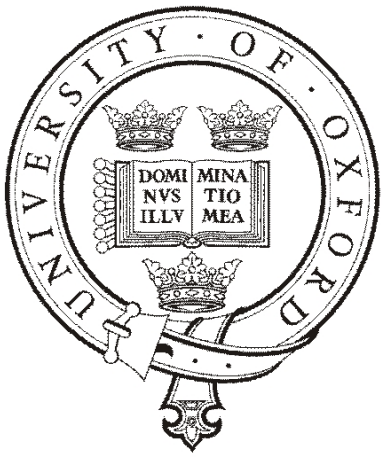
Dynamic DNA Motors and Structures

ALEXANDRA ELVA LUCAS

A thesis submitted in partial fulfilment of
the requirements for the degree of
Doctor of Philosophy at the University of Oxford



New College
University of Oxford
2016

Dynamic DNA Motors and Structures

Alexandra Elva Lucas, New College.
(Departments of Physics)

Thesis submitted for the degree of Doctor of Philosophy
at the University of Oxford, Hilary Term 2016.

Abstract

DNA nanotechnology uses the Watson-Crick base-pairing of DNA to self-assemble structures at the nanoscale. DNA nanomachines are active structures that take energy from the system to drive a programmed motion.

In this thesis, a new design for a reversible DNA motor and an automatically regenerating track is presented. Ensemble fluorescence measurements observe motors walking along the same 42 nm track three times. A second new motor was designed to allow motors on intersecting tracks to block each other, which can be used to perform logical computation. Multiple design approaches are discussed. The chosen approach showed limited success during ensemble fluorescence measurements.

The 'burnt bridges' motor originally introduced by Bath *et al.* 2005[1] was also sent down tracks placed along the inside of stacked origami tubes that are able to polymerise to micrometre lengths. Preliminary optical microscopy experiments show promise in using such a system for observing micrometre motor movement.

Scaffold-based DNA origami is the technique of folding a long single-stranded DNA strand into a specific shape by adding small staple strands that hold it in place. Extended staple strands can be modified to functionalise the origami surface. In this thesis, the threading of staple extensions through a freely-floating origami tile was observed using single-molecule Förster resonance energy transfer (smFRET). Threading was reduced by bracing the bottom of the extension or by using a multi-layered origami. smFRET was also used to investigate the process of staple repair, whereby a missing staple is added to a pre-formed origami missing the staple. This was found to be successful when the staple is single-stranded, and imperfect when partially double-stranded.

Finally the idea for a new "DNA cage", a dynamic octahedron called the *"Holliday Octahedron"*, is presented. The octahedron is made of eight strands, one running around each face. Mobile Holliday junctions at each face allow the stands to rotate causing a conformational change.

Acknowledgements

Many people have supported me through my DPhil and the writing of this thesis, to whom I'm deeply thankful. First I would like to thank my supervisor **Prof. Andrew J. Turberfield** for his guidance, ideas, and the discussions that helped me to step away from the small details to consider the bigger picture. Special thanks also to **Dr Jonathan Bath**, who was consistently patient with me: whether it was when I needed help in the lab, when I needed to talk through the latest motor mechanism or whether I was sending him the latest thesis chapter for feedback. He taught me all I know (and more I'm sure I've forgotten) about Adobe Illustrator, without which I wouldn't have been able to produce all the (hopefully pretty) schematics for this thesis.

DNA group has been a wonderful place to work — I'll miss all the tea (including the often-renewed argument over whether it's better with the milk in first), delicious cakes, fantastic banter, and the odd bit of lab squash and tennis. A few previous labmates in particular deserve a special thanks for providing moral support in my first few years: **Carlos Sanchez-Cano**, **Adam Wollman**, **Aiman Entwistle** (thanks Aiman for reading through the *Holliday Octahedron* chapter for me!) and **Helen Carstairs**.

Michael Boemo's arrival in DNA group in my 3rd year to do logic-implementing DNA motors (which was one of my goals since the start of my DPhil) gave me a good kick up the backside, and finally broadened my research outside of a reversible motor. He deserves a very special thanks for introducing me to 'Chicken & Rice', and letting Aiman and me stay with his ridiculously friendly and welcoming parents. Thanks also to **Florence Benn** and **Natalie Haley** for putting up with me through the motors & tubes project and for giving me feedback on the chapter. It was really lovely to work so closely with my friends.

Dr Timothy Craggs kindly offered to help me investigate some unexpected data I was getting with his single-molecule set-up. I am very grateful for his time, our discussions over the data and for his feedback on the FRET chapter. Thanks also to **Dr Robert Schreiber** for helping me assemble his multi-layered origami.

Family and friends have been essential for support outside of the lab. In particular I would like to thank my dad, **Kevin Lucas**, for nurturing my love of science from a young age; and my mum, **Elva Ainsworth**, for giving me the determination and strength to pursue my DPhil. Both my **Granny** and **Grandma** have also inspired me with their love of research and academic achievement in later life.

Two particular friends deserve a special thanks: **Kate Reynolds** and **Oliver Barter**. Kate was always happy to let me rant about the latest experimental issues, and provided me with much needed tea, cinnamon bun and stress-relieving cooking. Oli has been been my Mathematica guru and a fantastic emotional support, even whilst he's been doing his own thesis writing. I am also grateful to Oli's parents for providing us with an out-of-Oxford writing refuge.

Finally, I must also thank **Shelley Wickham** who gave a talk on DNA motors at a 'Physics Meets Biology' conference that I attended — it looked so awesome, I immediately knew I wanted to apply for a DPhil in DNA group to explore the exciting world of DNA nanotechnology.... and now look what's happened.

Dedicated to
my father for the inspiration
and
my mother for the determination

Contents

1 Introduction **2**
- 1.1 DNA-based self-assembly . . . 2
  - 1.1.1 The structure of DNA . . . 2
  - 1.1.2 DNA structures . . . 4
  - 1.1.3 DNA machines . . . 7
- 1.2 Motors . . . 11
  - 1.2.1 Biological motors . . . 11
  - 1.2.2 Synthetic motors . . . 12
- 1.3 Observation techniques . . . 21
- 1.4 Thesis structure . . . 21
- 1.5 Thesis contributions . . . 22

2 Reversible Motor **23**
- 2.1 Design . . . 24
  - 2.1.1 Overall mechanism . . . 25
  - 2.1.2 Director, remover and anchor structure . . . 28
  - 2.1.3 The ends of the track . . . 32
- 2.2 Sequence characterisation . . . 35
  - 2.2.1 Enzyme cutting near a vertex . . . 36
  - 2.2.2 Optimising the lengths . . . 38
  - 2.2.3 The final sequences . . . 40
- 2.3 Implementation on an origami tile . . . 41
  - 2.3.1 General assembly protocol . . . 43
  - 2.3.2 Walking down simple tracks . . . 44
  - 2.3.3 The ‘stations’ at the ends of the track . . . 47
  - 2.3.4 Normalisation levels . . . 50
  - 2.3.5 Reversing . . . 57
  - 2.3.6 Controls . . . 64
- 2.4 Discussion & future work . . . 68

3 Logic Gates with a "Lollipop Track" 73
3.1 DNA computation . . . 73
3.2 Logic gates . . . 75
3.3 Mechanism . . . 77
3.3.1 Absorbing interaction site ideas . . . 80
3.3.2 The chosen approach: the lollipop track . . . 83
3.3.3 The layout of multiple tracks . . . 87
3.3.4 Timing . . . 88
3.4 Testing the components . . . 88
3.4.1 Enzyme choice . . . 89
3.4.2 Plain track . . . 92
3.4.3 Interaction site . . . 92
3.5 Fluorimeter measurements . . . 99
3.5.1 NOT track . . . 100
3.5.2 Changing the buffer . . . 103
3.5.3 A braced track . . . 105
3.6 Discussion & future work . . . 107

4 A Track Inside Tubes 109
4.1 Design . . . 110
4.1.1 Tube . . . 110
4.1.2 Track for a burnt bridges motor . . . 111
4.1.3 Observation plans . . . 114
4.2 Ensemble fluorescence measurements . . . 116
4.2.1 General set-up . . . 116
4.2.2 Walking down monomer and dimer tubes . . . 121
4.2.3 Walking as a labelled-motor . . . 123
4.2.4 Walking on a labelled-track . . . 125
4.3 Microscopy . . . 128
4.3.1 Enzyme cutting under microscopy conditions . . . 129
4.3.2 Stained tubes . . . 132
4.3.3 Labelled-motor tubes . . . 134
4.3.4 Labelled-track tubes . . . 136
4.4 Discussion & future work . . . 145

5 Investigations of DNA Origami with Single-Molecule FRET 148
5.1 Theory . . . 151
5.1.1 Fluorescence . . . 151
5.1.2 FRET . . . 152
5.2 Experimental set-up . . . 154
5.2.1 Single-molecule FRET & ALEX . . . 154
5.2.2 Data analysis . . . 155
5.2.3 FRET efficiency model . . . 156
5.3 Threading . . . 158

5.3.1 Origami tile . . . 159
5.3.2 Braced on an origami tile . . . 160
5.3.3 Multi-layered origami . . . 162
5.4 Staple repair . . . 163
5.4.1 Single cargo loading . . . 164
5.4.2 Loading two cargos at one site . . . 173
5.5 Discussion . . . 176

6 Holliday Octahedron 179
6.0.1 Molecular cages . . . 179
6.0.2 Holliday junctions . . . 180
6.1 Design . . . 183
6.1.1 Structure and movement . . . 183
6.1.2 Conformation change . . . 185
6.1.3 Initiation and locking . . . 187
6.2 Models . . . 188
6.3 Formation of a plain octahedron . . . 189
6.4 Discussion & future work . . . 192

7 Summary 194

A Appendix: Supplementary Results 197
A.1 Chapter 2 supplementary . . . 197
A.1.1 Externally-reset mechanism . . . 197
A.1.2 A Holliday junction initiation for the remover . . . 197
A.1.3 Enzyme cutting near a vertex . . . 199
A.2 Chapter 5 supplementary . . . 201
A.2.1 Accuracy of low-FRET peak . . . 201
A.3 Chapter 4 supplementary . . . 202
A.3.1 Tube detection . . . 202

B Appendix: Methods 203
B.1 DNA strands . . . 203
B.1.1 DNA sequence design . . . 203
B.2 Origami synthesis . . . 203
B.2.1 Origami tile . . . 204
B.2.2 Origami tube . . . 204
B.2.3 Multi-layered origami . . . 205
B.3 Origami repair . . . 205
B.4 Origami purification . . . 206
B.4.1 Size-exclusion columns . . . 207
B.4.2 Gel purification . . . 207
B.5 Gel electrophoresis . . . 208
B.6 Ensemble fluorescence measurements . . . 208

B.7 FRET measurements . . . 210
B.7.1 Sample preparation . . . 210
B.7.2 Microscope . . . 211
B.7.3 Data analysis . . . 211
B.7.4 Model fitting . . . 212
B.8 Microscopy . . . 212
B.8.1 Microscope details . . . 212
B.8.2 Filter and fluorescence spectra . . . 213
B.8.3 Flow channel preparation . . . 213
B.8.4 YOYO-1 Iodide staining . . . 215
B.8.5 Microscopy and anti-photobleaching buffer . . . 216
B.8.6 Leakage signals . . . 217
B.9 Image analysis . . . 217
B.9.1 Detecting spots . . . 218
B.10 Octahedron protocol . . . 220

C Appendix: DNA Sequences 221
C.1 Origami staple sequences . . . 221
C.1.1 Minimised-twist tile . . . 221
C.1.2 Multi-layered origami . . . 221
C.1.3 Origami tube . . . 223
C.2 Strands for Chapter 2 . . . 226
C.3 Strands for Chapter 3 . . . 228
C.4 Strands for Chapter 4 . . . 230
C.5 Strands for Chapter 5 . . . 232
C.6 Strands for Chapter 6 . . . 233

Acronyms

A adenine
AFM atomic force microscopy
ALEX alternating-laser excitation
BSA bovine serum albumin
C cytosine
Cy3 Cyanine 3 fluorophore
Cy5 Cyanine 5 fluorophore
DNA deoxyribonucleic acid
DNA-PAINT DNA points accumulation for imaging in nanoscale topography
ds double-stranded
dT a chain of multiple T bases
E FRET efficiency
EM electron microscopy
FRET Förster resonance energy transfer
G guanine
HPLC high-performance liquid chromatography
mRNA messenger RNA
NEB New England Biolabs
PAGE polyacrylamide gel electrophoresis
PCR polymerase chain reaction
R_0 Forster radius
RNA ribonucleic acid
smFRET single-molecule FRET
ss single-stranded
T thymine
TEM transmission electron microscopy
TET tetrachlorofluorescein fluorophore
TEX615 TEX615 fluorophore
TIRF total internal reflection fluorescence
Tris tris(hydroxymethyl)aminomethane

Chapter 1

Introduction

DNA nanotechnology is a booming field of research that makes use of the Watson-Crick base-pairing of DNA to self-assemble structures and machines at the nanoscale, including that of 'DNA origami'. The possible applications range from nanoconstruction to nanomedicine. Sensitive to small molecules in the environment, devices can be designed to respond to them, creating nanosensors.

The work presented in this thesis explores a number of dynamic DNA structures. The main focus is on DNA motors, inspired by motor proteins inside cells, that can autonomously walk down a DNA track in a directable fashion. The motors designed and explored in this thesis are based on that introduced by Bath *et al.* in 2005[1], the 'burnt bridges' motor that burns the track behind it, imposing directionality down the track.

1.1 DNA-based self-assembly

1.1.1 The structure of DNA

DNA is a polymer comprised of four types of subunits called nucleotides (nt). Each subunit is made up of a 5-carbon deoxyribose sugar, a phosphate group and a base.

There are four primary DNA bases: adenine (A), cytosine (C), guanine (G) and thymine (T). The nucleotides are covalently linked between the sugar and phosphate groups, which forms the phosphate "backbone" of the DNA strand. Each strand has a polarity, dictated by a phosphate group at one end (called the 5' end) and a sugar at the other (the 3' end). DNA sequences are conventionally written from 5' to 3' as a list of consecutive bases, e.g. ATGCGA. Schematics of DNA strands will often place an arrow at the 3' end of the strand (an example is shown in Figure 1.1a).

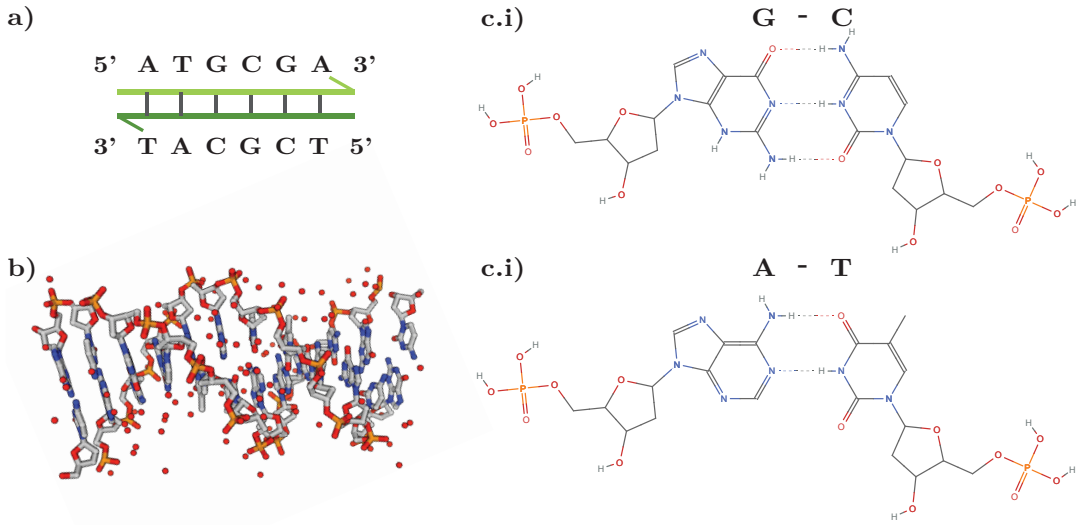


Figure 1.1: a) An example depiction of 6 bp of DNA with the sequence written next to each strand. The arrow denotes the 3' end. Sequences are not written 5' to 3' here as they are associated with the position on the strand. b) The structure of 12 bp of the B-form (the natural form) of DNA[2] (PDB: 10.2210/pdb1bna/pdb). c) The chemical structure of the bases with the hydrogen bonds (dashed lines) shown between Watson-Crick base pairs: i) G and C, ii) A and T (from left to right).

A single DNA strand can hybridise to its complement to form a double helix through Watson-Crick base pairing[3], whereby a G base on one strand forms hydrogen bonds with a C base on the other strand, and likewise for A and T bases (Figure 1.1). A G-C base pair (bp) is stronger than an A-T base pair as it forms three hydrogen bonds instead of two. The strands hybridise in an antiparallel fashion, such that the 5' end of one strand binds to the 3' end of the other. In this thesis, hybridised strands are denoted by a "." between the individual strand names, i.e. if strands X and Y are partially or completely hybridised together, the duplex is written "X.Y".

The double helix is roughly 2 nm in diameter[3], with 10.4 bp per turn and 0.34 nm up the helical axis between each base[4]. Double-stranded DNA (ds-DNA) has a persistence length of roughly 50 nm[5] and can be considered to be rigid at the lengths used throughout this thesis.

If a DNA strand has a sequence of bases (a 'domain' or 'section') that is a reverse complement to another section of the strand, these sections can hybridise together, giving the strand secondary structure. This is an important consideration when designing new DNA-based systems, as undesired secondary structure can hinder the desired functionality of the system. There are a number of tools that can be used to check and limit secondary structure in DNA sequences[6,7].

Two complementary DNA strands, or complementary domains of a single strand forming secondary structure, can be separated through a process of denaturation, for example by heating the strands up to 90°C. This breaks the hydrogen bonds between strands but does not break the covalent bonds holding each strand together.

It is the Watson-Crick base pairing that makes DNA an excellent material for self-assembled structures. Precise domains on different strands are "programmed" to hybridise together by controlling the sequences of the strands. These strands can be ordered from various companies that are able to synthesise specific sequences of DNA.

1.1.2 DNA structures

In 1982 Nadrian Seeman introduced the idea of using DNA to form lattices from immobile junctions that are joined together by complementary 'sticky ends'[8] (Figure 1.2a). Since then a wide range of DNA structures have been created using various approaches, such as 2D[9] and 3D DNA origami[10–12], polyhedra[13], hydrogels[14,15], and 3D crystals[16].

Scaffold-based DNA origami is the technique of folding a long 'scaffold' strand (e.g. M13mp18, a 7,247 nt strand) into a desired shape by annealing it with an excess of short 'staple' strands (roughly 30 nt)[9]. The staple strands are synthesised with a specific sequence so that they bind to specific domains on the scaffold strand,

holding it in place to form the desired shape (Figure 1.2b). This was initially demonstrated in 2006[9] with the assembly of 2D origami rectangles, triangles, stars and even smiley faces (with dimensions $\sim 100\,\text{nm}$). DNA origami structures have also been connected to form larger-spanning arrays, using "jigsaw piece" shapes[17] or complementary linking strands[18,19]. By introducing curvature into the origami, 3D structures are also possible. Computational tools exist to assist with the design of the staple strand sequences[20].

DNA origami has been used as a substrate for many functional molecules[23–26]. These can be precisely placed on the origami by attaching them to specific staple ends (this is explored in more detail in Chapter 5). As a prime tool in the field, DNA origami has incited various investigations into its formation process[27] and new methods for improving yield and stability[28–30].

Wei *et al.* 2012[31] have used a similar principle to the scaffold-based DNA origami to assemble 'single-stranded tiles' (SST) formed solely from short DNA strands. These 'DNA bricks' can also be used to construct complex 3D shapes[32].

DNA has been used to self-assemble a wide variety of 3D structures. Wireframe structures use ds-DNA to form the edges around open faces[33]. One of the smallest of these is a DNA tetrahedron composed of four strands that has an edge length of 6 nm[13] (Figure 1.2c). Each strand runs around a face of the tetrahedron, binding to the complementary sections of its neighbouring strands to make the edges. Other structures have included cubes[34,35], a bipyramid[36], an octahedron[37] and a truncated octahedron[38]. Polyhedra have also been designed with more complex edges[39], such as the DNA octahedron made from a single 1,669 nt strand[40] that uses two helices along its edges, and an icosahedron using six-helix bundles for its edges[11].

Another way to construct 3D structures is using DNA origami. 3D origami shapes can be hollow[22,41–43] or filled[11,12]. Hollow structures (whether wireframe or made from origami) can be used to enclose a cargo (forming a "DNA cage", described in more detail in Section 6.0.1). Amongst many other applications, Bell *et al.* 2012[22] used origami to form a nanopore with a precise pore size for detecting

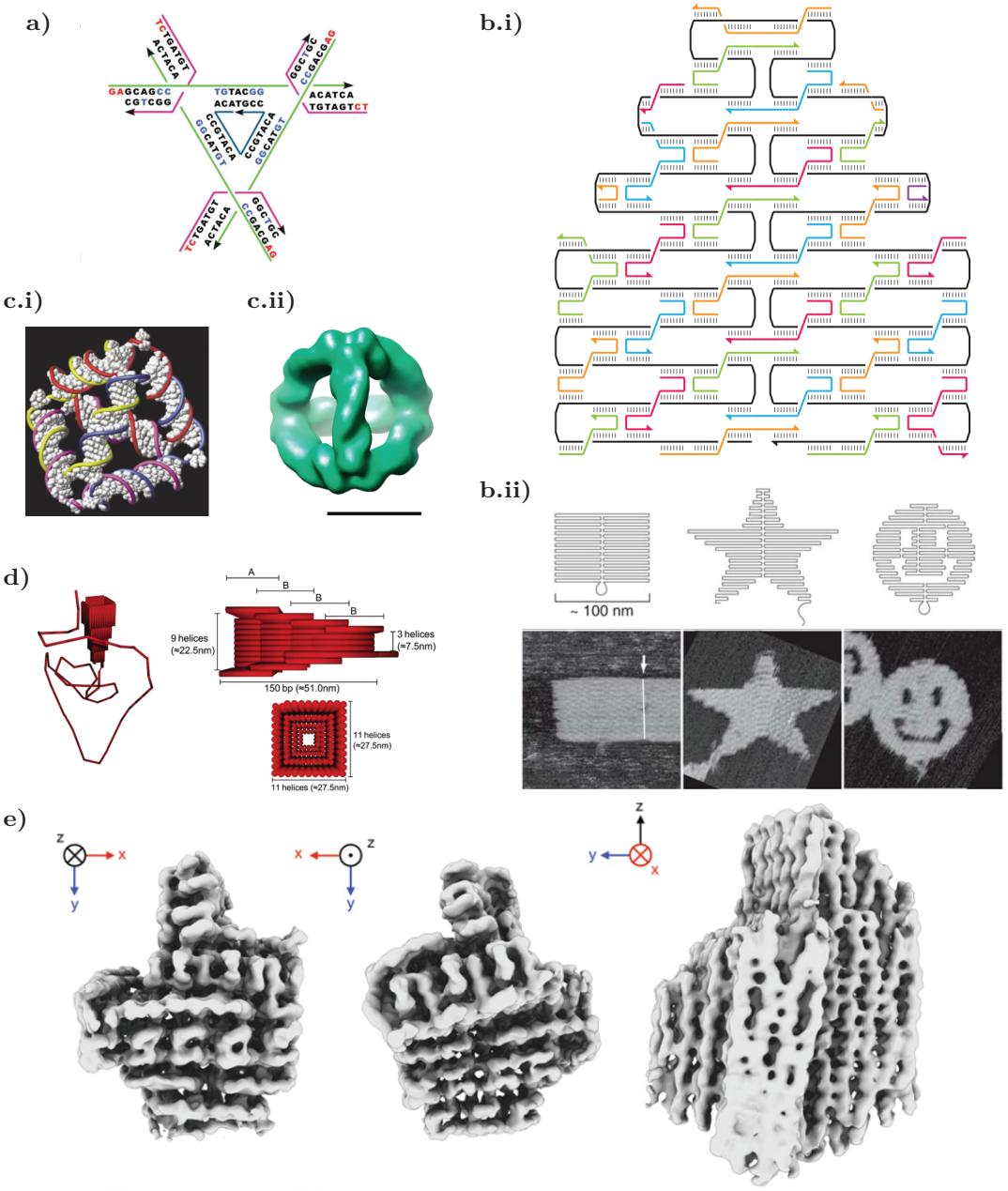


Figure 1.2: Examples of DNA structures. a) The subunits that bind together via 'sticky ends' to create a 3D DNA crystal. b) DNA origami: i) the principles of formation, the scaffold strand (black) is held in place by staple strands (coloured), ii) an origami tile, star and smiley face (from top to bottom: the raster of the scaffold strand and AFM images of the structures). c) DNA tetrahedron formed of four strands: i) a model of the strands, ii) a cryo-EM image of the structure, with a 5 nm scale bar. d) Origami nanopore for detecting single molecules. e) Cryo-EM images of a 3D origami structure from multiple views.

The images were taken with permission from: a) Zheng *et al.* 2009, Macmillan Publishers Ltd: Nature[16] ©2009; b) Rothemund *et al.* 2006, Macmillan Publishers Ltd: Nature[9] ©2006; c.i) reproduced (adapted) from Goodman *et al.* 2004[13] with permission of The Royal Society of Chemistry; c.ii) reprinted (adapted) with permission from Kato *et al.* 2009[21], ©2009 American Chemical Society; d). reprinted (adapted) with permission from Bell *et al.* 2012[22], ©2011 American Chemical Society; e) Bai *et al.* 2012[12], National Academy of Sciences of the United States of America ©2012.

single λ-DNA molecules as they traversed through (Figure 1.2d). Filled structures are often used for substrates with greater rigidity, e.g. that displayed in Figure 1.2e).

1.1.3 DNA machines

Dynamic DNA structures that can be programmed to move in specific ways (DNA machines) have been inspired by both biological systems[44–46] at the nano- and micro-scale, and larger man-made machines[10,47,48]. They can be both made and fuelled by DNA[42,49], or can be a hybrid of DNA and RNA[50], proteins[1] etc.

A few key properties and mechanisms that are often exploited in DNA machines are described briefly here, so that the terminology is explained in advance of the examples that follow.

Toehold-mediated strand displacement

DNA fuelled mechanisms normally involve a process called 'toehold-mediated strand displacement'. Strand displacement is when an invader strand replaces an incumbent strand that is bound to a target strand, forming a more stable complex (depicted in Figure 1.3a). The rate of strand displacement is significantly increased if the target strand has a single-stranded domain (a "toehold") that is complementary to a domain on the invader strand. The toehold allows the invader strand to bind to the target.incumbent duplex to initiate branch migration: as some of the incumbent bases melt apart from the target they can be replaced by base pairs with the invading strand. This is reversible, and so the branch point between the invader and incumbent diffuses up and down the target strand, until finally the incumbent is fully displaced.

The kinetics of toehold-mediate strand displacement can be controlled by altering the length or G-C content of the sequences[52,53], by placing mismatched base pairs between the strands[54] or by separating the toehold from the displacing domain by a linking section (called a "remote toehold")[55].

Toeholds can be hidden through secondary structure or within a duplex (as in Figure 1.3c). A cascaded reaction can be performed by sequential activation of

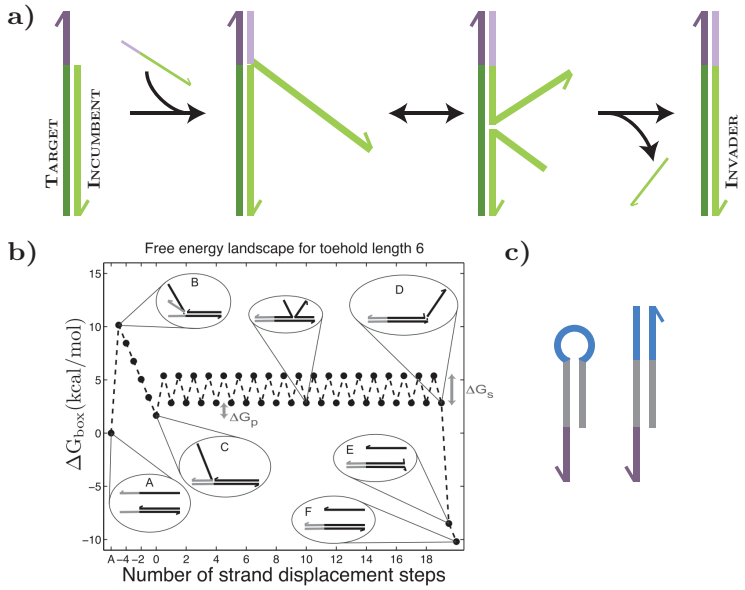


Figure 1.3: a) Depiction of toehold-mediated strand displacement. An invader strand can displace an incumbent from the target strand by binding to the target's **toehold**. Branch migration occurs when partially displaced bases between the incumbent and target are then formed by the invader and target, until finally the invader is fully bound. b) The free energy landscape for toehold-mediated strand displacement with a 6 bp toehold[51]. c) A hairpin and a duplex, each with two toeholds highlighted: an **accessible toehold** and a **hidden toehold** (this is inaccessible as long as the loop of the hairpin is small enough).
b) The image was taken from Srinivas *et al.* 2013[51] by permission of Oxford University Press: Nucleic Acids Research.

toeholds; for example, by the opening of a hairpin[56,57], or the removal of a covering strand (either by displacement[58] or cleavage via an enzyme[1]).

Examples

One of the first, and most versatile, DNA machines is the DNA "tweezers" reported by Yurke *et al.* in 2000[49] (Figure 1.4a). The tweezers are made up of three strands of DNA. A central 40 nt strand has one of the other (peripheral) strands hybridised to the 18 nt at each end, leaving 4 nt unbound in the middle to act as a flexible hinge. The peripheral strands have an extra 24 nt section that are unbound in the 'open' state. A 'closed' state is formed when a closing fuel strand is added that binds to both single-stranded extensions of the peripheral strands, bringing the ends of the central strand together. The closing fuel strand has an unbound section that

serves as a toehold for a removal fuel strand, which can displace the closing strand, returning the tweezers to the open state. This process can be repeated, driven by the hybridisation of the fuel strands.

Since then, the DNA tweezers concept has been modified by others; for example, opening has been triggered by a messenger RNA (mRNA) strand during *in vitro* studies[50], and the state of the tweezers has been switched by light irradiation which minimises the waste of DNA fuel strands[59,60]. Theoretical studies have also been made using a coarse-grained model to calculate the free-energy landscape of a full cycle of states[61].

Other DNA machines have been developed for a range of applications, including: to provide a conformation change in response to a signal such as a change in salt[64], temperature[65] or pH[66–68], to encapsulate and release a cargo (further described in Section 6.0.1), and to perform logic operations for DNA-based computation (further described in Section 3.1). DNA motors that can step down tracks have also been created. As they are a focus of the research in this thesis, they are specifically discussed in Section 1.2.

One of the many pH-detecting DNA nanomachines, the "I-switch", was reported by Modi *et al.* in 2009[62]. The I-switch is similar in structure to the DNA tweezers, except that the ends are brought closer together by the formation of an i-motif by the cytosine-rich extensions of the peripheral strands in acidic conditions (Figure 1.4b). This has been used for mapping spatial and temporal changes in pH inside living cells[62], in a multicellular organism[67], and (with the addition of a second type of pH detector) mapping two separate endocytic pathways inside a single cell in real-time[69]. A limitation of most pH-detecting DNA machines is the constrained region of pH values that the machine is sensitive to. Idili *et al.* 2014[68] have reported a design that is able to detect differences in pH over 5.5 units of pH.

Shen *et al.* 2004 introduced a DNA machine that is able to detect a protein binding, and estimate the work done by the protein on bending the DNA[63] (Figure 1.4c). When the protein bends the DNA, it breaks base pairs within the device. By changing the strengths of those base pairs (with a known energy of association), and observing when the protein no longer breaks all the bonds, an estimate

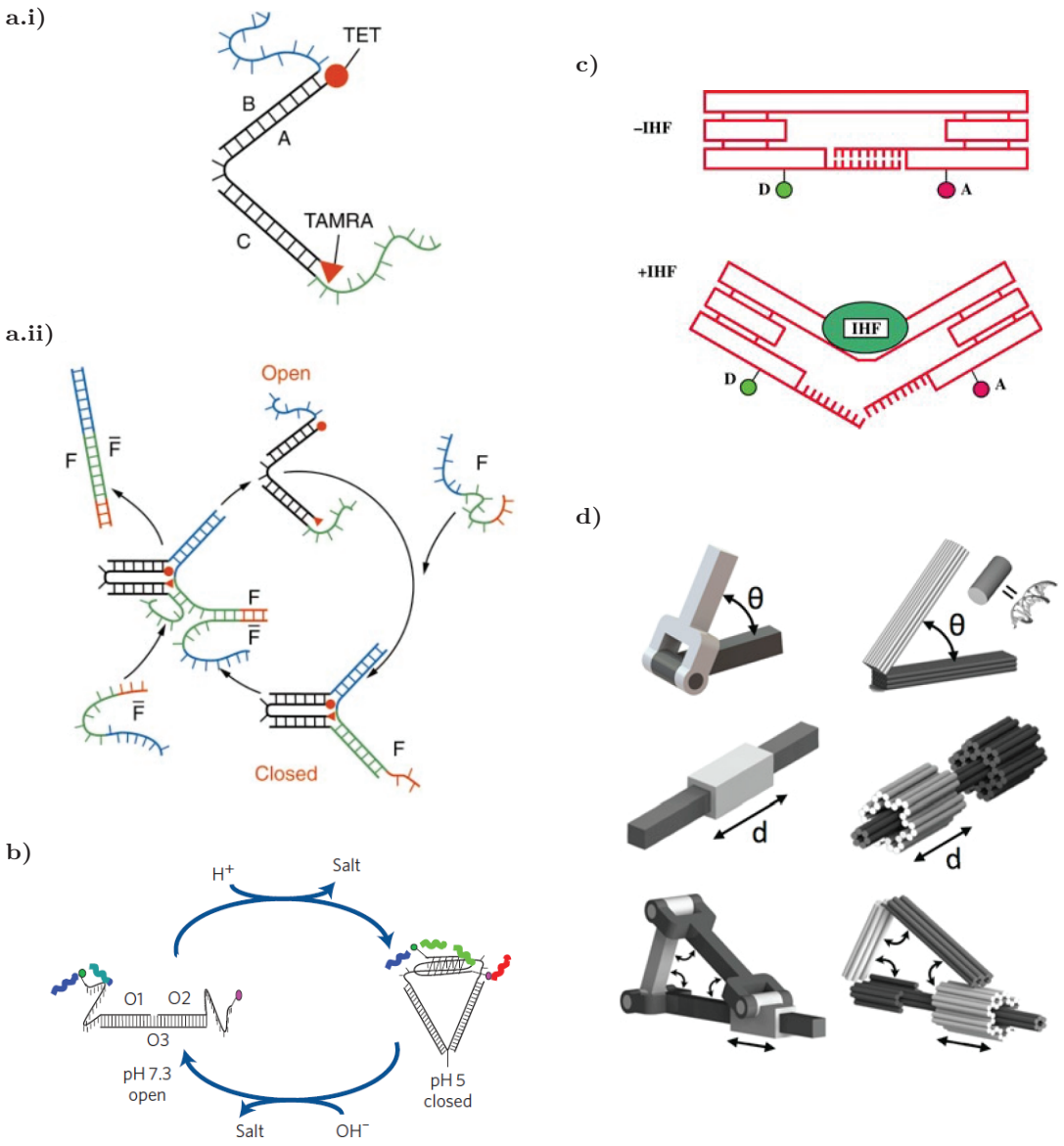


Figure 1.4: Examples of DNA machines. a) The DNA "tweezers": i) the main three strands, ii) the cycle switching from an open to closed state and back again through the addition of closing fuel strands (F) and removal fuel strands ($\bar{F}$) respectively. b) A pH nano-detector that forms an i-motif in acidic conditions, pulling the ends of the central strand (O3) close together. c) A protein-binding machine that is able to estimate the work done by the protein (integrated host factor, IHF, in this case) when binding and bending the DNA. The top schematic is the protein-free structure. The below schematic is the protein-bound structure: the protein bends the DNA, separating some base pairs, dependent on their energy of association. d) DNA origami mechanism design: from top to bottom are depictions of a rotational joint, a machine with linear motion, and a crank-slider mechanism that is a combination of a rotational and linear motion. The left images depict macroscale models, the right images show origami counterparts.

The images were taken with permission from: a) Yurke *et al.* 2000, Macmillan Publishers Ltd: Nature[49] ©2000; b) Modi *et al.* 2009, Macmillan Publishers Ltd: Nature Nanotech[62] ©2009. c) Shen *et al.* 2004[63], Wiley-VCH Verlag GmbH & Co ©2004; d). Marras *et al.* 2015[47], National Academy of Sciences of the United States of America ©2015.

of the binding energy can be made. The same method was later used for estimating the free energy of binding of another protein, MutS, when binding to unpaired bases and bending the DNA[70], and for a Apo-SoxR protein that untwists the local DNA helix[71]. These show the power of DNA machines to analyse molecules at the nanoscale.

A number of mechanically-functional structures have also been made. Zhou *et al.* 2014[72] created deformable objects, utilising single-stranded springs between rigid double-stranded helix bundles. The angle between two rigid bundles is altered by changing the length of the ss-springs between them. Marras *et al.* 2015[47] used a similar approach to form rotational and linear joints that have only one degree of freedom (Figure 1.4d), which are tunable in flexibility and the range of motion. They also combined a rotational and linear joint to form a DNA crank-slider, with reversible motion on a time-scale of the order of minutes. The ability to build a higher-ordered structure with a 2D or 3D motion through the combination of 1D joints opens up many new possibilities for DNA nanomachines.

1.2 Motors

1.2.1 Biological motors

Looking at the nanomachines at work within cells has inspired many synthetic nanomachines, including molecular motors. Biological motors provide linear and rotational movements: for example, a DNA helicase can move down a DNA helix unwinding it in preparation for replication (at rates of several hundred nucleotides a second[73]), and the bacteria flagellar motor rotates (at seveal hundred Hz[74]) to propel a bacterium.

Cytoskeletal motor proteins are used for intracellular movements. There are three types: the myosin family, the kinesin superfamily and the dynein family[4]. They all use "head" regions to bind to their associated filaments, and are able to step unidirectionally by hydrolysing one adenosine triphosphate (ATP) per step.

Motors from the myosin family step down actin filaments (with step sizes of roughly 5 nm, travelling up to 60 μm/s[75]), which can produce relative sliding between filaments for muscle contraction or to transport a cargo. Kinesin and dynein motors both step down microtubules, though normally in opposite directions (with speeds up to 2-3 μm/s and 14 μm/s respectively[4]). Kinesin-I (a specific type in the superfamily) moves 8 nm per step[76] and can walk processively down a microtubule over micrometre lengths before dissociating[77].

The activity of motor proteins is regulated through multiple pathways in the cell (e.g. myosin-II is regulated by phosphorylation at key sites on the protein[78]). Many of the capabilities of motor proteins would be desirable in synthetic nanomachines, but as these complex systems are not completely understood, they are hard to manipulate. The self-assembly and designability of DNA nanostructures offer an easier tool to wield: DNA-motor protein hybrids can be created (as accomplished by using DNA to create teams of kinesin[44,79,80]) or using DNA itself to form a motor (examples of which are provided in the following section).

1.2.2 Synthetic motors

There have been numerous designs for DNA motors over the years. The name "motor" is used here in reference to the "motor proteins" previously discussed. It is worth noting that some systems are reported using the name "walker" instead. Initially tracks for the motors were set-up on single DNA helices, but since then DNA origami structures are often used as a substrate (offering greater rigidity, and the option of non-straight tracks). Ideally a DNA motor would step in a directed, processive and autonomous fashion. Initial research often showed 'proof of concept' designs without implementing them on an extended track, some requiring external signals to be given for each step. More recent work has shown it is indeed possible for DNA motors to walk down extended tracks (with up to at least 30 steps[81]) and single-molecule measurements have opened up new validation of the operation, analysis into the stepping rates and yield (how successfully the motors step down the track) and real-time observations[82–87]. A few examples are described in detail

here to highlight the variety of the designs and possible applications.

As with any machine, motors require a source of energy to drive the system. One of the earliest DNA motors, reported by Yin *et al.* in 2004[88], is powered by the hydrolysis of ATP (the same fuel used by the cytoskeletal motor proteins). Many other motors use strand hybridisation to fuel each step[84,89–91], or the hydrolysis of the DNA or RNA backbone[1,92–95], and some have been designed to take a step when irradiated with light[85].

Shin *et al.* 2004[89] reported a bipedal motor, inspired by kinesin, that is formed of two strands that are hybridised together with unbound ss-domains (the "legs") at one end. The legs bind to a track of ss-extensions from a DNA helix via attachment fuel strands (Figure 1.5a). A leg is lifted from the track by an added detachment strand that displaces the attachment strand. The leg can then bind to the next extension on the track by an added appropriate attachment strand. The design was later adapted by Tomov *et al.* in 2013[87], who were able to use smFRET to observe individual motors on a track across an origami tile. They found that by using hairpin fuel strands they were able to increase the yield, by avoiding trapped states occurring between the fuel strands and the motor. The same design was also used to check that a motor could step between two origami tiles[86], which would be necessary for movement down extended tracks at the micrometre-scale.

Other motors have been designed with more than two legs, for example the "spiders" introduced by Pei *et al.* in 2006[94]. The spiders are formed of one or two streptavidin molecules with two to six legs. Each leg is a nucleic acid catalyst deoxyribozyme 8-17; when bound to the 'substrates' that make the track, the legs cleave them, turning them into 'products'. The legs remain bound to products for less time than substrates, which gives the spider a biased diffusion on the track. This system was extended by Lund *et al.* in 2010[97], who created a track on DNA origami that autonomously directed the spiders to start, follow, turn and stop (Figure 1.5e), and observed individual spiders with high-speed atomic force microscopy (AFM). The spiders were found to have an average speed of $\sim 0.05\,\mathrm{nm/s}$[97].

Single-footed motors have also been developed. A programmable and autonomous single-footed motor was reported by Muscat *et al.* in 2011[91], where hairpin fuel

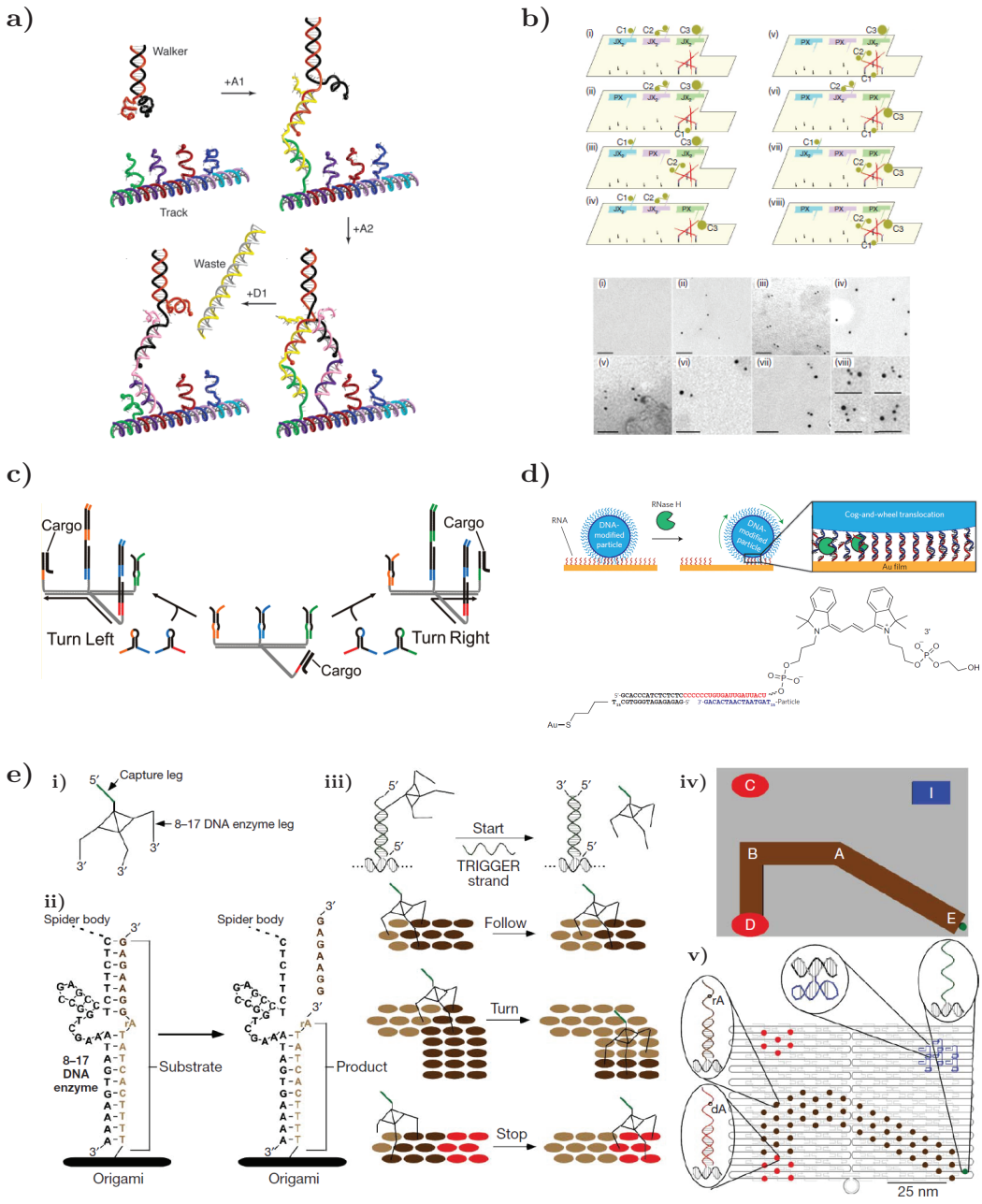


Figure 1.5: Examples of DNA motors. a) A bipedal motor that walks on a track of ss-extensions. Attachment strands (A) bind each leg to the track, and can be removed with detachment strands (D) to lift a leg. b) A multi-legged motor moves down an assembly line and can pick up a selection of three types of cargo depending upon the input signal. Top images depict each track and the selected cargo; the bottom panels show corresponding TEM images. c) A programmable, autonomous motor that can be directed at junctions, using DNA hairpins as fuel. d) A spherical, rolling motor covered in DNA that uses RNAse H to cut the complementary RNA track. e) A "spider" motor can walk down a track and respond to signals in the track.

The images were taken with permission: a) reprinted (adapted) with permission from Shin *et al.* 2004[89] ©2004 American Chemical Society; b) Gu *et al.* 2010, Macmillan Publishers Ltd: Nature[96] ©2010. c) reprinted (adapted) with permission from Muscat *et al.* 2011[91] ©2011 American Chemical Society; d) Yehl *et al.* 2015, Macmillan Publishers Ltd: Nature Nano.[95] ©2015; e) Lund *et al.* 2010, Macmillan Publishers Ltd: Nature[97] ©2010.

strands were used to direct the motor at a branched track (Figure 1.5c). The track is made up of single strands (anchorages) bound to blocking strands; each anchorage has an addressable toehold for a fuel strand and a domain that is complementary to the motor. The motor steps down the track when the fuel strand for its current location binds to the anchorage and transfers the motor on to the next anchorage, also removing the blocking strand from the anchorage. This process is autonomous as each toehold that initiates stepping is only activated sequentially through removal of the blocking strands. By adding a certain set of fuel strands, the motor's path down a branched track can be determined. Muscat *et al.* 2012[98] used the same motor system, but with a different directing mechanism: that of an adenosine aptamer. An aptamer is an oligonucleotide sequence that binds to specific molecules. The anchorages at a junction were designed such that the presence or absence of adenosine would determine which anchorage had a free toehold for the fuel strand to initiate strand displacement, enabling the motor to step across. This suggests that a motor could be directed down a network of tracks by various chemical signals in the environment; the motor's end location would be an indication of its surroundings, serving as a nanosensor.

Programmable motors are not only able to transport an attached cargo to a specific location, but can also create an assembly line whereby different cargos are collected at specific sequential sites down the track. DNA-templated reactions for the synthesis of a specific molecule have already been shown[99,100], a step towards the synthetic ribosome proposed by Bath *et al.* 2007[101]. Gu *et al.* 2010[96] created an assembly line for a motor that could receive signals to pick up (or not) a collection from three identifiable cargos (a small, a large and a coupled-pair of small gold nanoparticles) resulting in eight potential products (Figure 1.5b). The products were detected by transmission electron microscopy (TEM), and gave a yield of 43% for the triple addition of cargo, $\sim 70\%$ for the double additions and $> 90\%$ for the single additions. These yields could be improved by modifications to the collection mechanism, and show promise for assembly lines as an application of DNA motors.

DNA motors are not yet able to reach the speeds of motors found in biology. However, a spherical, rolling motor reported by Yehl *et al.* in 2015[95] has recently

helped to bridge the gap. The motor is formed of a spherical particle coated in DNA strands that are complementary to RNA strands that coat a surface. RNAse H is added to hydrolyse the RNA when hybridised to the DNA strands, freeing the DNA. This method of using an enzyme to cleave a track strand which frees a motor strand is used in many other systems, but the benefit of RNAse H is that its hydrolysis rate is roughly two orders of magnitude higher than other endonucleases[95]. This directly impacts the motor's speed, which was found to reach up to $\sim$ 80 nm/s (which is still 2-3 orders of magnitude slower than biological cytoskeletal motors). When the DNA strands were used with a single nucleotide mismatch, the speed was reduced by 60%, showing that this sort of system could be used for biomedical applications to detect single nucleotide polymorphisms.

'Burnt bridges' motor

The 'burnt bridges' motor was introduced by Bath *et al.* in 2005[1] on a double-stranded track on which the motor made two consecutive steps with an average speed of 0.1 nm/s. It is a single-footed, directional and autonomous motor. The motor was later used by Wickham *et al.* 2011[82] to send a motor down an extended track, and by Wickham *et al.* 2012[102] for directing motors at branched tracks. The latter experiments were performed with a track on DNA origami, as used in this thesis. Therefore, the specific details of the track design refer to these latter set-ups. Often the terms 'top' and 'bottom' will be used to refer to positions on the strands: these refer to locations far and near to the origami surface respectively.

The track is made of origami staple extensions that are complementary to the motor sequence. These are called "stators" in the original paper, but are called "anchorages" here. Figure 1.6 shows such a track running across an origami tile and a breakdown of the stepping mechanism. The anchorages have a TTT linker section between the motor-binding site and the staple sequence, to provide flexibility.

When a motor is hybridised to an anchorage, it completes a restriction site for a nicking enzyme, Nt.BbvCI, which cuts the anchorage 6 nt from the top (its 5' end). The small top fragment melts away, freeing a 6 nt toehold on the motor. The

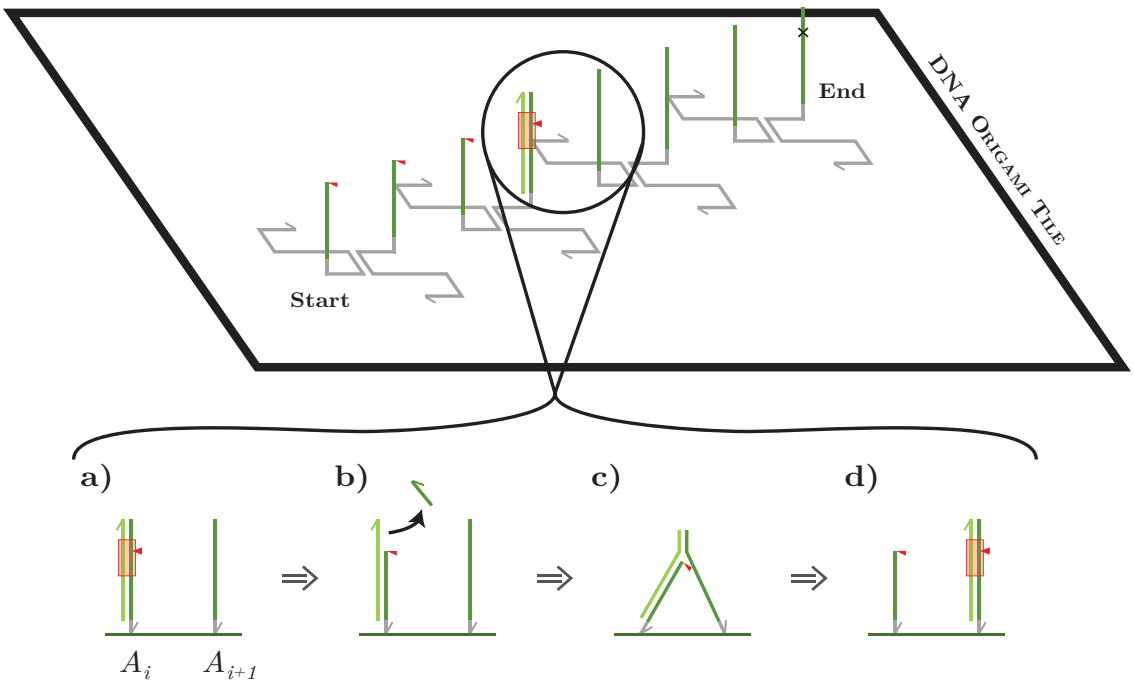


Figure 1.6: Schematic of the 'burnt bridges' motor on an origami track. The track is formed from anchorages, which are single-stranded extensions from origami staples. a) The motor strand is hybridised to a complementary anchorage, completing a restriction site for a nicking enzyme. b) The enzyme cuts the anchorage at a specific site. The small section at the top of the anchorage melts away, releasing a 6 nt toehold on the motor. c) The motor undergoes toehold-mediated strand displacement with the next, complete anchorage. d) Finally the motor is fully bound to the next anchorage and the process can start again for additional steps. Backwards motion is inhibited by the burnt track behind the motor, which is energetically unfavourable.
Reproduced with permission from ACS Synth. Bio., in press. Unpublished work copyright 2016 American Chemical Society.

motor then steps onto a next, complete anchorage through toehold-mediated strand displacement (as previously described in Section 1.1.3) and the process repeats. The energy for this driven motion comes from the hydrolysis of the phosphate backbone of the anchorages. Directional motion arises from the 'burnt' (cut) track behind the motor, which is energetically unfavourable compared to complete anchorages ahead of the motor.

The motor is stopped at the end of the track by a mismatch in the restriction site on the end anchorage, which inhibits enzyme cutting. Diffusion back down the track is inhibited as the motor makes more base pairs with the end anchorage than it could to a cut anchorage.

As the motor is complementary to all the anchorages, it must be specifically loaded onto the anchorage at the beginning of the track. This is done via a staple repair process: the motor is first pre-annealed with the first anchorage, and then incubated with the pre-formed origami missing the staple for the first anchorage. Diffusion of the motor down the track is inhibited through two mechanisms: the presence of two extra base pairs that are made between the motor and the first anchorage (making it more energetically favourable to remain on the first anchorage until actively stepping), and the use of blocking strands that cover the toehold on the other anchorages. Release strands are added immediately prior to stepping activation, which have a toehold to displace the blocking strands from the anchorages.

Wickham *et al.* 2011[82] reported the movement of the motor down a 100 nm track, consisting of 16 6 nm steps. Real-time AFM was able to detect individual steps of the motor (Figure 1.7b). Ensemble fluorescence measurements were also used to observe movement. The motor was labelled with a quencher, which reduces the fluorescence of different fluorophores placed along the track. The fluorophores were attached to the origami via modified staple strands. Control experiments suggested that undriven stepping is an order of magnitude slower than stepping driven by enzymatic cleavage[82]. An additional control checked for stepping between tiles, indicating that inter-tile stepping was 5000x more slow than stepping on the same tile[82].

Wickham *et al.* 2012[102] programmed the 'burnt bridges' motor to take specific paths at a branched junction in the track. Two methods of directing the motor were explored: an external instruction added to the sample (found to correctly direct 87% of the motors), and an internal instruction carried by the motor (found to correctly direct 71% of the motors). The anchorages at the junction had unique blocking strands bound to them, covering the toehold for the motor. The external instruction was given by adding the appropriate release strand to open up that branch of the track. The internal instruction was provided by a toehold on the motor that initiates the displacement of the appropriate blocking strand itself (Figure 1.7c).

The origami tile used in these previous experiments[82,102] and also in this thesis is a minimised-twist[82] version of the tile presented in Rothemund *et al.* in 2006[9].

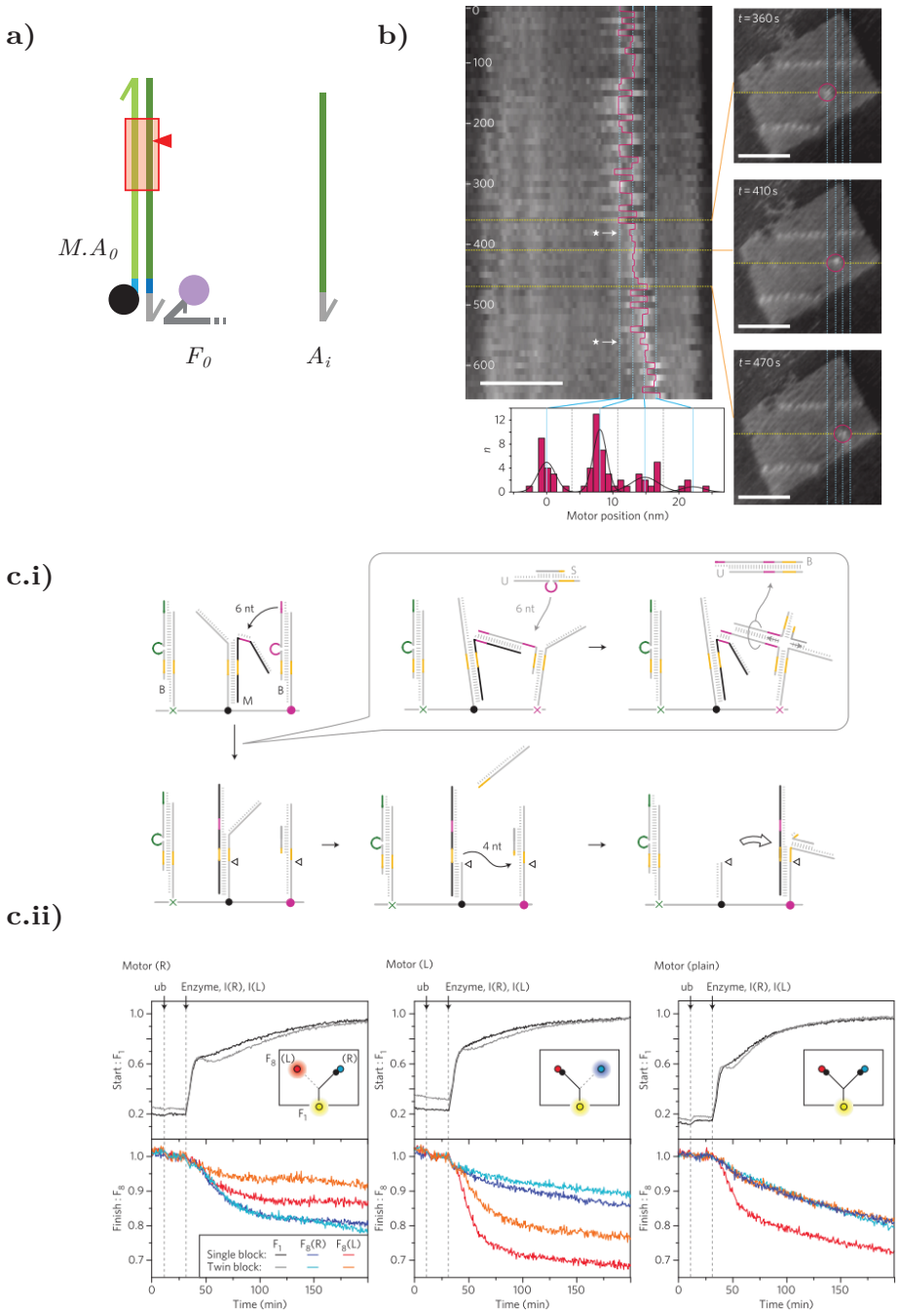


Figure 1.7: a) A schematic showing the 'burnt bridges' motor (M) bound to the first anchorage (A_0). The motor carries a quencher (black circle) that reduces nearby fluorescence, e.g. F_0 (light purple circle). The motor and first anchorage have two extra base pairs to inhibit diffusion onto the mid-track anchorages (A_i) before activation. b) AFM observation of individual steps of the motor on a linear track across an origami tile. The main panel shows a kymograph, where slices from consequetive images are stacked. The bright points are interpreted to be the motor, which can be seen to move across the slices over time. c) Ensemble fluorescence measurements of a motor directed at a branched track. The motor carries an internal signal, depicted in i). ii) The ensemble fluorescence measurements when the motor carries a signal to go right, left, and with no specific signal (in the panels from left to right).

The images were taken with permission: b) Wickham *et al.* 2011, Macmillan Publishers Ltd: Nature Nano.[82] ©2011; c) Wickham *et al.* 2012, Macmillan Publishers Ltd: Nature Nano.[102] ©2012.

This tile has 10.4 bp between crossovers in the tile (where staple strands are exchanged between the parallel helices). However, 3D modelling of the origami with CanDo[103,104], a computational tool that uses the finite element method, suggests that there is still curvature in the tile (Figure 1.8a).

Figure 1.8b) depicts the eight anchorage straight and bent track used in this thesis (with steps sizes of roughly 6 nm). Both tracks start at the top middle of the origami.

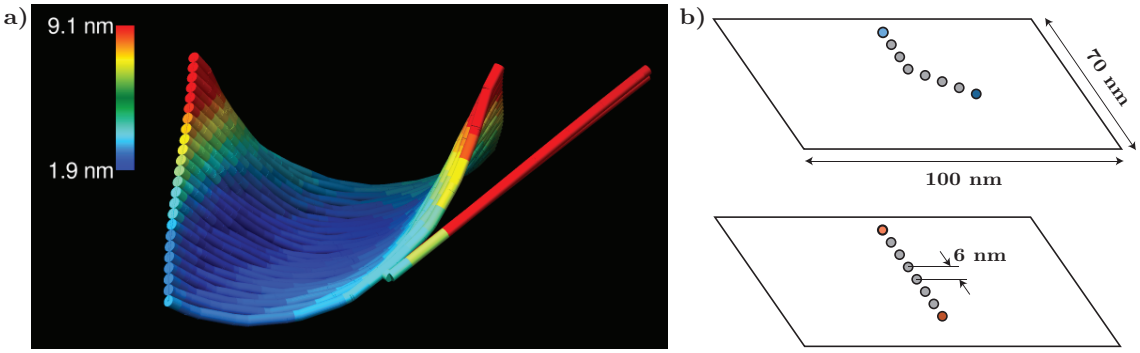


Figure 1.8: a) The structure of the minimised-twist tile used in this thesis, as modelled by CanDo[103,104]. It is coloured according to the local root mean square fluctuations (it is not related to the "height" of the structure, which is coincidental in this image). This shows clear flexing of the origami, particularly across opposite corners of the tile. b) Depictions of the origami tile with a straight and bent track, laid out as for the experiments used in this thesis.

1.3 Observation techniques

Many different observation techniques have been used for detecting and analysing DNA structures and machines. Fluorescence has been widely used in many disciples[105], including biotechnology, medical diagnostics and forensics, and was the principle method of observation for the experiments described in this thesis. Fluorescence can be used to explore the structure of molecules that cannot be easily imaged, even allowing the dynamics of them to be explored in real-time. It can be used for ensemble fluorescence measurements or for single-molecule measurements. The former records an average for the system, whilst the latter is able to measure individual molecules, highlighting any heterogeneity in the system.

Fluorescence measurements are normally performed by labelling the molecule of interest with a fluorophore or quantum dot. Over time they will photobleach and no longer produce a signal, which means that experiments are often limited to observation windows before photobleaching occurs. An alternative labelling technique is to use DNA-PAINT (DNA points accumulation for imaging in nanoscale topography)[106,107]. This technique uses short fluorescently-labelled strands of DNA that transiently bind to a complementary domain on the strand that is to be labelled. As the labelled strands only bind transiently, bound strands are routinely exchanged with different ones in solution. This reduces the limitations due to photobleaching, as the labelled strands in the solution are not illuminated during TIRF (total internal reflection fluorescence) microscopy, and provide a large reservoir of unbleached strands. DNA-PAINT not only combats the effects of photobleaching, but can also be used for super-resolution microscopy, as transiently-bound strands can bind at different times, giving single point spread functions that can be localised with a Gaussian fit.

1.4 Thesis structure

In Chapter 2, the ‘burnt bridges’ motor is adapted into a reusable and reversible system. A motor is shown to walk down a track with seven steps, three times. In

Chapter 3 the 'burnt bridges' motor is adapted to perform logic operations using interacting motors (the basics for DNA computation). In Chapter 4 the 'burnt bridges' motor is sent down extended tracks that are located inside stacked tubes made from DNA. This shows preliminary results aiming to observe micrometre movement of individual motors using optical microscopy.

Chapter 5 investigates DNA origami using single-molecule Förster resonance energy transfer (smFRET), offering guidance for future designs for functionalising origami surfaces. Chapter 6 presents a new design for a dynamic DNA octahedron composed of eight strands, named the *'Holliday Octahedron'*, that could be used as a DNA "cage" for drug delivery. Finally, Chapter 7 summarises the results of the preceding chapters. Additional experimental methodology and the strand sequences can be found in the Appendices.

1.5 Thesis contributions

Some of the work in this thesis was part of a joint collaboration, and other work has benefited from smaller contributions of image work, simulations etc. Therefore, each chapter is introduced with a statement of any specific contributions from others for the work therein.

Chapter 2

Reversible Motor

This chapter presents a DNA motor and an automatically regenerating track. It is based on the 'burnt bridges' motor[1], one of the simplest and most effective synthetic molecular motors made from DNA, previously described in detail in Section 1.2.2. The 'burnt bridges' motor uses a nicking enzyme to cut the DNA anchorage (the piece of track, frequently called 'stator' in the literature) to which the motor is bound, freeing a toehold on the motor that is used to step onto the next, complete anchorage. Directed motion requires energy. In the case of the 'burnt bridges' motor, the energy comes from the hydrolysis of the phosphate backbone of each anchorage strand by the nicking enzyme. Its motion is highly directional due to the 'burnt' track behind it: it is energetically unfavourable to bind to a cut anchorage rather than the complete anchorages ahead of it.

The aim was to not only design a mechanism for a regenerating track, so that motors could be reversed or multiple motors could traverse the same track, but to do so autonomously in a one-pot system. Ideally the mechanism would allow for tracks to be reprogrammed and for motors to be directed at junctions enabling DNA-based computation (as in Wickham *et al.* 2012[102] with the 'burnt bridges' motor).

To adapt the 'burnt bridges' motor for a renewable track, it may seem like a trivial case of repairing the 'burnt' track by ligating the cut anchorages. This would

require a 'splint' to hold the two parts of the anchorage in place for a ligase to ligate them back together. The splint would have to have the same sequence as the top of the motor for this (as both must be able to bind to the anchorage), and hence would also be able to bind to complete anchorages. This system would need alternating flows of nicking enzyme and ligase with the splint strand. Otherwise the splints could also initiate cutting of the anchorages, and the motor could also act as a splint for a ligase, potentially causing multiple rounds of nicking and ligating before the motor can step on. This simple approach is not able to provide an autonomously regenerating track, which was the aim of this thesis and hence was not pursued.

An alternative approach is to allow the nicking enzyme to cut a replaceable strand. The replaceable strand can be considered as 'fuel' for this process as it is used up as the motor moves down the track.

The reusable track presented in this chapter uses a sacrificial strand called a 'director' that binds to a staple extension called an 'anchor', completing the anchorage and "directing" the motor onto it. It is the director that is cut by the enzyme: this not only allows the motor to move forwards, but also initiates a mechanism for the removal and replacement of the cut sacrificial strand. In this way a 'burnt' track is regenerated and a motor is able to move down it again.

In this chapter, the design and characterisation of the regenerating track are first described. A number of designs for holding the motor at the end of the track are then compared. Finally, ensemble fluorescence measurements show motors stepping down the same track of eight anchorages three times, requiring two reverses.

2.1 Design

The aim was to create an autonomous system for a motor that is able to move down an automatically regenerating track. Given a circular track, the motor would go round and round until the fuel for regenerating the track runs out. Placed on a linear track, the motor would go forwards and backwards down the full length of the track in a controllable fashion (i.e. not by diffusion). The simplicity of the

'burnt bridges' motor allowed minimal revisions to produce a reversible motor. To maintain directional movement, there must exist a temporary wake of burnt track behind the motor. The wake must not get replenished at a rate faster than that of the motor's stepping. A precise investigation into the wake and how to control its length and replenishment rate were not made in this thesis.

A simpler system could be designed if one accepted re-initiating the entire track externally. However, such a system would be limited and hence was not aimed for, despite the merits of simplicity. For example, continuous rotary movement about circular tracks would not be possible; and stop-and-start rotation would lose the motor's previous directionality on re-initiation (due to the lack of a wake).

For an autonomous, one-pot system the design had to allow all of the component strands to be added from the start. The exceptions to this are release strands to initiate stepping of the motor from the ends of the track. These are required in order to acquire coherent signals from the motors during ensemble fluorescence measurements (described in detail in Section 2.1.3).

The new system described in this chapter was intricately designed to allow for autonomy. In the following section, the overall mechanism will first be described, so that it can be borne in mind when the specific details of the design are then subsequently explained in Section 2.1.2. A less powerful, but simpler design for an externally re-initiated track is also provided for completeness (Appendix A.1.1).

Experimental characterisation and implementation of the system can be found in Sections 2.2 and 2.3.

2.1.1 Overall mechanism

The mechanism for stepping along a series of anchorages is the same as that of the 'burnt bridges' motor. However, whereas the 'burnt bridges' anchorage consists of just one strand, the anchorage of the renewable track is a complex of two strands: a director and and an anchor. Figure 2.1 displays the overall mechanism of motor movement and track renewal; Figure 2.2 complements this by highlighting the key complexes and their interactions.

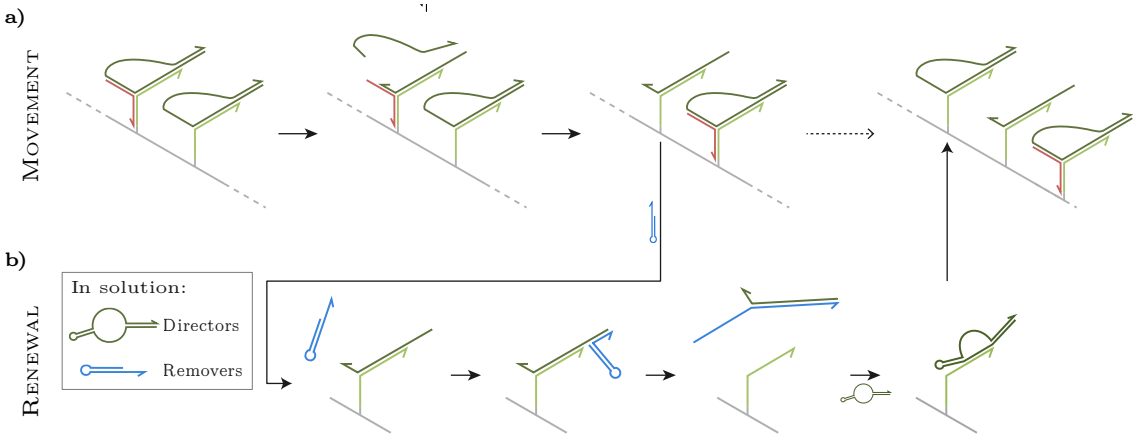


Figure 2.1: The overall mechanism for the movement of a motor down an autonomously regenerating track.
a) Motor movement — the **motor** binds to an anchorage formed of an **anchor** and a complete **director**. The nicking enzyme cuts the director, revealing a toehold on the motor. The motor steps onto the next anchorage through toehold-mediate strand displacement with the next anchorage, and so on for subsequent steps.
b) The track renewal — a cut director is removed from its anchor through the strand displacement by a **remover** strand. The empty anchor binds to a director in solution, regenerating a complete anchorage. Until the replenishment process is completed, backwards motion of the motor is inhibited.

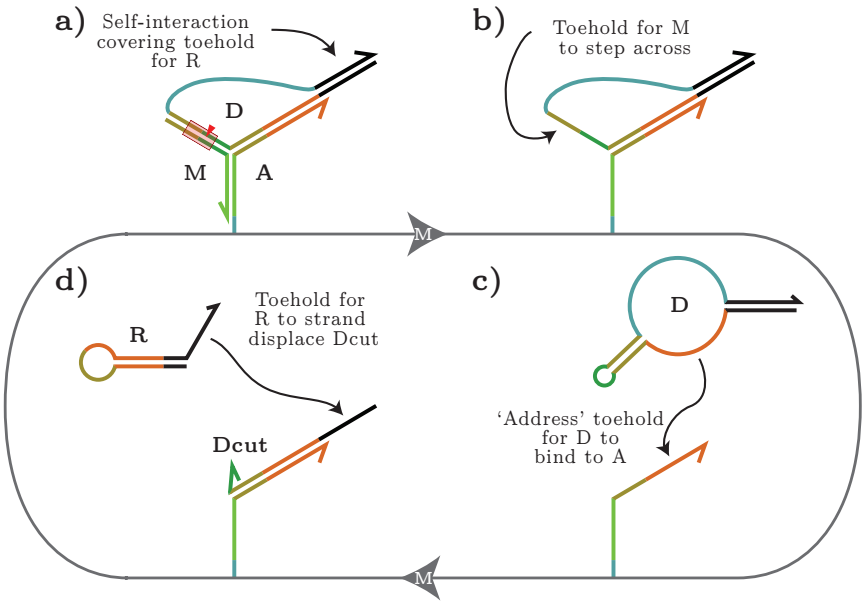


Figure 2.2: Schematic of a circular track with each anchorage showing some of the key stages of use. The domains of each strand are highlighted, matching those in Figure 2.3 which shows the breakdown of the sequence design for each strand. The motor's movement is in the direction of the arrow. a) The motor (M) is bound to a complete anchorage made of a hybridised anchor (A) and director (D). The restriction site (red box) and nicking site (red triangle) are shown. b) The anchorage ahead of the motor has an accessible toehold for the motor to use to initiate stepping onto it. c) A director in solution binds to a bare anchor using its 'address' toehold to complete the anchorage. d) A cut anchorage has an accessible toehold for a remover (R) to use to displace the cut director.

A director uses an addressable toehold (the 'address') that can be used for binding to specific anchors. An anchor without a bound director would provide fewer bases for the motor to bind to than even an anchorage with a cut director (and would not include the complement for the motor's toehold). A bare (unbound) anchor can, therefore, be considered inert.

Once bound to an anchor, the director forms a large loop such that the self-complementary ends of the director bind together. When the motor is present, it binds to the anchorage to form a 3-way junction. The motor.director arm completes a restriction site for the nicking enzyme Nt.BbvCI, which cuts the director 6 bp from the vertex. The short segment of the director that is bound to the top of the motor melts off, freeing a toehold on the motor which is able to bind to a nearby complete anchorage. The motor undergoes strand displacement, stepping from the old anchorage to the new director and then its anchor until it has fully stepped across. This process repeats down the track (Figure 2.1a).

Each step is driven by the ability of the motor to make more base pairs to an anchorage ahead of it than to the cut anchorage behind it or at its current position.

Once the enzyme has cut the director, the loop formed by the interaction between the two ends of the director also melts and the unbound portion of the director diffuses away. This uncovers a toehold at the 5' end of the director that a remover strand (which is in solution) can use to strip the cut director off the anchor by toehold-mediated strand displacement. *NB: "cut director" is used to refer to the cut part at the 5' end of the director, whereas the cut part at the 3' end of the director will only be referred to explicitly.* This leaves a bare anchor, which a director in solution can bind to using its addressable toehold, opening up some of its secondary structure to produce a regenerated anchorage (Figure 2.1 b).

The secondary structures of the directors and removers are key to limiting undesired interactions. The logic behind them is described in the following section, and the different interactions are experimentally checked in Section 2.2.

2.1.2 Director, remover and anchor structure

To benefit from the work already done on the 'burnt bridges' motor, the design for this renewable track was modelled closely on the base sequences of previous work[1]. The intricate design of the directors and removers is vital to control their interactions (Figure 2.3).

Directors

The sections of the anchor and director that bind to the motor are constrained by the motor sequence (Figure 2.3b). The 7 bp restriction site for the nicking enzyme Nt.BbvCI is in the motor.director duplex. To keep the strands short, the restriction site was located as close as possible to the vertex of the 3-way junction formed by the motor, director and anchor.

For an autonomously renewing system, there will be an excess of directors in solution. As the directors are partially complementary to the top of the motor, directors in solution could bind to the motor, slowing it down. Therefore, the director's sequence that is complementary to the motor's toehold is hidden in the stem of a hairpin. The rest of the domain of the director that is complementary to the motor forms the hairpin loop. The restriction site for the enzyme covers the stem and loop of the hairpin, i.e. it is partially single-stranded, and cannot be cut on the director alone.

Directors in solution must be able to bind to bare anchors, opening their hairpins to allow binding to the motor. This is initiated through the 'address' (Figure 2.3c), an addressable toehold for binding to specific anchors with a complementary toehold.

In order to remove a cut director from an anchor, there is a toehold at the 5' end (the end of the director that is bound to the anchor) that can be used by a remover strand to displace it using toehold-mediated strand displacement (Figure 2.3d). To stop the removers accessing the toehold before the director has been cut, the toehold is hidden by a complementary section at the 3' end of the director (Figure 2.3e). When the two ends of the intact director form a hairpin, the stem of the hairpin

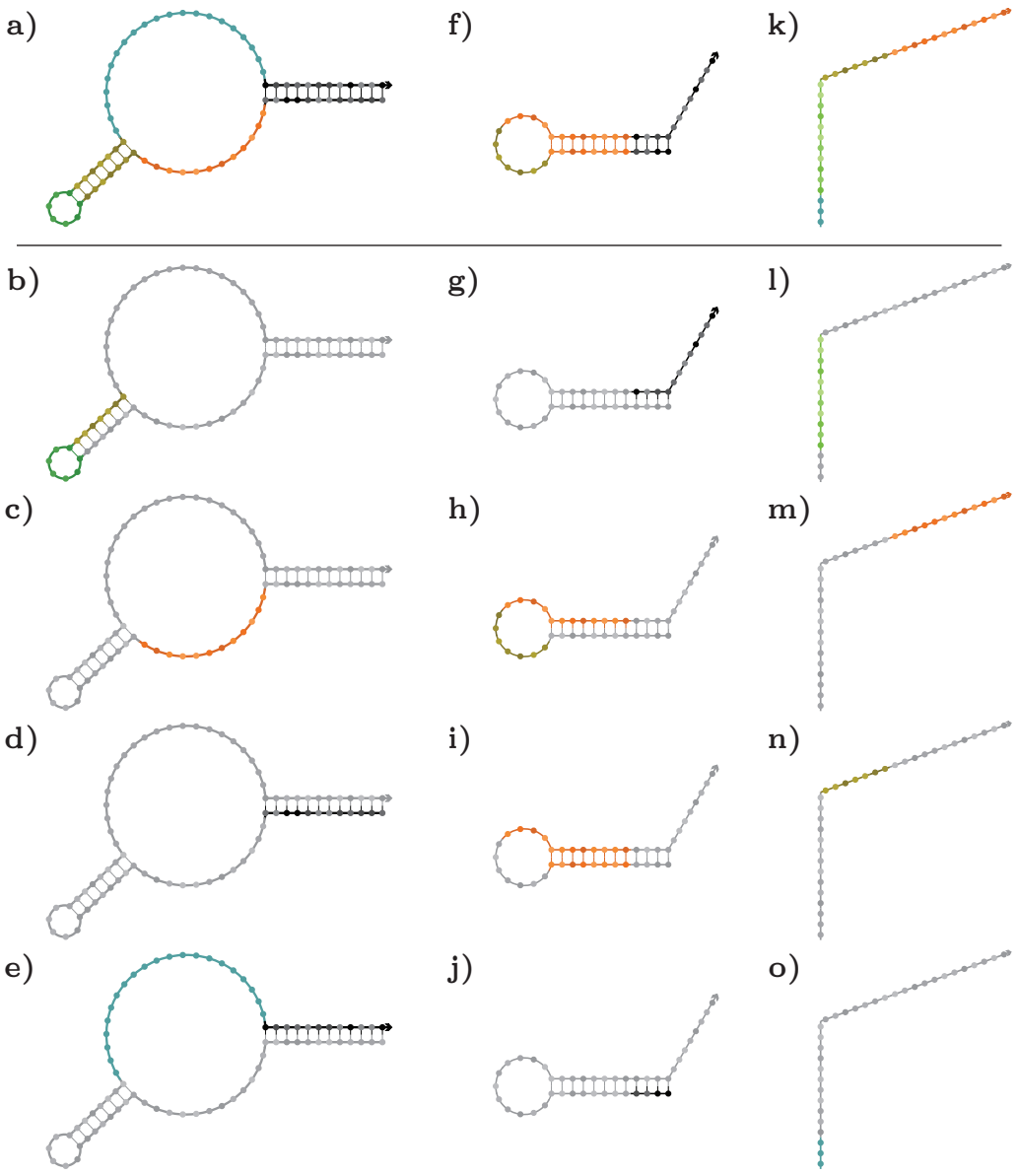


Figure 2.3: The structures of a director (D), remover (R) and anchor (A). a), f) and k) the full structure coloured into sections for D, R and A respectively. The images are adapted from NUPACK's structures[6].
Specific sections are highlighted in D: b) the sequence constraints set by being complementary to the top of the motor, c) the 'address' toehold for D to bind to A, d) the toehold for R, and e) the self-interaction to cover the toehold for R until D is cut.
Specific sections are highlighted in R: g) the toehold to bind to a cut D, h) the sequence constraints set by being complementary to the part of D that is bound to A, to strand displace it from A, i) some of the complement to D's 'address' is covered by a hairpin stem to stop interactions with Ds in solution, and j) some of the toehold for the cut D is hidden in the stem to make it less energetically favourable for R to bind to an uncut D.
Specific sections are highlighted in A: l) the sequence constraints set by being complementary to the bottom of the motor, m) the 'address' for D's toehold, n) the sequence constraints for D to open up its hairpin, and o) 3 dT as a flexible linker to the origami tile.

covers the toehold and stops the removers from being able to bind to it. A flexible dT section between the main body of the director and the toehold cover at the 3' end allows the two ends of the director to remain bound when it is bound to the anchor. Once the enzyme cuts the director, the two ends of the director are able to separate, freeing the toehold for the remover. This requires the melting temperature of the director's self-interaction to be below that of the working temperature, 37°C, when the director is cut (the sequence used in the experiments in Section 2.3 has a melting temperature of 32°C[6], where the melting temperature is defined as the temperature at which half of the bases are unbound).

Removers

For each version of a director there is a specific remover. This means that anchorages on specific sections of track can be made reusable and others "one-use" by adding or omitting the relevant removers respectively.

The removers have a toehold that is complementary to the free end of the cut director, followed by a section that is complementary to the part of the director that is bound to the anchor (Figure 2.3g-h). This can be used to remove the cut director from an anchor by strand displacement. As this requires the remover to share the 'address' region of the anchor, it could also interact with and open up directors in solution, in the same way that an anchor opens up a director. This would cause an unnecessary waste of directors and removers. To inhibit this interaction, the remover forms a hairpin, covering the majority of the address in the stem (Figure 2.3i). The uncovered portion of the address is in the hairpin loop. This has potential for another undesired interaction, between a remover and an anchor (Figure 2.4a). Once a remover has stripped off a cut director from an anchor, the end of its hairpin stem is uncovered. This is complementary to part of the anchor's address, and if the melting temperature of these sections is too high, the cut director.remover will bind to an empty anchor, inhibiting track renewal. Therefore, the amount of the remover's address hidden in the hairpin stem is a fine balance between limiting the undesired interactions between a remover and director (by hiding more of the

address in the stem) and between a cut director.remover and an anchor (by limiting the amount of the address in the stem).

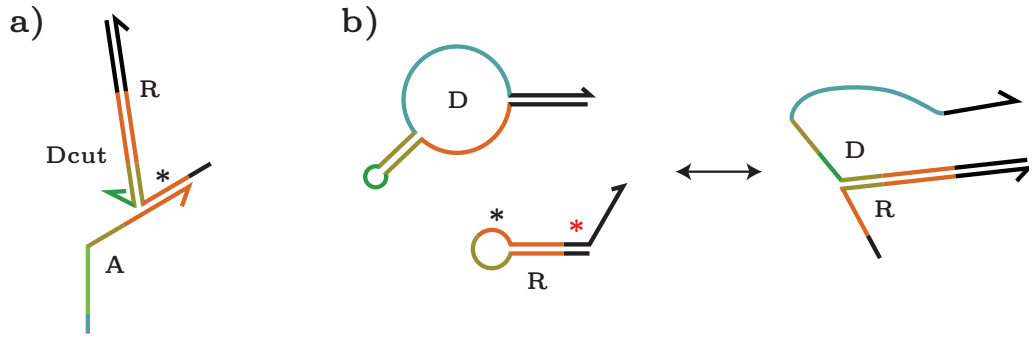


Figure 2.4: Schematics of undesired remover-based interactions. a) After strand displacing a cut director (Dcut) from an anchor (A) (as depicted in Figure 2.2d), the remover (R) is able to partially bind to the anchor. This domain is highlighted by *. To inhibit this interaction, the * domain must have a melting temperature below the working temperature. b) Directors (D) and removers in solution can potentially interact to form a duplex (this must be suppressed through careful sequence design). The base pairs highlighted by * on R are base pairs to be gained by binding to D. These are neutralised by a toehold cover-up on R, highlighted by * which are base pairs to be lost if R binds to D.

Any of the address in the remover's hairpin loop are base pairs to be gained if a director and remover bind (an undesired interaction, depicted in Figure 2.4b). To neutralise this, the remover's hairpin stem can be extended to cover up part of the toehold for the director (Figure 2.3j). This "cover-up" provides base pairs that would be lost if the director and remover bind. By considering only the energy gained from forming base pairs, ignoring any sequence and entropic effects, the toehold cover-up length must be larger than the length of the address in the loop to be energetically unfavourable for the director and remover to interact. Any superfluous base pairs formed by the toehold cover-up makes it even more unfavourable for the two strands to interact.

Anchors

The anchor has an address region for directors with the complementary sequence to bind to (Figure 2.3m). This is the toehold to mediate the binding of the director and anchor.

The rest of the anchor is constrained by the sequences of the motor and director that bind to the other main sections (Figure 2.3l and n). As in a typical 'burnt bridges' track, the anchors have a flexible TTT section between the staple sequence and the main body of the anchor (Figure 2.3o).

A possible addition to the anchors is a few extra nucleotides at its 3' end, forming an additional toehold that the remover can use to form a mobile Holliday junction when displacing the cut director from the anchor. However, this was not deemed necessary and also encouraged the remover to displace a complete director from an anchor, which is not desired, and so was not used (Appendix A.1.2).

2.1.3 The ends of the track

Ensemble fluorescence measurements were used to observe the motors' positions on the track. Each motor carries a quencher that reduces the fluorescence signal from nearby fluorophores (the same reporting mechanism as in previous work[82,102]). The movement of the motor from the beginning to the end of the track can be observed by the unquenching and quenching of different fluorophores at those locations. As all the motors in a sample would no longer be well co-ordinated by the end of a track of eight anchorages, the motors must be stopped at the end of the track and later actively released to re-establish a coherent signal. These end locations are referred to as 'stations', which use holding directors to stop the motor.

Previous work on the 'burnt bridges' motor[1] used a mismatch next to the nicking site on the end anchorage to stop the enzyme from cutting. This stops the motor's toehold from being actively exposed by the enzyme, and the additional base pairs the motor can make compared to those on the cut anchorages stops the motor from diffusing back down the track. Bath *et al.*[1] also used an extra 2 bp between the bottom of the motor and the first anchorage to make it more energetically favourable for the motor to remain on the first anchorage until stepping is initiated by the addition of the enzyme.

Diffusion of the motor down the track was further inhibited by Wickham *et al.* 2011[82] by using blocking strands to cover the toeholds of the mid-track anchorages.

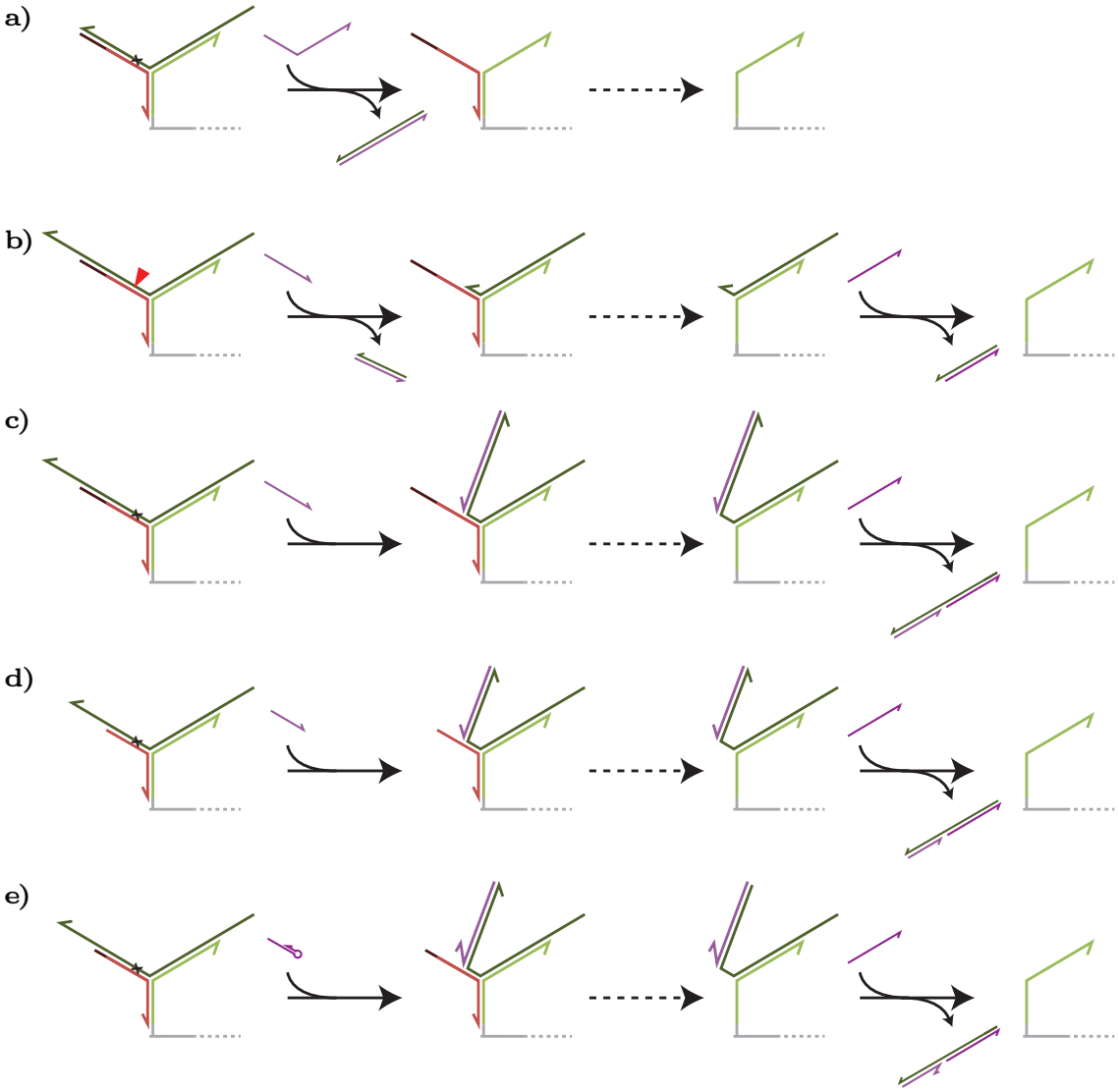


Figure 2.5: Various mechanisms for holding and releasing a **motor** at a 'station' at the beginning or end of the track. The holding of the motor makes use of two traits. First, a mismatch in the restriction site (used in a, c-e) to stop the enzyme from cutting. This is depicted by a cross here, whilst a complete restriction site has the nicking site shown at the red triangle. Secondly, extra bases are provided for the motor to bind to the **holding director** (9 nt for a-c) and 4 nt for e). These holding sections are highlighted by the extended, darker regions of the motor. Both techniques make it energetically favourable for the motor to stay on this **anchor** until it is released. Release mechanisms make use of one or two **release** strands to displace all or part of the director (a) and b-e) respectively). A hairpin first release strand is used in e). The dotted arrow depicts the motor having stepping away, and when this anchorage needs replenishing.

The blocking strands were removed just prior to movement initiation by adding release strands that are able to displace them from the anchorages. Blocking strands of this type are not easily used for a renewable track as they would require timed binding to the track, linked to an individual motor's movement and hence were not considered.

For the renewable track, a combination of a restriction site mismatch to stop the enzyme cutting (in the same place as for the 'burnt bridges' motor) and extra bases to reduce motor diffusion away were tested (Figure 2.5). These are required at both ends of the track as the motor must be able to be held and released at both for multiple traverses of the track. All tests used the extra 2 bp between the bottom of the motor and anchorage. Additional extra bases (the 'holding section') of 0, 4 and 9 bp between the top of the motor and the holding director were considered.

In all cases, release of the motor from a 'station' is initiated by a release strand that uses toehold-mediated strand displacement to displace enough of the holding director from the motor to free the motor's toehold for stepping. Initial tests using a single release strand to entirely remove the holding director from the motor and anchor (depicted in Figure 2.5a) showed very slow movement of the motor away from the station, possibly due to undesired binding between the free tops of the motor and anchorage. Therefore, a two-step strategy was developed in which a first release strand displaces enough of the motor to allow movement, and a second release strand is used to remove the holding director from the anchor so that it can be replaced.

An alternative not investigated in this thesis would have been to use the second release strand to remove the first release strand from the holding director, returning the anchorage to its previous state, as opposed to removing the holding director. This mechanism could be used with an anchor that fully binds to the motor, with no holding director necessary. However, only systems using removable holding directors would be able to make complete track redesigns mid-experiment, which is why mechanisms involving the removal and replacement of the holding directors were considered in this thesis.

After a number of experiments, a further alteration to the release strands was

made. Only the toehold between the holding director and the first release strand is unique for each end of the track. Therefore, when initiating motor movement by adding an excess of the first release strands for the beginning of the track, the release strands will also partially bind to the end holding director. This may hamper motor movement onto the last anchorage as the release strands would cover the complement to the motor's toehold. Therefore, the first release strand was redesigned as a hairpin, with the unvarying section hidden in the stem and loop. The extra holding section was reduced to 4 bp, as if it is too large the release strand may bind to the top of the motor, covering the region the motor uses to stay held at the next station.

2.2 Sequence characterisation

The key sections of the directors, removers and anchors were tested for their optimum lengths. Some interactions between the strands are necessary for the system to work, and some must be hindered to avoid slowing the motor down, cause unnecessary waste of strands, or cause the decoherence of motors during bulk measurements. The interactions that were considered are as follows, where M, A, D, Dcut and R denote the motor, anchor, director, cut director and remover respectively.

- Necessary interactions that should be strong (i.e. with an equilibrium shifted to the desired end product, minimising the free energy of the system) and/or rapid (i.e. with a fast rate of reaction and a minimal free energy barrier for completion):
  - A + D → A.D *(formation of a complete anchorage)*
  - A.D + M → M.A.D *(binding of the motor to the anchorage)*
  - M.A.D + Enzyme → M.A.Dcut + D3'cut + Enzyme *(enzyme cutting in the presence of the motor)*
  - M.A.Dcut + A.D → A.Dcut + M.A.D *(stepping of the motor)*
  - A.Dcut + R → A + Dcut.R *(removal of the cut director from its anchor)*

- Interactions to be hindered (if not stopped entirely):
  - A.D + Enzyme $\nrightarrow$ *(enzyme cutting in the absence of the motor)*
  - D + R $\nrightarrow$ *(director and remover interacting while free in solution)*
  - A.D + R $\nrightarrow$ *(remover interacting with the director before the anchorage is cut)*
  - A + R.Dcut $\nrightarrow$ *(remover binding to the address of the anchor)*

This section investigates the optimisation of the strands and their section lengths, given the desired interactions of the system. This leads to a demonstration of the chosen sequences for the strands (Section 2.2.3), before they are implemented on origami (Section 2.3). The tests were done by annealing or incubating certain complexes/strands together. All anneals involved heating the sample to 95°C, before cooling to 20°C by 1°C/min in 0.1°C steps. All incubations were done for 1 hr at 37°C. The samples were made in 1x Origami buffer (12.5 mM MgOAc, 40 mM (1x) Tris-acetate, pH 8.3) with 50 mM NaCl (as used for running ensemble experiments in previous work[1,82,102]). Samples were checked using polyacrylamide gel electrophoresis (PAGE) to observe the new populations.

2.2.1 Enzyme cutting near a vertex

A long motor would require increased separation between adjacent anchorages to prevent over-stepping and would limit the track length (in terms of the number of anchorages/steps) possible on a single origami tile. Therefore, to keep the motor sequence short, the nicking site was located as close to the vertex of the motor.director.anchor as possible.

The nicking site must be a short distance from the top of the motor.director so that the cut component at the top can melt off quickly at the working temperature (37°C here). The restriction site must therefore be placed close to either the 5' end or the 3' end of the motor (Figure 2.6). As the nicking site is asymmetric within the restriction site (with 5 bp and 2 bp on either side), the restriction site's placement

has the consequence of having the bulk of the restriction site either close to the vertex of the 3-way junction, or within the motor toehold and hence constraining the toehold sequence.

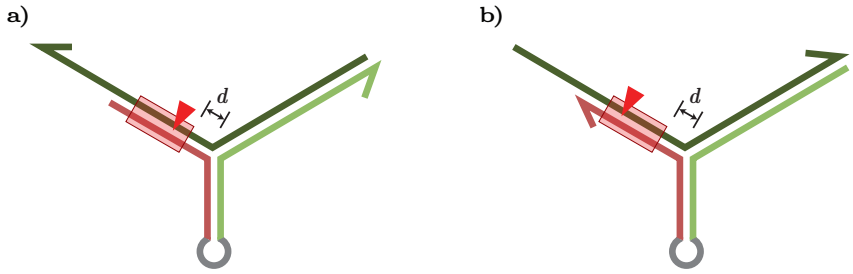


Figure 2.6: A schematic of the strands for testing how the possible placements of the restriction site affects the cutting efficiency of Nt.BbvCI. A hairpin represents the **motor** and **anchor**, which is bound to a **half director**, a simplified director strand with no loop or self-interaction at the ends. The restriction site is depicted by a red box, and the nicking site by the red arrow. a) The restriction site is at the 5' end of the motor. b) The restriction site is at the 3' end of the motor. d is the distance between the restriction site and the vertex.

The restriction site's distance to the vertex is limited by the amount of space the nicking enzyme needs. The cutting efficiency of Nt.BbvCI was tested when the 7 bp restriction site was 3, 4 and 5 bp from the vertex at the 3' end of the motor, and 2, 3 and 4 bp away at the 5' end of the motor.

Simplified strands and complexes were used for this test, not the exact sequences subsequently tested. For each orientation of the restriction site, a single 'half director' (Dhf) was used, which does not have the extensions at the ends to form a loop. The motor and anchor were represented by a single hairpin (MA), the stem of which acts as the motor.anchor arm. Extensions from the MA hairpin bind to the half director to form a 3-way junction. Different MA hairpins are used to shift the position of the restriction site compared to the vertex for the same half director. This ensures that the local sequence around the restriction site stays the same, and that only the distance and effect of the vertex cause any difference in cutting efficiency.

Pre-annealed complexes of MA.Dhf were incubated with the enzyme for 1 hr at 37°C, and then compared using PAGE. The analysis from the gels is summarised in Table 2.4.

Placement of the restriction site on the motor	Distance between the vertex and restriction site /bp	Percentage cut
3' end	3	61%
	4	72%
	5	75%
5' end	2	47%
	3	78%
	4	88%

Table 2.1: Cutting efficiencies of Nt.BbvCI over 1 hr at 37°C of various locations of the restriction site. The percentage of the cut population was calculated as the band intensity of the cut population divided by the sum of the band intensities of the cut and uncut populations on polyacrylamide gels (Appendix A.1.3).

The enzyme was more efficient at cutting closer to the vertex when the restriction site was placed at the 5' end of the motor. For example, when the restriction site was 3 bp from the vertex, the percentage that was cut was 61% and 78% when placed at the 3' end and 5' end of the motor respectively.

The restriction site was chosen to be 4 bp away from the vertex at the 5' end of the motor. It is worth noting that this is the opposite placement to the 'burnt bridges' motor where the restriction site is at the 3' end.

2.2.2 Optimising the lengths

Assuming that the toeholds of all the strands are able to initiate strand displacement sufficiently quickly, optimising the lengths of all the sections of the strands increases performance by controlling and limiting the undesired interactions. Various strands were tested, with address toeholds of 8, 12 and 15 nt, director self-interactions/remover toeholds of 9 and 12 nt, and remover toehold cover-ups of 0, 2 and 3 nt (see Figures 2.2 and 2.3 for depictions of these sections). All the removers tested had a fully bound address sequence, such that none of it was in the hairpin loop (unlike the example in Figure 2.3 f).

All matching variants were tested for the potential undesired interaction between stoichiometric amounts of the complete directors and the removers during a 1 hr

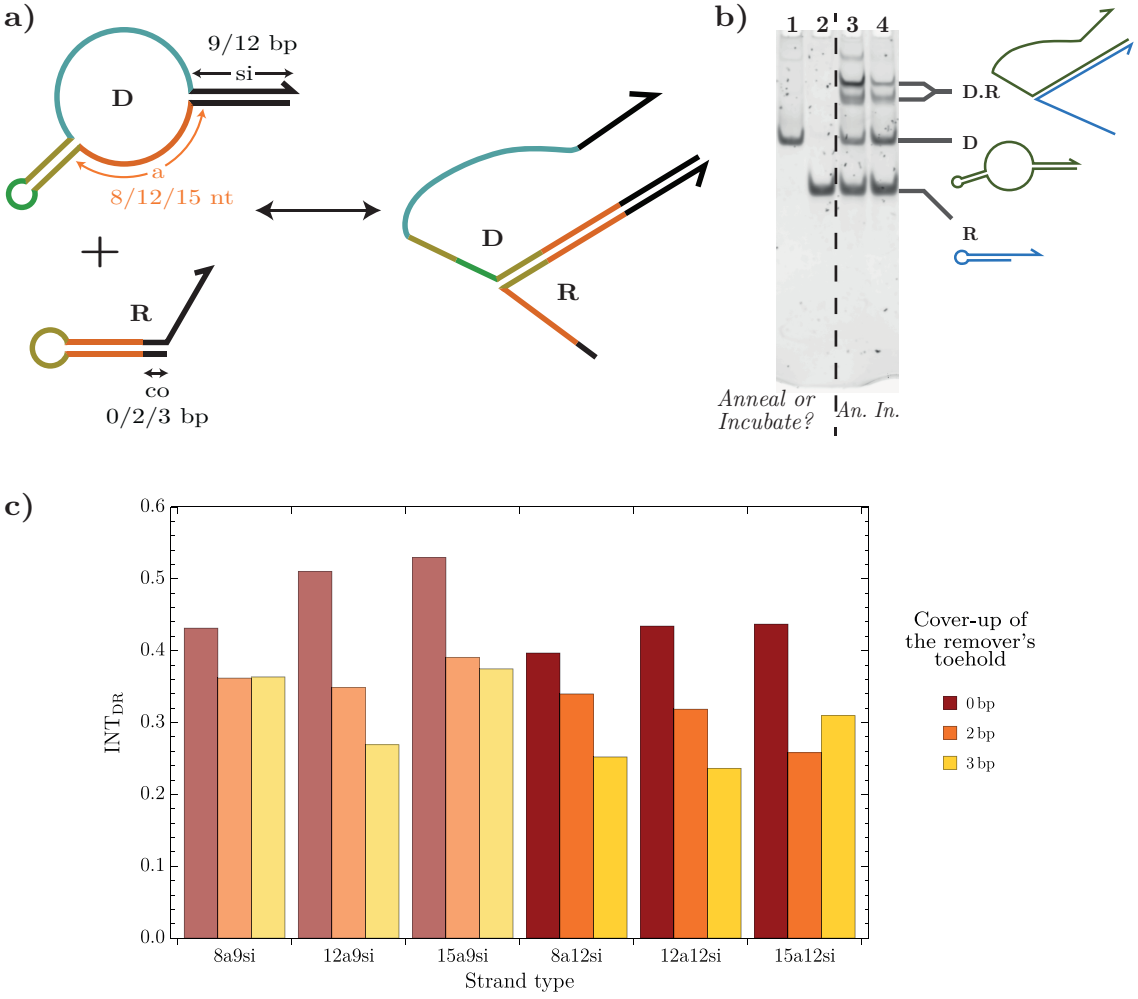


Figure 2.7: Various directors (D) and removers (R) were compared for the amount of interaction they have during a 1 hr incubation at 37°C. a) A depiction of D and R. b) Samples were run on polyacrylamide gels for analysis, an example of which is shown here for strands with a 12 nt address, a 12 bp self-interaction and a 2 bp cover-up. Lanes 1 and 2 — D and R alone respectively. Lanes 3 and 4 — a 100 nM mix of D and R annealed and incubated respectively. Multiple bands can be seen for the D.R duplex as there are different conformations that can form due to the repeated domains. c) The comparison metric, INT_{DR}, was calculated by normalising the D.R bands to the sum of the D.R and R bands. Strand types are named according to their address and self-interaction length, e.g. 8a12si has an address length of 8 nt and a self-interaction of 12 bp.

incubation at 37°C. All combinations were compared by PAGE analysis (an example of which can be seen in Figure 2.7b). A metric of the level of this interaction (INT_{DR}) was calculated by dividing the intensity for the director.remover bands by the sum of the director.remover and remover bands (to normalise against any differences between the gels or the amounts of sample run in the gel). A summary of INT_{DR} for each combination is shown in Figure 2.7.

The covering of the remover's toehold reduces INT_{DR}, as expected as more bases are lost by the director and remover binding together. The greater the cover-up, the lower the interaction. However, there will be a limit to its usefulness; if it is too long, it will not be energetically favourable for the remover to strip off the cut director from its anchor.

A self-interaction and remover toehold of 12 nt tends to have a lower INT_{DR} than that of 9 nt, though this trend is less obvious with a remover toehold cover-up of 2 bp. A larger self-interaction may keep the director closed more of the time, reducing the chances for an interaction. The various lengths for the address do not have an obvious effect on INT_{DR}. Consequently, strands with an address region of 12 nt, a self-interaction and remover toehold of 12 nt and a remover toehold with a cover-up were decided as the starting point for further testing.

2.2.3 The final sequences

As the remover has the complement to the director's address hidden in a hairpin stem, the remover also contains the complement to the anchor's address. Initial experiments suggested that a 12 nt address was sufficient for the remover to bind to the anchor once it had displaced the cut director (as previously depicted in Figure 2.4a). This would not be a useful interaction, as the anchor must be free for another director to bind once the cut director has been removed. Therefore, the remover was modified to hide only 8 nt of the complement to the director's address in its stem, so that it contained less of the complement to the anchor's address. The other 4 nt was placed in the hairpin loop. To ensure that it is still energetically unfavourable for the remover and director to interact in solution, a toehold cover-up

of 4 bp was required (depicted in Figure 2.4b). However, this binding between the anchor and cut director.remover has not been subsequently observed, and may have been due to the original gel being run at a sufficiently low temperature to allow an anchor.cut director.remover complex to form.

A consideration of all the key interactions for the final sequences as described in the preceding sections is shown in Figure 2.8a). These used directors with a 15 dT flexible region; however, this was subsequently increased to 21 dT before the experiments on origami were undertaken. This is not expected to change any of the interactions previously described, as the extra length should only increase the stability of the complete director to form its self-interaction when bound to the anchor. The extra length in the flexible region was added after some preliminary experiments suggested that the enzyme cut the director better when the flexible region was longer; on repetition of this test it was found not to make a significant difference. Enzyme cutting over 1 hr at 37°C of the motor.anchor.director, where the directors have a 21 dT section, is shown in Figure 2.8b).

2.3 Implementation on an origami tile

Simple tests were performed on different parts of the system. Fast movement was seen down a track bound with directors, with a similar rate to that of the 'burnt bridges' motor (Section 2.3.2)[1]. Slower movement was observed when tracks were made with reusable holding 'stations' at the ends of the track. Various designs for the stations were tested to ensure no significant diffusion of the motor away from the ends of the track (Section 2.3.3). The reversible track was then successfully tested for two reversals of the motor down an eight-anchorage straight track in the presence of removers (Section 2.3.5).

The quenching of fluorophores at the beginning and end of the track (F_0 and F_{end}) was used to report the presence of quencher-carrying motors during ensemble fluorescence measurements. The signals, therefore, come from multiple origami-tracks in solution. The fluorophores were attached to the ends of the staples adjoining

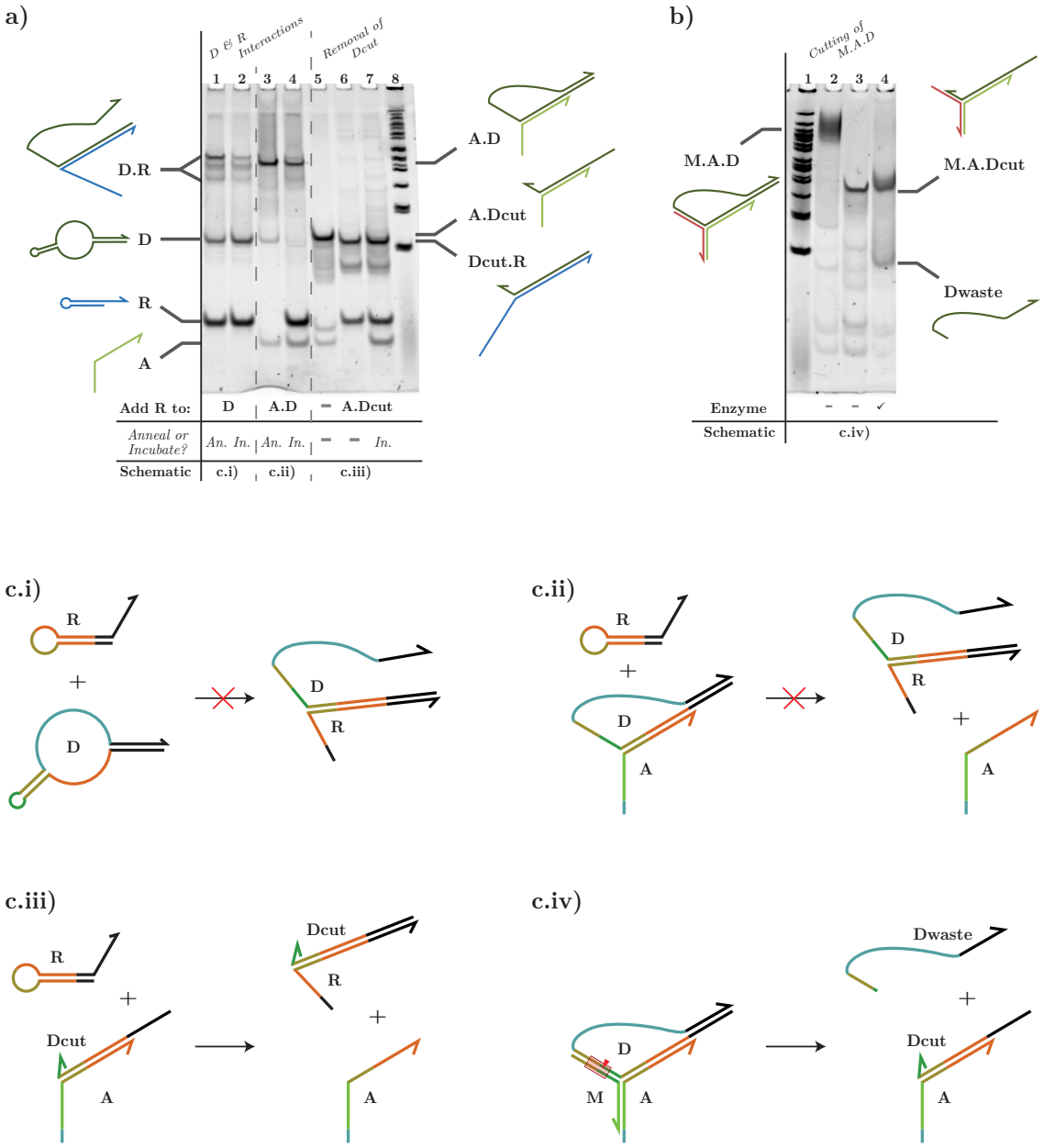


Figure 2.8: Polyacrylamide gels showing all the key interactions for strands with a 12 nt address (4 nt of which is in the remover hairpin loop), a 12 bp self-interaction, and a 4 bp toehold cover-up.
a) The interaction between **directors** (D) and **removers** (R) in solution: lanes 1-2 — R annealed and incubated with D respectively. The interaction between R and D when it is bound to an **anchor** (A): lane 3 — A.D, lane 4 — R incubated with A.D. The removal of a cut direction (Dcut) from A by R is also tested: lane 5 — A.Dcut, lane 6 — Dcut.R, lane 7 — R incubated with A.Dcut. Directors with a 15 dT flexi region were used here; lane 8 — NEB's 50 bp DNA ladder.
b) The director is cut by Nt.BbvCI when bound to the **motor** (M) and anchor: lane 1 — NEB's 50 bp DNA ladder; lane 2 — M.A.D, lane 3 — M.A.Dcut, lane 4 — the enzyme incubated with M.A.D for 1 hr at 37°C. Directors with a 21 dT flexi region were used here.
c) Schematics for the desired interactions tested: i) no interactions between the D and R in solution; ii) no interactions between A.D and R; iii) R displaces Dcut from A; iv) the enzyme cuts D on the M.A.D complex.

the first and last anchorages (for more details, see Appendix C.2). The fluorescence levels during motor movement are discussed and a calculation is made for an estimate of the percentage of motors initially bound to the track and the percentage of motors reaching the end of the track (Section 2.3.4). Finally, a number of controls are discussed to check for motor movement directly between the beginning and end of the track, and movement down a cut track (Section 2.3.6).

2.3.1 General assembly protocol

The origami tile was annealed at 54 nM in 1x Origami buffer (12.5mM MgOAc, 40mM (1x) Tris-acetate, pH 8.3) with a 5x excess of staples and anchors by heating the strands up to 95°C and cooling to 20°C over 90 mins. A straight track of eight anchorages running along the middle of the origami tile was used for all the experiments except for those in Section 2.3.2 which used a bent track of eight anchorages. This gives step sizes of roughly 6 nm.

The motor was pre-hybridised to the first anchorage by a 15 min annealing with a M:A_0:Dh_0 ratio of 0.9:1:3 with A_0 at 5 μ M in 1x Origami buffer. The motor was loaded onto the tile by adding M.A_0.Dh_0 to the origami in a A_0:tile ratio of 0.95:1, and incubated at 37°C for 2 hrs unless otherwise stated. The sample was then purified with size-exclusion resin to remove the excess strands, and diluted two-fold to be run in the fluorimeter. The experiments were run in one of two buffers: 1x Origami buffer + 50 mM NaCl (as in previous 'burnt bridges' experiments[1]) or 1x NEB's CutSmart buffer (to maximise the cutting efficiency of the nicking enzyme).

Various strands were added to the samples during the experiment, as noted on the graphs and in the text. To normalise the fluorescence levels an excess of motor (8x the amount of anchorages) was added at the end of the experiment to give the signal of the fully-quenched state. Further details can be found in Appendix B.

2.3.2 Walking down simple tracks

First the motor's movement was tested on a bent track of eight anchorages (Figure 2.9). The track started at the top middle of the origami tile, extending four anchorages into the middle (step sizes of roughly 5.8 nm) and then four anchorages in a line at a 62° angle (with step sizes of roughly 6.2 nm).

The interaction between the two ends of the director constrains the conformation of the vertex of the 3-way junction formed by the motor, director and anchor, which could slow down movement of the motor. Therefore, the movement down a track is compared for a simpler 'half director' (Dhf), which lacks the interaction between the two ends, and the full director with its self-interaction (Dsi).

The origami was annealed with all the anchors for the track except for the first anchor (A_0). As the motor was only sent down the track once, no holding directors at the ends of the track were necessary. Therefore, the motor was pre-annealed to the first anchor with the same type of director used for the rest of the track. This was loaded into the pre-formed origami over a 1 hr incubation at 37°C. The end anchorage required no director, and was able to bind fully to the motor except for a mismatch in the restriction site. This prevented enzyme cutting, to stop the motor at the end of the track.

These experiments were run in 1x Origami buffer and 50 mM NaCl, as in the original 'burnt bridges' motor experiments. The track was prepared by the addition of the directors (a stoichiometric amount compared to the anchors, calculated assuming full retention of origami after purification). The motor's movement was then initiated by the addition of the nicking enzyme, after which F_0 increased as motors moved away from the first anchorage and F_{end} decreased as motors arrived at the end anchorage. Finally excess motor was added to provide a baseline fluorescence level of the fully quenched state and to allow an estimate of how many motors reached the end of the track. The percentage of motors reaching the end of the track was 48% and 46% for the Dhf and Dsi track respectively (as calculated using Equation (2.5) of Wickham *et al.* 2012[102]).

Bath et al. 2005[1] thought that the nicking enzyme releasing the product was

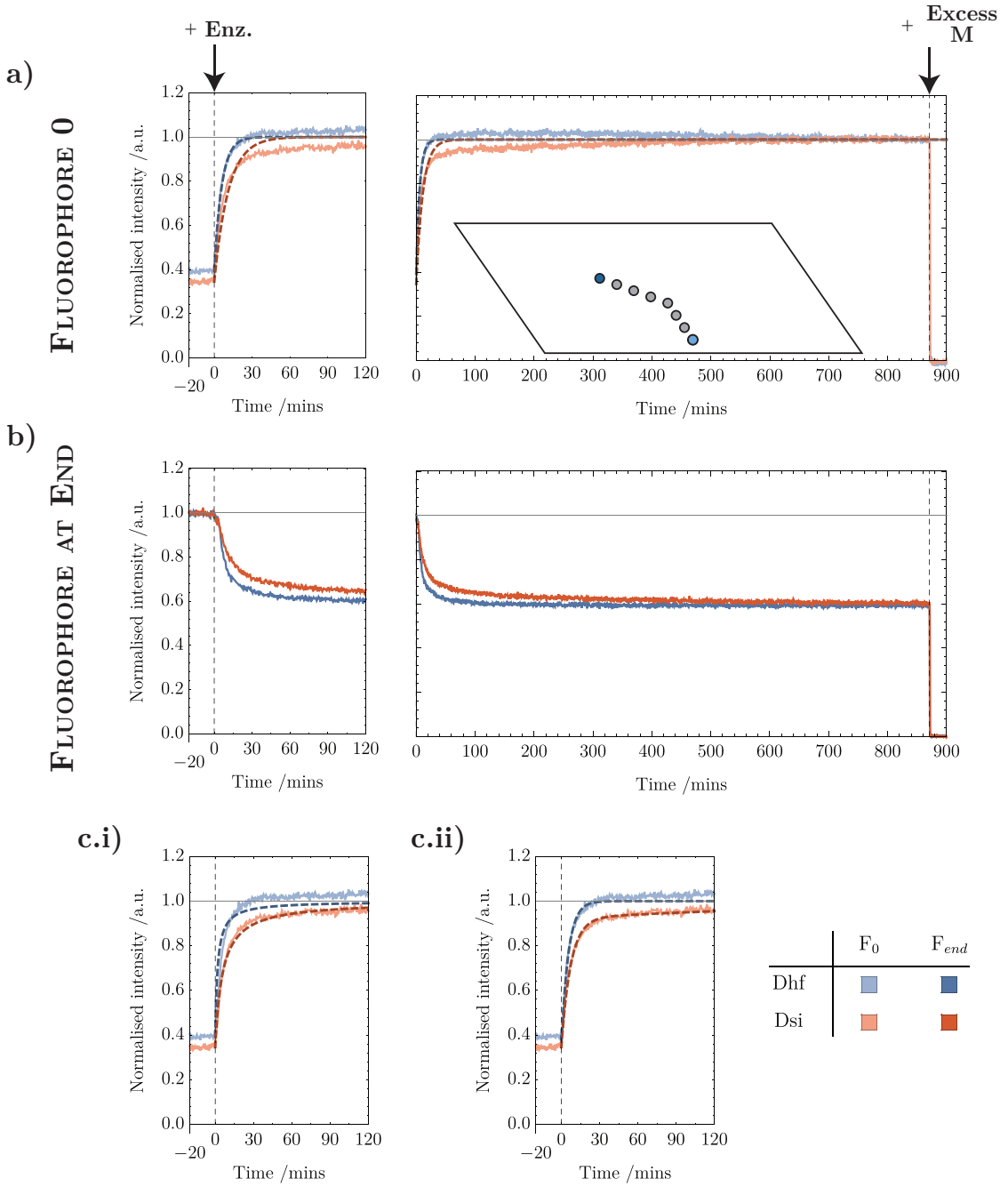


Figure 2.9: Fluorescence traces of the fluorophore at a) the beginning of the track (F_0) and b) the end of a bent track (F_{end}) are compared for two versions of the director: a half director (Dhf) that would require external renewal of the track, and a full director (Dsi) that is required for an autonomously renewing track. The motor was initiated by the addition of the nicking enzyme at $t = 0$ mins. The dotted lines show a fit to the F_0 data using a first-order model, as used in Bath *et al.* 2005[1]. c.i) and c.ii) show the initial F_0 data fit as a second order rate and as a system with two populations of track with their own first order rates respectively. Similar colours match the fit to the data. A depiction of the track on the origami tile is displayed in the inset of a). The circles depict the anchorages: light blue for the first anchorage, gray for mid-track anchorages and dark blue for the end anchorage.

the rate limiting step for the stepping of the 'burnt bridges' motor. As such, they fit a first-order rate equation to their data. Likewise, here, the leaving of the motor from A_0 was modelled using a first-order rate equation

$$\frac{dc_0(t)}{dt} = -k_1 c_0(t), \tag{2.1}$$

where c_0 is the fraction of A_0 bound to the motor, t is the time, and k is a first-order rate constant. The model fits to the Dhf track better than the Dsi track. The rate constants for the track of Dhf and Dsi are $k_1 = 0.003\,s^{-1}$ and $0.001\,s^{-1}$ respectively. These compare well with the rate $k_1 = 0.003\,s^{-1}$ of the 'burnt bridges' motor in Bath *et al.* 2005[1], and implies that the motor is not slowed down significantly by walking on a track of director-bound anchors.

As the F_0 signal for the Dsi track deviates from that of a first-order process, a second-order rate equation,

$$\frac{dc_0(t)}{dt} = -k_2 c_0^2(t), \tag{2.2}$$

where k_2 is the second-order rate constant, was also fit to the data (Figure 2.9c.i). Though this fits the Dsi data better than the first-order rate equation, it is not perfect.

Finally a model that assumed that there were two populations of tracks in the system, with different first-order rates (e.g. complete and partially-defective tracks) was fit to the F_0 data (Figure 2.9c.ii). This showed the best fit to the Dsi data, but as it has three free parameters (two rates and the relative ratios of the populations), this is not unexpected.

In general, this suggests that the Dsi track behaves slightly differently to the Dhf track, and perhaps no longer has the release of the enzyme as a rate limiting step, and/or has multiple populations. Despite the differences in the stepping process, the Dsi and Dhf tracks still show relatively similar speeds (i.e. the motor does not take an order of magnitude longer to reach the end of the track) and hence the slight increase in speed seen with Dhf is not significant enough to merit the sacrifice of the ability to regenerate the track autonomously. Therefore, the addition of full directors was considered for all future experiments.

2.3.3 The 'stations' at the ends of the track

In order to observe motors traversing reusable tracks multiple times using ensemble fluorescence measurements, it is necessary to wait a sufficient period of time for the majority of the motors to converge at the end of the track before the next release signal is given. Otherwise the de-coherence of the motors would lead to a reduced signal. Tracks using these 'stations' show much slower motor release than those for which there was no special end anchorages (as in the previous section). This means that the experiments often run for thousands of minutes, and therefore requires motors to be held stably at the stations, so that they do not diffuse back down the track. This is implemented by the use of holding directors (Dh) as previously described (Section 2.1.3).

Straight release strands

The diffusion of the motor from the beginning of the track was specifically investigated for the three station designs using two release strands with no designed secondary structure (see Figure 2.5b-d) for the depictions of the designs, and Figure 2.10 for the results). A straight track of eight anchorages running down the seam of the tile from the top was used. The pre-annealed $M.A_0.Dh_0$ was loaded into the origami over 2 hrs, and the samples were run in 1x CutSmart buffer.

Once the directors and the holding director for the end of the track were added to the samples, they were kept at 37°C for over 1,000 mins to observe any diffusion of the motor down the complete track. The nicking enzyme was then added, followed by another wait of over 1,000 mins at 37°C to check the diffusion of the motor in the presence of the enzyme. After which the first release strand for the beginning of the track ($Rl1_0$) was added to actively initiate motor movement. Finally, excess motor was added to fully quench both fluorophores for normalisation purposes. Observation over such long time-scales is necessary as the diffusion is not always obvious over shorter time-scales.

Station design 1 has 9 extra base pairs between the motor and the holding director to reduce diffusion. There is no mismatch in the restriction site, so the

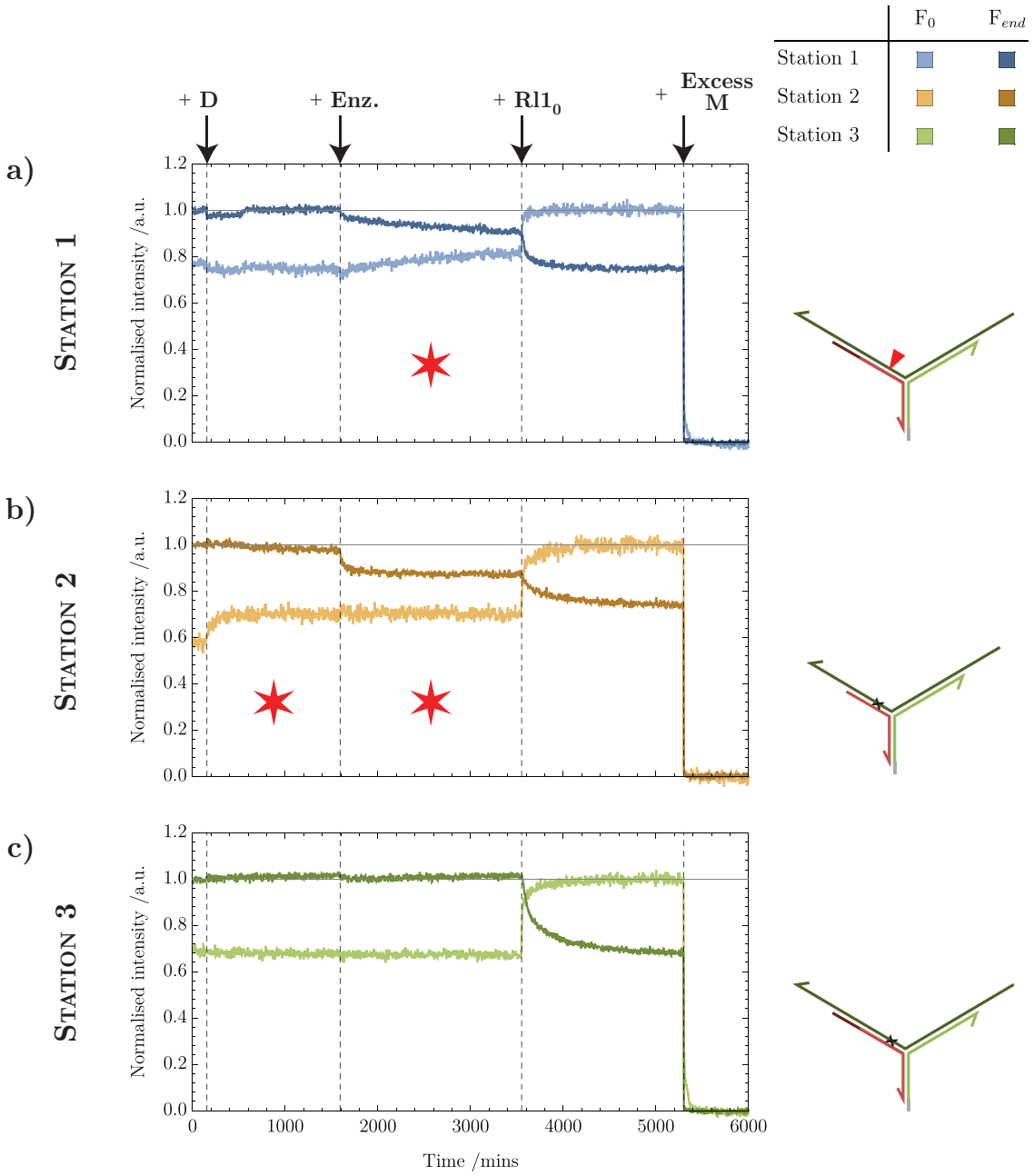


Figure 2.10: Diffusion of the motor (M) away from three possible holding directors (Dh) for the ends of the track. The three station designs here use two release strands with no designed secondary structure, as detailed in Section 2.1.3 and depicted alongside their respective data. Only the first release strand ($Rl1_0$) is used here to initiate motor movement. a-c) Ensemble fluorescence measurements for each design, with the additions of the enzyme and $Rl1_0$ made after over 1,000 mins to check the diffusion of the motors away from the stations and down the track. Significant diffusion is highlighted by a ✶. a) Station design 1: Dh and M form 9 extra base pairs. b) Station design 2: a mismatch in the restriction site of Dh stops the enzyme from cutting it. c) Station design 3: Dh and M form 9 extra base pairs and have a mismatch in the restriction site.

enzyme is able to cut the holding director. The cut portion covering the top of the motor is inhibited from melting away (as in normal stepping) due to the extra base pairs increasing the cut section's melting temperature. No obvious diffusion was observed after the addition of the directors to complete the track. Some diffusion was seen after the addition of the enzyme. It is possible that the small cut portion of the director nearest the vertex may partially melt from the motor, freeing some bases that may act as a toehold to initiate stepping.

Station design 2 does not have any extra base pairs between the motor and holding director, and relies upon a mismatch in the restriction site to stop the enzyme cutting and releasing the motor's toehold. Diffusion away from the starting anchorage was observed after the addition of the directors. Addition of the enzyme did not change the signal of F_0 near the starting anchorage, but did show a quenching of F_{end} near the end anchorage, suggesting that motors were arriving at the end of the track. Motors that had managed to diffuse away from the starting anchorage onto the complete mid-track anchorages after the addition of directors must have then been actively driven along the track (in both directions) once the enzyme was added.

Station design 3 uses 9 extra base pairs between the motor and holding director and a mismatch on the director in the restriction site (a combination of both strategies used by Station designs 1 and 2). No obvious diffusion of the motor was observed after director or enzyme addition on these time-scales.

Hairpin release strand

Station design 4 uses a hairpin first release strand and makes sure of 4 extra base pairs and a mismatch in the restriction site to hold the motor (depicted in Section 2.1.3e). No specific diffusion test was run on this design, but a lack of significant diffusion over similar time-scales can be seen in Figure 2.16. This station design was used for all the following experiments.

2.3.4 Normalisation levels

The fluorescence signals for the fluorophores at the beginning and end of the track (F_0 and F_{end}) were normalised as in Wickham *et al.* 2012[102]. A signal of 1 denotes the absence of the motor (the unquenched state). The signal in the presence of an excess of motors (the fully quenched state) was set as a baseline to normalise each fluorophore. This section explores a couple of controls to determine the proper baseline for a fully quenched stated. First, the loading of the motor.first anchorage into the origami is observed. Secondly, differences in the F_0 signal are investigated when the first anchorage is at some point single-stranded compared to always being double-stranded, implying that the loading of the first anchorage into the origami is imperfect. The importance of this on the baseline fluorescence levels is then considered. These experiments were performed on a straight track of eight anchorages down the middle of an origami tile.

Observing the loading of the motor

The loading of the motor pre-hybridised with the first anchorage was observed, to check the fluorescence signal for a 100% loaded sample in the absence of enzyme (Figure 2.11) (which may include misfolded origami that is unable to bind the first anchorage next to F_0). Origami was annealed, purified and diluted roughly two-fold to be put in the fluorimeter. This was tested for both buffers of interest: 1x Origami buffer and 1x CutSmart buffer. The pre-annealed complex of the motor, first anchor and holding director ($M.A_0.Dh_0$) was then added to the origami for loading. The normal protocol involved loading the motor by adding the complex with a (first anchorage):(origami tile) ratio of 0.95:1, incubating at 37°C for 1-2 hr and then purifying. In this case, the origami tile was purified before loading. The origami loss after purification is estimated to be 20% (Figure B.1), hence $M.A_0.Dh_0$ was added with an (A_0):(tile before purification) ratio of 0.8*0.95:1. This means that the relative amount of $M.A_0.Dh_0$ loaded would be similar to that in the normal protocol (though here the origami is roughly twice as dilute, and hence the loading rate is expected to be slower).

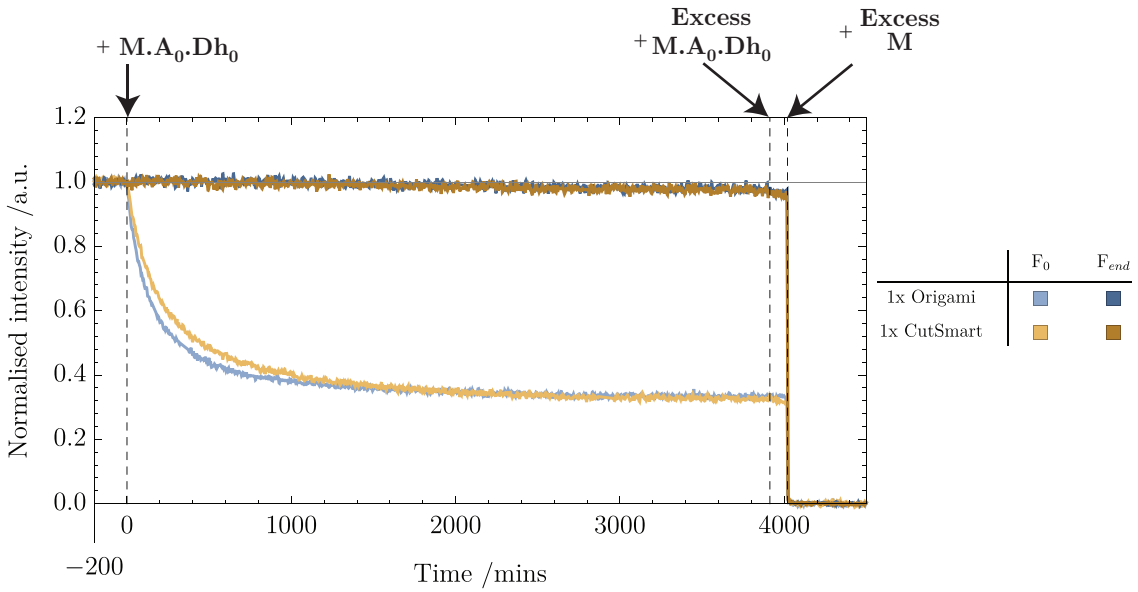


Figure 2.11: Origami missing the staple of the first anchorage was loaded with the pre-annealed motor.first anchor.holding director ($M.A_0.Dh_0$) at $t = 0$. Excess $M.A_0.Dh_0$ was later added to check for maximal loading. The samples were finally normalised by adding excess M to give a baseline fluorescence level. This was tested in two buffers: 1x Origami and 1x CutSmart buffer.

Once $M.A_0.Dh_0$ was added, a decrease in F_0 was seen, indicating that the quencher-carrying motor was loaded into place (Figure 2.11). It is interesting to note that the loading of the motor was faster in 1x Origami buffer than in 1x CutSmart buffer.

Once a plateau had been reached, suggesting that all of the motors had been loaded, an excess (3x the initial amount) of $M.A_0.Dh_0$ was added to check for maximal loading. This caused almost no effect on the fluorescence signal, implying that the origami was already 100% loaded (and suggesting that, in this case, less than 80% of the origami had been retained after purification).

The sample was then normalised by adding an excess of motor. As the $M.A_0.Dh_0$ was annealed in the ratio of $M:A_0:Dh_0 = 0.9:1:3$, the signal would be expected to further decrease as the excess M hybridises to the unbound A_0, such that the maximally-loaded plateau is normalised to 0.1. However, the plateau was seen at 0.33: more quenching is occurring than expected. This may be due to extra quenching from motors bound to the neighbouring anchorage, A_1, as quenchers are

expected to be able to affect a fluorophore over the distance between anchorages (roughly 6 nm). A similar effect is likely to also occur for F_{end}, by motors bound to the penultimate anchorage; the exact extent of this effect will be dependent on the distance to that anchorage and the exact fluorophore used.

Assuming no quenching from neighbouring anchorages, this signal would have suggested that 67% of origami was loaded with $M.A_0.Dh_0$, whereas it was actually 100% as $M.A_0.Dh_0$ was added in excess. All ensemble fluorescence measurements in this chapter used TET as the F_0 fluorophore and should be comparable to this maximally-loaded level.

F_0 dependency on the state of A_0

Additional quenching of the F_0 fluorescence was seen when adding the second release strand ($Rl2_0$) to remove the holding director and the first release strand ($Dh_0.Rl1_0$) from the beginning of the track leaving A_0 single-stranded (Figure 2.12). As $Dh_0.Rl1_0$ is unmodified and not bound very close to F_0 (16 nt up A_0 from the base of the origami), it should not significantly affect the fluorescence directly.

Two samples were compared with different orderings of the addition of $Rl2_0$ and excess M (to normalise the track), both run in 1x CutSmart buffer. Both samples were loaded with $M.A_0.Dh_0$. After the quenching of F_0 had plateaued, the track was prepared by adding directors, the holding director for the end of the track and the nicking enzyme. The first release strand ($Rl1_0$) was then added to initiate motor movement. The F_0 signal returned to a similar level to the one before the motor was loaded into the origami, suggesting that nearly all of the motors moved away from the beginning of the track successfully.

At this stage, the first anchorage should have just $Dh_0.Rl1_0$ bound to it (as depicted in the 3rd panel in Figure 2.5e). To normalise the data, excess M should be added to the sample; but to check that the bound $Dh_0.Rl1_0$ does not stop the excess M from binding to A_0 to quench F_0, $Rl2_0$ was added to displace it (as depicted in the 4th panel in Figure 2.5e). One sample was given a 3x excess of $Rl2_0$ and

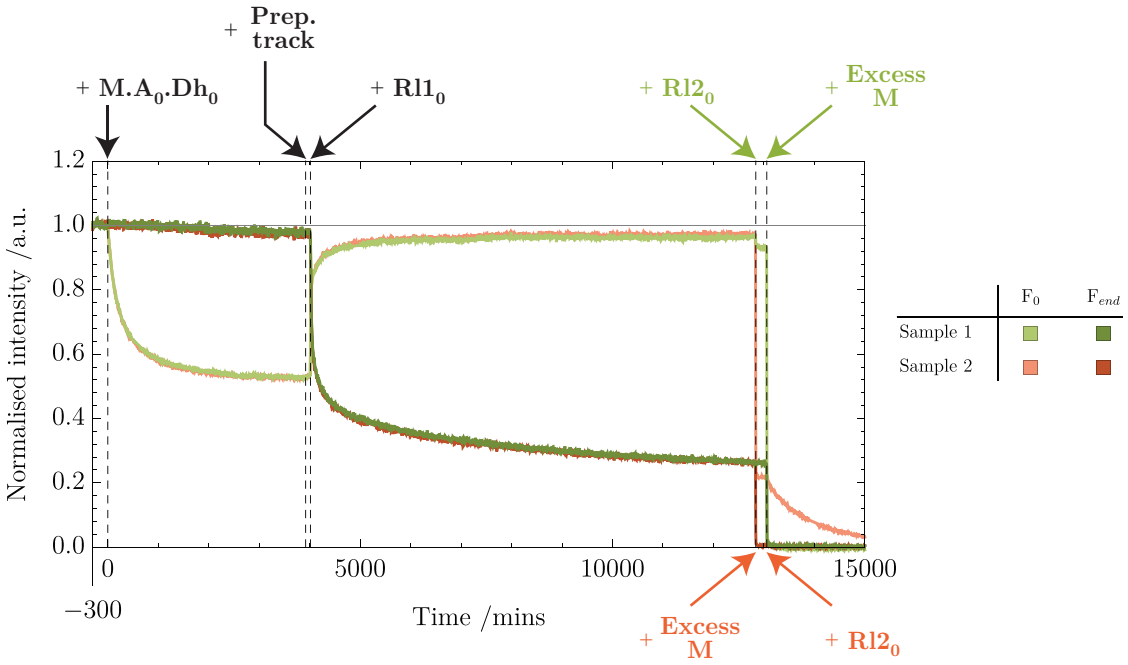


Figure 2.12: Additional quenching of F_0 is seen when adding $Rl2_0$ to displace $Dh_0.Rl1_0$ from A_0. This can be separated from the quenching when adding excess M by adding $Rl2_0$ afterwards (red trace) — a very slow quenching is seen that finally plateaus to the same level as when $Rl2_0$ is added before excess M (green trace).

approximately 3.5 hrs later excess M was added. The second sample had the reverse sequence of additions.

The first sample showed a small drop in the fluorescence of F_0 on addition of $Rl2_0$, followed by a significant drop to a constant level on addition of excess M. The second sample showed a drop in the fluorescence of F_0 on addition of excess M and then a very slow additional quenching of the fluorescence when $Rl2_0$ was added. When both samples were normalised with respect to their initial (unloaded) and final fluorescence levels, the traces match up very closely until the last two additions. This implies that whatever state the first sample is in quickly after the final additions is very slowly reached by the second sample with the reversed sequence of additions.

It is thought that this is due to the incomplete binding of the first anchor's staple sequence with the scaffold strand when loading the pre-annealed $M.A_0.Dh_0$ into the origami. This is supported by single-molecule observations using Förster Resonance

Energy Transfer (FRET) which suggest that the loading of a cargo-bound extended staple is not able to bind as fully with the scaffold strand as when the extension is single-stranded, i.e. without any cargo (Section 5.4.1).

Once $Rl2_0$ is added to the first sample, it will displace $Dh_0.Rl1_0$ from A_0, leaving it with a single-stranded extension. If the first anchor has loaded incompletely with the origami, the flexible ss-extension should then be able to wind through the origami to bind fully. The now nearby presence of a G base on the anchor strand would account for the small drop in fluorescence of F_0 here (due to proximal G base quenching[108]). The excess M is then able to bind to the fully incorporated A_0 and quenches F_0 maximally.

The second sample does not leave A_0 with a ss-extension, so when excess M is added, significant but not maximal quenching is seen as the motor (and hence the quencher) is not as close to F_0 as it could be. When $Rl2_0$ is subsequently added, this displaces $Dh_0.Rl1_0$ from A_0, leaving only M bound to it. It is hypothesised that the excess M in solution enables A_0 to fully bind with the scaffold strand — hence the very slow additional quenching.

Partial melting of the bottom of M from A_0 could allow A_0 to thread a small section through the origami to hybridise completely to the scaffold. Excess M in solution would then be able to bind to this section and displace the other M from A_0. This would allow the extension of A_0 to pass through the origami and for its staple to finally bind completely. This process of competition between motors strands would be slow, explaining the slow additional quenching seen.

The additional quenching accounts for 21% of the normalised signal here. For a single traverse of the track, a normalised signal should be compared to the quenched F_0 signal without $Rl2_0$ addition, so that the state of A_0 remains unchanged. However, it is more complicated for multiple traverses of the track, as $Rl2_0$ must be added to allow the motor to return to the beginning of the track. Once $Rl2_0$ is added, A_0 can readjust, such that when M returns to A_0 it quenches it more than it had originally. Any additional traverses would be comparable as no further change to A_0 would occur.

An alternative station mechanism, briefly mentioned in Section 2.1.3, where $Rl2_0$ displaces $Rl1_0$ instead of Dh_0, would not have had this issue as the extension to A_0 would always remain partially double-stranded. This alternative may have allowed the fluorescence signals for multiple traverses to be better compared.

The raw signal from F_{end} had the same level of quenching after excess M when as a ss-extension (as in Figure 2.11) or when bound to a holding director (as in Figure 2.12). This is expected if the additional quenching of F_0 is occurring due to the loading of the motor at the beginning of the track, whereas A_{end} should be completely bound with the scaffold strand as it was included in the origami anneal.

Calculations: percentage initially bound

When pre-loading the origami with $M.A_0.Dh_0$ before purification, it is not known how many of the tiles were successfully loaded with a motor during the loading incubation. An estimate of the percentage of motors successfully loaded can be made from the initial quenched state of F_0. For this, the fluorescence must be normalised between the unquenched (unbound) state and the level after the addition of excess motor. The estimate must account for any proximal quenching from motors bound to mid-track anchors (A_m) and the additional quenching seen on adding $Rl2_0$, as previously described.

Figure 2.12 shows that the fluorescence returns to a similar level as that of the pre-loaded state once motor movement is initiated, implying that almost all of the motors successfully leave A_0. This level reflects the 100% unbound state and is normalised to 1.

The expected upper-bound for the percentage of motors initially bound at the beginning of the track ($P_0(0)$) is 86%, as the motor was added annealed to the first anchorage in the ratio $M:A_0 = 0.9:1$, where A_0:origami = 0.95:1.

If a single traverse of the track is made, and $Rl2_0$ is not added, $P_0(0)$ can be calculated as in Equation (2.3) and depicted in Figure 2.13a).

$$P_0(0) = \frac{1 - f_{Initial}}{1 - f_{MaxLoad}} \tag{2.3}$$

If $Rl2_0$ has been added, allowing the single-stranded A_0 to readjust and bind fully with the scaffold strand (such as for multiple traverses), $P_0(0)$ can be calculated as in Equation (2.4) and depicted in Figure 2.13b).

$$P_0(0) = \frac{1 - f_{Initial}}{(1 - f_{MaxLoad})(1 - f_{Rl2effect})} \tag{2.4}$$

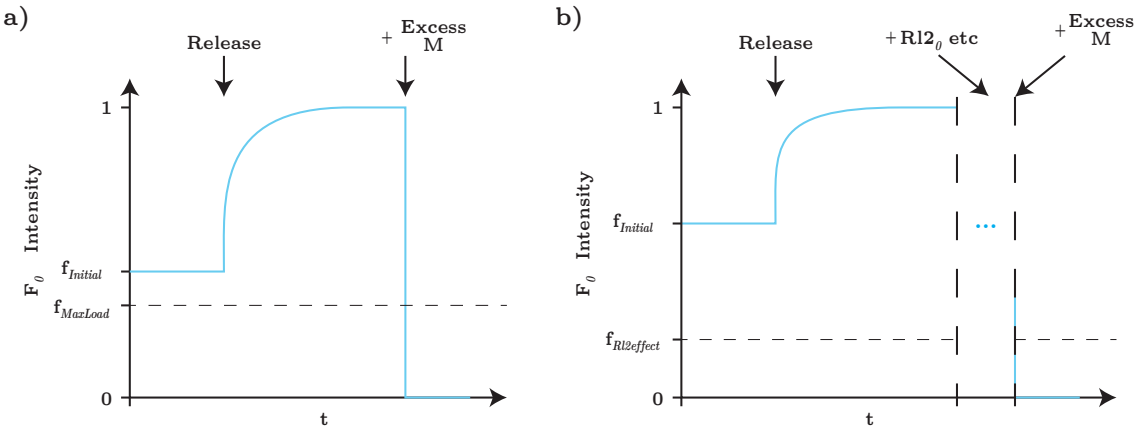


Figure 2.13: Schematics of F_0 traces for a) a single traverse and b) multiple traverses of a track. The effects of proximal quenching and the additional quenching when $Rl2_0$ is added must be taken into account when calculating the percentage of motors initially bound to the track. The plateau reached after motor movement is thought to give a good representation of the pre-loaded state (as in Figure 2.12) and is normalised to 1. The level after excess M is added provides the baseline.

The preceding results provide values of $f_{MaxLoad} = 0.33$ and $f_{Rl2effect} = 0.21$ for this set-up, where F_0 is a TET fluorophore. $f_{Initial}$ is the starting normalised fluorescence of F_0.

Calculations: percentage reaching the end

Wickham *et al.* 2012[102] used Equation (2.5) to calculate the percentage of motors reaching the end of the track ($P_{end}(Final)$). They used the upper-bound of 85.5% for $P_0(0)$, giving a lower-bound for $P_{end}(Final)$. Alternatively, the calculation could be made with the estimated percentage of motors initially bound, as per Equation (2.6). A schematic of a F_{end} trace is provided in Figure 2.14. If suitable controls have been made (as in this Chapter) to accurately determine $P_0(0)$, then Equation (2.6) should provide a better estimate for $P_{end}(Final)$ than Equation (2.5).

However, F_{end} is likely to also be affected by proximal quenching of motors bound to A_m when adding excess motor. The percentage found using Equation (2.5) or Equation (2.6) should provide a lower-bound estimate.

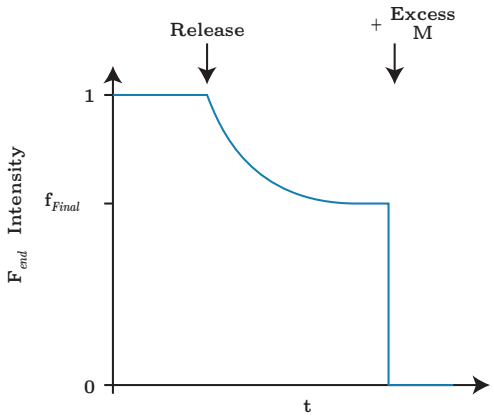


Figure 2.14: Schematic of a F_{end} trace for a single traverse of a track.

$$P_{end}(Final) = \frac{1 - f_{Final}}{0.855} \tag{2.5}$$

$$P_{end}(Final) = \frac{1 - f_{Final}}{P_0(0)} \tag{2.6}$$

f_{Final} is the normalised fluorescence level of F_{end} once motor movement has plateaued, before excess M is added.

2.3.5 Reversing

The motor was sent along an eight-anchorage, straight track and reversed successfully. This is shown here for three traverses of the track (i.e. two reverses) with the removers in solution so that track replenishment could occur autonomously. This is compared with two traverses of the track with the removers externally-added for track repair after a single traverse, to check for any unwanted effects from remover-director interactions.

As mentioned in the preceding section, though changes in the fluorescence levels indicate motor movement, the exact levels change depending upon the state of the

local system. The impact of this on the ability to estimate the percentage of motors moving down the track is discussed.

All the samples in this section were run in 1x CutSmart buffer.

Traverses with removers included

The motor was sent along a track of eight anchorages three times. This shows controlled movement over 21 steps of 6 nm each, equating to a movement across 126 nm, including two reversals from the ends of the track. This was done in the presence of the removers, which had been carefully designed to have minimal interaction with the directors before they are cut (as previously described in Section 2.2). All of the additions to the sample are listed in Table 2.2 and highlighted alongside the fluorescence traces in Figure 2.15.

Reason	**Addition**	**3x excess to**
Prepare the track	**D** **Dh**$_{end}$ **R** Enzyme	A$_m$ A$_{end}$ A$_m$ -
1st release	**Rl1**$_0$	A$_0$
Remove cut anchorages	**Rl2**$_0$	A$_{end}$
Replenish cut anchorages	**Dh**$_0$	Rl2$_0$
2nd release	**Rl1**$_{end}$	Dh$_{end}$
Extra D	**D**	A$_m$
Remove cut anchorages	**Rl2**$_{end}$ **R**	Dh$_{end}$ A$_m$
Replenish cut anchorages	**Dh**$_{end}$	Rl2$_{end}$
3rd release	**Rl1**$_0$	Dh$_0$
Normalisation	**M**	10x A$_m$

Table 2.2: The additions made for the motor movement down three traverses of the track. The corresponding fluorescence traces are shown in Figure 2.15. Abbreviations for the strands are used as follows: M = motor, A = anchor, D = director, Dh = holding director, R = remover, Rl1 = first release strand, Rl2 = second release strand. Subscripts refer to the location on the track, where "0", "*m*" and "*end*" refer to the start, middle and end of the track, e.g. A$_0$ is the first anchor.

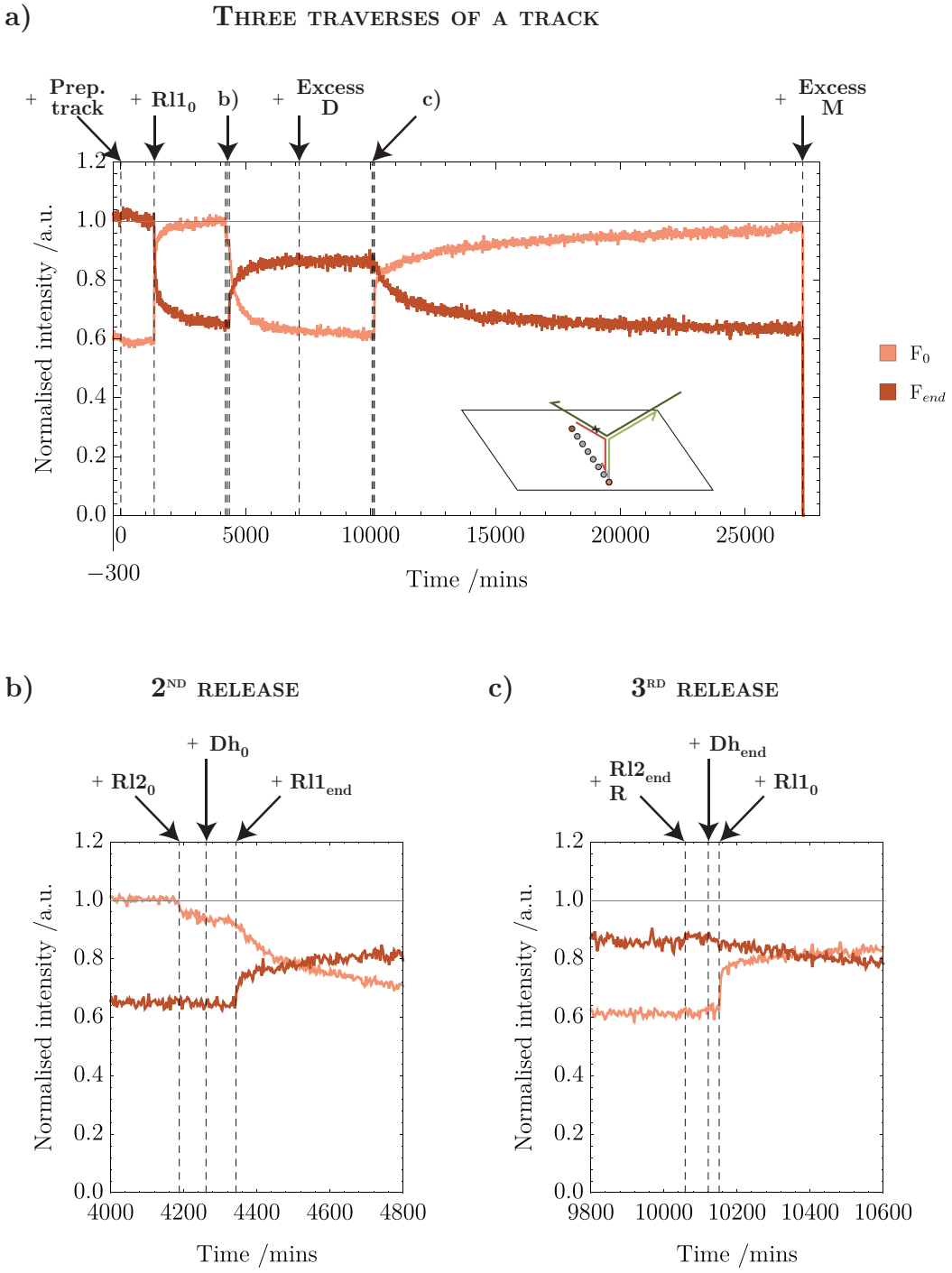


Figure 2.15: a) Fluorescence traces of fluorophores at the beginning and end of a track (F_0 and F_{end}) as a motor (M) was directed along a reusable track three times. M was held at the ends of the track by stations of design strategy 4. Movement away from the ends of the track was initiated by the first release strand (Rl1). As removers were included in the preparation for the track, the track was otherwise able to repair itself continuously. Additions to the sample are listed in Table 2.2. Zoomed-in views are provided for b) the second release (from A_{end}) and c) the third release (from A_0). The fluorescence was normalised to the 100% unbound state and the fully quenched state after excess M was added.

The origami was pre-loaded with $M.A_0.Dh_0$ (with 77% of tiles initially bound with a motor, as calculated by Equation (2.4)). The track was initially prepared by adding the directors for the mid-track anchorages (D), the holding director for the end anchorage (Dh_{end}), the removers (R) and the enzyme. Motor movement was initiated by the first release strand for the beginning of the track ($Rl1_0$). As expected, the signal of F_0 increased, indicating that the motors (and their quenchers) moved away. Correspondingly the signal from F_{end} decreased, indicating motor arrival at the end of the track. According to Equation (2.6), 47% of the motors reached the end of the track (a lower-bound estimate).

Once the F_{end} signal was no longer reducing significantly, it was assumed that the majority of the motors had reached the end of the track, and the second traverse of the track could occur. The second release strand for the beginning of the track ($Rl2_0$) was added to displace $Dh_0.Rl1_0$ from A_0 (as depicted in the 4th panel of Figure 2.5e). After roughly 70 mins, new Dh_0 were added to replenish the first anchorage. The motor was then released from A_{end} by the addition of $Rl1_{end}$. This caused an increase in F_{end} and a reduction in F_0 as the motor moved back down the track. The increase in F_{end} is initially quick, and then slower. This may be due to some of the track not yet being replenished with new directors. Motors that are able to step onto a complete next anchorage would step quickly, whilst motors that can't would have delayed stepping across the gap to the next complete anchorage.

The fluorescence signal for F_{end} did not return to its starting value, suggesting that not all of the motors were released from the end of the track. In case this was because of insufficient directors in solution to replenish the track (due to undesired interactions with the removers), extra directors were added. No change to the signal was seen, implying that a lack of directors was not the problem.

The unquenching of F_{end} only returned roughly 60% of the initial signal, suggesting that 40% of the motors remained at A_{end}. This is supported by the fact that, when rescaling the F_0 signal to compensate for the additional quenching after $Rl2_0$ has been added, the quenching of F_0 returns roughly 70% of its initial signal.

The third traverse of the track was made in a similar manner. The second release strand for the end of the track ($Rl2_{end}$) was added with extra removers. New Dh_{end}

were then provided to replenish A_{end}. Finally the motor was released from A_0 by $Rl1_0$. Once again the unquenching of F_0 and the quenching of F_{end} was seen. This movement was much slower than the initial movement for the first traverse of the track, but as no extra enzyme had been added, it should not be surprising that the enzyme's rate of cutting would be reduced after 8 days at 37°C.

The fluorescence levels returned to similar values as after the first release. They should be comparable as F_0 is in the unquenched state and the additional quenching after adding $Rl2_0$ only affects quenched F_0.

Traverses with externally-added removers

Including the removers in the solution whilst the motor is moving down a track has the potential to go wrong in two ways: firstly they may interact with directors (whether in solution or bound to anchors), which would use up the directors and stop them from being available for track replenishment; secondly they may remove the cut directors from the track, and complete directors may replenish it so fast that the motor is no longer directed down a track due to the cut anchorages behind it, but instead just diffuses up and down. This effect was checked by only adding the removers at the stage that they are required, i.e. after the motor has already moved down the track once and the track needs to be replenished for a second traverse.

All of the additions to the sample are listed in Table 2.3 and highlighted alongside the fluorescence traces in Figure 2.16. Larger excesses were used than for the three traverses with the removers included, to overcompensate for any potential undesired interactions between the components.

The origami was pre-loaded with $M.A_0.Dh_0$ (with 87% of the tiles initially bound with motors, as calculated by Equation (2.4)). The track was initially prepared by adding the directors for the mid-track anchorages (D) and the holding director for the end anchorage (Dh_{end}). The nicking enzyme was added over 1,000 mins later, and showed no significant diffusion of the motor away from the beginning station down the complete track. Motor movement was then initiated by the first release strand for the beginning of the track ($Rl1_0$) over another 1,000 mins later. No

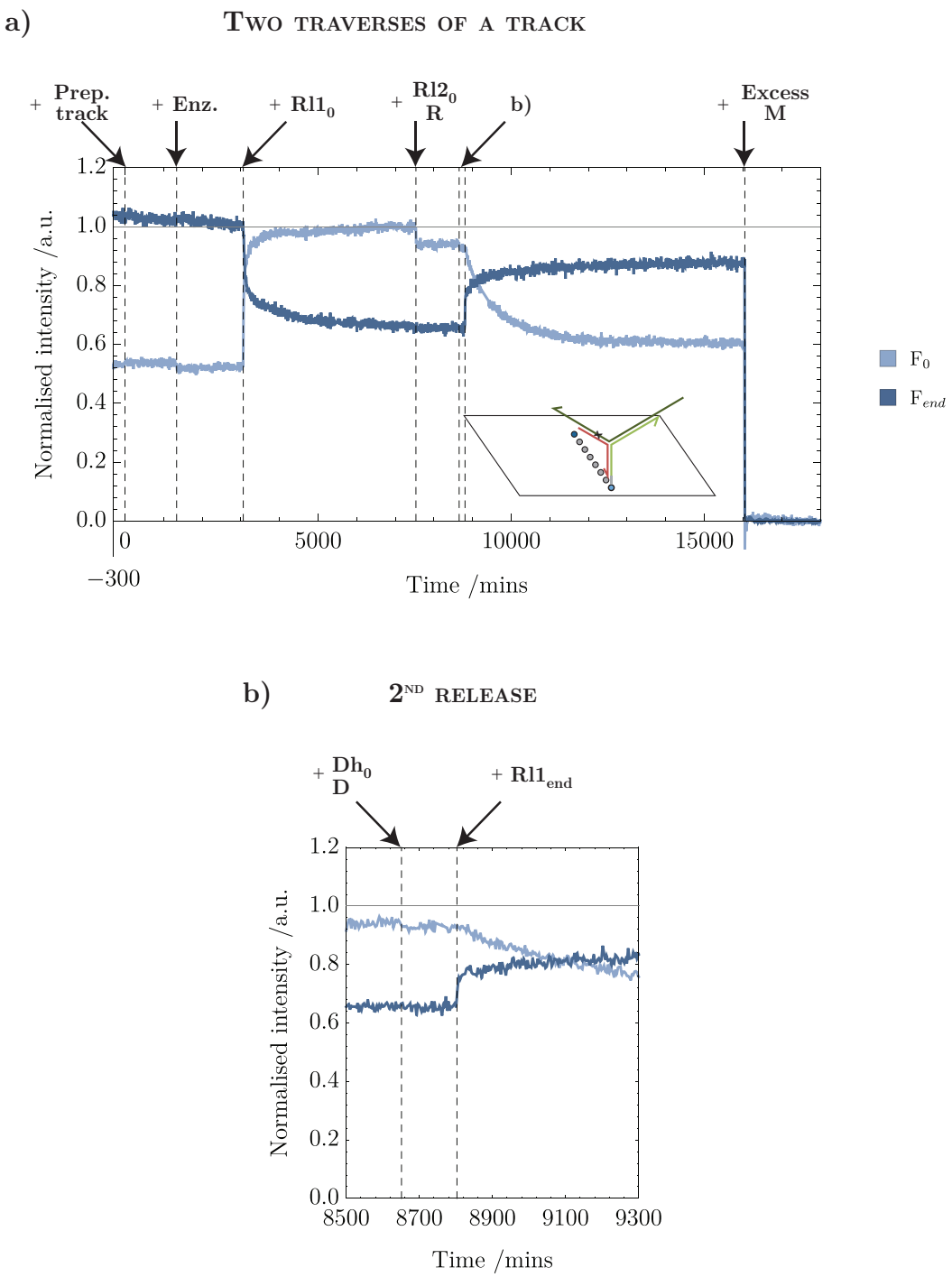


Figure 2.16: a) Fluorescence traces of fluorophores at the beginning and end of a track (F_0 and F_{end}) as a motor (M) was directed along a reusable track twice with the removers (R) added just before the second traverse of the track. M was held at the ends of the track by stations of design strategy 4. Movement away from the ends of the track was initiated by the first release strand (Rl1). Additions to the sample are listed in Table 2.3. b) A zoomed-in view is provided for the second release (from A_{end}). The fluorescence was normalised to the 100% unbound state and the fully quenched state after excess M was added.

Reason	**Addition**	**Excess**
Prepare track	**D**	3x A_m
	Dh_{end}	3x A_{end}
Add enzyme	Enzyme	-
1st release	**$Rl1_0$**	3x A_0
Remove cut anchorages	**$Rl2_0$**	3x A_{end}
	R	6x A_m
Replenish cut anchorages	**Dh_0**	3x $Rl2_0$
	D	12x A_m
2nd release	**$Rl1_{end}$**	3x Dh_{end}
Normalisation	**M**	10x A_m

Table 2.3: The additions made for the motor movement down two traverses of the track. The corresponding fluorescence traces are shown in Figure 2.16. Abbreviations for the strands are used as follows: M = motor, A = anchor, D = director, Dh = holding director, R = remover, Rl1 = first release strand, Rl2 = second release strand. Subscripts refer to the location on the track, where "0", "*m*" and "*end*" refer to the start, middle and end of the track, e.g. A_0 is the first anchor.

significant diffusion of the motor was seen once the enzyme was added over this period, indicating that these stations are able to hold the motor well in the presence of enzyme and a complete track.

As expected, on release, the signal from F_0 and F_{end} increased and decreased respectively, indicating that the motors moved away from the beginning of the track to the end. According to Equation (2.6), 39% of the motors reached the end of the track (a lower bound estimate).

To prepare for the second traverse of the track, the second release strand for the beginning of the track ($Rl2_0$) and the removers (R) were added to displace Dh_0 and the cut directors respectively. Dh_0 was subsequently added to replenish A_0, along with excess directors in case the removers had interacted with the directors already in solution. Having replenished the track, the second traverse of the track was initiated by the first release strand for the end of the track ($Rl1_{end}$).

Similar to the sample with the removers included initially, the F_0 and F_{end} signals did not return to their initial levels after compensating for the effects of the additional quenching after the addition of $Rl2_0$. The F_0 and F_{end} signals returned

by roughly 70% and 60% respectively.

Comparison

The samples with the removers included initially and externally-added were compared to check for any impact of the removers on the motor movement. A simple first-order model did not fit the data well, and so the rates are compared qualitatively by normalising the fluorescence to the initial and end levels for each release.

The leaving and arrival rates of the motor during its first traverse of the track were similar regardless of the presence or absence of removers (Figure 2.17a), implying that the removers were not adversely interacting with the directors bound to the anchors. However, a difference was seen during the second traverse of the track (Figure 2.17b). The leaving rate of the motor from A_{end} is similar in both cases, but the arrival of the motor back to A_0 is slower when the removers were not initially included. Other than the timing of the remover addition, the difference between these two systems is that the 'externally-added R' sample had 2.5x the excess of directors as the 'R included' sample. As the directors are in excess in both cases, and additional excess should not be able to slow the motor, the slower arrival rate of the motor is expected to be due to the timing of the remover addition.

This implies that the time it takes to replenish the track is not insignificant. When the removers are included from the start, the replenishment process is able to take place whilst waiting for signal of F_{end} to plateau. Whereas when the removers are added and the motor is released from the end (relatively) soon after, the track is still undergoing replenishment and hence the motor is delayed by defects down the track.

2.3.6 Controls

The following experiments were compared to check that the motor was really moving down the track, as opposed to jumping directly between the ends of the track. Four samples were compared: a full track, a cut track, and tiles with no mid-track

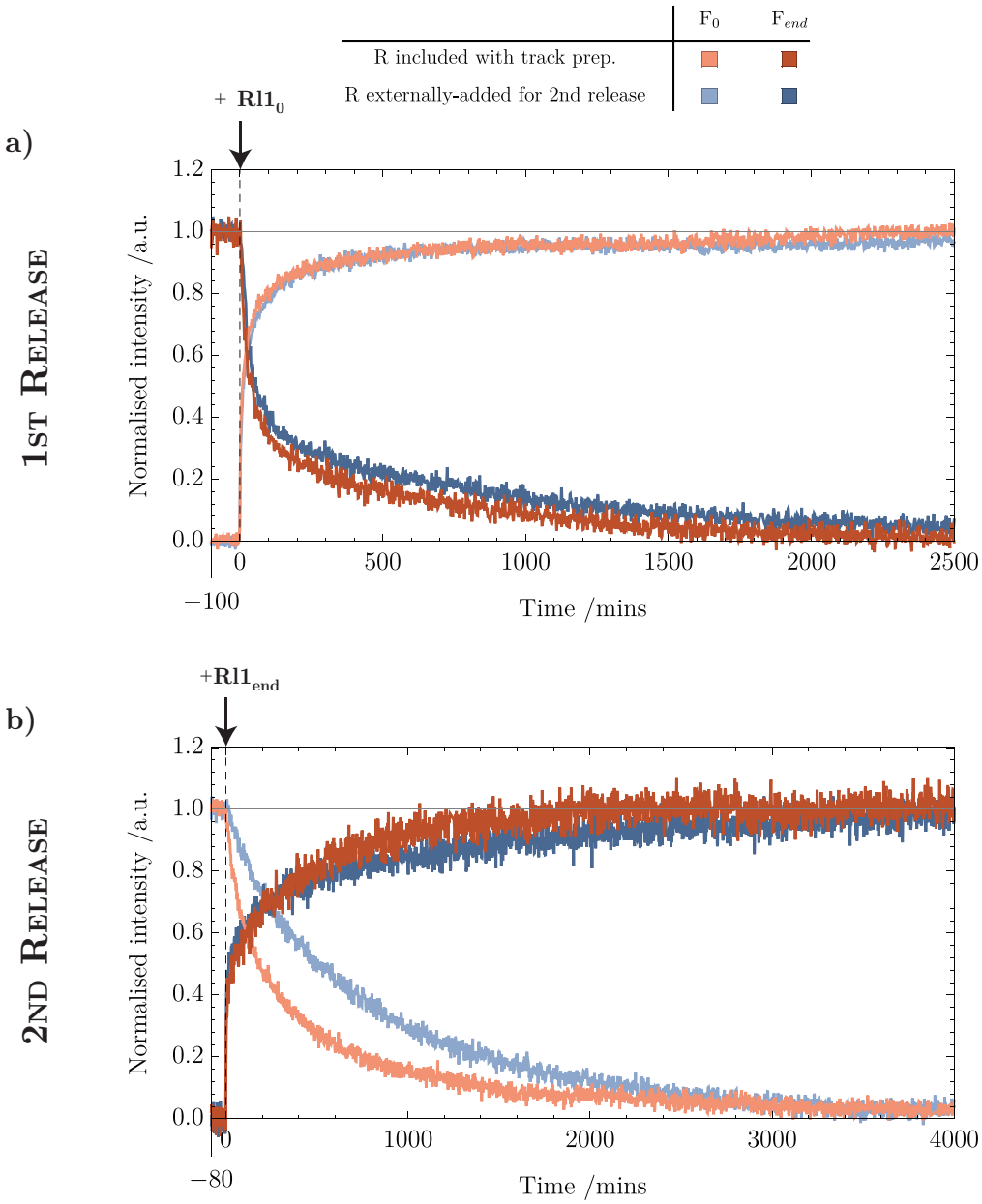


Figure 2.17: A comparison of the fluorescence traces for the fluorophores at the beginning and end of the track (F_0 and F_{end}) after a) the first release of the motor (from A_0 to A_{end}) and b) the second release of the motor (from A_{end} to A_0). The red traces are from the sample that included the removers with the track preparation (Figure 2.15). The blue traces are from the sample where the removers were added just prior to the second release (Figure 2.16). For comparison, the fluorescence was normalised to the initial and end fluorescence levels for each release, the time-scales were also shifted so that the release occurs at $t = 0$ mins.

but with A_0 and A_{end} either on the same tile or on separate tiles (as depicted in Figure 2.18c). The same straight track layout was used as throughout this section. The ends of the track were separated by roughly 42 nm, with six possible mid-track anchorages every 6 nm between them. The motor is 31 nt long, corresponding to a length of 10 nm if straight and double-stranded. Therefore, the motor should not be able to reach the other end of the track without first travelling down it, unless the origami tile is able to flex and bring the ends of the track within range.

The samples were pre-loaded with $M.A_0.Dh_0$ and run in 1x CutSmart buffer. The tracks were prepared by the additions of the relevant directors, cut directors, the holding director for the end of the track and the nicking enzyme as required. Motor movement was initiated by the addition of the first release strand for the beginning of the track ($Rl1_0$).

The motor's presence at A_0 or A_{end} is indicated by the quenching of the nearby fluorophore, F_0 or F_{end}. All track types showed movement of the motor away from A_0 (an unquenching in F_0) and arriving at A_{end} (a quenching of F_{end}) but with very different kinetics (Figure 2.18). The signals were normalised to account for different amounts of sample in each case: the initial fluorescence level prior to the addition of $Rl1_0$ is set to 1. The increase above this level indicates how many of the motors have left A_0.

As no simple model could be fit to the data to acquire rate constants, the half-times for the increase in F_0 are listed in Table 2.4 for comparison. The F_0 signals for all the track types seem to be plateauing to the same level. The increase in F_0 is fastest for the complete track and its F_0 level prior to excess motor being added (at $t = 5,800$ mins, where t is the time after $Rl1_0$ is added), which is relatively stable, is used as an estimate of the plateaued level. Therefore, the half-times were found as the time at which the increase in F_0 is half the plateaued increase in F_0 for the complete track. The F_0 levels at $t = 5,800$ mins for the different track types are also compared in Table 2.4.

When a full track was present, relatively fast motor movement was seen (with $t_{1/2} = 10$ mins). The other three control tracks were much slower (with $t_{1/2} > 410$ mins). As expected, the tiles with no mid-track and A_0 and A_{end} on separate

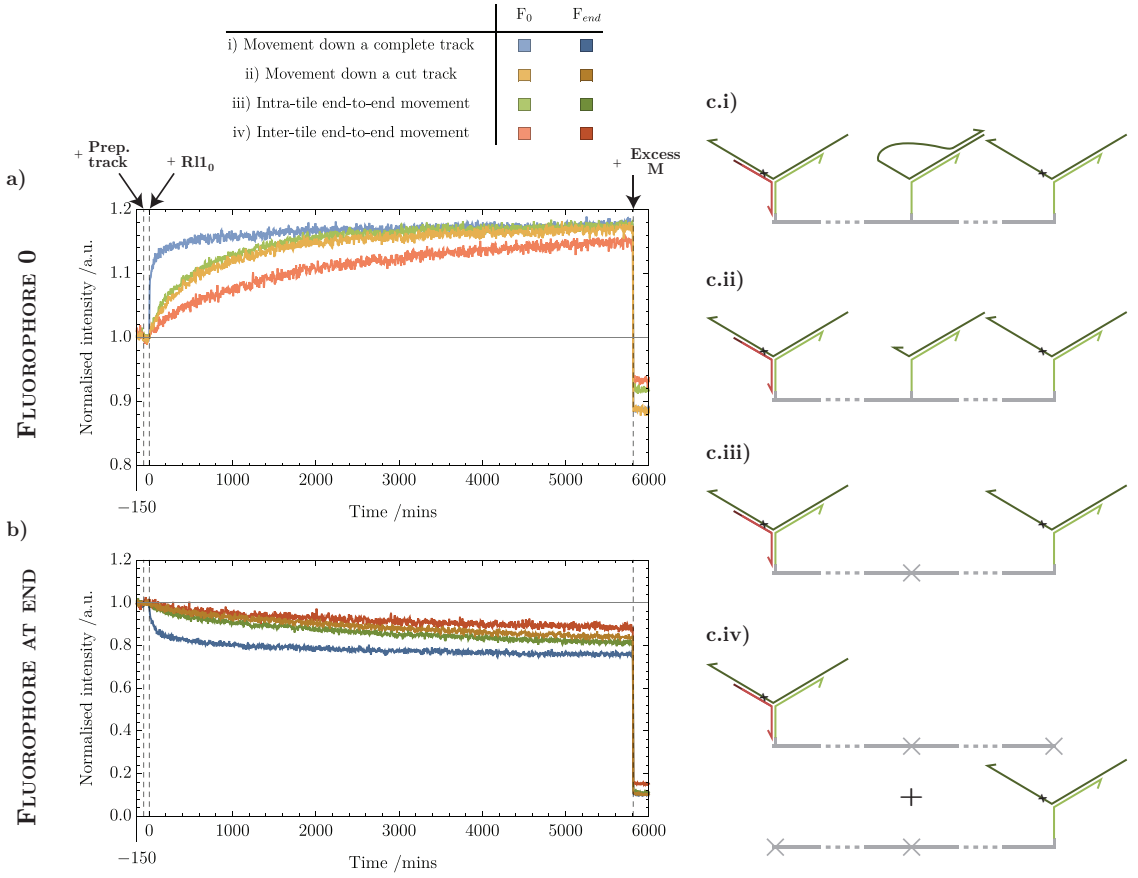


Figure 2.18: A comparison of the fluorescence traces for fluorophores at a) the beginning (F_0) and b) the end of the track (F_{end}) for four control tracks. The control tracks are compared for i) a complete track, ii) a cut track, iii) no mid-track with A_0 and A_{end} on the same tile, and iv) no mid-track with A_0 and A_{end} on the different tiles. The fluorescence is normalised with respect to the level just before the first release strand ($Rl1_0$) is added, and a recorded fluorescence intensity of 0 — this was to account for different amounts of sample in each case. c) Depictions of the tracks.

Track version	F_0 level at 5,800 mins, F_0(5800)	$t_{1/2}$ to F_0(5800) for track i) /mins
i)	1.177	10
ii)	1.170	490
iii)	1.175	410
iv)	1.150	1,330

Table 2.4: The normalised F_0 levels for each track type at $t = 5,800$ mins. The complete track (track i) seems to have mostly plateaued by this time, and the other tracks are tending towards it. The half-times were found by assuming that all the tracks are tending towards the F_0(5800) of track i).

tiles had the slowest unquenching of F_0, as all the other track types could allow this movement as well as on-tile movement.

This suggests that the motor is able to move between the two ends of the track, without the need for a track in-between. Given the motor is not long enough to reach the other end of the track, this must be enabled by flexing of the origami tile, bringing the other end within reach. These rates could be reduced by using a stiffer origami as a substrate for the track. Nevertheless, the significantly faster increase in F_0 (and decrease in F_{end}) for the complete track compared to the others confirms that travel along the track is much faster than alternative pathways.

2.4 Discussion & future work

This chapter has outlined a new design for a DNA motor and renewable track. A renewable track offers many possibilities, for example: reversing motors down a track; multiple motors can move down the same track; decisions made by a motor that is programmed to make a specific turn at a junction in a branched track could be "rewritten". A motor was shown to successfully reverse down a track of eight anchorages using ensemble fluorescence measurements.

The design makes use of a sacrificial 'director' strand that binds to an anchorage, providing the extra base pairs required for the motor to walk down the track. The

directors bind to anchorages through an 'address' sequence. This gives the system flexibility in setting up track layouts, even when not used as a renewable track. For example, an origami could be made with a "lawn" of bare anchors: all of the staples having a 3' extension. Each anchor could have its own address, allowing specific paths to be set up for the motors by adding the corresponding directors. Directors enable the anchors by turning them into anchorages, creating a track and "directing" the motor down them. After the motors have all arrived at 'stations' at the ends of the paths, new paths could then be provided by adding removers for the previous directors (to clear all the tracks so that some of the anchors could be reused) and adding appropriate directors to set up the new paths. Remover strands are used to strand displace a cut director from an anchorage for track replenishment.

Two desired properties of the system increased the design complexity: autonomous replenishment, and the stations at the beginning and end of the track to hold the motor.

Autonomous replenishment

For autonomous replenishment, directors and removers are included in excess in solution and must have limited interactions so that they do not bind together and get used up before track renewal. This requires the secondary structure of the strands to be carefully designed. Simpler directors (e.g. the 'half director') and removers could be used for a system where the track renewal is initiated externally. Though a reversal down such a track was not tested, a single traverse of a track was compared for the self-interacting directors (for autonomous renewal) and half directors. The motor moved faster down a track of half directors than complete directors, with a similar first-order reaction rate to the original 'burnt bridges' motor[1] ($k = 0.003\,\mathrm{s}^{-1}$).

The reversing experiments suggested that the process of replenishing the track is slow, as the movement away from an end anchorage for a second and third traverse of the track showed a fast and slow population. This is thought to be from motors that are able to step onto replenished anchorages (a fast process) and from motors

that either have to wait for anchorages to be replenished or for the origami to flex so that they can jump across a gap onto a replenished anchorage (a slow process). Comparing the reversal of motors in a system that contains the removers initially and another that received the removers after the first traverse of the track, the motors return to the beginning of the track faster when the removers were included initially, presumably due to the removers having had more time to replenish the track. This is good evidence that the motor is indeed using the track to move between the two ends of the track, and not just stepping there directly. It also suggests that the replenishment rate is slow and would benefit from optimisation.

Future work could investigate the wake of burnt anchorages behind the motor, and optimisation of its replenishment rate. The replenishment process has a number of steps, any of which could be rate-limiting and could be optimised by changing domain lengths or strengths: the melting apart of the two ends of a cut director (a 12 bp section for the strands used here); binding of the remover's toehold to the cut director (via a 8 nt toehold); strand displacement of the cut director from the anchorage (the hairpin remover may benefit from a mobile Holliday junction for this, see Appendix A.1.2); and finally a complete director binding to the anchor (via the 12 nt address toehold). The kinetics for each step could be investigated by adding a fluorophore and a quencher to one or two component strands to act as molecular beacons. For example, to test the removal of the cut director from an anchorage, the 3' end of the cut director and the 5' end of the anchor (the opposite ends from the toehold for the remover) could be labelled with a fluorophore and a quencher respectively. These would initially be close as the strands are bound together, giving a quenched signal. After the strand displacement by the remover, the cut director and anchor would separate and the fluorescence would increase. The rate of increase indicates the rate of the process. Coarse-grained simulations, such as oxDNA[109,110] (which treats DNA strands as strings of rigid nucleotides, taking into account hydrogen bonding, coaxial stacking, excluded volumes etc), that have shown promise at simulating strand displacement[54] may be able to guide further alterations to the system design.

The 'stations'

The stations that hold the motor at the beginning and end of the track were required to obtain coherent signals during ensemble fluorescence measurements. When stepping down an eight-anchorage track, the motors fall out of sync. Therefore, they must be held at the ends of the track to get a clear signal, before they are then restarted together for a reversal. Release of a motor from a station was achieved by the addition of the first release strand (a hairpin), which frees the motor's toehold through toehold-mediated strand displacement. However, as the holding director is not removed from the anchor or motor, the first release strand and motor remain in competition with each other. Release of the motor from the station at the beginning of the track was slower than for a track without stations (initiated by addition of the enzyme), with twice the half-time. A station design where the first release strand completely displaces the portion of the holding director that covers the motor's toehold showed faster stepping away of the motor; but as it also allowed a noticeable fraction of the motors to diffuse down the track, the slower, better-holding station design was used.

Insight into staple repair

The system also highlighted something interesting about the process of staple repair, used for loading the motor onto the origami at the beginning of the track. The motor is pre-annealed to the first anchor and its holding director in a sub-stoichiometric amount. This complex is then incubated at 37°C for 1-2 hr with the pre-formed origami missing the staple from which the first anchor extends.

At the end of the experiment, to normalise the fluorescence traces, excess motor is added to bind to all of the anchorages. This provides a baseline for the fully-quenched state. A difference was seen in the fluorescence levels depending upon whether the second release strand (which displaces the holding director from the anchorage, leaving the anchor single-stranded) was added before or after the excess motor.

The results suggested that the process of staple repair does not allow the anchor to bind fully with the origami, but if it is left single-stranded it is able to bind (more) completely. This was seen as a larger decrease in the F_0 signal on adding excess motor when the first anchor had been single-stranded than if it had always been partially double-stranded, suggesting that the quencher-carrying motors are closer to F_0. This would be possible if the anchor's staple sequence had not been completely bound up to the start of the neighbouring staple that is modified with F_0; and once single-stranded, the anchor is able to wind its way through the origami to bind completely (minimising the free energy), and is closer to F_0. This is supported by results using single-molecule Förster Resonance Energy Transfer (FRET) in Section 5.4.

Future work

Future work would benefit from single-molecule experimental techniques. This would eradicate the need for the stations that not only complicate the design and require multiple external additions, but also slow down the motor. Another benefit would be that it would allow observation of the origami placed against a surface, which would prevent the issues due to tile flexibility and stepping between tiles (as revealed in the control experiments). For example, a labelled motor could be sent around a circular track, and high-speed AFM or super-resolution microscopy could be used to observe the same motor as it moves around the track multiple times. If cut anchorages could also be labelled (e.g., for fluorescence microscopy, the 3' end of the cut director could be labelled with a fluorophore, and the 5' end with a quencher; cut anchorages would then show a fluorescent signal), then direct observation of the wake behind the motor could also be made.

It is possible that the rotational movement of a motor around a circular track could be useful. The fuel for the process would come from the directors and removers. For example, origami tubes with circular tracks around them could be rolled along a motor-covered surface. Instead of the motors moving, the track would move, causing the tubes to roll. Alternatively, if the motor was attached to something (e.g. an end of a long ss-strand), it could wind it around a central pillar.

Chapter 3

Logic Gates with a "Lollipop Track"

DNA has not only been used to "program" structures, but has also been used for computation more akin to *in silico* programming. This chapter explores the design of a DNA motor system that is able to perform logic operations for basic computation. All the designs are based on the ability of a motor to block another motor. A number of design approaches are discussed before one design, nicknamed the "Lollipop Track", is investigated in more detail. It is finally implemented on a full track on an origami tile with limited success.

3.1 DNA computation

The field of DNA computation started in 1994 when Adleman[111] used DNA to solve a directed Hamiltonian path problem, a special case of the travelling salesman problem. Combinatorial problems such as these are well suited to DNA computation , where even a fraction of Avogadro's number of DNA provides large parallelism. Since then, DNA has been used for a variety of computational problems ranging

from calculating the square root of a 4-bit number[112], to playing tic-tac-toe[113], to controlling gene expression[114].

DNA computation has some disadvantages compared to conventional electronic computing. For example, it is much slower with reactions taking minutes to hours, compared to the nanosecond-scale of silicon processing. Outputs are not necessarily easily read by human-counterparts and may require additional analysis, such as PCR amplification (to first increase the amount of an output signal strand so it can be further analysed) or gel electrophoresis (to filter out different sized components)[111]. However, DNA is much more suitable for interfacing with biochemical systems, where fast computation is not a primary concern and outputs need not be read by an external observer if they can be transmitted to another part of the system. Biomedical applications for cellular level diagnosis or treatment are possible with DNA computation[23].

Many mechanisms for computation have been created using interactions between DNA and enzymes[102,115–117], whilst DNA strand displacement enables computation to be made solely with DNA[58,118,119]. Lakin *et al.*[120] have developed a formal computing language for DNA strand displacement, which is incorporated into Microsoft Visual DSD[121], a computational tool for designing and analysing displacement reactions.

Freely-floating strands rely on orthogonality between sequences to prevent unwanted interactions. This increases the propensity for error as more sequences are required in the system. Localising strands minimises crosstalk between different parts of the system so that similar or even identical sequences can be used at different stages of the computation[122]. Localised computation has other possible benefits, such as increasing the speed of processing. This is because reaction rates are dependent on concentration and, by tethering strands near to each other, the local concentration is significantly increased. DNA origami is an ideal substrate for tethering components as it allows for well-controlled placement at the nanoscale. DNA origami would also enable computation components to be delivered into cells for diagnostic or therapeutic purposes — a large amount of single strands may not all get successfully delivered and would be more prone to enzymatic digestion once

inside (see Chapter 6 for details of delivering DNA structures into cells).

Directable DNA motors are an example of localised computation on DNA origami. Wickham *et al.* 2012[102] directed the 'burnt bridges' motor at junctions on an origami tile, using fluorescence signals at the ends of the branched track to determine the output. Dannenberg *et al.* 2014[123] have recently analysed the potential for DNA motor circuits, and Boemo *et al.* 2015[124] have created software to automatically design DNA circuits based on interacting motors.

3.2 Logic gates

Luca Cardelli of Microsoft Research suggested the implementation of a number of logic gates using interacting DNA motors[124]. The notation for the logic gates is shown in Figure 3.1 (including the functionally complete NOR and NAND gates). Each gate relies on a motor being able to block another motor as it travels down its track.

For a given logic gate, some of the motors are necessary and must always be used (ancilla bits, labelled as '1'). Others are logical inputs for the gate, and their presence or absence down their track represents a logical proposition of 1 or 0 (these are labelled 'A' or 'B'). There are two ways to implement this: an input of 1 (or 0) can be set by the loading (or omission) of the input motor, or by the addition (or omission) of a release strand to initiate the movement of the motor.

The calculation of the gate output occurs when the motors move down the tracks and interfere (or not) with each other.

The subsequent output is the presence (output = 1) or absence (output = 0) of one of the motors at the end of its track. This can be reported in numerous fashions, such as by the strand displacement of a DNA or RNA strand (possibly bound to a cargo) or the initiation of another motor. In this chapter, the output was measured during ensemble fluorescence measurements by the quenching of a fluorophore at the end of the track in the presence of a quencher-carrying motor. It

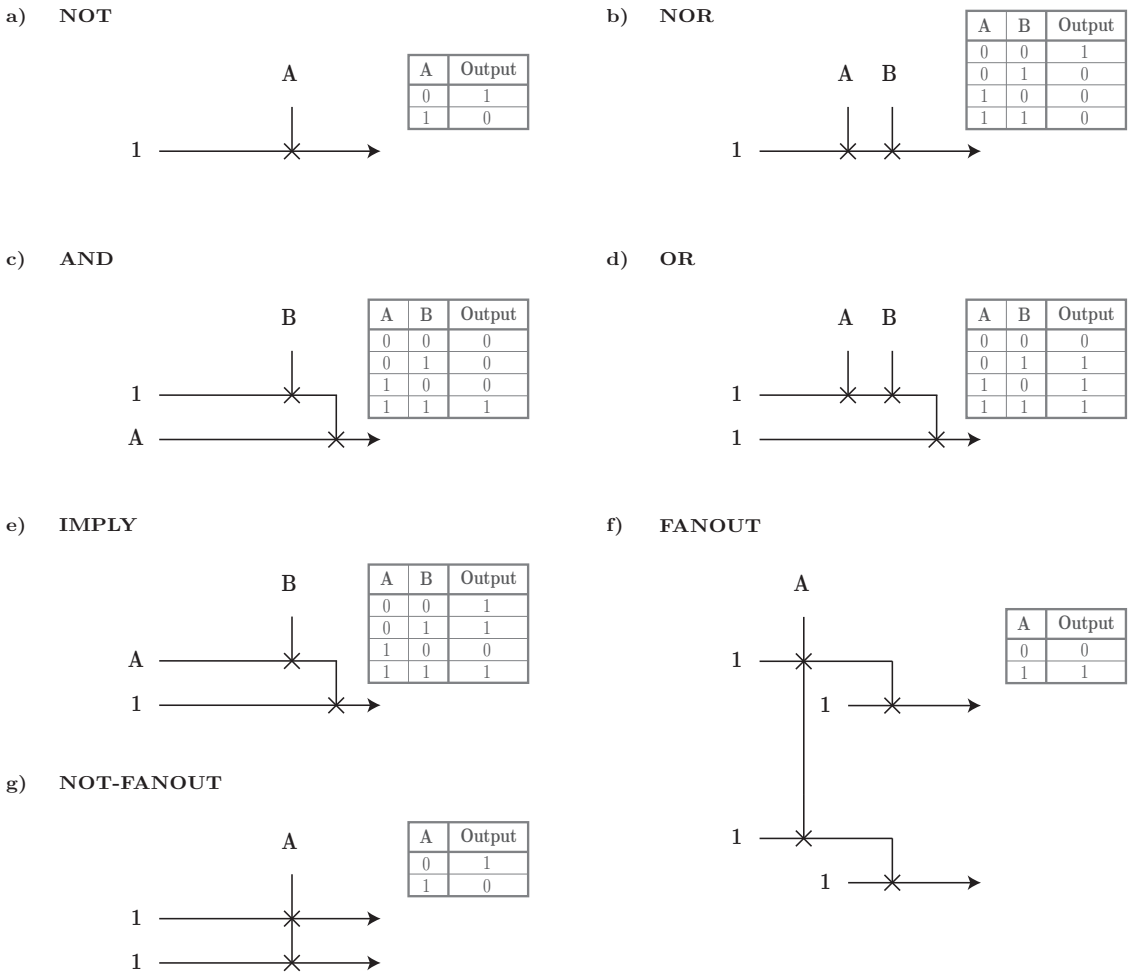


Figure 3.1: Luca Cardelli's proposed logic gates made from interacting tracks for DNA-motors are displayed alongside their truth tables. Lines represent tracks, with the relevant motor starting at the labelled end of a track. A '1' motor is always able to move down its track. 'A' and 'B' motors are logical inputs to the gates: input = 1 if the motor is able to move down its track, and input = 0 if it cannot. Crosses at the junction of a horizontal and vertical line denote the blocking of the horizontal track by the motor on the vertical track. An arrow at the end of a track represents the output of the logic gate: if a motor arrives at the end the output = 1, if no motor arrives the output = 0.
a-b) The NOT and NOR gates only require a motor to to be block another motor. c-e) The AND, OR and IMPLY gates also require a motor that can be blocked to be able to block. f-g) The FANOUT and NOT-FANOUT additionally require a motor to be able to block and move on to block again.

is worth noting that the output state of 0 is merely the absence of a signal. It is, therefore, important to ensure fast motor movement so that a decision of the output can be made within a reasonable time frame. Alternatively, dual-rail logic can be used, whereby the same logic gate is set up but with a NOT gate preceding the output to switch the output state — comparing the two signals will help determine whether the signal has been processed yet and what it is.

The simplest gate is the NOT gate; where the input motor is able to block the output motor. If the input motor is able to step (input = 1), it moves down its track and blocks the output motor, which then cannot reach the end of its track (output = 0). Whereas when the input motor is omitted or not released from the start of its track (input = 0), the output motor is able to pass down its track unimpeded to reach the end (output = 1).

If a motor is able to block multiple tracks, a FANOUT operator can be constructed that is able to reduce the number of tracks needed by replicating an output. This can be used as an input for multiple other gates without having to replicate the entire previous processing.

3.3 Mechanism

The aim was to design a new DNA motor that is able to implement Luca Cardelli's proposed logic gates based on motors blocking each other. Necessary properties for such motors are:

- for a motor to be able to block
- for a motor to be able to be blocked
- that the timing of motor operation can be predicted, such that one blocking can be made to occur before a second one with a high probability (this requires the motors to step at well-understood rates)

An additional desirable property that allows for more complex logic gates:

- for a motor to be able to block and move on to block again

This new system was based on the 'burnt bridges' motor,[1] a simple and versatile DNA motor, the details of which have been previously described in Section 1.2.2. General desirable system properties for a similar system are:

- to be simple, i.e. not to require too many additional strands, enzymes etc,
- to have relatively compact motors and anchorages (avoiding the need for large step sizes between anchorages that would restrict track layouts on a single origami tile),
- for different motors to have distinct sequences so that different tracks can come together without motors crossing onto the wrong track.

Making no initial assumptions, there could be two species of motor — one a "blocker" and another a "blockee". However, if the system is able to implement the AND, OR, or IMPLY gate, a single motor must be able to act as both a blocker and a blockee. For simplicity it was decided that all motors would be of the same type, i.e. the same length, directionality and blocking mechanism, such that any motor can block any other motor. Therefore, the term "blocker" refers to a motor that blocks another motor and "blockee" refers to a motor that is blocked at a specific junction between two tracks.

The desired property of a motor being able to block multiple motors means that the process of blocking must not permanently inhibit the stepping of the blocker motor, nor its blocking ability.

There are a number of possibilities for a blocking mechanism, some of which are mentioned here briefly before moving on to discuss the chosen approach in Section 3.3.2. Examples of these mechanisms can be found in Boemo *et al.* 2016 (in press)[125] with a discussion of how to optimise compound logic gates made from such interacting motors.

The track destroyer The blocker could destroy one or more anchorages at the junction, leaving a gap in the track that the blockee cannot step over. However, the origami tile planned as a substrate for these experiments is flexible and is expected to flex along particular axes (see Figure 1.8). This means that tracks in different locations and directions on the tile may need different minimum gaps to stop a motor stepping across. This would require assessment for all blocking locations (called the 'interaction site') on the tile, or the use of a stiffer origami as a substrate.

The motor destroyer The blockee could be destroyed at the interaction site. For the ensemble fluorescence measurements used here, it would be sufficient for the blockee to have its own blocking ability ruined and its quencher removed (as it is the quencher that impacts the output signal). In this state, even if the remnants of the blockee stepped or diffused down its track, it would not be able to interfere with the rest of the tracks or impact the fluorescence output. For example, this could be initiated by the blocker freeing a second restriction site for an enzyme that cuts off the bottom of the blockee. If the sequence that does this is at the bottom of the blocker, the blockee would lose both its quencher and its blocking ability.

The remover The blockee could be removed from the origami tile into solution through toehold-mediated strand displacement, initiated by the blocker. The benefit of this is that the blockee would not be near the tracks or other motors, and hence any interactions or diffusion encouraged by co-localisation would be less likely due to lowering the effective concentration. However, the blockee would need to be well-bound to its remover strand to ensure it does not rebind to another origami tile. This approach would work better at lower concentrations, or if the origami tiles were settled on a surface and the solution was washed past.

The absorber The blocker could initiate an absorbing mechanism to hold the blockee at the interaction site. This would control the location of the blockee and hence its interactions.

The final option of an absorption mechanism is investigated in this chapter. First, a few ideas for the interaction site are discussed (Section 3.3.1) before the chosen mechanism is described in more detail (Section 3.3.2). Track layout and blocking timing are also considered. Preliminary characterisation of the system is then explored (Section 3.4), and some initial measurements for a NOT track on an origami tile are described (Section 3.5).

3.3.1 Absorbing interaction site ideas

The 'burnt bridges' motor can be held at the end of a track by a mismatch in the restriction site to inhibit enzyme cutting. As the motor is able to bind by more bases to the end anchorage than to the cut track behind it, diffusion back down the track is limited. Unfortunately, this trick could not easily be used to hold a blockee motor at the interaction site, as the mismatch is a permanent feature at the anchorage and would not be able to be "turned on" by a blocker motor. Therefore additional/stronger bases or another sort of bond, must be made available by the blocker. Obviously, any mechanism designed to hold a motor must also allow motor movement in the absence of a blocker.

There were many possible strategies for this, three are described here. The final strategy was investigated further, and its initial characterisation and implementation are explored in the rest of this chapter.

The absorbing blocker The simplest way for the blocker to provide extra bases for the blockee is for it to provide them itself. This would only allow the blocker to block once, and so could not be used for the FANOUT or NOT-FANOUT gates that are useful for simplifying a network of gates.

This could be implemented through extensions at the top and bottom of 'burnt bridges'-like motors. A blocker would have a complementary bottom extension to bind to the blockee's top extension (Figure 3.2). An interaction site would consist of a double-length anchorage: the anchorage sequence for the blockee would be at

the base as normal, and the anchorage sequence for the blocker would be above with a mismatch in the restriction site to stop the blocker.

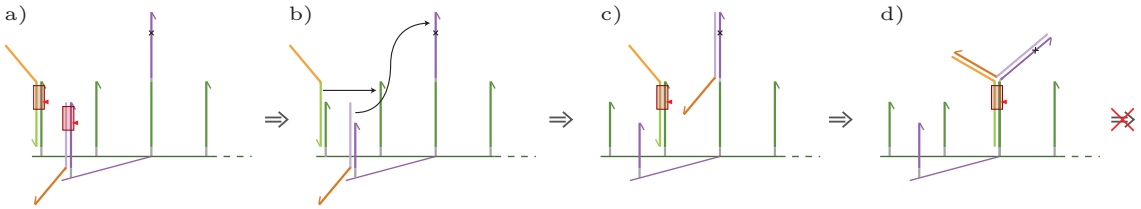


Figure 3.2: A possible approach for an interaction site that uses the blocker motor to hold the blockee motor using extra extensions on the motors. The main body of the motor is used for stepping down the track as with the 'burnt bridges' motor. The red box denotes the restriction site for the enzyme, and the nicking site is highlighted by the **triangle**. For clarity, as only the 3' extension of the blocker and the 5' extension of the blockee are important at an interaction site, the possible 5' blocker extension and 3' blockee extension are not shown here (these would be used for different interactions at other interaction sites).
a) Two motors are present on their own tracks. A double-length anchorage is present at the interaction site between the two tracks. b) The motors step down their tracks. The blocker (with a **purple body**) binds to the top part of the interaction anchorage. c) The blocker arrives at the interaction site first, and is unable to move away as a mismatch in the restriction site inhibits enzyme cutting. d) The blockee (with a **green body**) steps onto the interaction site. Due to the presence of the blocker, the blockee's **top extension** binds to the blocker's **bottom extension**, forming a stable complex and preventing it from stepping down its track.

In the absence of the blocker, the blockee could pass through the interaction site as normal. If the blocker were present, the blockee's top extension would bind to the the blocker's complementary bottom extension, forming a 3-way junction. Even if the enzyme was still able to cut the blockee's anchorage, the extra bases bound to its top should stop the cut anchorage from melting away, keeping the blockee's toehold covered. It's possible that careful placement of the restriction site would allow the 3-way junction to inhibit enzyme cutting for even greater control (sensitivity to nearby junctions was seen in Section 2.2.1).

A general problem with a double-lengthed anchorage is that it can reach further across the origami tile, potentially binding to a motor multiple steps down the track. However, it should not be an issue here as it is the blocker's anchorage sequence that has the extra reach. This may encourage the blocker to arrive at the interaction site faster than normal, but this would only help to ensure that the blocker arrives before the blockee.

An interesting characteristic of this mechanism is that the holding sequence between a blocker and blockee could be designed to allow a specific blocker to hold a specific blockee.

Hairpin interaction anchorage Another strategy uses the blocker to initiate the release of extra bases for an extension of the blockee (its 'tail') to bind to at the interaction site (Figure 3.3). The two motors would walk on anchorages with opposing polarity, using anchorages coming from the 3' and 5' ends of staples. The interaction site could be located at a single join between two staples in the origami tile. One staple would have a 3' ss-extension at this point, forming a classic anchorage for the blockee to step onto. In the absence of any change, the blockee would pass straight through the interaction site as normal

The neighbouring staple would also be extended from the same point, but from its 5' end. This would act as an 'interaction anchorage' for the blocker, a modified version of its normal anchorage. The top of the interaction anchorage would be complementary to the bottom so that it forms a hairpin. This would cover in its stem a domain that could bind to the tail of the blockee motor.

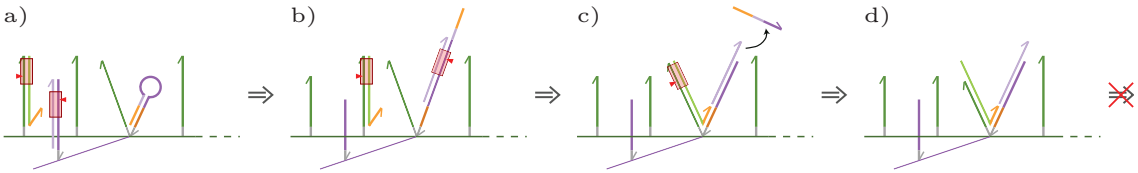


Figure 3.3: A possible approach for an interaction site that uses the blocker to initiate the release of extra bases for the blockee to bind to. These extra bases inhibit the blockee's movement away from the site. The motors step like the 'burnt bridges' motor, but have an additional ss-extension (the 'tail') at the bottom. For clarity, as only the tail of the blockee is important at an interaction site, the tail of the blocker is not shown here.
a) Two motors are present on their own tracks. One track has anchorages that are 5' extensions to origami staples, whilst the other are 3' extensions. b) The motors step down their tracks; the blocker opens up a hairpin anchorage at the interaction site, using a toehold in the loop. c) The end of the hairpin anchorage is cut off in the presence of the blocker. Its stem will remain uncovered. d) The blockee reaches the interaction site and its tail binds to complementary bases on the blocker's anchorage, which are now uncovered.

Once the blocker arrives at the interaction site (using a toehold in the hairpin

loop to initiate stepping onto the interaction anchorage), the nicking of the anchorage would release the end of the hairpin that completes the stem, which would diffuse away and would not rebind as it is too short (and no longer co-localised). Therefore, once the blocker has moved on, the complementary bases for the blockee's tail would remain uncovered. Therefore, when the blockee arrives at the interaction site, its tail will bind to the neighbouring cut anchorage, providing extra bases to inhibit the motor from stepping away.

However, this mechanism may be difficult to implement in practice. It would be necessary to carefully tune the hairpin stem to remain closed when an unblocked blockee arrives (as the blockee can make similar base pairs with its tail) and to remain uncovered when cut.

Lollipop track A final strategy is for the blocker to disrupt the enzyme's ability to cut the blockee's anchorage at the interaction site. To achieve this, part of the restriction site or any stabilising double-stranded sections either side of it is removed by the blocker. This was the chosen approach and is discussed in more detail in the following section.

3.3.2 The chosen approach: the lollipop track

The chosen mechanism that allows motors to block one another is to trap a blockee motor at an interaction site between two tracks by enabling a blocker motor to disrupt the enzyme's ability to cut the blockee's anchorage.

The design of the motor was based on the 'burnt bridges' motor[1]. The original design was modified by changing the restriction site for the nicking enzyme, to allow it to be disabled by a blocker. The restriction site is moved up the motor such that it requires a ds-region above the motor for the enzyme to be able to cut (Figure 3.4). This could either be because the restriction site extends above the motor, or because the enzyme is sensitive to having a restriction site located at the end of a DNA strand (in this case, the motor) and requires an extra ds-region next

to the restriction site[126]. It is this extra ds-region that is destroyed by the presence of a blocker, inhibiting enzyme cutting and further movement of the blockee.

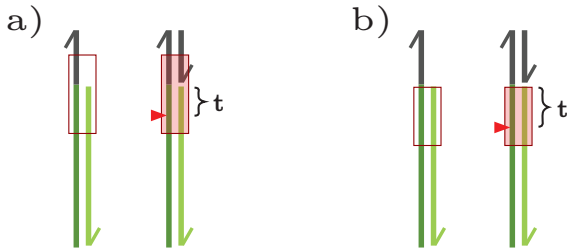


Figure 3.4: Repositioning a restriction site over or next to the end of a strand can make a **ds-region** above it necessary for the enzyme to cut. The restriction site and nicking location are highlighted by the red box and **triangle** respectively. An outlined red box highlights the restriction site when the enzyme cannot cut. Examples of a **motor**-bound **anchorage** requiring a ds-region above the motor: a) the restriction site extends above the motor and a ds-region above the motor is required to complete it, b) the enzyme requires a ds-region next to the restriction site as it is too close to the end of a DNA strand[126]. When the enzyme is able to cut the anchorage, the motor is left with the toehold 't'.

Normal track

For this design, as the motor is not sufficient to complete the restriction site on an anchorage and enable the enzyme to cut, a normal anchorage must be able to form the ds-region above the motor itself. Therefore, each normal anchorage has a hairpin top (Figure 3.5) — this is what gives the track the name "The Lollipop Track". The hairpin stem extends down to the top of the motor, and is placed close enough or within the restriction site such that its presence is required for the enzyme to cut.

Interaction site

The interaction site is formed of two nearby anchorages, one for the blocker and the other for the blockee (Figure 3.6). The tops of the interaction anchorages are complementary to each other and are able to bind to form a link. This linking section fulfils the same purpose as the hairpin stem on a normal anchorage: its presence is necessary for the enzyme to cut.

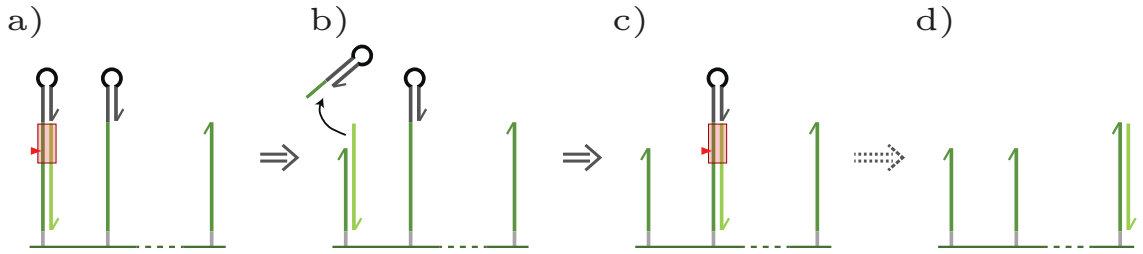


Figure 3.5: The motor moves down a plain lollipop track. The track is made up of anchorages with **hairpin tops**, the stems of which are necessary to complete ds-regions next to the restriction site that are required for the enzyme to work. The restriction site and nicking location are highlighted by the red box and triangle respectively.
a) A motor completes the restriction site at the beginning of the track. b) The enzyme nicks the first anchorage, the top of which melts off. c) The motor is then able to move onto the next complete anchorage through toehold-mediated strand displacement. d) After further movement down the track, the motor moves onto the end anchorage. The end anchorage does not have a hairpin top to allow the enzyme to cut, stopping the motor.

When the first motor arrives at the interaction site (the blocker), it is able to pass through. This step may take longer than a normal step, as the linking section may transiently bind and unbind. When bound, the restriction site is functionally complete and the enzyme cuts the interaction anchorage, freeing the motor toehold. The cut linking section then melts away from the top of the other anchorage.

This leaves the second interaction anchorage with no link at the top. When the second motor arrives (the blockee), the nicking enzyme is unable to cut due to the missing ds-section above the motor.

Extra base pairs between the bottom of the motor and its interaction anchorage make it energetically unfavourable for the motor to diffuse forwards down the track. These extra bases also slow the motor's movement away from a complete interaction site, but as long as they are less than the motor toehold length (bases to be gained by moving onto the next anchorage), the motor is still driven forwards.

This mechanism relies upon the blocker motor arriving at the interaction site first. The interaction site is symmetric in that either motor is able to pass through and block the other motor, it just depends upon which motor arrives at the interaction site first. This satisfies the condition for motors to be able to block and be blocked. As the motors themselves are not changed or used up by the blocking

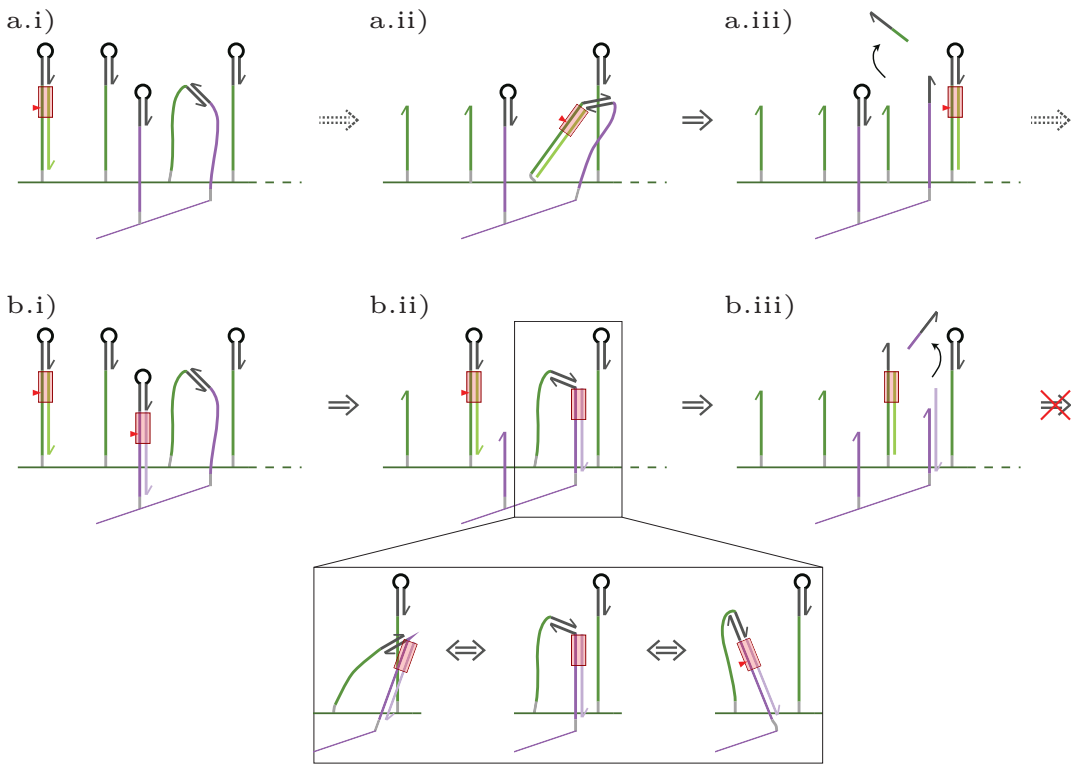


Figure 3.6: The tracks of two interacting motors forming a NOT gate. One motor (the blocker) is able to stop the other motor (the blockee) from reaching the end of its track. The presence or absence of the blocker determines the input of the gate, whilst the presence or absence of the blockee at the end of its track determines the output.
Input = 0 a.i) Only one motor is able to move down its lollipop track. a.ii) The motor reaches the interaction site, which is formed of an interaction anchorage from each track. They have complementary tops so that they bind together to form a double-stranded link. This link is necessary for the nicking enzyme to cut either anchorage. a.iii) Once the enzyme has cut, the linking section melts off into solution, and the motor is able to step forwards. The motor moves down the track until it reaches the end. **Output = 1**
Input = 1 b.i) Both motors are present on their own lollipop tracks. b.ii) The motors move down their tracks, with the blocker motor reaching the interaction site first. b.iii) Once the enzyme has cut, the linking section melts off into solution. When the blockee motor subsequently arrives at the interaction site, it cannot move forwards as the enzyme cannot cut its interaction anchorage. **Output = 0**

mechanism, the motors are able to block other motors multiple times down its track — a desirable extra condition for the system.

3.3.3 The layout of multiple tracks

Tracks of interacting motors can be positioned to cross each other, to briefly come close at the interaction site and then diverge without crossing, or to run alongside each other (Figure 3.7). Their sequences must be sufficiently orthogonal so that a motor would not accidentally step onto the wrong track.

Parallel tracks allow a dense track network to be made, making economic use of the limited space on an origami tile. They also keep the stepping distances for each motor the same, which stops specific motors going faster than expected due to having smaller step sizes. It is worth noting that track trajectories could be manipulated to speed up or slow down certain motors, the purpose of which is explained in more detail in the following section.

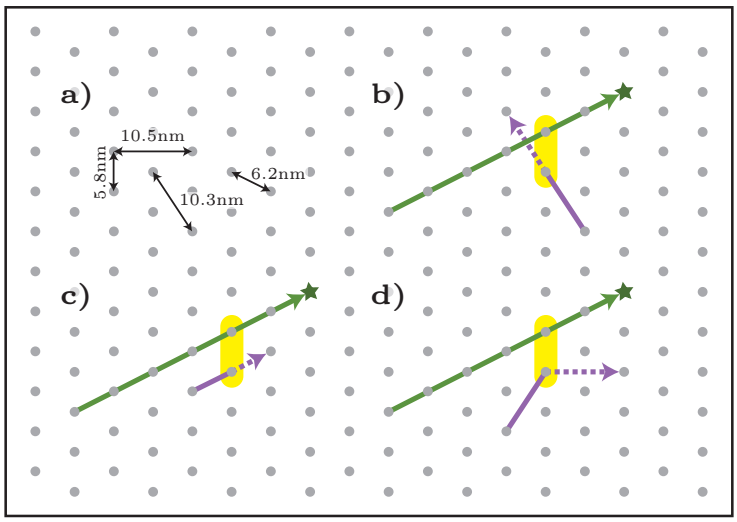


Figure 3.7: The possible ways to lay out interacting tracks. a) The four smallest step sizes for possible trajectories across the tile. b-d) Track layouts for a NOT gate. Motor movement is in the direction of the arrow, and dashed lines indicate additional movement that is not necessary for the NOT gate computation. The motor for the green track quenches the fluorophore at the end of its track unless blocked by the motor on the purple track. Tracks can be laid out to b) cross each other, c) run parallel to each other, and d) "reflect" each other.

3.3.4 Timing

This mechanism relies on the blocker arriving at the interaction site, enabling its anchorage to be cut and the cut linking section to melt away before the blockee arrives. There are a number of ways to manipulate the timing of a motor's arrival. The simplest is to change the track length before the interaction site, giving more steps for the blockee to walk down than the blocker. This is useful up to a point, but with complex logic gates, this could lead to excessive use of space on a single origami tile[125].

Alternatively, a motor could be slowed down by decreasing its toehold, or using mismatches to slow down the strand displacement of the motor between two anchorages when stepping[54]. As mentioned in Section 3.3.3, different track directions across the origami tile have slightly different stepping distances which could also be used to intentionally slow down or speed up a motor. A more brute force method is to simply remove anchorages, creating a gap in the track to slow down the motor moving across it. A sufficiently large gap would require the motor to wait for opportune flexing of the origami to bring the next anchorage within reach.

Given the sensitivity of some of these methods to anchorage separation, if the flexing of the origami were not necessary, it would be desirable to build the track on a stiff origami to remove the effects of the tile flexing from the system. The origami tile described in Section 1.2.2 was used to test this mechanism despite its flexibility, due to its simplicity in formation and purification.

3.4 Testing the components

This section details the preliminary characterisation of the components of the Lollipop Track. Starting with the choice of enzyme and the placement of the restriction site, which is an integral part of the basic mechanism. The successful cutting of mid-track lollipop anchorages is then shown, followed by an investigation into the operation of the interaction site.

3.4.1 Enzyme choice

Although the general stepping mechanism is the same as that of the 'burnt bridges' motor, another restriction enzyme could be used to cut the anchorages. Different enzymes have their own sensitivities to the completeness of their restriction site[127] and require different amounts of double-stranded DNA next to their restriction site[126] (for stability). Therefore, a number of potential enzymes were tested to find the most suitable.

The requirements for the enzyme were:

- to release a motor toehold of around 4-8 nt. Too small a toehold and the initiation of strand displacement for stepping onto a new anchorage will be too slow. Too long a toehold and the cut top of the anchorage will not melt off. This restricts the possible locations of the nicking site relative to the end of the motor.
- to require a double-stranded section above the motor. This is necessary for the blocking mechanism.
- to have an optimum incubation temperature of 37°C. This allows some of the kinetics of this system to be compared to previous 'burnt bridges' experiments which were run at 37°C.

The restriction enzymes that were readily available from New England Biolabs (NEB) were narrowed down to four possibilities: Nt.AlwI, Nt.BbvCI, Nt.BsmAI and SexAI (Table 3.1).

The restriction site for the nicking enzymes (Nt.AlwI, Nt.BbvCI and Nt.BsmAI) can be varied in position along the motor.anchorage duplex to release different length toeholds on the motor (as the toehold is the domain from the top of the motor down to the nicking site, depicted within Figure 3.8 for each enzyme). The use of the restriction enzyme SexAI is more restricted, as it cuts both strands of the duplex and hence the second nicking site must be above the motor so as to not destroy it. This gives an upper limit of 5 nt for the motor toehold using SexAI.

Enzyme	Restriction site
Nt.AlwI	3'...C C T A G N N N N N...5' 5'...G G A T C N N N N N...3'
Nt.BbvCI	3'...G G A G T C G...5' 5'...C C T C A G C...3'
Nt.BsmAI	3'...C A G A G N N...5' 5'...G T C T C N N...3'
SexAI	3'...T G G W C C A...5' 5'...A C C W G G T...3'

Table 3.1: The restriction sites for the possible enzymes: three nicking enzymes (Nt.AlwI, Nt.BbvCI and Nt.BsmAI) and one restriction enzyme (SexAI). 'A', 'T', 'G' and 'C' refer to the standard nucleotides. 'N' refers to any of the four nucleotides, and 'W' refers to either 'A' or 'T'. The **triangle** shows where the enzyme cuts the phosphate backbone.

The nicking enzymes were tested to see whether a suitable motor and interaction anchorage were possible (Figure 3.8). This involved incubating each enzyme with a pre-annealed motor and interaction anchorage (with no ds-region above the motor). To be compatible with the blocking mechanism, the interaction anchorage must not be cut by the enzyme. Various motors, containing different amounts of the restriction site, were tested. The strands were annealed in 1x Origami buffer + 50 mM NaCl (the buffer used during the 'burnt bridges' experiments[1,102,128]). They were then incubated with the relevant enzyme for 1 hr at 37°C and finally heat inactivated at 80°C for 20 mins. Samples were run on polyacrylamide gels to determine which motors did not enable the enzyme to cut the interaction anchorage.

Nt.AlwI did not cut the interaction anchorage when bound to motors with toeholds of 4 and 5 nt (Figure 3.8a). For these motors, 5 or 4 nt of the restriction site (a sequence-specific region) would need to be completed by the ds-link at an interaction site. This would constrain the sequence of the link. As this constraint must be fulfilled at both ends of the link (so that it can work for both anchorages at the interaction site), this requires the linking sections to have reverse-complementary sections at either end. This was later found to allow the interaction anchorage to

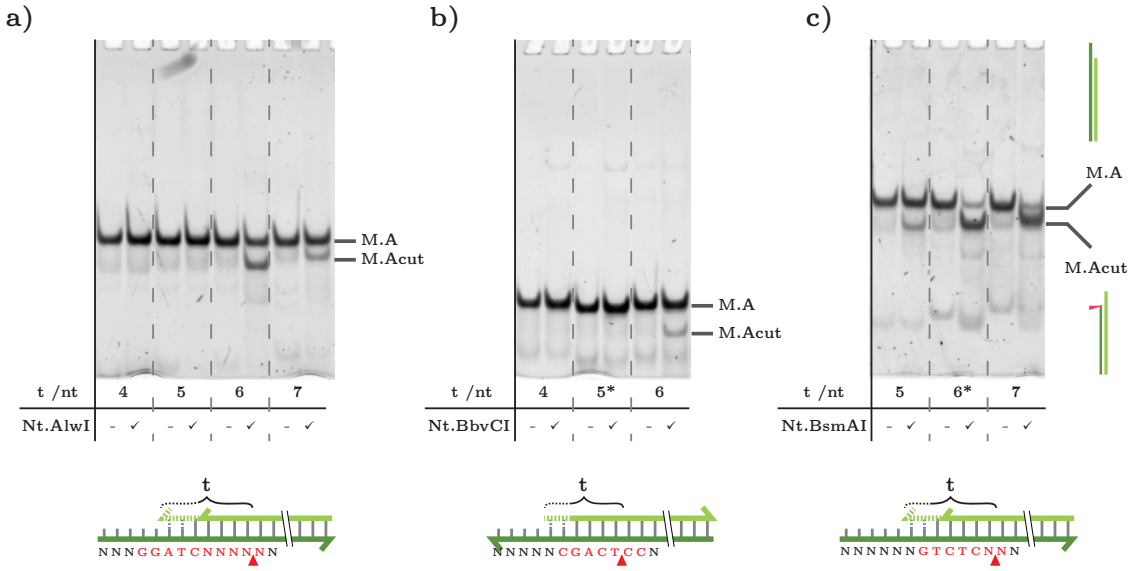


Figure 3.8: Polyacylamide gels used to check for inhibited enzyme cutting of an **interaction anchorage** (A) with various **motors** (M) pre-annealed to it. The different motors completed different amounts of the restriction site, and would have different toehold lengths (t) to initiate stepping. Three enzymes were tested: a) Nt.AlwI, b) Nt.BbvCI and c) Nt.BsmAI. Gel details: 15% 29:1 polyacrylamide gels, run at 250V for a) 72 min, b) 68 min and c) 61 min. Sample details: stoichiometric amounts of the strands were annealed in 1x Origami buffer + 50 mM NaCl at 113 nM. 12.5 units of enzyme were added to each 50 μl sample.

enable its own cutting by transiently forming a hairpin with a stem above the motor, much like a normal lollipop anchorage.

Nt.BbvCI did not cut the interaction anchorage for motors with toeholds of 4 and 5 nt (Figure 3.8b). Whilst Nt.BsmAI cut the interaction anchorage for all motors tested, with toeholds of 5-7 nt (Figure 3.8c). The enzyme SexAI showed no enzymatic activity, even with a full duplex, and so was not further investigated.

Consequently, Nt.BbvCI was the best choice, allowing a motor toehold of 5 nt without having to constrain the link sequence, and hence with no worry of the interaction anchorage self-enabling cutting.

Buffers

As Nt.BbvCI must also be able to cut an anchorage when the section above the motor is double-stranded (regardless of the nick in the duplex at the junction between the strands), various buffers were tested to ensure efficient cutting of a normal lollipop anchorage annealed to a motor (Figure 3.9). These tests were done with a lollipop anchorage with a 7 nt hairpin stem and a 4 dT loop.

Buffers varied between 1x Origami buffer + 50 mM NaCl (the original 'burnt bridges' buffer) and CutSmart® buffer (NEB's current recommended buffer for the enzyme: 50 mM Potassium Acetate, 10 mM Magnesium Acetate, 20 mM Tris-acetate, 0.1mg/ml BSA). The enzyme cut most efficiently in CutSmart buffer. A replicate CutSmart buffer without the BSA was used as a replacement buffer for 1x Origami buffer + 50 mM NaCl in some of the experiments when the system was implemented on an origami tile (see Section 3.5.2 for a comparison of the buffers).

3.4.2 Plain track

In order to test the simplest gate, the NOT gate, two motors (M1 and M2) on their own tracks (of A1 and A2) are needed, requiring two different motor sequences. Therefore, the two versions of lollipop anchorages and motors were tested to ensure that both were cut in the presence of Nt.BbvCI. The lollipop anchorages have an orthogonal 7 bp hairpin stem and a 4 dT hairpin loop.

Test anchorage strands were used without their staple sequence, as the staple section would be bound into the origami during full experiments. They were annealed to the motors in replicate CutSmart buffer, and then incubated with Nt.BbvCI for 1 hr at 37°C before running on a polyacrylamide gel. Both sequences showed similar cutting efficiencies and were used for the subsequent experiments (Figure 3.10).

3.4.3 Interaction site

Polyacrylamide gels were used to test for the formation of the link between two interaction anchorages, and the link-requiring cutting of one of the anchorages when

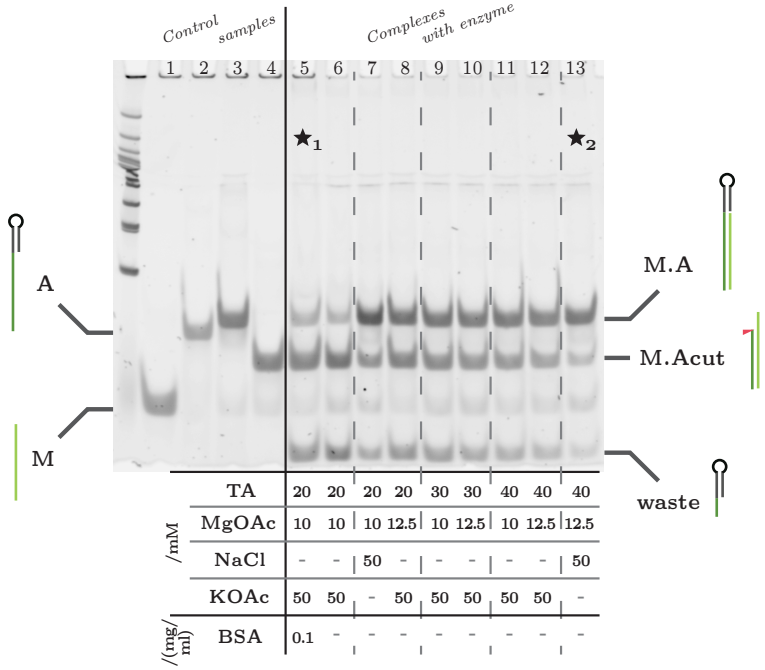


Figure 3.9: The cutting efficiency of the **lollipop anchorage** (A) annealed to the **motor** (M) was checked in various buffers. ★1 highlights CutSmart buffer as provided by NEB. ★2 highlights the original 'burnt bridges' buffer. Lanes 1-4 — control samples of M, A, M.A and M.Acut respectively. Lanes 5-13 — M.A incubated with Nt.BbvCI at 37°C for 1 hr in various buffers. Gel details: 15%, 29:1 polyacrylamide gel, run at 250V for 63 min in a cold room. Sample details: strands were annealed in the ratio of A:M = 1:1.25, where A was at 100nM. 0.5μl of Nt.BbvCI (10,000 units/ml) was added to 20μl samples.

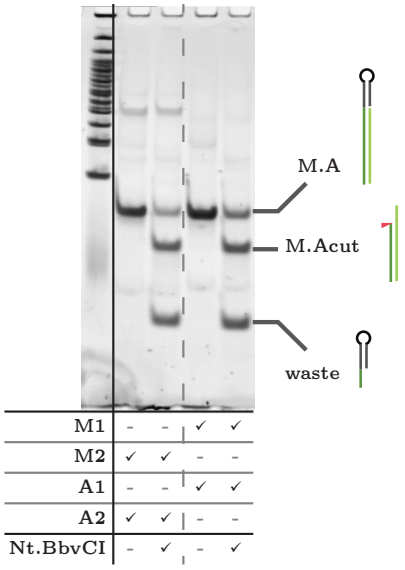


Figure 3.10: Two different motor and lollipop anchorage sequences were tested to ensure cutting by Nt.BbvCI. Stoichiometric amounts of the **motor** and **anchorage** were annealed in replicate CutSmart buffer and incubated with Nt.BbvCI for 1 hr at 37°C. Gel details: 15% 29:1 polyacrylamide gel, run at 250V for 60 min in a cold room. Sample details: strands were annealed in 20 μl at 113 nM; 0.5 μl of Nt.BbvCI (10,000 units/ml) was added.

bound to its motor (Figure 3.11).

In order to test this with a few strands rather than on origami, the interaction anchorages were given complementary extensions in place of their staple sequences. This forces them to bind together, simulating the localisation when bound in the origami (see the depiction of M2.A1$_I$.A2$_I$ in Figure 3.11). The binding section was 16 bp ($\approx$ 1.5 turns), so that the anchorage sequences came from the same side of the binding helix. This does not exactly replicate the separation on the origami tile, which differs depending upon the track orientation. In the origami experiments in Section 3.5 they are separated by roughly 6.2 nm (calculated from measurements of a plain tile observed with AFM[**Wickham201**]), whilst these non-origami tests had a separation of 5.4 nm (calculated using a length of 0.34 nm per base[3]).

When a motor was annealed with both interaction anchorages, it gave a significantly slower band on a gel than when the motor was annealed with a cut control for the interaction site (lanes 9 and 10 in Figure 3.11). This implies a marked difference in shape of the structure, as the small reduction in the number of bases is not sufficient to account for the change. This is evidence of the link forming between the interaction anchorages, creating a loop-like structure when the interaction site is complete.

Efficient cutting of the interaction site was seen when the motor was annealed with both interaction anchorages and incubated with Nt.BbvCI for 1 hr at 37°C (lane 11 in Figure 3.11). Whereas no cutting was observed when the motor was annealed to only its interaction anchorage (so no ds-link could form) and incubated with the enzyme for 1 hr at 37°C (lane 7 in Figure 3.11). This demonstrates that the link enables the cut as designed.

Not forming dimers

In order to prove that the extra slow band of the motor-interaction site complex (M.A1$_I$.A2$_I$, where A$_I$ refers to an interaction anchorage) was forming a link with itself and was not a dimer ((M.A1$_I$.A2$_I$).(M.A1$_I$.A2$_I$)), a light and heavy version of the interaction site were created using a 1:1 mix of a light and heavy A2$_I$ strand.

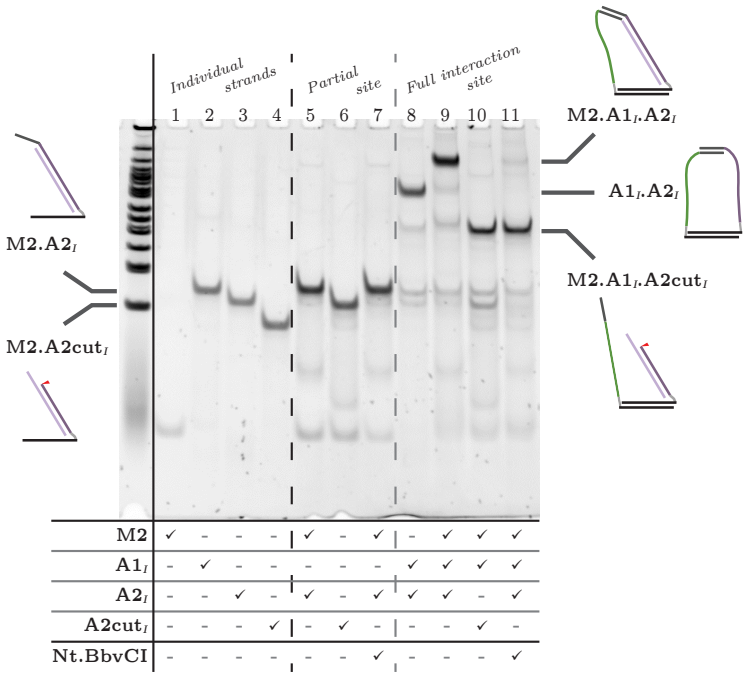


Figure 3.11: The formation and cutting of the interaction site was tested with a single **motor** (M2) annealed to it. Lanes 1-4 — control samples of individual strands. Alongside is NEB's 50bp DNA ladder for reference. No cutting of a single **interaction anchorage** when no **ds-link** is present: lanes 5-6 — control samples of the uncut (M.A2$_I$) and cut form (M.A2cut$_I$) respectively; lane 7 — M.A2$_I$ incubated with Nt.BbvCI for 1 hr at 37°C. Formation of a structure-changing ds-link: lanes 8-9 — the interaction anchorages annealed without and with the motor respectively; lane 10 — control for the cut form of the interaction site (M2.A1$_I$.A2cut$_I$), which rus much faster than the uncut form; lane 11 — M2.A1$_I$.A2$_I$ is incubated with Nt.BbvCI for 1 hr at 37°C, and is efficienctly cut. Gel details: 15%, 29:1 polyacrylamide gel, run at 180V for 80 min in a cold room. Sample details: strands were annealed in 1x Origami buffer + 50 mM NaCl at 113 nM; 0.5 μl of Nt.BbvCI (10,000 units/ml) was added to 20 μl samples.

"Light" and "heavy" refer to strands/complexes with a smaller and larger molecular weight respectively, which are often distinguishable using polyacrylamide gel analysis. When annealed with a motor and the other interaction anchorage, two populations should form if they are monomers (P_{Light} and P_{Heavy}), and three populations should form they are dimers (P_{Light}.P_{Light}, P_{Light}.P_{Heavy} and P_{Heavy}.P_{Heavy}).

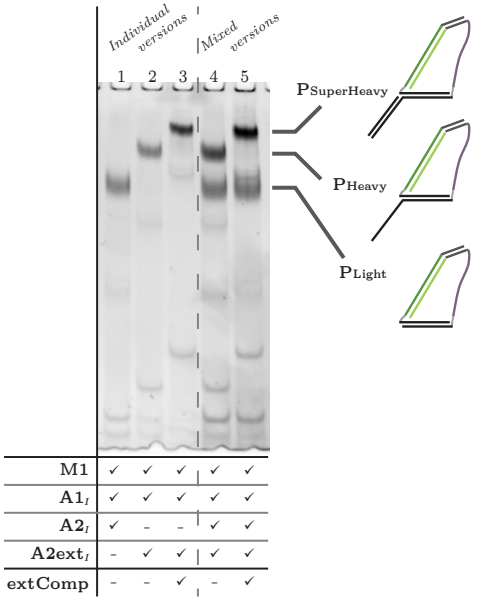


Figure 3.12: PAGE analysis to check that the interaction site is forming looped monomers instead of dimers. A light and heavy version of one of the interaction anchorages (**A2**$_I$ and **A2ext**$_I$ (with and without **extComp** bound to its extension)) were annealed with the **motor** (M1) and the other interaction anchorage (**A1**$_I$). Lanes 1-3 — samples of the interaction site formed using A2$_I$, A2ext$_I$, and A2ext$_I$ + extComp (producing the light, heavy and super heavy structures). Lanes 4-5 — the interaction site is annealed with an equal mix of A2$_I$ and A2ext$_I$ with and without extComp. Two populations are seen, as expected if the structures are monomers. Gel details: 15%, 29:1 polyacrylamide gel, run at 190V for 190 min in a cold room. Sample details: strands were annealed in 1x Origami buffer + 50 mM NaCl in the ratio of A2$_I$:A2ext$_I$(:extComp):A1$_I$:M1 = 2:2(:4):4:5, where A2$_I$ was at 113 nM.

The light version of A2$_I$ was the same strand used for Figure 3.11. The heavy version had an extra 16 nt extension from its 5' end: when bound to a complementary strand (extComp), a super-heavy version was created — this was useful for further band separation on a polyacrylamide gel.

Two populations were seen on a polyacrylamide gel (both with and without extComp to create the super heavy structure), implying monomer formation as

desired (Figure 3.12).

Intra-molecular cutting

It is possible that interaction anchorages may bind to waste cut links or other origami floating in solution. If this were the case, a blocked motor would still be able to pass through the interaction site using intra-molecular binding to enable the enzyme to cut its interaction anchorage, though at a lower rate than if the interaction site were complete.

This was tested using interaction anchorages that can only bind together via their linking section, which were annealed with one of the motors. After incubation with the enzyme over 1 hr at 37°C, ∼5% of the duplex was cut (Figure 3.13). As the enzyme has been shown not to cut M2.A2$_I$ by itself (lane 7 in Figure 3.13), this cutting must be due to transient binding with A1$_I$.

The strands were used at the same concentration as the other preliminary characterisation tests so that they could be compared (113 nM). However, this is roughly 4 times the concentration of the origami in the ensemble fluorescence measurements, and so cutting in those experiments is expected to be even less.

Cutting with flexi linker length

Lollipop anchorages on an origami tile have a 3 dT linker between the anchorage sequence and the origami staple sequence, to give the anchorages flexibility when bound to a motor. In order to ensure sufficient flexibility to allow the tops of the interaction anchorage to bind together, forming the link, a 12 dT flexible linker was used in the initial experiments of the preceding sections.

Longer linkers increase the chances of motors skipping anchorages as they step down the track, so the minimum length flexible linker for the interaction anchorages was investigated. This was tested by considering the cutting efficiency of the interaction site for a 3, 6, 9 and 12 dT linker length. The interaction anchorages were annealed with one of its motors, and then incubated with Nt.BbvCI for 1 hr at

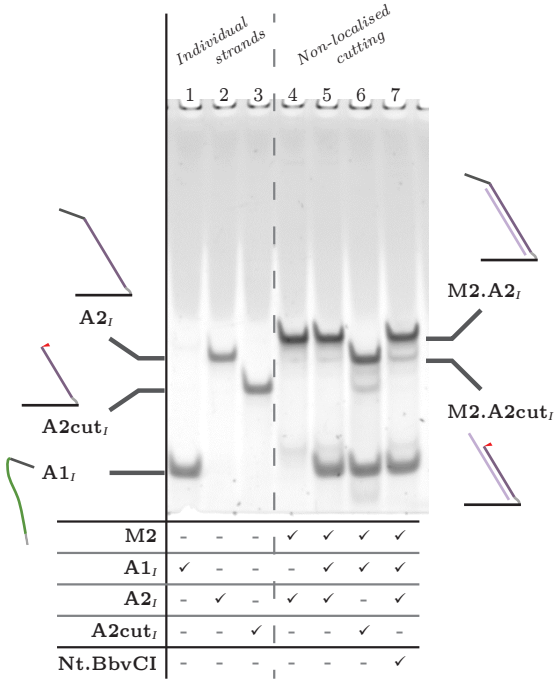


Figure 3.13: A test for intra-molecular binding enabling enzyme cutting of an interaction anchorage ($A2_I$) annealed to its motor (M2). Lanes 1-3 — control samples of individual strands. Lanes 4-5 — M2.$A2_I$ in the absence and presence of $A1_I$ (which remains unbound) respectively. Lane 6 — a control for M2.$A2cut_I$ in the presence of $A1_I$. Lane 7 — M2.$A2_I$ with $A1_I$, incubated with the enzyme for 1 hr at 37°C. This shows a small amount of cutting. Gel details: 15%, 29:1 polyacrylamide gel, run at 109V for 110 min in an ice bath. Sample details: strands were annealed in 1x Origami buffer + 50 mM NaCl at 113 nM; 0.5μl of Nt.BbvCI (10,000 units/ml) was added to a 20 μl sample.

37°C. Samples were run on polyacrylamide gels to determine the cutting efficiency, the results of which are summarised in Table 3.2.

Flexible linker	**Motor**	**Percentage cut**	**Average over the motors**
3 dT	M1	53%	49% ± 5%
	M2	45%	
6 dT	M1	65%	68% ± 4%
	M2	71%	
9 dT	M1	67%	70% ± 4%
	M2	73%	
12 dT	M1	67%	69% ± 3%
	M2	71%	

Table 3.2: Cutting efficiencies of Nt.BbvCI (over 1 hr at 37°C) of an interaction site annealed with one of its two motors. The interaction site was formed of two anchorages bound by a 16 bp (≈ 5.4 nm) complementary section in place of the origami support. This underestimates the separation on the origami tile and is expected to overestimate the cutting efficiency. The percentage cut was calculated as the band intensity of the cut population divided by the sum of the band intensities of the cut and uncut populations on a polyacrylamide gel. The average percentage cut over both motors is also provided.

The cutting efficiency for a 3 dT linker was lower than that of 6, 9 and 12 dT linkers, which all gave similar values. This indicates that a short linker does indeed restrict the interaction site from easily forming the linker to allow enzyme cutting. As previously mentioned, these non-origami tests underestimate the separation between the interaction anchorages on the origami. Therefore, to be on the safe side, a linker length of 9 dT was used for the following ensemble fluorescence experiments.

3.5 Fluorimeter measurements

In order to show that the mechanism works, a NOT gate was implemented on an origami tile (Section 3.5.1). The absence or presence of the blocker motor was simulated by using an unblocked (uncut) and blocked (cut) form of the interaction anchorage. To compare the impact of the interaction site on the motor's progress,

the track was also prepared with a normal lollipop anchorage in place of the interaction site. The sequences used were those tested in the preceding section.

The motor was observed using ensemble fluorescence measurements. Fluorophores were placed at the beginning and end of the track (F_0 and F_{end}), and were quenched in the presence of the quencher-carrying motor. The unquenching of F_0 confirms that the motors are able to move away when the enzyme is added, and the quenching of F_{end} serves as the output signal for the gate. It is worth noting that the F_0 signal is not necessary for the function of the logic gate as it is not part of the output; however, it is useful for ensuring that the motors have been successfully initiated and are stepping down the track well.

In initial experiments, a low percentage of motors reached the end of the track (Section 3.5.1). The use of replicate CutSmart buffer (instead of the original 'burnt bridges' buffer) was found to increase the percentage of motors arriving at the end (Section 3.5.2).

The track was also given bracing at the base of the anchorages to discourage them from threading through the origami to point out from the wrong surface (Chapter 5). This gave a slight improvement in the amount of motors reaching the end of the track (Section 3.5.3).

3.5.1 NOT track

A track of eight anchorages was run diagonally across an origami tile, spanning roughly 43 nm. The movement of a motor down the track was compared for a full lollipop track, a track with a complete interaction site, and a track with the cut form of an interaction site (Figure 3.14). The cut form simulates how the interaction site would be once a blocker motor had passed through. This allowed the blockee's movement to be tested without any complications arising from incorrect motor timings, which could cause the blockee to arrive at the interaction site before the blocker.

The mid-track anchorages were lollipop anchorages, separated by 6.2 nm. The interaction anchorage of the motor was placed at the penultimate anchorage posi-

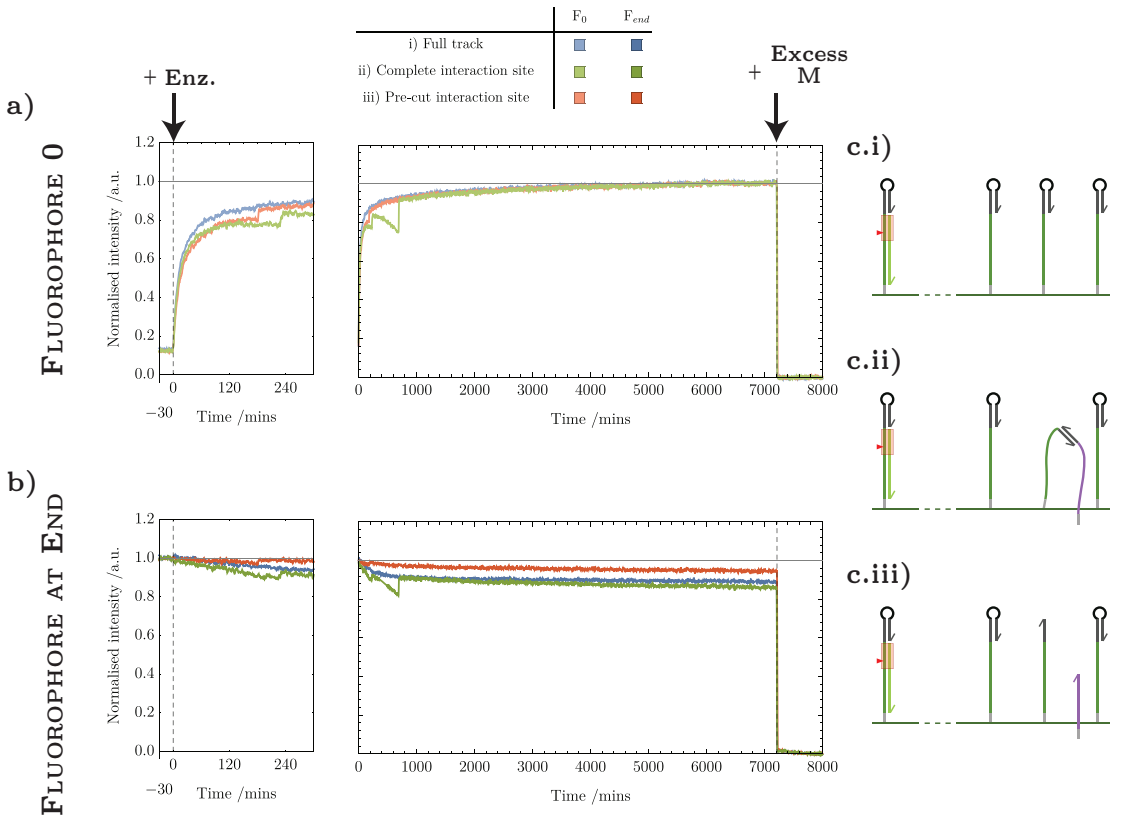


Figure 3.14: Fluorescence traces of fluorophores at a) the beginning (F_0) and b) the end (F_{end}) of the track for i) a full lollipop track, ii) a track with a complete interaction site, and iii) a track with a pre-cut interaction site. The fluorescence was normalised with respect to the unquenched and fully quenched state. c) Depictions of the tracks, formed of eight anchorages running diagonally across an origami tile. The penultimate anchorage was i) a lollipop anchorage, ii) an interaction anchorage that is able to form a ds-link with an interaction anchorage for another track, and iii) an interaction anchorage that is unable to form a ds-link as the other interaction anchorage was pre-cut.

tion. The second interaction anchorage to complete the interaction site was extended from a staple 6.2 nm away and had the sequence for an orthogonal second motor. The end anchorage was complementary to the motor but with no hairpin top, in order to stop the enzyme from cutting it, and hence holding the motor at the end of the track. Backwards motion is inhibited by the cut track behind it.

The first anchorage was similar to the mid-track anchorages, but with three extra bases at the bottom, complementary to extra bases on the motor. This was to reduce diffusion of the motor down the track before its movement was initiated, by making it energetically more favourable to remain bound to the first anchorage. The motor was loaded into place by being pre-annealed to the first anchorage in a M:A ratio of 0.9:1 with A at 5 μm. The complex was then added to the pre-formed origami (missing the staple for the first anchorage) in a A:origami ratio of 0.95:1, and incubated at 37°C for 2 hrs.

The sample was run in 1x Origami buffer + 50 mM NaCl. The motor's movement was initiated by the addition of Nt.BbvCI. After which F_0 increased and F_{end} decreased, indicating the motor moving away from the first anchorage to the end of the track.

All three tracks had similar loading efficiencies (as indicated by their initial normalised fluorescence levels (Section 2.3.4)) and movement away from the beginning of the track. A small quenching of F_{end} was seen for the full track, when normalised to the fully quenched state once excess motor was added. The percentage of motors reaching the end of the track was calculated as per Wickham *et al.* 2012[102] (Equation (2.5)), and suggested that 13% of the motors reached the end of the track. This is much less than previous experiments using the 'burnt bridges' motor on an eight anchorage track, where roughly 50-70% of the motors reach the end of the track (using the same calculation method).

When a complete interaction site was present, 16% of the motors reached the end of the track. It is not known whether or not this increase compared to a full lollipop track is significant. Though it is possible that the extra long flexible linker at the bottom of the interaction anchorage may allow it to reach further back down

the track to bind to a motor stuck behind a track defect, increasing the chances for a motor to reach the end of the track.

In the case where the second interaction anchorage is pre-cut, and hence no enzyme-enabling link is able to form, the percentage of motors reaching the end of the track drops to 6%. The likely reason why this is not closer to 0% is because the interaction anchorage did not have any additional bases to keep the motor from diffusing forwards onto the end anchorage. Therefore, any motors arriving at the interaction anchorage are likely to end up roughly equally-distributed between the interaction anchorage and the end anchorage. This explains getting roughly half the amount of motors at the end for a cut interaction site as for a complete interaction site.

The main problem is that so few motors are reaching the end, even with a plain track with no interaction site. The motors seem to be leaving the first anchorage well, so must either be getting stopped or lost down the track. This could be due to the enzyme's ability to cut the lollipop anchorages or due to track defects; these possibilities were further investigated in the next two sections.

3.5.2 Changing the buffer

Section 3.4.1 showed that using replicate CutSmart buffer improved the cutting efficiency of the enzyme. Therefore, a repeat of the motor walking down a plain lollipop track was made in this buffer.

In order to make sure that the origami formed in the same way, all the experiments used 1x Origami buffer to anneal the origami tile. When using the original 'burnt bridges' buffer, NaCl was added after purification during a roughly two-fold dilution of the sample. The annealed samples that were to be run in replicate CutSmart buffer were diluted two-fold in a translation buffer (7.5 mM MgOAc, 100 mM KOAc) after purification.

The percentage of motors reaching the end of the track is much higher in replicate CutSmart buffer than the original buffer (Table 3.3). The motors also moved away from the first anchorage faster (Figure 3.15), with a 2.5-fold difference in $t_{1/2}$, the

half-time for the unquenching of F_0 caused by the motors leaving the beginning of the track. Faster movement away from the first anchorage is consistent with improved cutting in CutSmart buffer (Figure 3.9). It is possible that the CutSmart buffer might increase enzyme stability as well as efficiency, which could then explain the increased percentage of motors reaching the end of the track as well as increasing the rate of arrival.

Buffer	**Percentage of motors reaching the end**	**$t_{1/2}$ of motors leaving the start /mins**
1x Origami + 50 mM NaCl	14 ± 1 %	20 ± 7
1x CutSmart	39 ± 3 %	8 ± 1

Table 3.3: Comparison of the motors walking down a straight track in either 1x Origami buffer + 50 mM NaCl or replicate CutSmart buffer. The percentage of motors reaching the end of the track is calculated as in Equation (2.5). $t_{1/2}$ is the half-time of the motors leaving the first anchorage. Errors were calculated as the standard deviation from multiple experiments.

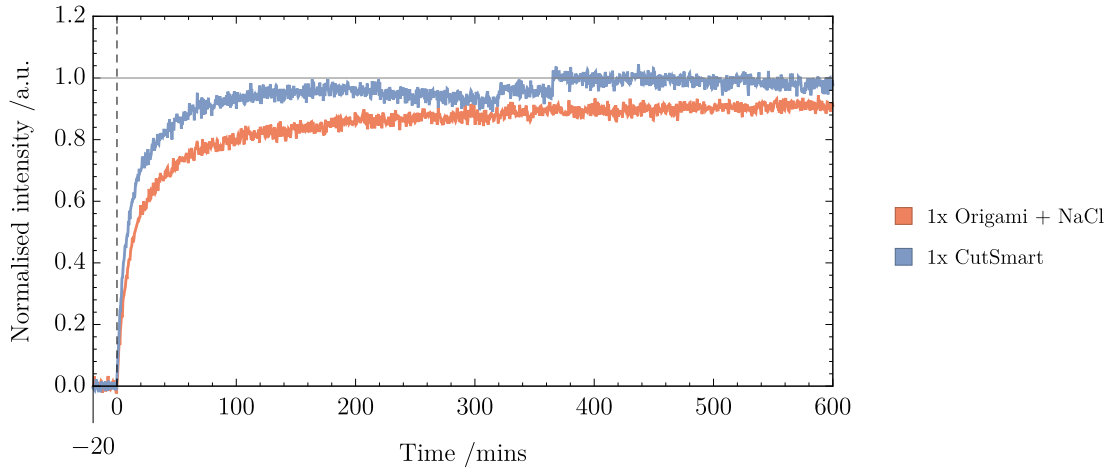


Figure 3.15: Examples of the motor leaving the first anchorage when run in the original 1x Origami buffer + 50 mM NaCl or replicate CutSmart buffer. This is seen by the unquenching of F_0. The traces were normalised so the starting signal is at 0 and the released plateau is at 1 so that the kinetics could be compared. Motor movement was initiated at $t = 0$ mins by the addition of Nt.BbvCI. The motors leave the first anchorage slightly faster in 1x CutSmart buffer.

3.5.3 A braced track

Another hypothesis for a small percentage of motors reaching the end of the track is that, during origami formation, some of the anchorages are threaded through holes in the tile, and their hairpin tops stop them from being able to thread back through once the origami has formed. This would trap some of the anchorages on the "wrong" side of the origami. It is possible that this could cause enough of a track defect to stop motors from reaching the end. Therefore a track was designed with 'bracing' at the bottom to promote the correct orientation of the anchorage relative to the origami tile.

Section 5.3 considers the threading of extensions in much more detail, and includes analysis of the different states using single-molecule measurements. A similar sort of 'bracing' seemed to reduce the amount of threading of ss-extensions through an origami tile.

The bracing was formed at the base of the anchorages by including an extra 12 nt section that binds to the complementary extension of the neighbouring staple (see the inset in Figure 3.16). The two staples (that of the anchorage and its neighbour) and the scaffold strand create a three-way junction at the staple join. Two unbound A bases on both staples were placed at the junction to allow the scaffold strand to remain stacked at the junction[129].

The bracing sequence was unique for each anchorage, so that only the correct pair of anchorage and neighbouring staple bind together. If the wrong pairs were able to form, it could hamper origami folding.

Motors moving down an eight-anchorage straight track were compared for a normal and braced track (Figure 3.16), run in replicate CutSmart buffer. A braced track gave a slightly higher percentage of motors reaching the end of the track (Table 3.4).

Though both track types have similar $t_{1/2}$, the overall plateau is reached faster for the braced track. The unquenching of F_0 was modelled according to a first-order rate equation (Equation (2.1)). The model fits the shape of the data for the normal track poorly ($k = 0.000\,9\,s^{-1}$), but fits the braced track data well ($k = 0.002\,s^{-1}$).

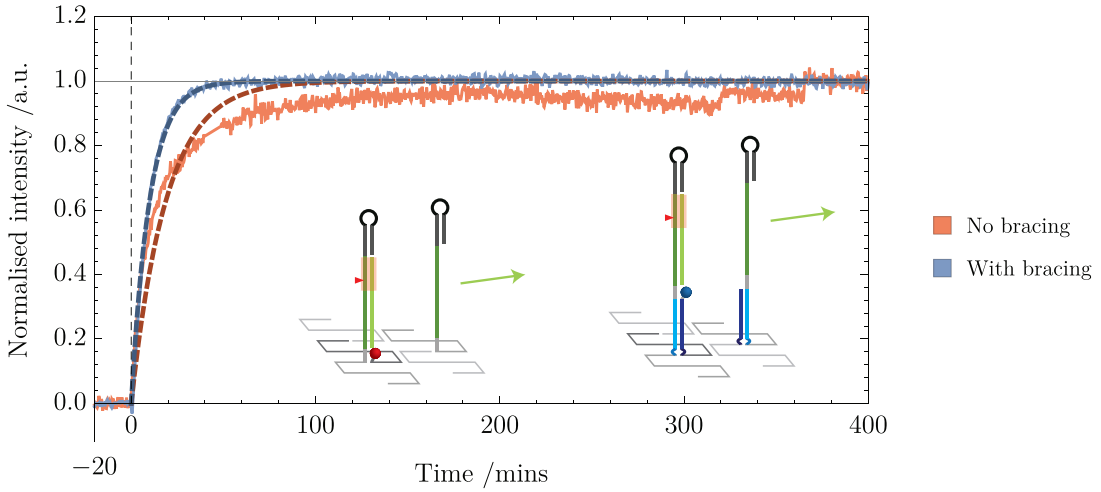


Figure 3.16: Examples of the motor leaving the first anchorage when the track has bracing at the bottom to encourage the anchorages to point away from the origami tile. This is seen by the unquenching of F_0. The traces were normalised so the starting signal is at 0 and the released plateau is at 1 so that the kinetics could be compared. Motor movement was initiated at $t = 0$ mins by the addition of Nt.BbvCI. The dashed lines are the fits of a first-order model to the data.

Bracing present?	**Percentage of motors reaching the end**	**$t_{1/2}$ of motors leaving the start /mins**
No	39 ± 3 %	8 ± 1
Yes	51 ± 4 %	6 ± 1

Table 3.4: Comparison of the motors walking down a straight track with and without bracing at the bottom of the anchorages. All experiments were run in replicate CutSmart buffer. The percentage of motors reaching the end of the track is calculated as in Equation (2.5). $t_{1/2}$ is the half-time of the motors leaving the first anchorage. Errors were calculated as the standard deviation from multiple experiments.

This may indicate that there are two populations: one with the first and second anchorages in an unthreaded state, with quick stepping between them; and another with threaded anchorages that can slowly unthread, causing slower stepping. If the braced track has only the unthreaded population, this explains all the quick stepping from the first anchorage. If the normal track has a mix of unthreaded and threaded populations, the first movement seen would be that of the quick unthreaded populations (explaining the similar $t_{1/2}$ values), followed by a slower stepping from the threaded populations as they take time to unthread into position.

Though a braced track speeds up the motor it has not drastically improved the

percentage of motors reaching the end of the track.

3.6 Discussion & future work

In this chapter, a number of design approaches for a DNA motor system that uses blocking to perform logic operations were discussed. The chosen approach, the "Lollipop Track", was based on the 'burnt bridges' motor. It places the restriction site for a nicking enzyme at the top of the anchorage such that it requires a ds-region above it. The enzyme is integral for motor movement; blocking occurs when a blocking motor disrupts the restriction site that another motor needs to continue stepping down its track.

As a simple test, a NOT track was implemented on an origami tile. The presence of the blocking motor was mimicked by forming the origami with the blocked form of the interaction site. Tracks with an unblocked and blocked form of the interaction site had 16% and 6% of the motors reach the end of the track respectively. One reason why the blocked form of the interaction site did not have a percentage closer to 0% is because the interaction site did not have extra bases to stop the motor from diffusing away down the track. Motors are, therefore, expected to end up on the end anchorage and the interaction anchorage with equal probability. The presence of the motor at the end of the track is indicated by the quenching of a fluorophore at the end of the track by the quencher-carrying motor. As the interaction site was located at the penultimate anchorage, only 6.2 nm away, it is possible that motors that remained at the interaction site were still able to quench the fluorophore. This could be tested by forming the origami with the end fluorophore staple and the penultimate anchorage, and adding the motor to check for fluorescence changes.

These experiments show roughly the right sort of behaviour, i.e. a reduced percentage of motors reaching the end of the track when it has a blocked interaction site; but the low percentages make it hard to assess properly. When a similar system was implemented with a full track of normal lollipop anchorages, only 14% of motors reached the end of the track. This is low compared to typical 'burnt

bridges' experiments which have previously shown 50-70% of motors reaching the end of the track. Two hypothesises for the small amount of motors reaching the end of the track were tested. The first was that the cutting efficiency of the nicking enzyme was too low. By changing the buffer to one shown to increase the cutting efficiency, an increase to 39% of motors reached the end of the track.

The second hypothesis was that there are more track defects on this track than the classic 'burnt bridges' track. The main difference between them is that the lollipop anchorages have hairpin tops that provide the ds-region that enables the enzyme to cut. During origami self-assembly, it is possible that some of the anchorages are threaded through holes in the origami lattice. Whilst ss-extensions would be expected to be able to unthread, the hairpin tops may inhibit them from doing so, causing them to get stuck on the wrong side of the origami. Other work in this thesis (Section 5.3.2) has shown that bracing the bottom of staple extensions (which is what an anchorage is) with extra base-pairs with the extension of the neighbouring staple reduces threading. When a lollipop track with braced anchorages was tested in the cutting-efficient buffer, an additional increase to 51% of motors reached the end of the track.

The use of a multilayered origami was shown to be even more successful at reducing threading (Section 5.3.3). Therefore using a multilayered origami as the platform for a lollipop track could further improve the percentage of motors reaching the end. To check more directly if the hairpin tops are causing a significant difference to the track, the 'burnt bridges' track could be replicated with hairpin tops on the anchorages. If this shows reduced numbers of motors reaching the end of the track compared to a track without the hairpin tops, this would be evidence that these are indeed the problem.

If the issues with a general low percentage of motors reaching the end of a plain track can be overcome, it would be worthwhile for the interaction site to be retested with its position moved further away from the end anchorage and with the appropriate extra bases provided to stop the motor diffusing away.

Chapter 4

A Track Inside Tubes

This chapter presents a system for observing movement of a 'burnt bridges'[1]-like motor over micrometre distances with an optical microscope. Origami tubes that are able to polymerise to form stacked tubes provide a substrate for a repeating track. Tubes also provide a way of enclosing a track within an origami structure, potentially shielding it from interference from other components in solution. This requires the motor to be able to step down a track whilst in an enclosed space, and to step between connected origami.

Two approaches for observing the motor are considered: labelling the motor directly, and labelling the track such that the fluorescence is removed from the 'burnt' track behind the motor. Preliminary microscopy experiments are explored for both approaches. The modifications to the 'burnt bridges' motor and track were also checked using ensemble fluorescence measurements, to ensure a feasible system was being considered.

The work in this chapter was a collaboration with Florence Benn and Natalie Haley. The strategy for this project and the majority of the experiments were made jointly. However, some parts of the project were accomplished by one person as follows. The tube was designed solely by Florence Benn prior to this project

(a summary of the design is made here). The tubes were assembled by her, and she provided the AFM images of the structures. Schematics of the 3D tubes were adapted from her original images. Natalie Haley provided the microscopy expertise and took the images on the microscope. She also provided the gels that tested enzyme cutting in the microscopy conditions. I analysed the microscopy images, under advice from the others, and wrote the analysis scripts.

4.1 Design

4.1.1 Tube

Chiral origami tubes were designed by Florence Benn. The staples were designed to give the origami curvature, allowing it to fold up into a tube. The tube is made from 20 helices that wrap around the tube to give it a right-handed twist (confirmed with circular dichroism by Florence Benn, results currently unpublished). The length of the tubes, measured from an AFM image (Figure 4.1), is 117±6 nm. The tubes are able to stack, polymerising to μm length-scales.

To allow for modification of the inside of the tube, the staple nicks were designed to be on the inside surface. Therefore, anchorages (which are extended staples) can be used to set up a track inside the tube. In some cases it was useful to modify the outside of the tube, e.g. for biotinylated strands to tether the tube to a microscope slide surface for imaging. To move the nick position to the outside surface, two neighbouring staples are slightly modified by making one longer and the other shorter by 0.5 turns.

End-to-end stacking of the tubes can be promoted or suppressed through the addition of specific end staples that bind to free loops of scaffold at the ends of the tube. poly(dT)-end staples can be added to suppress stacking of the tubes, giving discrete ∼100 nm monomer tubes (Figure 4.2a). Each poly(dT)-end staple is a U-shaped staple that is complementary to two parts of neighbouring free loops of scaffold at the end of a helix, with 8 dT domains on the ends pointing away from

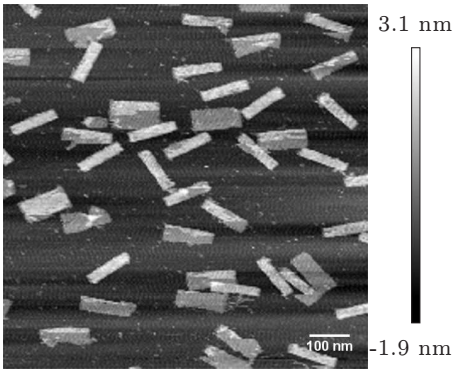


Figure 4.1: AFM image of the tubes taken by Florence Benn. Some of the structures are wider and flatter; they are interpreted as opened-up tubes, possibly from the AFM tip pulling them open. The less wide and thicker structures are expected to be the complete tubes; these have a length of 117±6 nm.

the tube. This uses the steric repulsion of a DNA brush to prevent non-specific stacking[130]. Without any end staples, the tubes may still stack via non-specific end-to-end stacking of the helices alone.

Alternatively, linker staples can be added to promote stacking, forming continuous micrometre-scale tubes (Figure 4.2b). Half the linker strand is complementary to the free scaffold at the end of one helix, whilst the other half is complementary to the free scaffold at the end of another helix on the other side of the tube. The linker staples were designed such that the end of a track on one tube would align with the start of a track on another tube.

AFM images of the tubes with poly(dT)-end staples and linker staples show successful promotion and suppression of stacking (Figure 4.2). As many of the stacked tubes have lengths >0.5 μm, it should be possible to observe them with optical microscopy.

4.1.2 Track for a burnt bridges motor

A track of 21 anchorages was placed on the inside of the tube, starting at one end of the tube and finishing at the other in ∼6.2 nm steps (Figure 4.3). The set of linker staples used to connect the tubes aligns the end anchorage of one tube to the

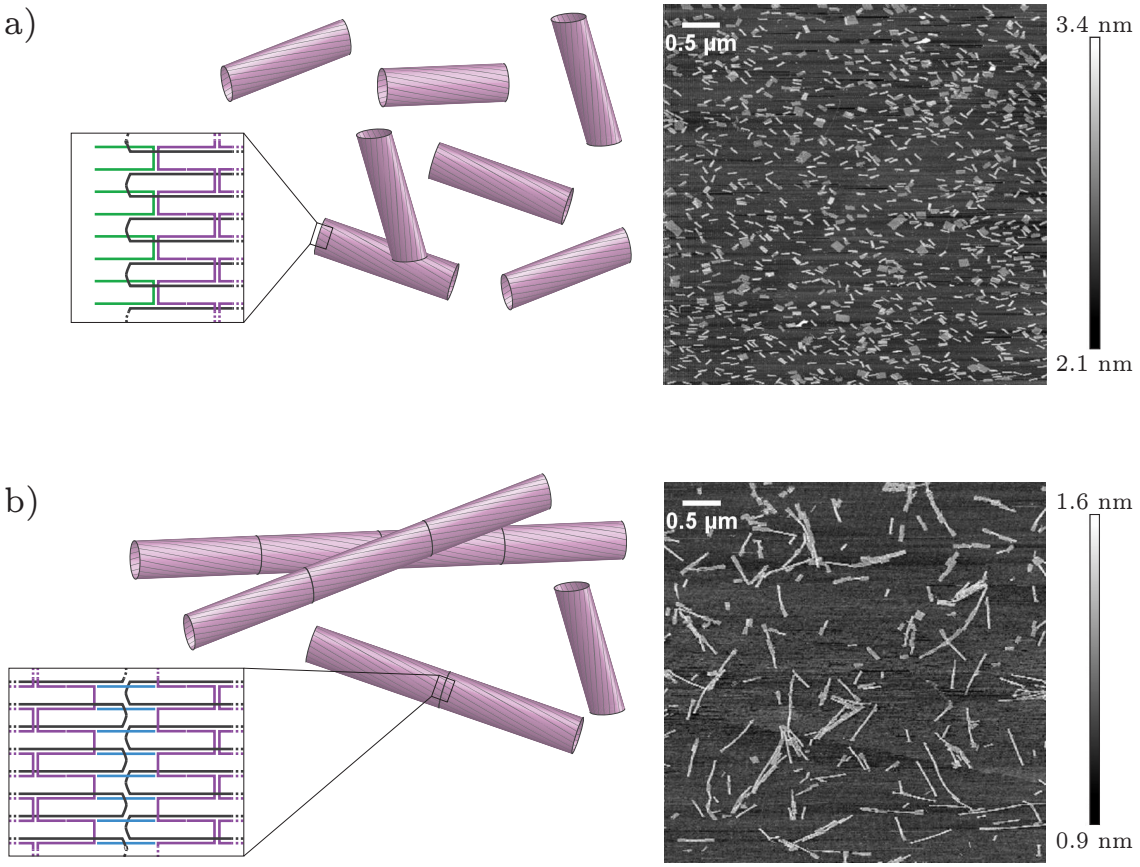


Figure 4.2: Depictions of the tubes alongside an AFM image of a sample. Insets shows the special end staples used at the ends of the tubes. a) Tubes made with **poly(dT)-end staples** to suppress stacking. b) Tubes with **linker staples** to promote stacking. AFM images were taken by Florence Benn.

first anchorage of another tube. The stepping distance between these anchorages is ∼12 nm.

It is possible that the anchorages might thread through the origami lattice holes of the tube to the outside. However, the plan was to transport a motor through the confinement of an enclosed origami. As bracing of an extension has been shown in Chapter 5 to reduce threading, a similar technique was used here. It is worth noting that the relative sizes of the extension and bracing differ to the previous tests and so its success at reducing threading is not known precisely. The bracing used here was made up of an 8 nt section on the anchorage that binds to a complementary 8 nt section on the neighbouring staple (its 'bracing neighbour') at its adjoining end. Two unbound A bases on each staple between the staple and bracing sections give

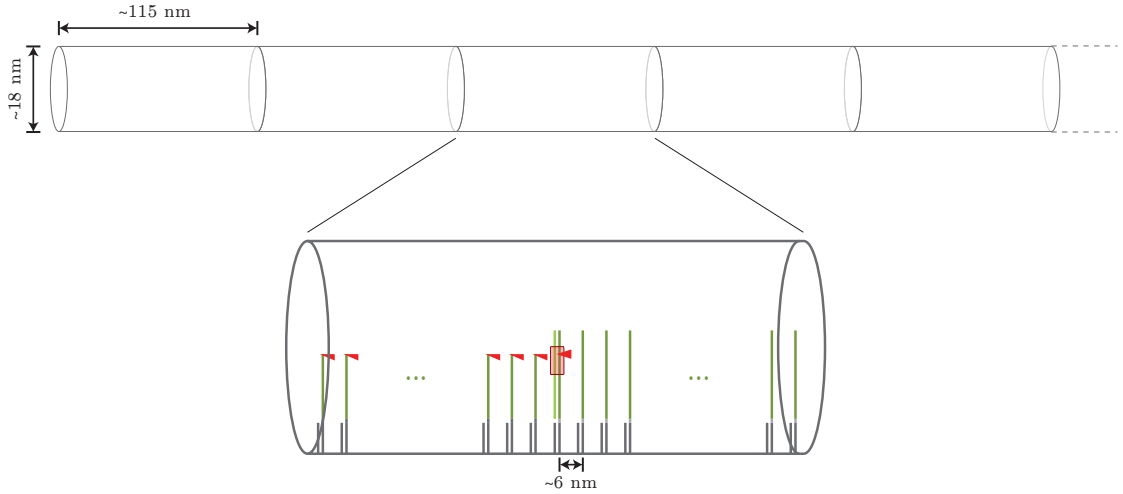


Figure 4.3: Schematic of a 'burnt bridges'-like track[1] running inside stacked tubes. The **motor** is complementary to the **anchorages**. When bound together, the motor completes a restriction site for the nicking enzyme (depicted as a red box) that cuts the anchorage strand 6 nt from the top. The cut top melts away, freeing the toehold on the motor to initiate stepping onto the next anchorage. The zoomed-in view of a single tube shows a motor in the middle of a track with cut ('burnt') track behind it. The anchorages have an 8 nt **bracing** at the bottom, formed by hybridisation to an extension of the neighbouring staple, to reduce threading of the anchorages at their base to the outside of the tube.

the anchorage some flexibility and allow the scaffold strand to be stacked at the 3-way junction formed here[129].

The motor is loaded into place at the beginning of the track by pre-annealing to the first anchorage (A_0), and incubating the complex with the defective tube missing the staple for A_0. This process of staple repair is the same as used elsewhere in this thesis. A_0 has an extra 2 nt at the bottom to bind to complementary nucleotides on the motor. This limits diffusion of the motor down the track before the enzyme is added, as it is energetically favourable to remain bound to A_0 compared to stepping forwards. Movement is then initiated by the addition of the nicking enzyme, Nt.BbvCI.

4.1.3 Observation plans

The motor

There are a number of ways to observe a motor moving down a stacked tube using optical microscopy. The most direct way is to label the motor with a fluorophore or quantum dot or using a transiently-bound DNA-PAINT strand[106,107]. A reference signal would be required so that the position of the motor could be observed relative to a fixed position on the tube or on the microscope slide surface. For example, the first tube on which the motor is loaded could also be labelled with fluorophores, quantum dots or DNA-PAINT strands or could be stained with a nucleic acid stain. The benefit of a stain is that it could stain the first tube with up to one dye per base pair, giving a very strong signal that will take longer to photobleach below observable limits. One possible issue with a stain is its effect on the motor's stepping: the cutting efficiency of the enzyme on a stained duplex or the kinetics of the strand displacement between the stained anchorages may be adversely affected.

An indirect way of observing motor movement is by labelling the top of all the anchorages. When the nicking enzyme cuts the anchorage, the labelled top will diffuse out of the tube (either through the walls of the tube or out an end). By using Total Internal Reflection Fluorescence microscopy (TIRF microscopy), freely-diffusing fluorophores will not be observed as only a small region (on the order of 100 nm) near the surface of the microscope slide is illuminated. Once the motor has moved down part of the track, its location can be determined at the boundary between the visible track ahead of it and the dark 'burnt' track behind it.

Both a direct (labelled-motor) and indirect (labelled-track) method of observing the motor are explored in this chapter. For the labelled-motor system, the motor was extended with multiple copies of a complementary domain for a dual-labelled Cy3 strand ($Cy3_M$). Due to limited space inside the tube (the diameter is ∼18 nm), the length of $Cy3_M$ was kept relatively short at 10 nt. Adding two copies of the domain to the motor, along with some unbound linker bases between ds-regions to give it flexibility, gives the motor a contour length of ∼17 nm. This enables each motor to be labelled with four Cy3s. Two options were considered: one where the

motor has one copy of the labelling domain at each end ($M_{1,1}$), and another where the motor has two copies of the domain at the 3' end ($M_{0,2}$).

For the labelled-track system, the anchorages were extended with a 16 nt domain that is complementary to a Cy3-labelled strand ($Cy3_A$). Staining the tubes with a dimeric cyanine nucleic acid stain called YOYO-1 Iodide serves as a reference signal. YOYO-1 and Cy3 act as a FRET pair when co-localised[131], whereby excited YOYO-1 molecules (the donors) can transfer their energy to nearby Cy3 fluorophores (the acceptors) causing them to emit. The YOYO-1 signal is expected to be bright enough to be observed regardless of this, as it is a bis-intercalator that binds 1 molecule for 4 base pairs of the DNA at saturation[132].

Preliminary microscopy experiments are discussed in Section 4.3. Firstly, to check the viability of the systems, ensemble fluorescence measurements were performed on similar tracks and are discussed in Section 4.2.

The movement

Ideally, movement of a motor down a single stacked tube would be observed within a single observation window. Bath *et al.* 2005[1] calculated a first-order rate constant for stepping of the 'burnt bridges' motor as $k = 0.009\,\mathrm{s}^{-1}$, giving an average speed of 0.1 nm/s. It is worth noting that an origami tube is expected to flex less along the direction of the track ($\sim$ down the axis of the tube) than the origami tile used in the 'burnt bridges' experiments, so the speed of stepping down the tube is likely to be slower. To see clear movement down a stacked tube of μm length, this would take approximately 5 hrs. Experimentally, this is quite difficult, due to drift of the microscope slide and bleaching of the dyes.

To avoid photobleaching, snapshots of a single field of view could be taken every hour. Software can be used to automatically keep the sample in focus. This could be done by observing the nucleic acid stain with a mercury lamp, instead of illuminating the sample with the (more powerful) laser. This would ensure a better overall signal, as the signal from the nucleic acid stain will be bright and will produce an observable signal for longer than the Cy3 signal for the motor or track. $x - y$ drift of the

microscope slide could be accounted for as long as the tubes remained within the field of view.

An alternative is to initiate the motor before putting the sample on the microscope, and view aliquots every hour. The distance between the motor and the reference dye for numerous tubes could be compared between the aliquots at different times. Between viewings, the sample could be kept at 37°C, the optimum working temperature for the enzyme, and would not have the disadvantage of being restricted to the 20°C of the microscope, which would reduce the cutting efficiency of the enzyme and hence slow down the motor. The preliminary experiments discussed in Section 4.3 used this approach, but snapshots of movement down specific tubes are planned for future work by collaborators Florence Benn and Natalie Haley.

4.2 Ensemble fluorescence measurements

Before attempting to observe motor movement with the microscope, ensemble fluorescence measurements were used to check that the motor can move down the tube despite all of the required modifications to the simpler 'burnt bridges' motor and track.

Having the track inside of the tube restricts not only all of the strands that must be contained within it, but also the enzyme which must be able to diffuse into and around the inside of the tube. A simple track and motor scheme was tested to ensure that the motor could move down the tube and between tubes (Section 4.2.2). Versions of a labelled-motor and labelled-track set-up were also checked (Sections 4.2.3 and 4.2.4).

4.2.1 General set-up

Two track layouts were used for the ensemble fluorescence measurements in this section: a track of 5 anchorages on a single tube (a monomer) and a track of 26 anchorages crossing between two tubes (a dimer) (Figure 4.4). Both tracks start at

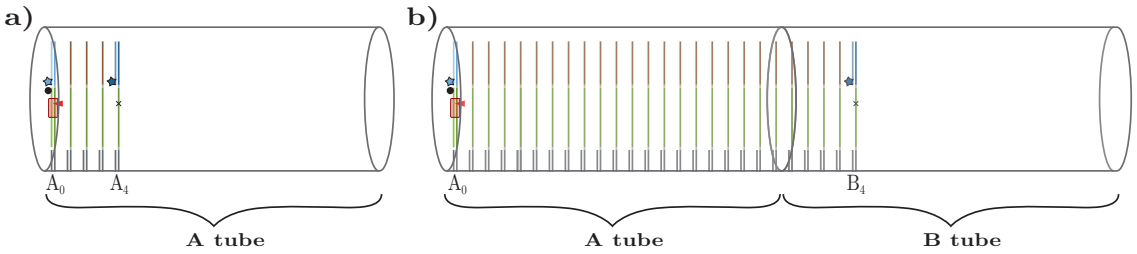


Figure 4.4: Schematics of the monomer and dimer tube track layout with fluorophores at the beginning and end of the track (stars) to detect the presence of a quencher-carrying motor (the quencher is represented as a black circle). The tube that the motor is loaded onto is referred to as an 'A tube'; any connecting tubes are referred to as 'B tubes'. a) The monomer has 5 anchorages: A_0-A_4. b) The dimer has 26 anchorages, 21 on the A tube and 5 on the B tube: A_0-B_4.

one end of a tube (the front) and move inwards. The tube the motor is loaded onto is called an "A tube" (with anchorages A_i). The connecting tube in the dimer case is called a "B tube" (with anchorages B_i). Both tubes are made from the same staple mixes, and so must be annealed separately and purified before adding together.

Braced anchorages were used to reduce threading as previously described. Whenever an anchorage (A_i or B_i) is stated as being used, this implies that the anchorage's bracing neighbour staple is also included. The only exception is for A_0, on which the motor is pre-annealed for loading; the bracing neighbour for A_0 is included in the origami anneal and is not included in the motor loading complex.

Fluorescence signal & normalisation

The position of the motor along the track was reported by fluorophores at the beginning and end of the track (F_0 and F_{end}). In Sections 4.2.2 and 4.2.4, the motor is modified with a 3' quencher, and its presence at the beginning or end of the track is indicated by the decrease in fluorescence of F_0 or F_{end} respectively. In Section 4.2.3, the motor is labelled with Cy3 fluorophores and the FRET between the Cy3 and F_0 or F_{end} indicates the presence of the motor at the beginning or end of the track.

To mimic the planned microscopy experiments using anchorages with labelled tops, the anchorages here also have domains above the motor-binding site that could

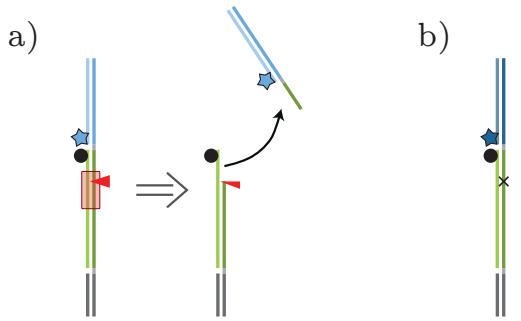


Figure 4.5: Schematics of the fluorophores at a) the beginning (F_0) and b) end of the track (F_{end}). The **anchorages** at the begining and end of the track have unique extensions at the top, that are complementary to a TET-labelled strand (**TET_0**) and a Cy5-labelled strand (**$Cy5_{end}$**) respectively. A **motor** is depicted here with a 3' quencher (black circle) that can reduce fluorescence of nearby fluorophores (the stars). The first anchorage is cut by the nicking enzyme at the **triangle** and the labelled top is removed. The end anchorage has a mismatch in the restriction site (at the 'X') and is not cut, and therefore remains labelled.

be used to bind a complementary fluorophore-labelled strand (Figure 4.5). The first and end anchorage were given unique sequences so that the first anchorage binds to a TET-labelled strand (TET_0), and the end anchorage binds to a Cy5-labelled strand ($Cy5_{end}$). This is unlike ensemble fluorescence measurements in other chapters of this thesis, where F_0 and F_{end} are directly conjugated to staples at the surface of the origami. This requires the normalisation and interpretation of the fluorescence traces to also change.

As F_0 is located above the motor, it is removed from the origami when the enzyme cuts the first anchorage (A_0). Therefore, the signal from F_0 does not show that the motor has stepped away from the beginning of the track (as it would elsewhere in this thesis), but shows that the enzyme has cut A_0, freeing the motor's toehold that is required for stepping onto the next anchorage. In previous 'burnt-bridges' studies[82,102,128], the fluorescence is normalised by adding excess motor that bind to the entire track, giving a baseline level that reflects a fully motor-bound state. However, in this case, because F_0 is removed from tubes that were loaded with a motor, the fluorescence level of F_0 after excess motor does not provide a suitable normalisation. Therefore, F_0 signals have been normalised with respect to their initial level and that just prior to adding excess motor.

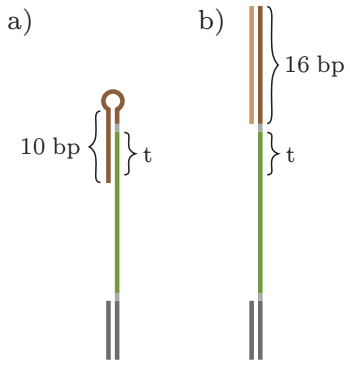


Figure 4.6: Schematics of a mid-track anchorage with a top **extension** that can bind to **another strand** (which is labelled with a Cy3 fluorophore for the microscopy labelled-track experiments). a) Undesired secondary structure allows the anchorage to create a hairpin that covers the 6 nt toehold (t) for the motor. b) The most stable structure when the complementary strand for the extension is included. The structures depicted here were predicted by NUPACK[6] at 37°C.

The end anchorage (A_{end} or B_{end} in the case of the monomer or dimer) has a mismatch in the restriction site to stop the enzyme from cutting, as in other 'burnt bridges' set-ups[1,82,102,128]. Once the motor has arrived at the end anchorage, the extra base pairs formed compared to the 'burnt' track inhibits the motor from diffusing away. This also means that F_{end} is not removed from the tube, and its fluorescence can still be normalised with respect to the fully motor-bound state after excess motor is added (a 6x excess compared to the anchorages). This gives a measure of how many motors have successfully reached the end of the track (as described in Section 2.3.4).

Mid-track anchorages

All the mid-track anchorages have the same domain above the motor-binding site that can be used to bind a fluorophore-labelled strand. This is used during microscopy experiments for labelling the track. Except for in Section 4.2.4, which aims to mimic the labelled-track experiment and binds an unlabelled strand to this domain, the domain was supposed to be unbound during the other ensemble fluorescence experiments.

However, after the experiments had taken place, it was realised that this domain

gave the anchorages undesired secondary structure (Figure 4.6). The top of the anchorage is able to bind to itself to create a hairpin, the 10 nt stem of which covers up the toehold used by the motor to step. This is expected to slow progress of the motor down the track, as the motor will not be able to bind to the next anchorage to initiate stepping until the anchorage's hairpin has sufficiently melted open to allow access.

Sample preparation

The tubes were annealed at 54 nM in 1x NEB 2.1 buffer with a 3x excess of staples, a 5x excess of anchorages and a 6x excess of $Cy5_{end}$ (if required). Any linker staples or poly(dT)-end staples for controlling stacking were added in a 5x excess to the tube. The monomer was annealed with A_1-A_4 anchorages, $Cy5_{end}$ and poly(dT)-end staples to suppress stacking. The dimer was made from an A tube with anchorages A_1-A_{20} and the poly(dT)-end staples for the front of the tube only; and a B tube with anchorages B_0-B_4, $Cy5_{end}$, the linker staples and the poly(dT)-end staples for the end of the tube only. Any anchorage sites not used (e.g. A_5-A_{20} for the monomer) were filled in by the normal staples for the sites.

After the tubes were annealed, they were purified using size-exclusion resin to remove the excess small strands from the larger origami structures. The A tubes were purified before loading the motor-A_0 complex to remove the excess neighbouring bracing staple for A_0. This staple has a complementary 8 nt domain to bind to A_0 and it is possible that the excess bracing staples could bind to the motor-A_0 complex, preventing the staple sequence from having free access to the scaffold strand in the origami, leading to a poor loading efficiency.

The motor was pre-annealed with A_0, TET_0 and any extra necessary strands (see each section for the different details of each experiment), with A_0 at 5 μM in 1x NEB 2.1 buffer. For the monomer, the pre-annealed complex was then loaded at the beginning of the track by incubating it at 37°C for 1 hr with the purified A tubes missing the staple for A_0, in a A_0:tube ratio of 0.95:1. For the dimer, the pre-annealed complex was added to purified A tubes with a full track and purified B

tubes for a 1 hr 37°C incubation. The A and B tubes were added in a 1:1 ratio. As the B tube was annealed with its first anchorage, the motor should only be loaded onto the A tube at the beginning of the track.

Finally, the samples were purified again and KOAc was added to give a final concentration of 50 mM KOAc (necessary for efficient cutting by the enzyme). The samples were placed in a fluorimeter for observation (at ~ 20 nM). Movement of the motor is initiated by the addition of 10 units of Nt.BbvCI, the nicking enzyme.

4.2.2 Walking down monomer and dimer tubes

The movement of a motor was compared for a track of 5 anchorages on a single tube (a monomer) and a track of 26 anchorages crossing two tubes (a dimer) (Figure 4.7). This test was necessary for checking that a simple motor (i.e. no bulky extensions) could move inside a tube and cross between tubes. The motor used was modified with a 3' quencher (at its top end). The motor-A_0 complex was formed by pre-annealing the quencher-modified motor (M_q) with A_0 and TET_0 in the M_q:A_0:TET_0 ratio of 0.9:1:3.

The enzyme should cut A_0 to free the motor's toehold with the same efficiency for both the monomer and dimer tubes, as their starting environments are the same. This would be seen as a similar fluorescence trace for F_0 in both cases. The motor is then expected to arrive at the end of the track more slowly for the long track of the dimer than the short track of the monomer, as the motor will have to take more steps. This would be seen as a slower decrease in the fluorescence signal of F_{end}.

The motor's stepping was initiated by the addition of the nicking enzyme (Figure 4.7). The unquenching of F_0 was indeed similar for both track types. The quenching of F_{end} was slower for the long track than the short track, as expected. Excess motor was finally added to provide a normalisation for F_{end}. These results not only imply successful stepping of the motor down a tube, but also from an A tube onto a B tube. No specific control was made to check that no $M_q.A_0.TET_0$ was initially loaded onto the B tube instead of the A tube (which is not expected as the B tube has no missing staple). However, if the signal from the dimer was actually

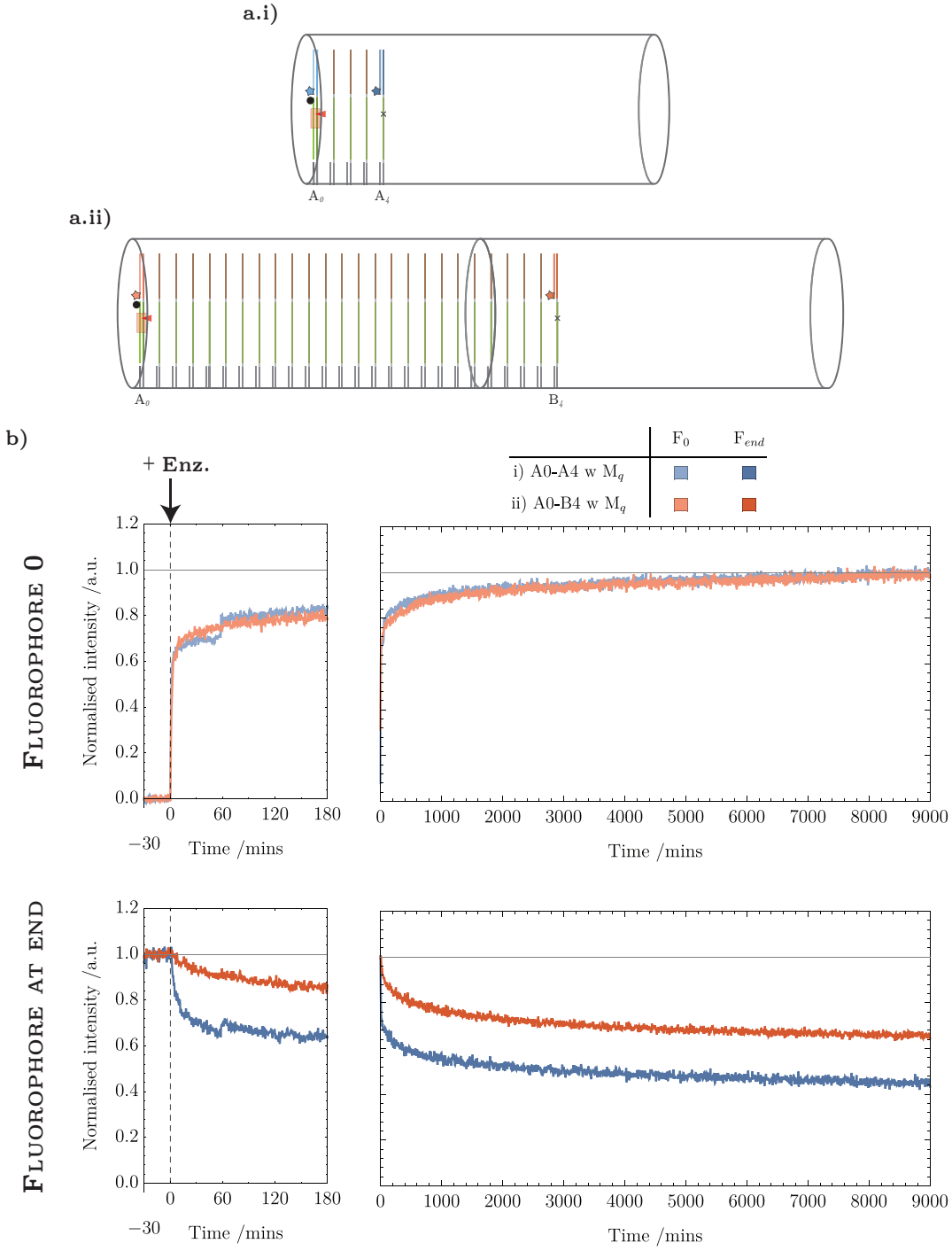


Figure 4.7: Comparison of motors walking down short and long tracks. a) Depictions of the tracks for i) a 5 anchorage track on a monomer tube; and ii) a 26 anchorage track that crosses between two connected tubes (a dimer). b) The normalised fluorescence traces of the fluorophore at the beginning and end of the track (F_0 and F_{end}). The motor was initiated by the addition of the nicking enzyme at $t = 0$ mins. The F_0 signal was normalised with respect to its initial level and the level just before excess motor was added. The F_{end} signal was normalised with respect to its initial and final levels after excess motor was added.

from motors loaded into place at B_0's site, the F_{end} signal would have had similar initial kinetics to the monomer's signal. To be certain that the dimer's quenching of F_{end} is not from motors initially loaded onto the B tube, future work should include a control experiment. For example, only the B tube could be incubated with the pre-annealed M_q.A_0.TET_0; if there is no undesired loading, the tube should not carry a F_0 signal.

As the F_0 fluorescence traces do not fit first-order rate equations well, the stepping rates cannot be easily compared to the rate of the original 'burnt bridges' motor. By comparing the rate of quenching of F_{end} for the short track of 5 anchorages to the Wickham *et al.*'s[102] 8 anchorage track, it seems (qualitatively) that the motor is slower here. This is not surprising, as the undesigned secondary structure of the mid-track anchorages and the more rigid origami platform for the track is expected to slow down the motor.

4.2.3 Walking as a labelled-motor

The microscopy set-up for the labelled-motor observation requires that the motor be able to carry fluorophores through the tube. The $M_{0,2}$ labelled motor was tested here. It has two copies of a domain that is complementary to the dual-labelled $Cy3_M$ strand. To check that this motor is not too bulky to fit inside and step down the tube, ensemble fluorescence measurements were undertaken on the dimer tube as previously described. In this case, the presence of the motor is indicated by FRET between the Cy3s it carries and F_0 and F_{end}. Figure 4.8 shows the energy transfer between the fluorophores, and the change to the recorded signals in the absence/presence of the motor. The motor-A_0 complex was formed by pre-annealing $M_{0,2}$ with $Cy3_M$, A_0 and TET_0 in the $M_{0,2}$:$Cy3_M$:A_0:TET_0 ratio of 0.9:2.25:1:3.

F_0 is a TET fluorophore. In the absence of the motor, the TET will emit at $\lambda_{TET,em}$ when excited at $\lambda_{TET,ex}$. In the presence of the motor, an excited TET will transfer its energy to a nearby Cy3, which will then emit at $\lambda_{Cy3,em}$. The F_0 signal is observed with the following fluorimeter settings: an excitation wavelength of $\lambda_{TET,ex}$ and an emission wavelength of $\lambda_{TET,em}$ (details can be found in Appendix B.6).

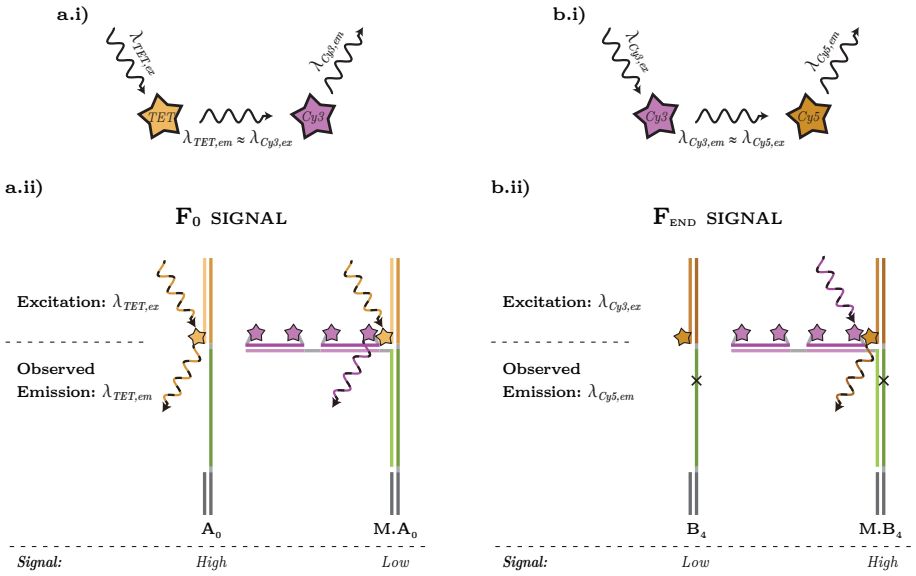


Figure 4.8: A schematic of the FRET between the Cy3 on the motor and a) the TET on the first anchorage and b) the Cy5 on the final anchorage. This allows the motor's presence to be detected at the ends of the track.

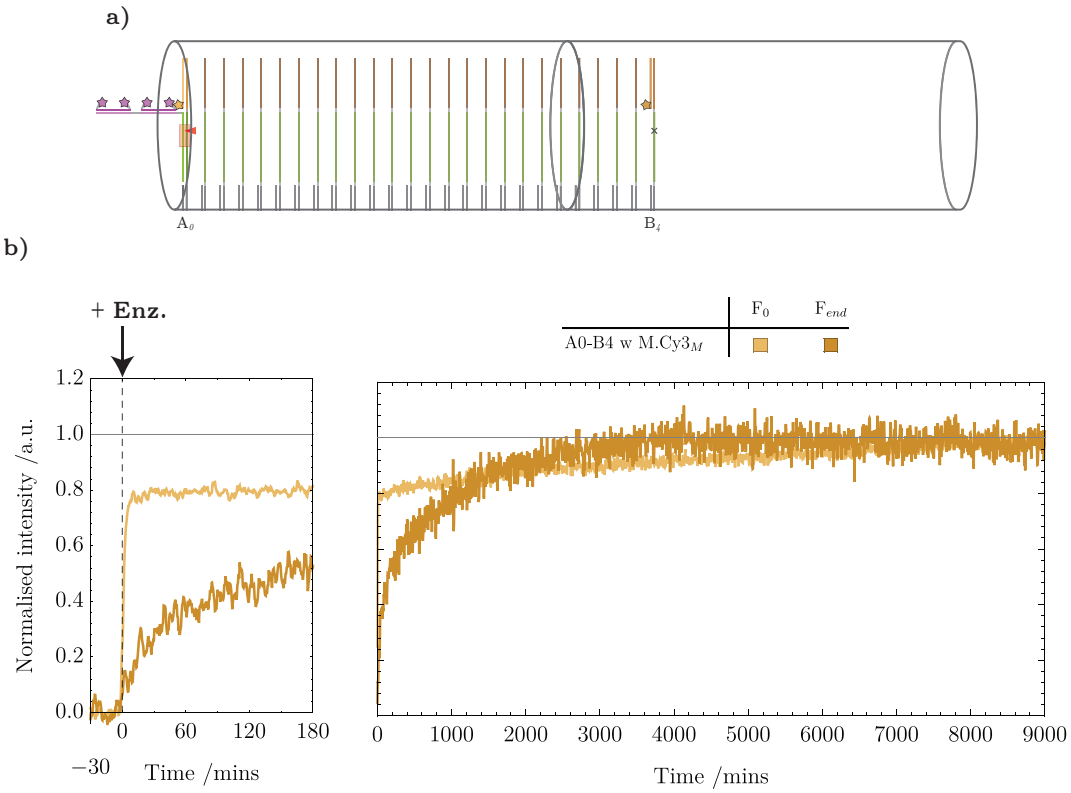


Figure 4.9: a) Depiction of the dimer track with a Cy3-labelled motor. b) The normalised fluorescence traces of the fluorophore at the beginning and end of the track (F_0 and F_{end}). The motor was initiated by the addition of the nicking enzyme at $t = 0$ mins. The fluorescence signals were normalised with respect to their initial level and final levels.

During the experiment, the signal should initially be low while the motor is bound to A_0 as the TET will transfer its energy to the nearby Cy3s instead of emitting itself; and once the movement is initiated, the signal should increase as the Cy3s move away from the TET, reducing the efficiency of the energy transfer between them.

F_{end} is a Cy5 fluorophore. In the absence of the motor, the Cy5 will emit at $\lambda_{Cy5,em}$ only when excited directly at $\lambda_{Cy5,ex}$. In the presence of the motor, an excited Cy3 will transfer its energy to a nearby Cy5, which will then emit at $\lambda_{Cy5,em}$. The F_{end} signal is observed with the following fluorimeter settings: an excitation wavelength of $\lambda_{Cy3,ex}$ and an emission wavelength of $\lambda_{Cy5,em}$ (with a slit width of 5 nm). During the experiment, the signal should initially be low in the absence of the motor as the Cy5 is not being excited; and once the movement is initiated, the signal should increase as motors arrive at B_4 and the Cy5 is excited by the energy transfer from the nearby Cy3s.

Movement was initiated by the addition of the enzyme (Figure 4.9). After which both signals for F_0 and F_{end} increased, as expected for the motor moving down the track. The signal of F_{end} increased more slowly as the motor has to step down the track to reach it. The fluorescence signals were normalised with respect to their initial and final levels. As no controls were performed to check the fluorescence levels in the complete absence or presence of the motor, an accurate percentage of motors reaching the end of the track could not be calculated. However, qualitatively this shows that it is possible for this bulky motor to move inside the tube.

4.2.4 Walking on a labelled-track

The microscopy set-up for the labelled-track observation requires all of the anchorages to have fluorophore-labelled tops. These would be chopped off by the passing of the motor and indirectly indicate the motor's presence along the stacked tube. To avoid having to purchase 21 modified anchorage strands (which is expensive), the anchorages were given the same extra domain above the motor-binding site that is complementary to a fluorophore-labelled strand. This way the entire track can

be labelled with a single strand type.

However, the inside of the tube is limited in space; it has an inner diameter of ∼18 nm. An anchorage is most constrained inside the tube when bound to the motor (with a contour length of ∼18 nm), as it is then made up of three rigid double-stranded domains: the bracing, the motor binding site and the domain binding to the fluorophore-labelled strand. Unbound linker bases between these regions give the strand some flexibility so it can reorientate itself within the tube. It is important for the anchorages to be able to move about within the tube, as a motor-bound anchorage must be able to move into proximity of the next complete anchorage to initiate stepping.

To check that a motor could walk inside a tube under these conditions, the microscope experiment was mimicked using ensemble fluorescence measurements on a dimer tube (Figure 4.10) as described previously. The motor-A_0 complex used here was formed by annealing M_q with A_0 and TET_0 in the M_q:A_0:TET_0 ratio of 0.9:1:3.

Instead of using $Cy3_A$, an unlabelled version was used here to avoid FRET between the Cy3 and F_0 or F_{end}. A 5x excess of the unlabelled strand was added to the mix for the motor-loading incubation. The lack of a fluorophore on these strands should not impact the results, as it is binding of this strand to give a rigid ds-region on the anchorage that is likely to present a problem, not the fluorophore. Due to the undesired secondary structure described in Section 4.2.1, not all of the mid-track anchorages may have bound to the unlabelled strand as planned. However, the positive control sample in Section 4.3.4 was prepared with an incubation of $Cy3_A$ and showed successful track labelling, indicating that it is at least partially effective.

On addition of the enzyme to initiate stepping, the signal of F_0 increased as the enzyme cut A_0, and the signal of F_{end} decreased as motor arrived at B_4 at the end of the track. This means it should indeed be possible to watch motor movement down a labelled-track on the microscope. Excess motor was finally added to provide a normalisation for F_{end}.

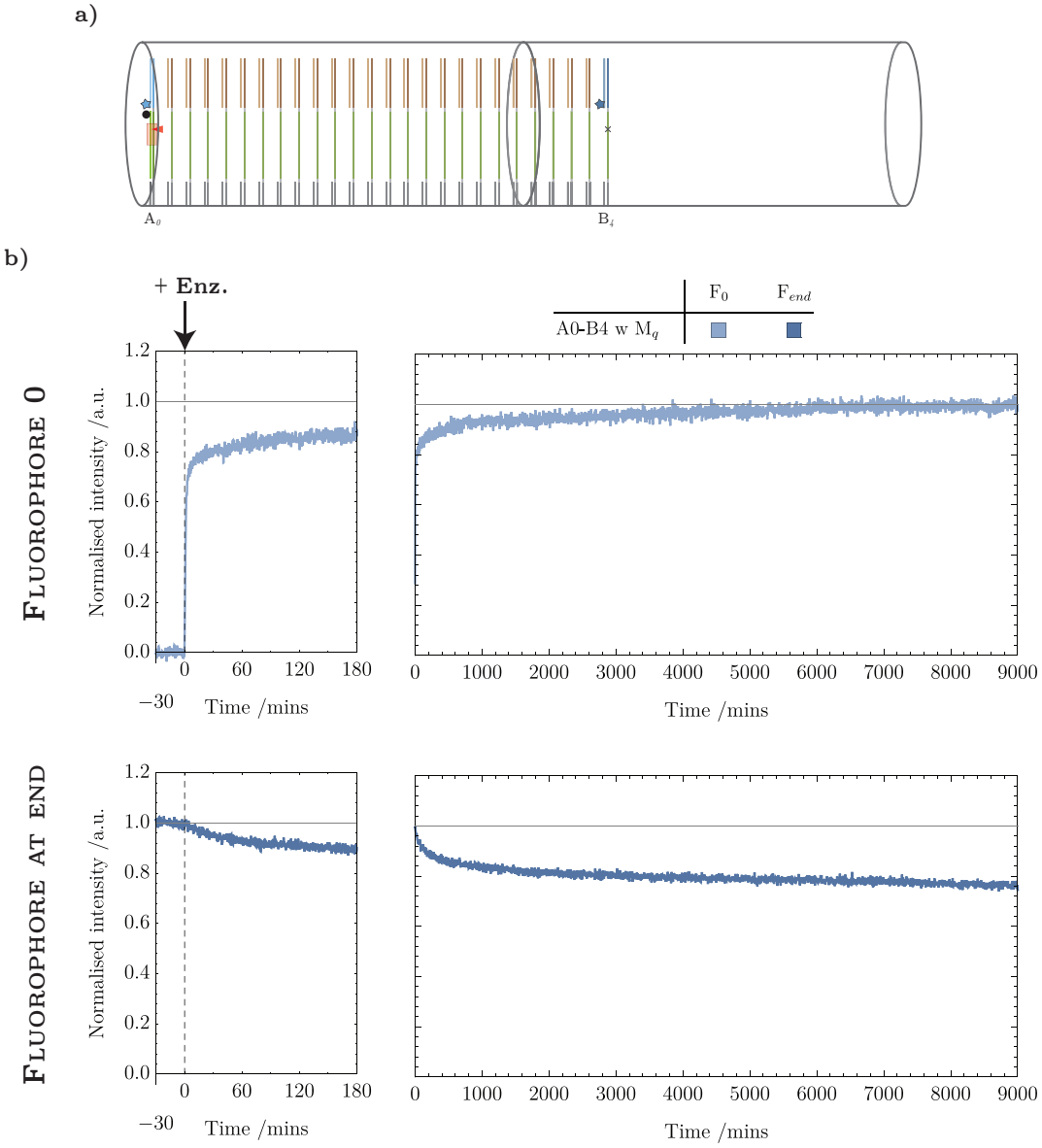


Figure 4.10: Motor movement down a dimer tube when the mid-track anchorages have double-stranded sections above the motor-binding site. This mimics the planned microscopy experiment when the track is labelled with Cy3-labelled strands. a) Depiction of the 26 anchorage track. b) The normalised fluorescence traces of the fluorophore at the beginning and end of the track (F_0 and F_{end}). The motor was initiated by the addition of the nicking enzyme at $t = 0$ mins. The F_0 signal was normalised with respect to its initial level and the level just before excess motor was added. The F_{end} signal was normalised with respect to its initial and final levels after excess motor was added.

4.3 Microscopy

Observations were performed using a Total Internal Reflection Fluorescence (TIRF) microscope[133,134]. A TIRF microscope uses an evanescent wave to illuminate the sample close to the microscope slide surface. This technique is very useful for reducing background fluorescence, as the bulk solution is not illuminated. In order to image the tubes, they were fixed to the surface of a microscope slide using biotin-streptavidin interactions. For the microscope experiments, seven biotins were attached to each tube by modifying seven pairs of staples to have their ends on the outside surface of the tube. One staple from each pair (a 'tether strand') was given a 16 nt extension that is complementary to part of a biotinylated anchor strand. A 14 nt domain separates the tether-binding domain from the biotin-modified 5' end. The biotinylated anchor was included in the origami annealing in a 1.2x excess compared to the tether staples.

The YOYO-1 signal was observed by illuminating with a mercury lamp and using a "wideband interference blue" (WIB) filter cube. The Cy3 signal was observed by illuminating with a 532 nm laser and using a Cy3/Cy5 filter cube (with a power density upper bound of 0.39 $W/\mu m^2$). There is no leakage of the YOYO-1 signal when observing the Cy3 (Appendix B.8.6). Although there is leakage of Cy3 signal when observing the YOYO-1, this is not an issue as the YOYO-1 acts as a bright reference dye and would overwhelm any Cy3 signal.

Slide preparation

A flow channel for the sample was created using an adapted protocol from Machinek 2014[135]. The surface of a microscope slide was treated to control the binding of the tubes. Sequential incubations of 300 nm latex beads, BSA and biotinylated-BSA, streptavidin and the origami sample were interspersed with washes of the origami buffer. The beads were added to help focus on the surface of the slide. The BSA blocks non-specific binding to the glass surface, whilst the biotinylated-BSA bound to streptavidin provides specific anchor points for any biotinylated sample. Finally the channel was washed with an anti-photobleaching buffer before being sealed with

Valap[136] to prevent evaporation and oxidation of the anti-photobleaching buffer (see Appendix B.8 for further details). If a sample required enzyme, the anti-photobleaching buffer contained 500 units/ml of Nt.BbvCI and 50 mM KOAc or NaCl.

4.3.1 Enzyme cutting under microscopy conditions

It was important to check that the nicking enzyme was able to cut a motor-bound anchorage in the different conditions required for the microscopy experiments. Enzyme cutting in three buffers was compared: microscopy buffer (1x TAE, 12.5 mM $MgCl_2$) with 50 mM NaCl, microscopy buffer with 50 mM NaCl and 1/100 YOYO-1 Iodide, and the anti-photobleaching buffer with 50 mM NaCl and 12.5 mM $MgCl_2$. The use of YOYO-1 Iodide here is not completely comparable to that of the staining of the tube samples, as the gel samples were left in a solution of YOYO-1, whereas the tubes were purified to remove any excess. Therefore, this should offer a pessimistic estimate of the cutting efficiency with YOYO-1.

Various versions of a motor-bound anchorage were tested: a simple motor and an unlabelled anchorage (M.A, annealed in a M:A ratio of 1.2:1), a simple motor and a labelled anchorage (M.A.$Cy3_A$, in a M:A:$Cy3_A$ ratio of 1.2:1:1), an extended motor labelled at both ends and an unlabelled anchorage ($M_{1,1}$.$Cy3_M$.A, in a $M_{1,1}$:$Cy3_M$:A ratio of 1.2:2.4:1), and an extended motor labelled twice at the 3' end and an unlabelled anchorage ($M_{0,2}$.$Cy3_M$.A, in a $M_{0,2}$:$Cy3_M$:A ratio of 1.2:2.4:1). Samples of each were prepared with the anchorage strand at 100 nM. 18 μl aliquots were mixed with 2 μl of 10x the appropriate buffer before annealing. One aliquot per sample was used as a reference for the uncut complex, and a second aliquot per sample received 0.5 μl of enzyme. All the samples were then incubated at 37°C for 1 hr. The samples were checked on separate polyacryladmide gels for each buffer condition (Figure 4.11), using a loading dye containing SDS. The gels were stained with Sybr Gold and scanned for the Sybr Gold and Cy3 fluorescence.

Cutting is seen clearly for all motor-anchorage complexes in microscopy buffer with 50 mM NaCl and the anti-photobleaching buffer mix. This is most obvious from

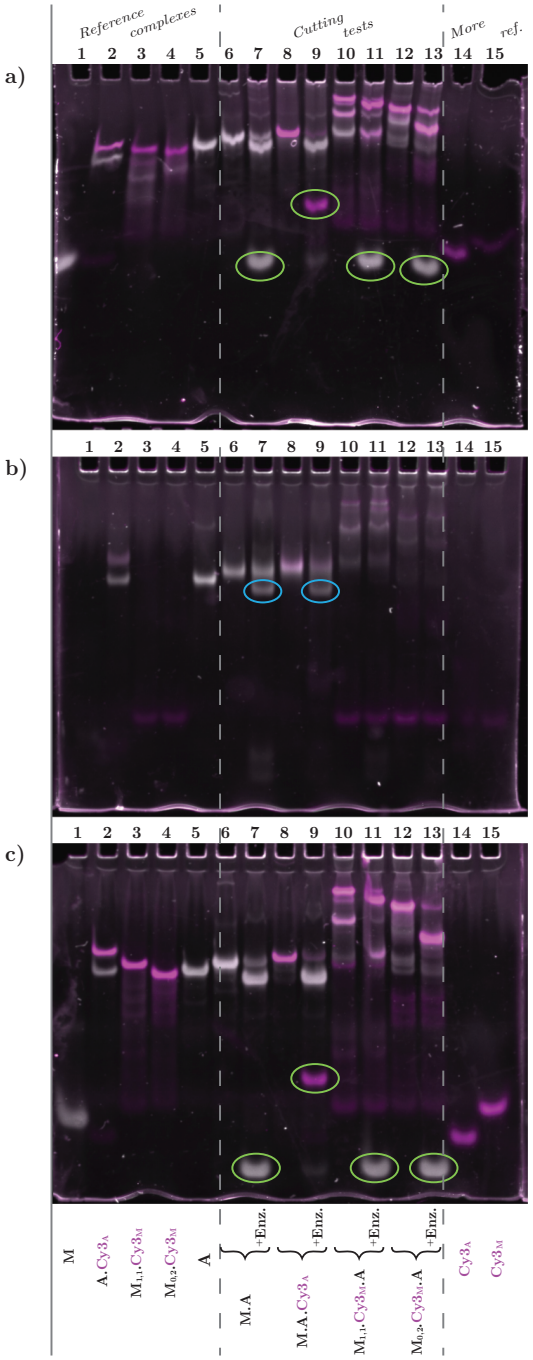


Figure 4.11: Enzyme cutting tests for the various buffer conditions expected for the microscopy experiments: a) microscopy buffer & 50 mM NaCl; b) microscopy buffer, 50 mM NaCl & 1/100 YOYO-1; c) anti-photobleaching buffer, 50 mM NaCl & 12.5 mM $MgCl_2$. Gels were scanned for Sybr Gold (white signal) and Cy3 (pink signal). Green circles highlight the tops of anchorages cut off by the enzyme; where this is not obvious, blue circles highlight the cut motor-anchorage complex. Lanes 1-5 — control samples of M, A.Cy3$_A$, M$_{1,1}$.Cy3$_M$, M$_{0,2}$.Cy3$_M$ and A respectively. Lanes 6-13 — pairs of lanes contain samples of annealed M.A, M.A.Cy3$_A$, M$_{1,1}$.Cy3$_M$.A and M$_{0,2}$.Cy3$_M$.A respectively; the latter of each pair is incubated with enzyme. Lanes 14-15 — control samples of Cy3$_A$ and Cy3$_M$ respectively. Gel details: 15% 29:1 polyacrylamide gels, run at 200V for ∼120 min. Sample details: enzyme digestion used 0.5 μl of Nt.BbvCI (10,000 units/ml) per 20 μl sample, and was incubated at 37°C for 1 hr.

the cut tops of the anchorages in lanes of the gels that had enzyme (highlighted by green circles in Figure 4.11a,c). The cutting in the gel with samples containing YOYO-1 was not as obvious. The signal from the Sybr Gold staining was reduced compared to the other gels as the intercalation of Sybr Gold was in competition with the YOYO-1. Very little Cy3 signal was seen. YOYO-1 and Cy3 can act as a FRET pair, so it is possible that the reduced Cy3 signal is due to accelerated acceptor bleaching of the Cy3[137]. Despite the poor fluorescence, it is still possible to see the cut form of the motor-anchorage complex for M.A and M.A.Cy3$_A$ (highlighted by blue circles in Figure 4.11b) suggesting the enzyme can still cut despite the presence of YOYO-1.

It does not seem that all the Cy3$_M$ is bound to the extended motors, particularly when in the presence of YOYO-1. Cy3$_M$ is only 10 nt long; it was designed to be short to allow two copies to bind to the motor but still fit inside the tube. The gels suggest that a higher GC-content strand or a longer strand should be considered for future work to ensure stable binding. Multiple bands for the motor-bound anchorages are seen, one that is unlabelled (no Cy3$_M$) and two heavier bands for a single-labelled and double-labelled complex. Faint bands for the Cy3$_M$ alone can be seen — the Cy3 signal from these may not be very strong due to self-quenching of the Cy3 fluorophores at either end when the strand is single-stranded and the two ends are closer together. This is supported by the 1.2x relative intensity of the Cy3$_M$ band compared to the Cy3$_A$ band in Figure 4.11c). If there was no self-quenching, the Cy3$_M$ band should be twice as bright as the Cy3$_A$ band, as it is dual-labelled and the same amount of each strand was added. The increase in unbound Cy3$_M$ in the presence of YOYO-1 (seen in lanes 3-4 and 10-13 of Figure 4.11b) may be due to the YOYO-1 causing underwinding in the DNA[138], further destabilising the short duplex.

Table 4.1 quantifies the cutting efficiency of the enzyme for M.A and M.A.Cy3$_A$ in each buffer as an indication of the effect of each buffer on the enzyme. The cutting of M$_{1,1}$.Cy3$_M$.A and M$_{0,2}$.Cy3$_M$.A could not be easily quantified due to the multiple bands for the complexes.

The slight increase in cutting efficiency seen with the anti-photobleaching buffer

Buffer	Complex	Percentage cut
Microscopy buffer & 50 mM NaCl	M.A	86%
	M.A.Cy3$_A$	89%
Microscopy buffer, 50 mM NaCl & YOYO-1	M.A	42%
	M.A.Cy3$_A$	50%
Anti-photobleaching buffer, 50 mM NaCl & 12.5 mM $MgCl_2$	M.A	91%
	M.A.Cy3$_A$	94%

Table 4.1: Cutting efficiencies of Nt.BbvCI over 1 hr at 37°C in various buffers. The percentage of the cut population was calculated as the band intensity of the cut population divided by the sum of the band intensities of the cut and uncut populations on the Sybr Gold stained polyacrylamide gels.

compared to the microscopy buffer is not thought to be significant, but does suggest that efficient cutting is possible in the anti-photobleaching buffer. YOYO-1 staining causes a reduction in the cutting efficiency and destabilises short duplexes. For the microscope experiments, YOYO-1 should be used in much smaller amounts to reduce these negative effects or should be used to stain only strongly-bound non- motor or anchorage strands.

4.3.2 Stained tubes

Stacked tubes were prepared and stained with YOYO-1 Iodide to check for formation. This was done with and without A tubes to cap the front of a stack of B tubes. A 1/100 final dilution of YOYO-1 Iodide was used to stain the tubes for 10-15 mins before the sample was purified. Purification with size-exclusion resin was then able to remove the excess YOYO-1 molecules (as previously used by Lo 2012[139]) as well as the excess staple strands.

The tubes were all annealed at 20 nM. The A tube sample included the poly(dT)-end staples for only the front of the tube, inhibiting any stacking on the front end. The B tube samples included 100 nM of linker staples to promote stacking, and the polymerisation was left at least over night at 4°C. For capped stacks, the separately purified A and B tube stocks were added together in a 1:20 ratio and incubated for

1 hr at 37°C — the A tubes are expected to bind to the front of a stacked B tube, capping it and preventing further polymerisation from that end.

Typical fields of view are shown in Figure 4.12 alongside a depiction of the capping. Figure 4.12c) shows a histogram of the lengths from multiple images (8 and 3 images for the B-only and A:B of 1:20 samples respectively).

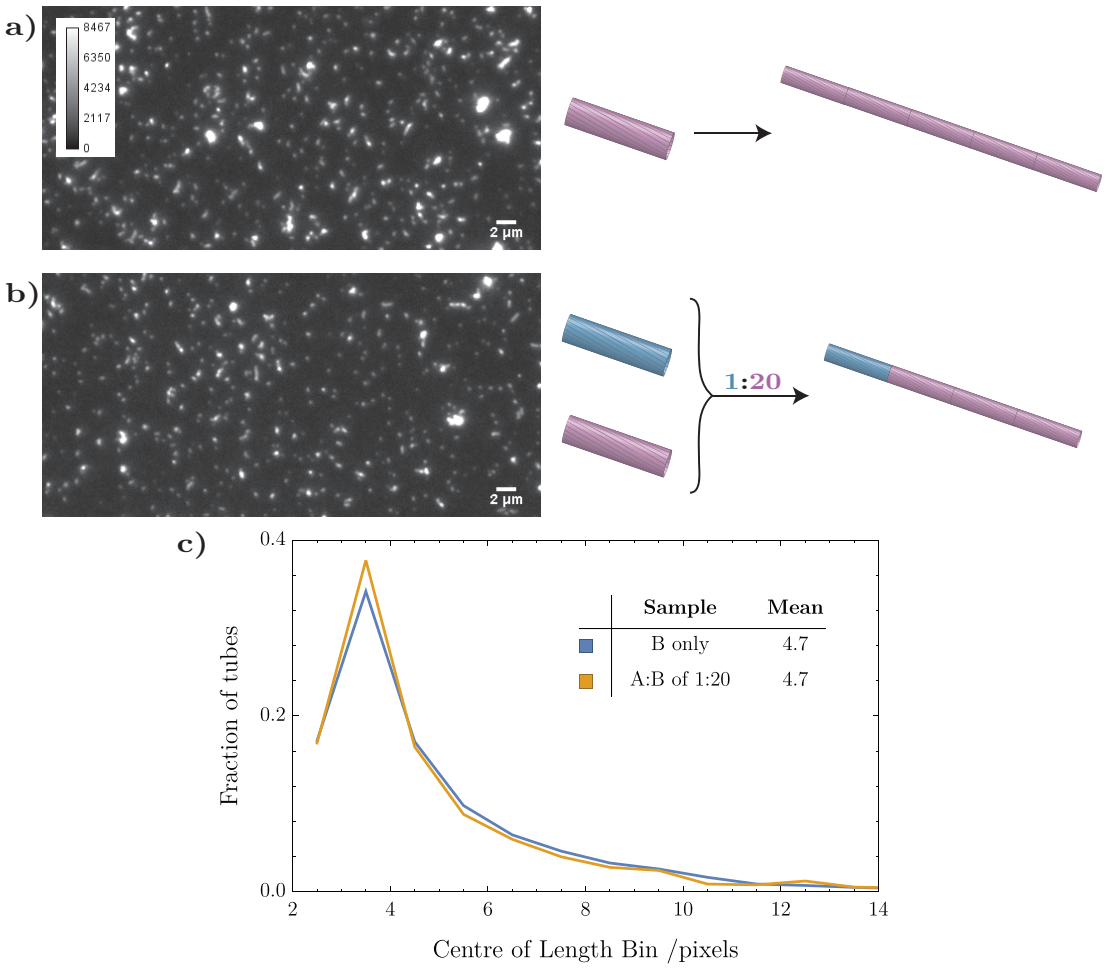


Figure 4.12: Formation of tubes with and without a capping tube ("A tube", in blue) that is able to bind to the front of the main stacking tubes ("B tubes", in purple). a) B-only tubes and b) A capped B tubes with an A:B ratio of 1:20, alongside depictions of the stacked tubes. Typical images are shown with the same brightness/contrast settings. A calibration bar of the pixel values is provided and relevant for both images. Microscope details: WIB filter, illuminated by Mercury lamp, 500 ms exposure, 100 EM gain. c) A histogram of the object lengths over all the images for each sample (8 and 3 images for the B-only and A:B of 1:20 samples respectively). The histogram data had a bin width of 1 pixel.

The length distributions were found by detecting the presence of the tubes, filtering out noise and aggregates, and finding the tube lengths. The tubes were found by using the Laplacian of the Gaussian for edge detection[140,141], then binarising the image and using Mathematica to detect the tubes (see Appendix B.9.1 for the details and Figure A.5 for corresponding images with the detections overlaid). This method makes a good attempt at detecting all of the spots in the image, but is not perfect. The spots that haven't been detected are lower brightness spots.

There was no significant change in the length distribution of the tubes when they were capped with A tubes, which might have been expected if A tubes limit polymerisation of a stack. Evidence of successful capping is being planned by collaborators Florence Benn and Natalie Haley at the time of this thesis's writing, where A tubes are labelled with gold nanoparticles, and stacked tube samples are imaged with a Transmission Electron Microscope (TEM).

4.3.3 Labelled-motor tubes

A labelled motor is the most direct way of being able to observe motor movement, but may give too small a signal or photobleach very quickly. Initial microscopy experiments were performed to check the feasibility of this approach. The labelled motor used here ($M_{0,2}$) has a 3' extension that has two copies of the same domain, which is complementary to a Cy3 strand. The Cy3 strand was dual-labelled at both ends ($Cy3_M$), and hence is able to label each motor with up to four Cy3 fluorophores. Ensemble fluorescence measurements previously discussed in Section 4.2.3 have shown that it is possible for this motor to walk down a track inside a tube despite its bulky extension.

The extended motor was pre-annealed to the Cy3 strands and the first anchorage with a $M_{0,2}$:$Cy3_M$:A_0 ratio of 0.9:2.25:1, with A_0 at 5 μM. Therefore all the motors should be bound to an anchorage strand and be labelled with up to four Cy3s, forming $M_{0,2}.Cy3_M.A_0$. A and B tubes were annealed at 20 nM separately. The A tube anneal included poly(dT)-end staples for the front of the tube and the anchorages for all the track except the first anchorage. The B tube anneal included

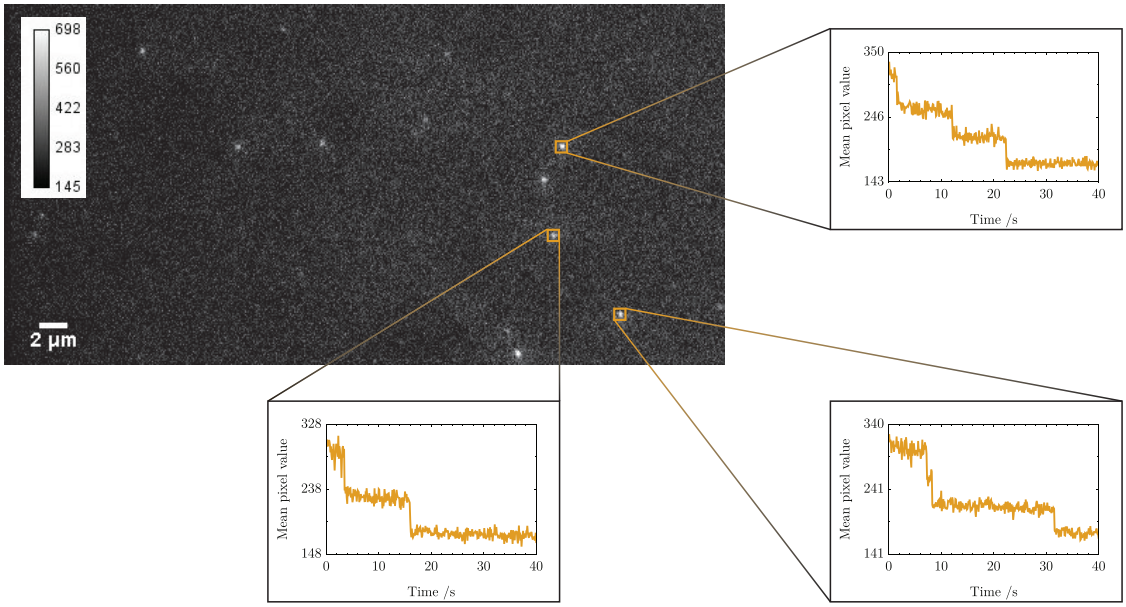


Figure 4.13: Labelled motors (with up to four Cy3 fluorophores) were added to tubes by pre-annealing to the first anchorage, incubating with the defective A tubes missing the staple for the first anchorage, then purifying. Purified B tubes were then added in an A:B ratio of 1:20 and incubated. Displayed here is the first image in a video of an example field of view. The tubes were not stained and so cannot be seen. Bright spots are seen to photobleach in multiple, roughly uniform steps. The intensity traces of three such spots are shown in the insets — the mean pixel value was found for the highlighted square region around each spot for each image in a video. Microscope details: Cy3/Cy5 filter, illuminated with a 532 nm laser, 100 ms exposure, 200 EM gain.

100 nM of linker staples to promote stacking and all the anchorages for the track. $M_{0,2}.Cy3_M.A_0$ was added to the A tubes and incubated at 37°C for 1 hr to load the motor. This was done with A_0 at a 5x excess to the A tubes. The loaded A tube stock and B stock were then purified separately with size-exclusion resin before being combined in a A:B ratio of 1:20. The sample was then incubated at 37°C for 1 hr to encourage capping of the A tube onto the front of the stacked B tube.

When the sample was imaged in the microscope, bright spots were seen to photobleach in steps (Figure 4.13). As fluorescence is proportional to the number of fluorophores, step-wise photobleaching provides a method of counting fluorescent sub-units in a molecule[142]. Up to three photobleaching steps per spot were observed, suggesting that bright spots correspond to motors successfully loaded with both dual-labelled Cy3 strands. Random fluorescent particles on the surface would

be unlikely to give this signal. Presumably a four-step photobleaching trace was not seen because of prior photobleaching and unsaturated binding of the motor with $Cy3_M$. Traces of the mean pixel value (indicating the brightness) within a 8 px×8 px square around three such spots over the course of 40 s are shown in the insets of Figure 4.13. The steps are of uniform height, as expected if each step corresponds to the photobleaching of an individual fluorophore. As the tubes were not stained, they could not be seen in the images, and hence this cannot be used to check for the placement of the motor on single or stacked tubes.

This suggests that it is possible to use this labelled motor for observing movement down a tube. However, the snapshots of the motor's position would need to be relatively infrequent and the sample would need to be protected from light in between observations as photobleaching is likely to be the biggest issue for this system.

4.3.4 Labelled-track tubes

A labelled track that loses its fluorescence once the motor has moved down it is an indirect way of observing the motor. Labelling the track instead of the motor provides a brighter signal that should be more resilient to photobleaching and hence is a worthwhile alternative to explore. The track is labelled by $Cy3_A$ strands that bind to complementary extensions at the top of the anchorages. Once the enzyme cuts a motor-bound anchorage, this labelled top will diffuse away, removing the fluorescent signal from 'burnt' track behind the motor. Ensemble fluorescence measurements described in Section 4.2.4 have shown that a motor is able to move down such a track despite the bulkier anchorages of this system.

Initial experiments with the microscope involved measuring the average brightness over time of aliquots of the same sample with and without enzyme (Figure 4.14a-b). The aliquot without enzyme serves as a negative control. $M.A_0$ was pre-annealed with a $M:A_0$ ratio of 0.9:1, with A_0 at 5 μM. The tubes were annealed with all of the anchorages and with $Cy3_A$ in a 1:1 amount relative to the anchorages. The $M.A_0$ stock was added to the defective A tubes to load the motor over 1 hr at

37°C. The A and B tube stocks were then purified separately and combined in a A:B ratio of 1:20 with extra linker staples (at 100 nM). Aliquots of the sample were put into different flow channels. The negative control sample received plain anti-photobleaching buffer, whilst the main sample received enzyme-containing anti-photobleaching buffer. The first images of the main sample and the negative control were taken roughly 15 mins after the anti-photobleaching buffer (with or without enzyme) had been put into the flow channels.

Figure 4.14a-b) shows typical images of the samples taken on the day of preparation (day 1) and a number of days afterwards. In the intervening times the samples were kept wrapped up in aluminium foil (to reduce photobleaching) in an incubator at 37°C. However, it is thought that the key changes to the sample would actually have happened within the first few hours and so these images are not able to really show the difference between the main sample and the negative control. As the samples were aliquoted from the same stock and the flow channels were prepared at the same time, the main sample before the enzyme was added should have looked similar to the negative control on day 1. The day 1 images for the main sample are less bright than the negative control (Figure 4.15), suggesting that the motor may have already moved down the track and the 'burnt' track is causing the reduced fluorescence. However, to be certain of these results it would be best to have images taken before and after the enzyme was added to the same sample.

A positive control was separately made by adding excess motor strands — this test would not require the motor to be able to move down the track, but checks for enzyme cutting of the anchorage and the reduction in signal from $Cy3_A$ diffusing away. The positive control was made in a similar way to the main sample and the negative control, except that the tubes were not annealed with the $Cy3_A$ strands; instead these were added to the A tubes at the same time as $M.A_0$ for the incubation step, and were added to the annealed B tubes for a 1 hr, 37°C incubation before purification. The sample was prepared and placed in a flow channel with anti-photobleaching buffer containing enzyme (as done with the main sample), imaged and then had its buffer replaced with anti-photobleaching buffer containing enzyme and excess motor (a 10x excess compared to the total number of anchorages that

was passed through the flow chamber). This allowed images to be taken before and after the excess motor was added, to better compare the changes to this exact microscope slide sample.

Figure 4.14c) shows typical images of the positive control taken on the day of preparation before and after excess motor, and a number of days afterwards. In the intervening times the sample was kept wrapped up in an incubator at 37°C. There is a sharp decrease in the sample brightness once excess motor was added (Figure 4.15). This suggests that the enzyme is successfully cutting off the labelled top of the anchorages in the presence of the motor, and that the labelled tops are able to diffuse into solution.

Incubating the annealed tubes with $Cy3_A$ compared to annealing the tubes with it was not initially expected to make a difference, as the $Cy3_A$ binds to extensions on the tubes and are not part of the integral origami structure. However, after the experiment it was realised that the top of the anchorage that binds to $Cy3_A$ has undesired secondary structure (as described in Section 4.2.1). This means that incubating the annealed tubes with $Cy3_A$ may be less effective at loading the strand than annealing it with the origami (when the anchorage secondary structure will have melted, making it easier for $Cy3_A$ to bind).

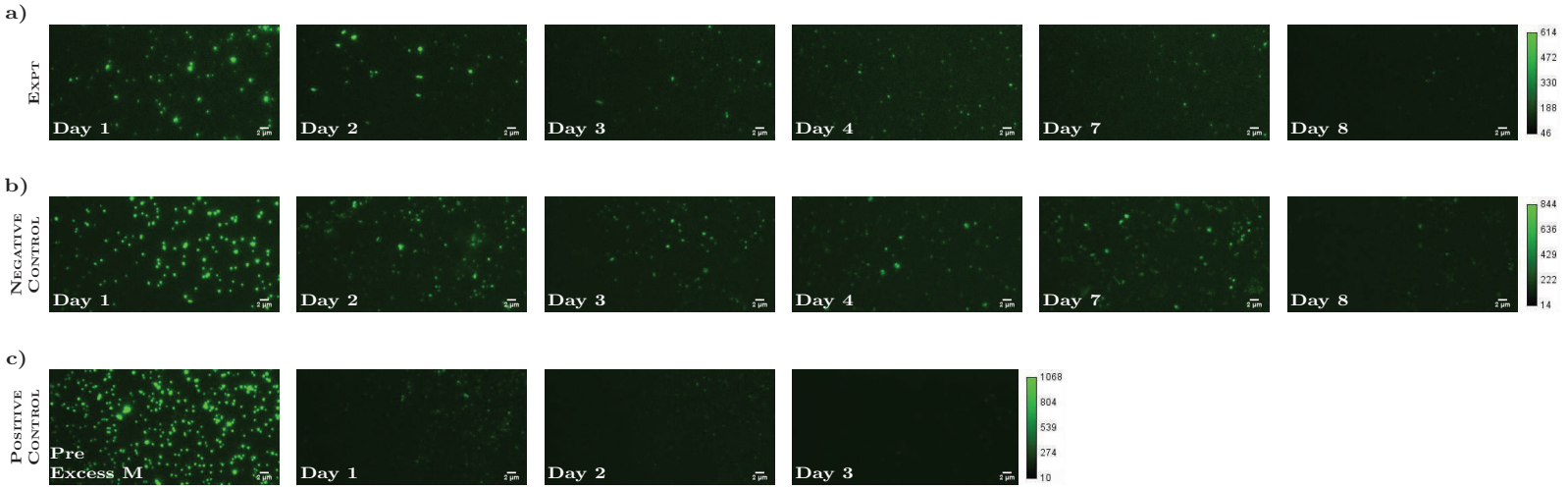


Figure 4.14: Examples of typical fields of view when observing stacked tubes with Cy3-labelled tracks over multiple days. A motor is loaded onto an A tube that is able to cap the front of stacked B tubes. The tubes have full tracks that are labelled with $Cy3_A$ strands that bind to the top of the anchorages by a-b) including $Cy3_A$ in the tube anneal or c) incubating annealed tubes with $Cy3_A$. a) The main sample has enzyme in the buffer to enable the motor to step down the track, chopping off the $Cy3_A$. b) The negative control without enzyme; photobleaching should be the only effect reducing the fluorescence. c) The positive control has excess motor strand and enzyme in the buffer; the motor strands bind to the entire track which should then get cut quickly by the enzyme. Images for the positive control were also taken prior to exchanging the buffer to add the excess motor. All the images for each sample have the same brightness/contrast settings and have a single appropriate calibration bar. Microscope details: Cy3/Cy5 filter, illuminated by the 532 nm laser, 100 ms exposure, 100 EM gain.

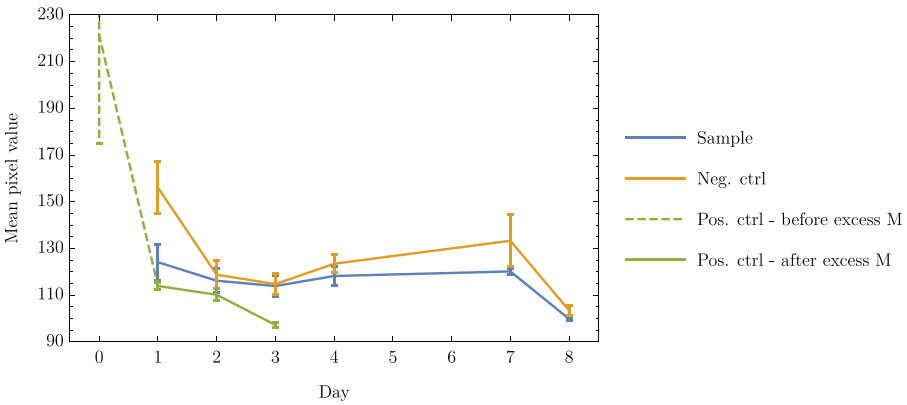


Figure 4.15: The mean pixel brightness over time for the main sample, the negative control and the positive control. This was averaged over 5-6 images taken each day per sample, the standard deviation providing the error bars. The dashed line and data point at "Day 0" for the positive control reflects the data before the excess motor is added.

Flashes of the $Cy3_A$

Videos of the enzyme-containing samples show flashes that are thought to be from the cut labelled-tops of the anchorages floating free in solution. Images from the videos are displayed here, but unfortunately are not as clear at showing the flashes as the videos. Flashes are most obvious in a video for the positive control, taken on the same day that the enzyme and excess motor was added (Figure 4.16). Snapshots from day 8 of the main sample also shows flashes (Figure 4.17), though these are not as numerous and were not obvious on the first day that the enzyme had been added. This is presumably related to the slower rate of cutting and the lower density of the sample. For comparison, snapshots of the video of the negative control on day 8 are also displayed, in which flashing signals were not seen (Figure 4.18).

As the video snapshots fail to show flashes clearly amongst the bright, static structures, median subtracted versions were made. First, the median pixel value for each pixel over all 10 images in the video was found. The median subtracted image was created by taking each pixel and subtracting its median value, and then dividing by the median value. The image was then normalised with respect to its 0.001th and 0.999th quantile values (the minimum and maximum values are too sensitive to outliers). Large pixel values, therefore, represent pixels that are

unusually bright compared to the entire video, and low pixel values are pixels that are unusually dark. The general image looks grey, showing little deviation from the median overall. This highlights the flashes, the temporary bright spots that are seen in the videos, as bright spots in the median subtracted images.

In a similar way to the tube detection in Section 4.3.2, the spots in the median subtracted images were detected and have been highlighted here in corresponding images with the displayed snapshots (details can be found in Appendix B.9.1). The total number of detected spots in the videos for the main sample, the negative control and the positive control are 58, 3 and 595 respectively.

Figure 4.16: a) Sequential snapshots of a video for the positive control, separated by 100 ms. Microscope details: Cy3/Cy5 filter, illuminated by the 532 nm laser, 100 ms, 100 EM gain. The calibration and scale bar are appropriate for all images. b) Median subtracted images corresponding to the images above. Bright spots show unusually bright pixels, most of which correspond to the flashes seen in the video. c) Detected spots in the median subtracted images are highlighted here by overlaying the images with their fitted ellipses in red. A total number of 595 detected spots were found over all 10 images in the video.

Figure 4.17: a) Sequential snapshots of a video for the main sample, separated by 100 ms. Microscope details: Cy3/Cy5 filter, illuminated by the 532 nm laser, 100 ms, 100 EM gain. The calibration and scale bar are appropriate for all images. b) Median subtracted images corresponding to the images above. Bright spots show unusually bright pixels, most of which correspond to the flashes seen in the video. c) Detected spots in the median subtracted images are highlighted here by overlaying the images with their fitted ellipses in red. A total number of 58 detected spots were found over all 10 images in the video.

Figure 4.18: a) Sequential snapshots of a video for the negative control, separated by 100 ms. Microscope details: Cy3/Cy5 filter, illuminated by the 532 nm laser, 100 ms, 100 EM gain. The calibration and scale bar are appropriate for all images. b) Median subtracted images corresponding to the images above. Bright spots show unusually bright pixels. c) Detected spots in the median subtracted images are highlighted here by overlaying the images with their fitted ellipses in red. A total number of 3 detected spots were found over all 10 images in the video.

4.4 Discussion & future work

This chapter has presented a couple of possible approaches for observing a 'burnt-bridges'-like motor that walks down a track inside an origami tube. This system is not unlike the transportation of kinesin or dynein motor proteins that step down microtubules inside cells[143]. The ability to stack the tubes to micrometer lengths extends the track to scales that are observable with an optical microscope even without super-resolution techniques. Preliminary tests were performed using two approaches for observing motor movement both directly and indirectly using Cy3 fluorophores. YOYO-1 Iodide was used to stain the tubes, providing a bright signal that could be used as a reference dye for tube position.

Ensemble fluorescence measurements were performed to check the feasibility of the proposed systems. The results suggested successful movement of the motor down the track. This shows not only walking of the motor within an enclosed origami, but also between two connected origami.

The motor was loaded onto the beginning of a stacked tube in a three-step process. The motor was attached to the first anchorage by pre-annealing them together. The motor-first anchorage complex was then incorporated into a single monomer tube (an A tube) via a staple repair incubation. The A tube, which can only connect to another tube from the opposite side to the motor's location, was finally incubated with stacked tubes (B tubes). The A tube should then cap a stack of B tubes such that the motor is at the front end of the stack, with anchorages only extending in one direction. Proof of successful capping is in progress by collaborators Florence Benn and Natalie Haley, who are aiming to confirm this method works by labelling the A tubes with gold nanoparticles, and using TEM to check that the A tubes (labelled) are capping the B tubes (unlabelled).

Direct observation of motor movement involved labelling the motor with two copies of dual-labelled Cy3 strands. Preliminary microscopy experiments were able to detect individual motors, with total photobleaching of the Cy3s occurring within $\sim 40\,\mathrm{s}$. The biggest problem with this approach is that a motor may not remain observable for long enough to step down the track. A few alterations could be made,

such as increasing the melting temperature of the domain for the Cy3 strand to ensure a fully-labelled motor (there was evidence that the strands did not bind fully), or the use of a motor synthesised using Cy3-dCTP bases (Amersham Biosciences). Cy3-dCTP bases could increase Cy3 labelling of the motor, attaching one Cy3 fluorophore for each C base in the motor's sequence. A benefit of directly labelling the motor is that it can be localised by super-resolution microscopy.

The indirect observations involved labelling the tops of the anchorages with a Cy3 strand, such that the fluorescence is removed from cut anchorages behind the motor. Images of a sample were taken after the enzyme was added, and compared to a negative control that did not receive the enzyme. The enzyme-added sample was darker than the negative control, suggesting that the motor was walking down the track and the labelled anchorage-tops were cut off. However, this would be more convincing if the experiment was repeated with images also taken prior to the enzyme addition, in case fewer tubes (or aggregates) were originally bound to the surface of the flow channel. A positive control, where excess motor was added with the enzyme to bind to all of the anchorages, allowing the enzyme to cut the entire track without the motor walking, acted as a proof of principle for the fluorescence change. Images were taken before and after the enzyme and excess motor addition, showing a sharp decrease in brightness after the addition. This indicates successful cutting of the anchorages and diffusion of the labelled tops out of the tube. Videos of the main sample and positive control also showed bright flashes that are interpreted as the cut labelled anchorage-tops diffusing free in solution. These were not observed for the negative control without enzyme, as expected; further evidence that the enzyme was successfully cutting the anchorages.

The preliminary investigations involved taking sets of images each day over multiple days. However, changes in the brightness of the labelled-track seemed to occur on a time-scale shorter than the separation of these images. Future experiments would benefit from ensuring that sets of images are taken before enzyme is added, and as quickly as possible after the addition. Subsequent images should then be taken roughly ever hour afterwards (or more frequently if photobleaching allows). Ideally the same tubes would be imaged over the entire period of time for real-time

observation. This would require the microscope set-up to allow enzyme to be added without moving the microscope slide, and for drift of the slide to be minimised.

An alternative labelling technique is to use DNA-PAINT (DNA points accumulation for imaging in nanoscale topography, previously introduced in Section 1.3)[106,107]. DNA-PAINT not only combats the effects of photobleaching, but can also be used for super-resolution microscopy. DNA-PAINT could be used for labelling the motor or the anchorages of the track. As the domains for the labelling strand must be short, this would also minimise the amount of DNA within the tube, which may speed up motor movement or leave space for a cargo to be transported through the tube.

Single-molecule observations of this system could allow analysis of how modifications to the motor and track change the speed of motor movement. Enclosing motors within origami structures could also be used for the transport of a cargo (attached to the motor) over micrometre length-scales. The tubes could provide protection of the motor and/or cargo from large components in solution.

Chapter 5

Investigations of DNA Origami with Single-Molecule FRET

This chapter reports on investigations of the structure of staple extensions, often used to functionalise DNA origami, using single-molecule Förster resonance energy transfer (smFRET). The sequence of a staple defines its position within the origami. Therefore, attachment of a functional molecule to an extension from a staple end can be precisely placed. Specifically in this thesis, this is used extensively for providing the tracks for motors (each anchorage is an extension to a staple) and fluorophores for detecting the presence of the quencher-carrying motor. More generally, this technique has been used for functionalising origami with a wide-variety of molecules including proteins[23,24] and inorganic nanoparticles[25,26].

Origami are often functionalised on a particular surface, e.g. a cargo inside an origami cage (see Chapter 6 for more details), or a continuous track of anchorages on the same side of an origami tile. However, it has been shown that ss-extensions are able to thread through holes in the origami tile[144], which would functionalise the wrong surface. Staple threading was previously shown by adsorbing origami to a surface, and using time-lapse AFM to observe streptavidin binding to biotin-modified extensions of a subset of the staples[144]. This was seen even when the

origami was face-down (with extensions originating from the side of the origami next to the surface), indicating that the extensions are able to thread through to the open side. The streptavidin binding rate was dependent on the extension length, plateauing around 10 dT. Although these experiments show that threading occurs when the extensions are trapped between the origami and the surface (where there are limited degrees of freedom), they do not say anything about threading through an origami free in solution. This chapter investigates the threading of a ss-extension through an origami floating free in solution. Two techniques for reducing threading are explored.

Figure 5.1 shows the relatively open weave of an origami tile. The parallel helices come together at 'crossovers', where a staple or scaffold strand is exchanged between two neighbouring helices. Between these crossovers, the helices separate, creating holes through which extensions can thread. There are three different-sized holes in the origami tile, the smallest and biggest at the 'seam', the centre of the origami where the scaffold strand is exchanged at crossovers.

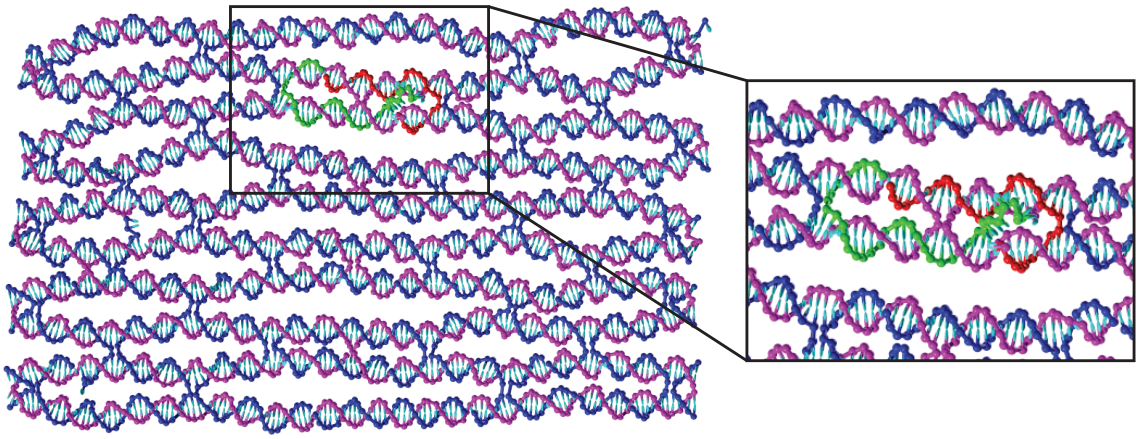


Figure 5.1: A simulated structure of a small DNA origami tile showing its open weave[109]. To help visualization, an attractive surface has been used to flatten the origami. The staple lengths and types, and the crossover points between parallel helices are the same as the full origami tile used in the experiments. Two neighbouring staples are highlighted: the red staple has a 2 dT extension and the green staple has a 10 dT extension. The extensions originate at the same join between the staples — the same as the staples used in the threading experiments in Section 5.3.1. The **scaffold** and the **unextended staples** are coloured in purple and blue respectively.

An alternative method of functionalising an origami is to anneal it with all

the staples except for the modified staple, and subsequently incubate the annealed ('defective') origami with the modified staple. The principle is that the origami is able to undergo 'staple repair': the staple initially binds to an accessible part of the ss-scaffold strand, and the rest of the staple winds around the helix to hybridise completely.

This technique is particularly useful for a couple of special cases. The first is if the staple of interest has a modification that would be degraded by the annealing process used to assemble the origami, e.g. by the buffer conditions or annealing temperatures. Secondly, it is useful for controlling the placement of an oligonucleotide cargo that hybridises to the staple extension, when similar extensions on other staples are also present. This is the case for the motor experiments in this thesis, which are based on the original method by Wickham *et al.* 2011[82] — the motor (a cargo) is pre-annealed to the first anchorage (an extended staple) to set its initial position on the track, before being loaded onto the origami via a staple repair incubation. As the efficiency of staple repair has not been quantitatively measured, experiments were performed to investigate the staple repair of a staple with a ss- or ds-extension.

Single-molecule FRET is a powerful tool for looking at individual structures. Not only is it sensitive to nanoscale changes in distance, it can also highlight heterogeneity in the system, allowing different populations with different structures to be identified. The basic theory of FRET is outlined in Section 5.1. The experimental set-up and data analysis is described in Section 5.2.

Threading of single-stranded extensions in an origami is explored in Section 5.3, and the repair of extended staples is discussed in Section 5.4.

The experiments in this chapter were done in collaboration with Dr Timothy D. Craggs, a FRET specialist who provided the microscope and helped run all of the FRET measurements on the samples. He also performed the data analysis as summarised in Section 5.2.2, and was instrumental at helping to interpret the data.

The multi-layer origami used in Section 5.3.3 was originally designed by Dr Robert Schreiber, a colleague, for another purpose. He was kind enough to provide

the strands and show me the protocol for assembly.

The simulation of the small DNA origami tile, used to show the weave of the helices, was produced by Flavio Romano. Behnam Najafi kindly provided the depiction of the structure in Figure 5.16.

5.1 Theory

5.1.1 Fluorescence

Fluorescence is a type of luminescence, which is the emission of light from a substance (e.g. a fluorophore) in an excited electronic state[105]. Jablonski diagrams are a useful way of showing the processes involved in the absorption and emission of light (an example is provided in Figure 5.2). Horizontal lines depict the electronic energy levels of the ground state (S_0) and excited states (S_1, S_2, etc); thick lines indicate the vibrational ground level of the state, and thin lines indicate higher vibrational levels of the state. The vertical height reflects the energy of the state. Transitions between states are depicted as arrows.

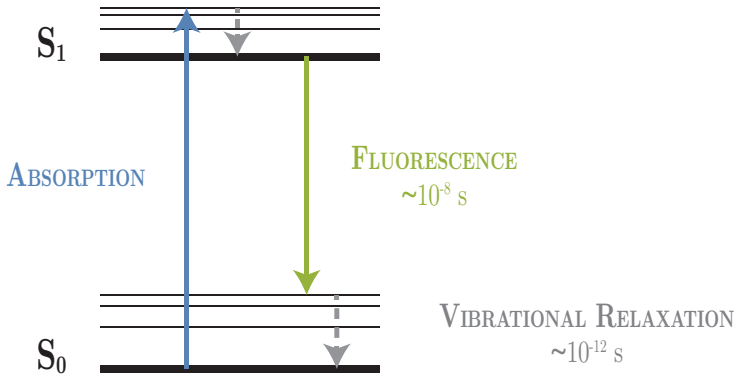


Figure 5.2: An example of a Jablonski diagram, depicting the ground state (S_0) and an excited (S_1) energy state. Ground levels are depicted by thick horizontal lines, whilst higher vibrational energy levels are depicted by thinner lines. Arrows show energy transfer between levels. Rough time-scales are provided for vibrational relaxation and flourescence[105].

A fluorophore is excited if an incoming photon has an energy that matches the energy difference from the ground state to a higher-energy state (e.g., $S_0 + hc/\lambda_{ex} \rightarrow$

S_1, where hc/λ_{ex} is the energy of the absorbed photon). When a photon is absorbed, an electron transitions from the ground state to an excited state; if it is excited into a high vibrational level, it will quickly undergo vibrational relaxation and fall into the lowest vibrational level of that state. The fluorophore can then return to the ground state in a number of ways, including: by fluorescence (return from an excited singlet state), phosphorescence (return from an excited triplet state), collisional quenching (by contact with another molecule) and non-radiative pathways. In this chapter, fluorescence and FRET (a non-radiative process) are most relevant and will be discussed in further detail.

During fluorescence, a photon is emitted by an excited fluorophore. It normally has a lower energy (longer wavelength) than the absorbed photon (e.g., $S_1 \rightarrow S_0 + hc/\lambda_{em}$+heat), as described by the Stokes shift (highlighted in Figure 5.3). Common causes are the loss of energy during vibrational relaxation in the excited state, and transitions to high vibrational levels of the ground state after emitting the photon (the Franck-Condon principle[105]).

5.1.2 FRET

Förster resonance energy transfer (FRET) is the non-radiative energy transfer between a 'donor' fluorophore and an 'acceptor' chromophore (which may also be a fluorophore)[145,146] . This occurs when there is spectral overlap of the emission spectrum of the donor and the excitation spectrum of the acceptor (Figure 5.3). An excited donor is able to return to the ground state by transferring its energy to an acceptor through dipole-dipole coupling. No photons are actually exchanged between the donor and acceptor, which makes the other often-used name of "fluorescence resonance energy transfer" a misnomer.

The rate of energy transfer ($k_T(r)$) is dependent upon the distance between the donor and acceptor, according to

$$k_T(r) = \frac{1}{\tau_D}\left(\frac{R_0}{r}\right)^6, \tag{5.1}$$

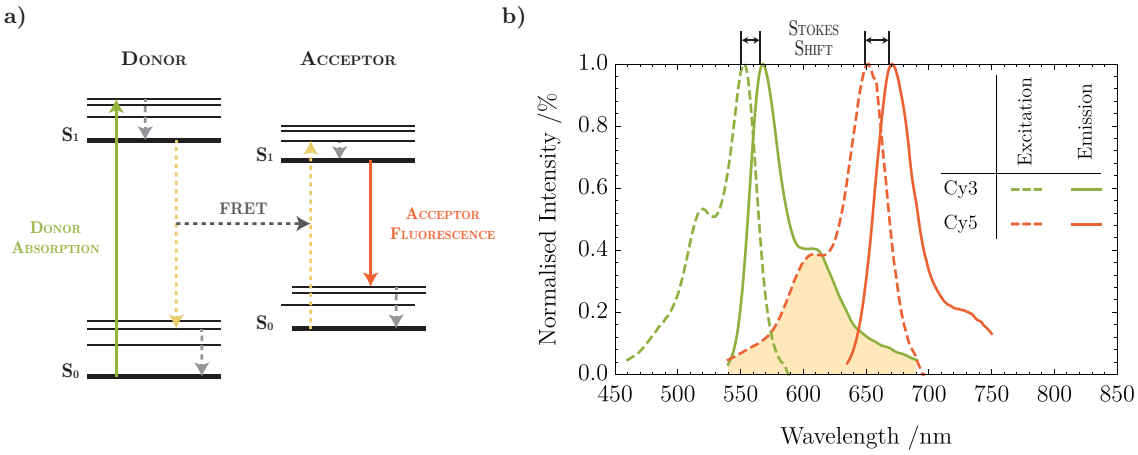


Figure 5.3: a) Jablonksi diagram to show FRET between a donor and an acceptor. An excited donor can return to the ground state via dipole-dipole coupling to an acceptor. The excited acceptor can then return to the ground state by emitting a photon. b) The excitation and emission spectra of Cy3 and Cy5 fluorophores (data provided by Chroma). The shift in peak position of the spectra to longer wavelengths (lower energies) is described by the Stokes shift. Cy3 (the donor) and Cy5 (the acceptor) are a FRET pair. The overlap of the Cy3 emission and the Cy5 excitation spectra is highlighted by the yellow shading.

where τ_D is the lifetime of the donor in the absence of the acceptor, r is the donor-acceptor separation, and R_0 is the Förster radius of the donor-acceptor pair. The r^{-6} dependence arises from the dipole-dipole interaction between the fluorophores. The interaction energy of two dipoles is proportional to the square of the electric field, which falls as r^{-3}.

The efficiency of energy transfer (E), which is the ratio of the energy transfer through FRET to the total energy transfer, is given by

$$\mathrm{E} = \frac{k_T(r)}{\tau_D^{-1} + k_T(r)} = \frac{1}{1 + (r/R_0)^6}. \tag{5.2}$$

R_0 is defined as the distance at which the FRET efficiency is 50%. It is dependent upon various properties of the donor and acceptor. A Cy3/Cy5 FRET-pair, as used in this chapter, has $R_0 \approx 6\,\mathrm{nm}$[147]. The distance-dependence of the FRET efficiency is plotted in Figure 5.4. As it is sensitive to nanoscale distances it can be used as a nanoscale ruler[145,148,149], which makes it a powerful tool for studying the structure and interactions of proteins[137,150,151], DNA[152], RNA[153] etc.

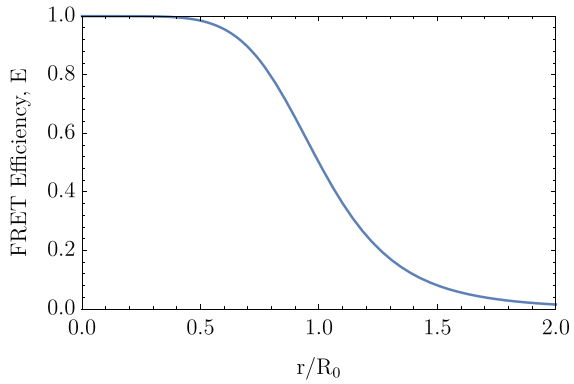


Figure 5.4: Plot of the FRET Efficiency (E) with r/R_0, where r is the distance between the donor and acceptor. R_0 (the Förster radius) is defined as the distance when $E = 0.5$.

5.2 Experimental set-up

5.2.1 Single-molecule FRET & ALEX

Single-molecule FRET[148,154] (smFRET) is able to detect different conformations of molecules, either immobilized on a surface or in solution. This makes it a powerful tool for investigating DNA origami whose natural environment is often floating free in solution. In this chapter, smFRET data was collected using a confocal microscope. A focused laser beam illuminates a femto-litre volume, in which freely-diffusing origami is excited and from which the emitted light is observed. The origami can only be viewed for $\sim 1\,\text{ms}$, the time is takes to diffuse through the volume; so it gives a snapshot in time of the structure but is unable to say anything about its history. As fluorophores outside this confocal volume are not illuminated, they do not photobleach and do not contribute to the background signal.

The sample was illuminated under alternating-laser excitation (ALEX) to excite first the donor and then the acceptor. The fluorescence intensities of the donor and acceptor emission were recorded after each excitation(in the 'donor channel' D and 'acceptor channel' A respectively). ALEX allows filtering for correctly-labelled species bearing an active donor and an active acceptor[148,155], briefly described in the following section.

5.2.2 Data analysis

As a labelled origami diffuses through the confocal volume, the background fluorescence is punctuated by bright bursts. For each burst, the apparent FRET efficiency (E^*) is calculated as

$$E^* = \frac{F_{DA}}{F_{DA} + F_{DD}}, \tag{5.3}$$

where F_{ij} refers to the fluorescence intensity collected in the j channel when excited in the i channel. Molecular conformations with different donor-acceptor distances are seen as peaks in a histogram of E^*. While this uncorrected FRET efficiency does not yield accurate, absolute distances, it does provide quantitative relative-distance information, which is sufficient for this study.

The selection criteria for the bursts and the data analysis of the E^* values were performed as detailed in Hohlbein *et al.* 2014[148]. Donor-only and acceptor-only species are identified by plotting a 2D histogram of E^* and the raw Stoichiometry (S^{raw}), as shown in Figure 5.5. S^{raw} is the ratio of the total fluorescence recorded after donor excitation to the total fluorescence recorded after both donor and acceptor excitation, given by

$$S^{raw} = \frac{F_{DD} + F_{DA}}{F_{DD} + F_{DA} + F_{AA}}. \tag{5.4}$$

Donor-only species have $S^{raw} \sim 1$, whilst acceptor-only species have $S^{raw} \sim 0$. These are removed from the final data before further analysis.

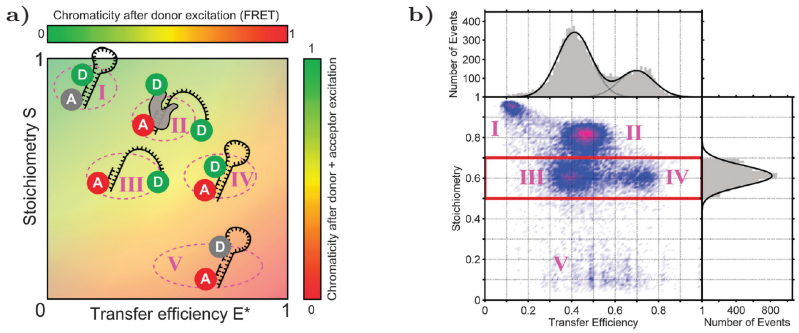


Figure 5.5: Illustration of how a 2D plot of FRET efficiency (E) and stoichiometry (S) can be used to filter out molecules that are not singularly-labelled with both a donor and acceptor fluorophore. Reproduced (adapted) from Hohlbein *et al.* 2014[148] with permission of The Royal Society of Chemistry.

5.2.3 FRET efficiency model

Though Gaussian peaks are normally fit to FRET efficiency histograms[148,150,156], a different model was sought to provide a better fit to the data for species with a high FRET efficiency ($E^* = 0.9 - 1$). As the FRET efficiency is limited to values between 0 and 1, the data distribution becomes distinctly asymmetric at high and low values. A Gaussian model is, therefore, not suitable as it has no such restrictions and is symmetric. Often experiments are designed to ensure that the fluorophores have a separation of $\sim R_0$ (where the efficiency is most sensitive to changes in distance), which gives efficiency values in the central region — the data distribution is approximately symmetric here, and is therefore acceptably fit with a Gaussian model. However, some of the experiments in this chapter had $E^* > 0.9$, for which a Gaussian model was unsatisfactory.

The alternative model was derived by assuming the separation of the fluorophores (r) fits a Gaussian distribution:

$$\phi(r) = N[\mu, \sigma] = \frac{1}{\sigma\sqrt{2\pi}} e^{-\frac{(r-\mu)^2}{2\sigma^2}}. \tag{5.5}$$

The distribution for E was then found using Wolfram Mathematica 10.2 to produce a transformed distribution for the efficiency using Equation (5.2) given Equation (5.5), resulting in:

$$\mathcal{D}(E;\mu,\sigma) = \frac{e^{-\frac{\left(\frac{1}{E}-1\right)^{1/3}+\mu^2}{\sigma^2}} \left(e^{\frac{\left(\left(\frac{1}{E}-1\right)^{1/6}-\mu\right)^2}{2\sigma^2}} + e^{\frac{\left(\left(\frac{1}{E}-1\right)^{1/6}+\mu\right)^2}{2\sigma^2}} \right)}{6\sqrt{2\pi}\left(\frac{1}{E}-1\right)^{5/6} E^2\sigma}. \tag{5.6}$$

Note that the μ and σ relate to the underlying distribution of r. The width of $\mathcal{D}(E;\mu,\sigma)$ depends on both μ and σ; holding σ constant, $\mathcal{D}(E;\mu,\sigma)$ will be broader if $\mu \approx R_0$ than if μ is much larger or smaller than R_0.

For a structure with two states, the fluorophore separation is bimodal, a linear combination of two normal distributions. The corresponding efficiency distribution that arises from the bimodal fluorophore separation is equivalent to a linear com-

bination of the efficiency distributions for each state with the same relative ratios. Therefore, the percentage of structures in each state can be calculated as the relative area of each separate efficiency distribution compared to the overall distribution. The two population efficiency distribution can be written as:

$$\mathcal{D}2(E;\mu1,\sigma1,\mu2,\sigma2) = p\mathcal{D}(E;\mu1,\sigma1) + (1-p)\mathcal{D}(E;\mu2,\sigma2), \tag{5.7}$$

where p is the percentage of the population with $\phi(r) = N[\mu1,\sigma1]$.

The model in Equation (5.6) or Equation (5.7) was used to fit one or two populations to the FRET efficiency histograms respectively. Resolvable peak values are noted on the histograms and discussed in the text. It is worth noting that the peak efficiency value is not the same as the mean efficiency value. Nevertheless, these values are still suitable for comparing samples.

Other distributions were also considered — a Gamma distribution would not be physical as it allows E > 1; a Beta distribution is restricted to values between 0 and 1 and has been used infrequently in the literature[157,158]. A comparison of the typical "Gaussian E" model, the alternative "Gaussian r" model and the "Beta E" model is shown in Figure 5.6. The Beta E and Gaussian r models have similar fits to the data, and are both significantly better than the Gaussian E fit (which predicts unphysical values). The Gaussian r model was used in this Chapter.

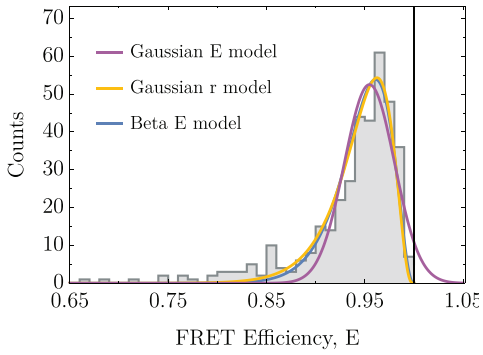


Figure 5.6: An example of how three models fit the data of a single species at high FRET values. The models: a Gaussian distribution for the efficiency values (often used in the literature), and a Gaussian distribution for the donor-acceptor separation (as derived here), and a Beta distribution for the efficiency values (sometimes used in the literature).

5.3 Threading

A 10 dT extension to an origami staple was used to investigate threading through an origami. The depth of an origami tile is the diameter of a DNA helix ($\sim 2\,\text{nm}$[3]). A 10 dT extension has a contour length of $\sim 6.7\,\text{nm}$[159] and is, therefore, long enough to thread through the origami (see Figure 5.7 for a depiction). If unthreaded, the extension will form a disordered coil above the origami surface with a root-mean-squared (RMS) end-to-end distance of $\sim 5.4\,\text{nm}$[160]. If threaded, the extension will pass through the origami to form a disordered coil on the other side.

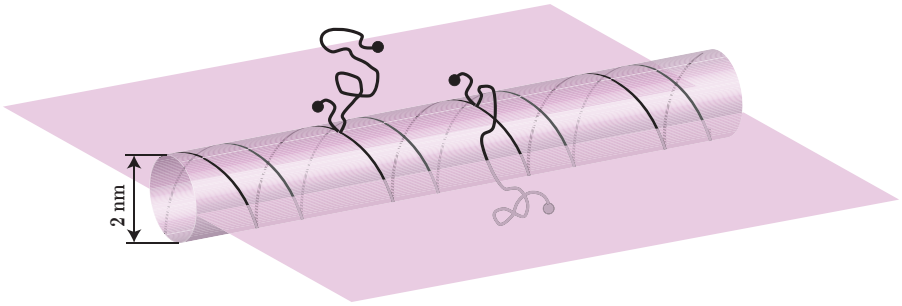


Figure 5.7: Depiction of the possible threading of a 10 dT extension through an origami. For clarity, only one helix of the origami is specifically shown. At two sites along the helix there is a 2 dT and 10 dT extension with fluorophore-labelled ends. On the left, the 10 dT extension is unthreaded and both fluorophores are on the same side of the origami. On the right, the 10 dT extension has threaded through the origami, separating the fluorophores.

To study the position of the extension using smFRET, the end of the extension (at the 3' end of the staple) was modified with a Cy3 donor fluorophore. The neighbouring staple provided a reference position through a Cy5 acceptor fluorophore on a 2 dT 5' extension (except for when it is repositioned at the 3' end where stated). Both extensions originate from the same nick between two staples. The 2 dT extension has a contour length of $\sim 1.3\,\text{nm}$[159] and is too short to thread through the origami. Its location is used to define the top of the origami, the surface from which the extensions originate.

The separation between the donor and acceptor will be larger if the 10 dT extension is threaded, as the extension will be more extended as it passes through a constricted gap in the origami. Therefore, unthreaded and threaded populations

should be identified as separate populations in a FRET efficiency histogram, at high FRET and low FRET respectively.

The structure of these extensions was explored in three systems: the basic system of plain extensions on an origami tile (Section 5.3.1), braced extensions on an origami tile (Section 5.3.2), and plain extensions on a multilayered origami (Section 5.3.3). The last two were studied to investigate their ability at reducing threading.

The origami tile was a 100 nm×70 nm minimised-twist tile[82]. The staples were located at the top middle of the tile, crossing the seam (where the scaffold weaves back on itself). Figure 5.1 shows the local environment of the staples. The multi-layered origami is roughly 50 nm×30 nm×7 nm. The staples were located in the corner of the top layer of the multi-layered origami (roughly 6 nm from each edge). In each case, the origami was formed by annealing the scaffold strand with an excess of all the staples, including the Cy3- and Cy5-labelled extended staples. The origami was then purified to remove the excess staples (by size-exclusion resin for the origami tile, and by extraction from an agarose gel for the multilayered origami).

5.3.1 Origami tile

First, a ss-extension on an origami tile was investigated using a 100 nm×70 nm minimised-twist origami tile[82]. The fluorophore-labelled staples are located at the top middle of the origami tile (as shown in Figure 5.1), running across the seam where the scaffold strand crosses between helices.

Figure 5.8 shows the histogram of the FRET efficiency values. The clear high-FRET peak at $E^* = 0.87$ is interpreted as arising from origami with unthreaded extensions. The broad range of low-FRET values may correspond to threaded extensions that have access to multiple holes in the origami lattice to thread through. A threaded state in each hole may have a slightly different average FRET efficiency; together these would merge to give a broad range, which was fit as a single population.

As the low-FRET values do not have a distinct peak, it is difficult to accurately fit the model to the data. A similar overall fit can be obtained by varying the ratio

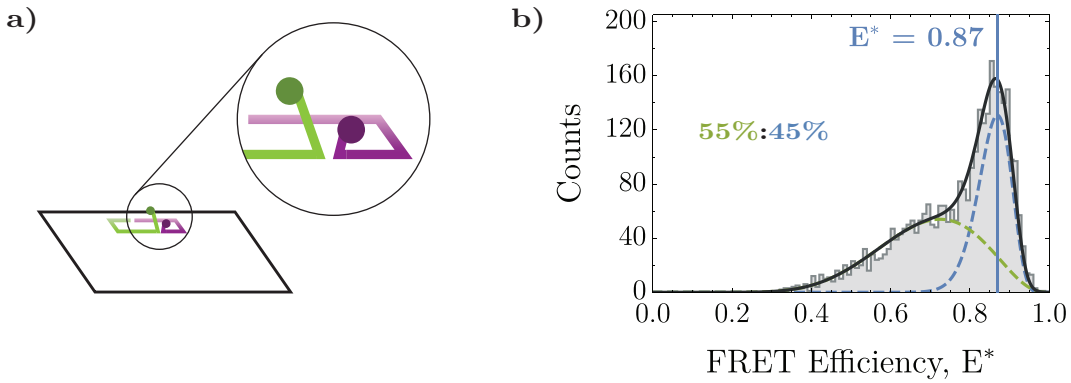


Figure 5.8: An origami tile has two modified staples: one with a Cy3 on the end of a **10 dT extension**, and another with a Cy5 on the end of a **2 dT extension**. a) A depiction of the structure with a zoomed-in view of the fluorophore-labelled staples. b) The distribution of FRET efficiency values with two fitted populations. The relative ratios of the two populations is provided, with colours and order matching that of the peaks.

of the populations and the underlying r distribution of the low-FRET population whilst retaining a similar goodness of fit (measured from the mean residuals and shown in Appendix A.2.1). This shifts the position of the low-FRET peak, but does not affect the position of the high-FRET peak. It is for this reason that the value for the high-FRET peak is stated throughout this chapter, whilst the low-FRET values serve only as an indication of other populations. The fit that is used in Figure 5.8 is the one that minimised the mean residuals of an unconstrained fit to the data. It suggests that approximately half the extensions are threaded through the origami.

5.3.2 Braced on an origami tile

One possible technique for reducing threading is to brace the extension at the surface of the origami, by forming a duplex pointing away from the surface at the beginning of the extension. The bracing is formed by the hybridisation of complementary domains on neighbouring staples at the nick from which the extensions originate. A three-way junction is formed here by the extended staple, the 'bracing neighbour' staple and the scaffold strand.

Three-way junctions with fully-complementary arms at the junction have been found to form with equal angles between the three arms[161,162]. Adding unbound

bases to one of the strands at the junction causes one of the other two strands to stack[129]; which one depends upon the strand sequences[163,164]. Unbound bases have also been found to increase the stability of the junction[161,165]: junctions with a bulge of two to five A bases have similar stability, and are more stable than junctions with a bulge of one A base. Junctions with two bulges are even more stable[165].

Bearing all of this in mind, the bracing was designed such that both staples have two unbound A bases at the junction, between the bracing domain and the scaffold-binding domains. This should increase the stability of the junction, compared to a design without any unbound bases. It should also allow the scaffold strand to remain stacked at the junction. The bracing domain is 4 nt ($\sim$ 1.4 nm); although this is short, the high effective concentration (given the staples are bound within the origami) should ensure the bracing hybridises successfully.

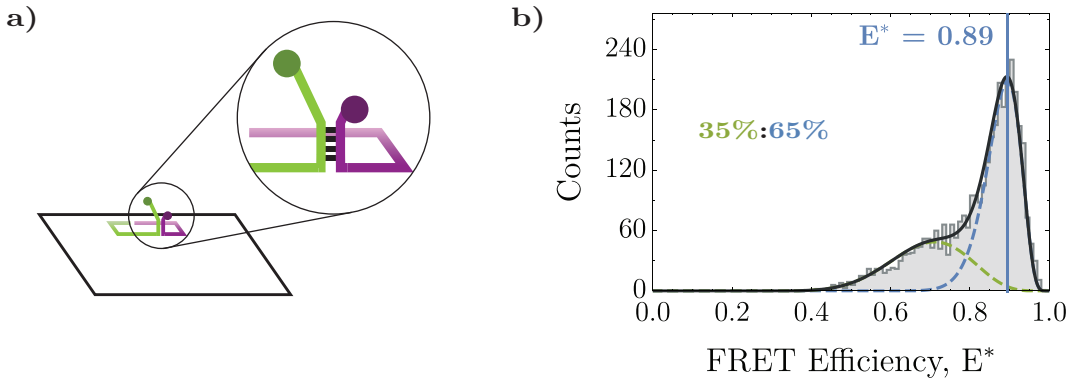


Figure 5.9: An origami tile has two modified staples that have complementary bracing domains to hybridise together. Above the bracing domain, one staple has a Cy3 on the end of a **10 dT extension**, and the other has a Cy5 on the end of a **2 dT extension**. a) A depiction of the structure with a zoomed-in view of the fluorophore-labelled staples. The two unbound A bases on each staple were omitted for clarity. b) The distribution of FRET efficiency values with two fitted populations. For comparison, the low-FRET values were fit with the same underlying mean fluorophore separation as in Figure 5.8. The relative ratios of the two populations is provided, with colours and order matching that of the peaks.

The bracing section is sufficiently short that the 10 dT extension is still long enough to thread through the origami. The histogram of FRET efficiency values shows a high-FRET peak at $E^* = 0.89$, closely matching that of the unbraced sample in the preceding section, and some low-FRET values (Figure 5.9). As the peak for

the low-FRET values remained unresolvable, for comparison, its fit was constrained to have the same underlying mean donor-acceptor separation (μ) as the fit to the unbraced data. The relative percentage of the low-FRET population is reduced, suggesting that the bracing has reduced the chance of threading by approximately 40%.

5.3.3 Multi-layered origami

The second technique that was tested for reducing threading was to use a multi-layered origami. It is formed of three-layers with a square lattice. Each staple hybridises to domains on the scaffold strand within each layer. As the origami design is different from the origami tile used in the preceding sections, the holes in the lattice for extensions to thread through will be different. The same Cy3 and Cy5-labelled extensions were used as in the origami tile experiments (a 10 dT and 2 dT extension), originating from the top surface of the top layer.

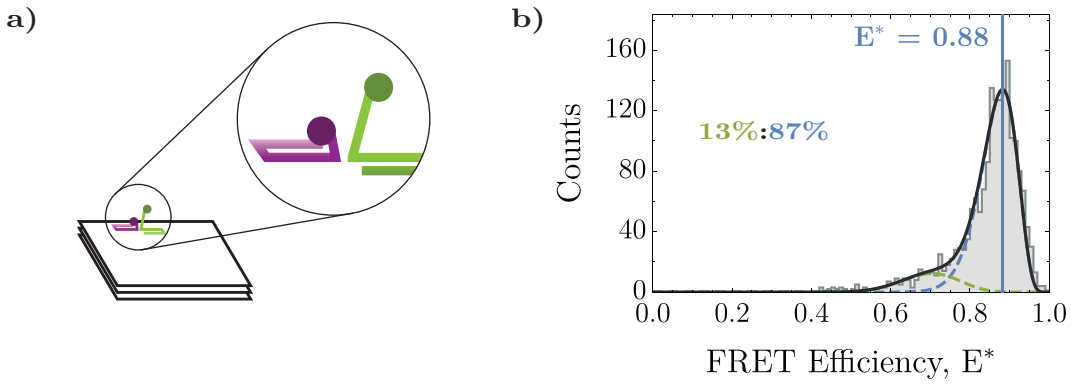


Figure 5.10: A multi-layered origami has two modified staples: one with a Cy3 on the end of a **10 dT extension**, and another with a Cy5 on the end of a **2 dT extension**. a) A depiction of the structure with a zoomed-in view of the fluorophore-labelled staples. b) The distribution of FRET efficiency values with two fitted populations. For comparison, the low-FRET values were fit with the same underlying mean fluorophore separation as in Figure 5.8. The relative ratios of the two populations is provided, with colours and order matching that of the peaks.

Threaded extensions would be constrained by the layers below, suffering an entropic penalty. Therefore, the use of a multi-layered origami is expected to reduce threading. The histogram of FRET efficiencies shows a clear high-FRET peak at

$E^* = 0.88$, similar to the tile experiments, and a small amount of low-FRET values (Figure 5.10). As for the fit to the bracing data, the fit for a second population at low-FRET was constrained to have the same underlying mean fluorophore separation (μ) as the fit in Figure 5.8. The relative percentage of the low-FRET population is significantly reduced, suggesting that the additional origami layers have reduced the chance of threading by roughly 80%.

5.4 Staple repair

The process of staple repair to load a cargo onto an origami was investigated using the same technique that Wickham *et al.*[102,128] used to load a DNA motor into place at the beginning of a track. The repair process was used to load oligonucleotide cargos onto a minimised-twist origami tile[82].

The general principle of cargo loading via staple repair is that the cargo strand is complementary to part of an extended staple. The origami is formed by annealing the scaffold strand with an excess of all the staples except for the staple of interest. The cargo and extended staple are pre-annealed, and then subsequently added to the pre-formed origami for an incubation at 37°C for 1 hr. The origami sample is then purified to remove the excess staples and cargo. The modified staples used throughout this section are the same as those used in Section 5.3 — located near the top of the origami, bridging the seam (where the scaffold strand crosses between helices), shown in Figure 5.1 and Figure 5.11.

Section 5.4.1 explores a simple system, wherein a single cargo strand is loaded onto an origami. Section 5.4.2 investigates two methods for loading two cargo strands to the same site on the origami (i.e. at the same nick between two staples): by hybridising both cargo strands to a single extension, forming a three-way junction; and by hybridising a cargo strand on both a 3' and 5' extension at the site. All these methods have relevance to DNA motor systems studied in this thesis.

5.4.1 Single cargo loading

The loading of a single cargo strand was studied using a staple with a 35 nt extension, 32 nt of which is complementary to the cargo strand. A 3 dT spacer separates the cargo-binding domain from the scaffold-binding domain. This is similar to experiments with the 'burnt bridges' motor, where the single cargo is the motor and the extended staple is the first anchorage (A.K.A. "stator") of a track[82,102].

The 3' end of the cargo (at the 'bottom', i.e. the end nearest to the origami) has a Cy3 fluorophore on a 2 dT linker. A reference signal is provided by a Cy5 fluorophore on a 2 dT extension of the neighbouring staple; as this extension is not long enough to thread, the Cy5 marks the 'top' of the origami. Both extended staples have their extensions originating at the same nick with the Cy5 on a 5' extension (except where stated).

If the staple repair is successful, the staple will be fully bound by 32 bp with the scaffold strand (16 bp on one origami helix and 8 bp on the neighbouring helix), and the cargo-bound extension will protrude from the top of the origami (see Figure 5.11a) for a depiction). In this case, the two fluorophores would be close to each other, leading to a high FRET efficiency.

Incomplete repair can lead to multiple conformations (depicted in Figure 5.11b-d). The single-stranded end of the staple is flexible and is expected to weave through the origami to hybridise with the scaffold strand. Whereas the cargo-bound end is more rigid: its 11 nm length is much less than the 50 nm persistence length of ds-DNA[5]. The ds-extension is expected to inhibit this end from weaving through the origami to bind completely. Therefore, the initial binding location of the staple to the scaffold may impact how well the staple is incorporated, leading to different kinetically-trapped states. These are expected to have a larger fluorophore separation than the desired structure, as the cargo-bound staple would not be hybridised to the scaffold next to the reference Cy5 extension, leading to a lower FRET efficiency.

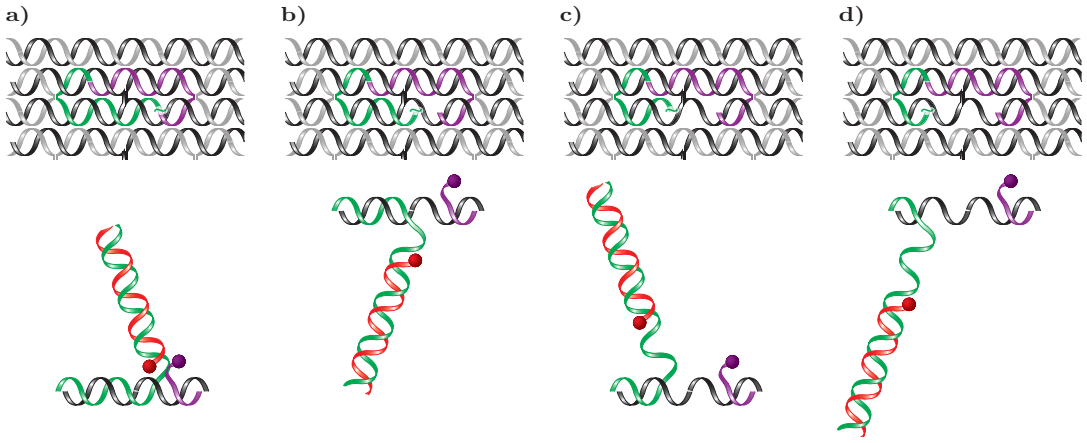


Figure 5.11: Schematics for a) the full-bound state, and b-d) partially-bound states after staple repair. The top panels show the top view of a section of origami tile, the bottom panels show side-on views of the helix from which the extensions originate. Partially-bound states are expected to be unbound only at the ds-extension end of the staple: b) unbound by half a turn, the cargo is therefore on the "wrong" side of the origami, c) unbound by a turn, d) unbound by 1.5 turns. The following components are highlighted here: the **scaffold strand**, **unmodified staples**, the **extended staple**, the **cargo**, and the **neighbouring staple** with a reference dye.

Non-origami controls

In order to get an idea for what FRET efficiencies would correspond to the various hypothesised partially-bound states, non-origami controls were performed. Simple structures were made by annealing the key strands (the cargo, extended staple and neighbouring staple) with a 'base' strand that acts as the scaffold strand. The base strand is complementary to the scaffold-binding domains on both staples, and so binds them together as if they were in the origami (see the insets in Figure 5.12 for depictions).

Partially-bound structures were formed by using versions of the extended staple modified with an orthogonal sequence to stop the relevant part of the scaffold-binding domain from hybridising to the base strand. Structures that were unbound by 5 nt, 10 nt and 16 nt (roughly 0.5, 1 and 1.5 turns respectively) were tested. In these cases, the base strand would have a single-stranded section due to the unbound bases. The corresponding unbound scaffold domain in the origami would be less flexible than a pure single-stranded domain, as it would be held in place by other parts of the origami structure. Therefore, a small strand to complete the

missing bases on the base strand was added to the 10 nt and 16 nt partially-bound samples, allowing the base strand to remain double-stranded and relatively rigid. This could not be done for the 5 nt partially-bound sample as a 5 nt strand will not bind stably to its complement at the pM concentrations used here[6].

It was not easy to purify out the excess strands, and so the strands were added such that all of the Cy3-labelled cargo was incorporated into a full structure. Post-processing was used to remove the data from Cy5-only labelled structures (as described in Section 5.2.2).

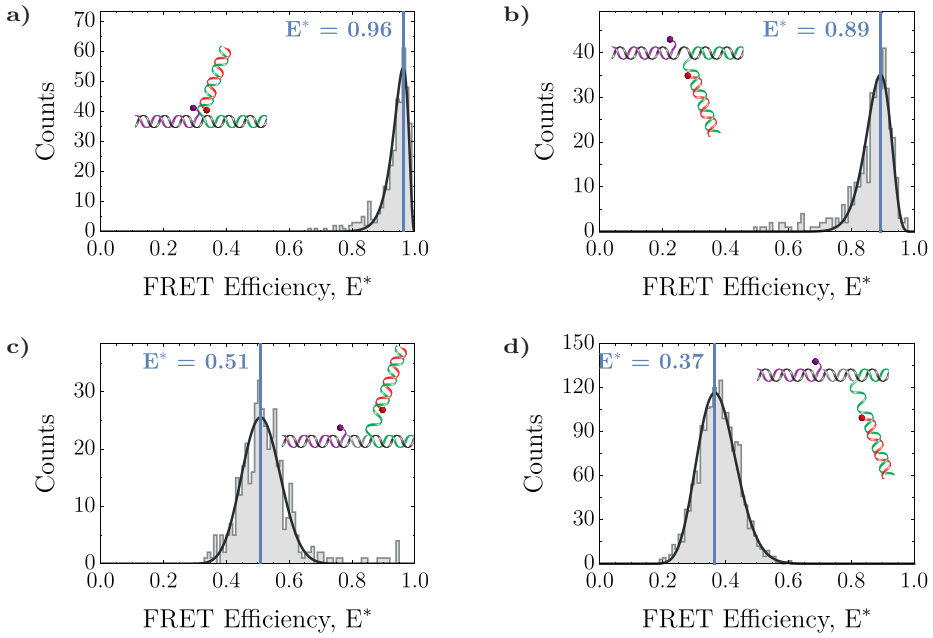


Figure 5.12: The histograms of FRET efficiencies for the non-origami controls with one fitted population. Insets show a depiction of the structure formed by a **base strand** (acting in the role of the scaffold), the **extended staple**, the Cy3-labelled **cargo** and the Cy5-labelled **neighbouring staple**. a) The fully-formed structure, b) unbound by 5 nt (∼ 0.5 turn), c) unbound by 10 nt (∼ 1 turn), d) unbound by 16 nt (∼ 1.5 turn).

Figure 5.12 compares the histograms of the FRET efficiencies for these non-origami structures. All samples showed a single peak in the distribution as expected. The fully-bound structure has a peak at $E^* = 0.96$; the 5 nt, 10 nt, and 16 nt partially-bound structures have peaks at $E^* = 0.89$, 0.51 and 0.37 respectively. The partially-bound structures have decreasing peak FRET efficiencies, as expected as the fluorophores are expected to move further apart.

Though these should serve as a useful reference (particularly in terms of the differences between these structures), the peak FRET efficiencies for the same structure within an origami may be slightly different due to the differences in the exact local environments of the fluorophores (such as the presence of the origami surface).

Initial experiments with close fluorophores

Figure 5.13 shows the histogram of FRET efficiencies for a sample of defective origami that has been repaired with a cargo-bound staple before purification. It shows a clear high-FRET peak at $E^* = 0.91$ and a very broad distribution of low-FRET values. The relative percentage of the low FRET states was found to have decreased substantially when the same sample was checked 16 days later (stored at 4°C in the intervening time); whilst the high-FRET peak remained the same over this period.

The distribution of low-FRET values is too broad to arise from a single population. These are attributed to origami with intermediate repairing states containing partially-bound staples. Comparing to the non-origami controls, they are likely to be unbound by less than 10 nt. The absence of these in the sample after 16 days suggests that the repair process has then gone to completion. The high-FRET peak arises from the structure with the closest separation of the fluorophores. A control of the structure with a fully-bound staple was required to check whether this peak corresponds to the desired structure.

Figure 5.14 shows the results of a control, where the origami was annealed with all the staples. The cargo strand alone was subsequently incubated with the origami at 37°C for 1 hr, and the sample finally purified. Given the results in Section 5.3, the extended staple is expected to be able to thread through the origami. Once the cargo strand is added to the sample, some may bind to an unthreaded extension and some to threaded extensions. It is not known how the cargo strand will affect the proportion of threaded states in this case or whether it inhibits a change in state; for example, cargo strands may preferentially bind to unthreaded extensions as the complementary domain would be more accessible.

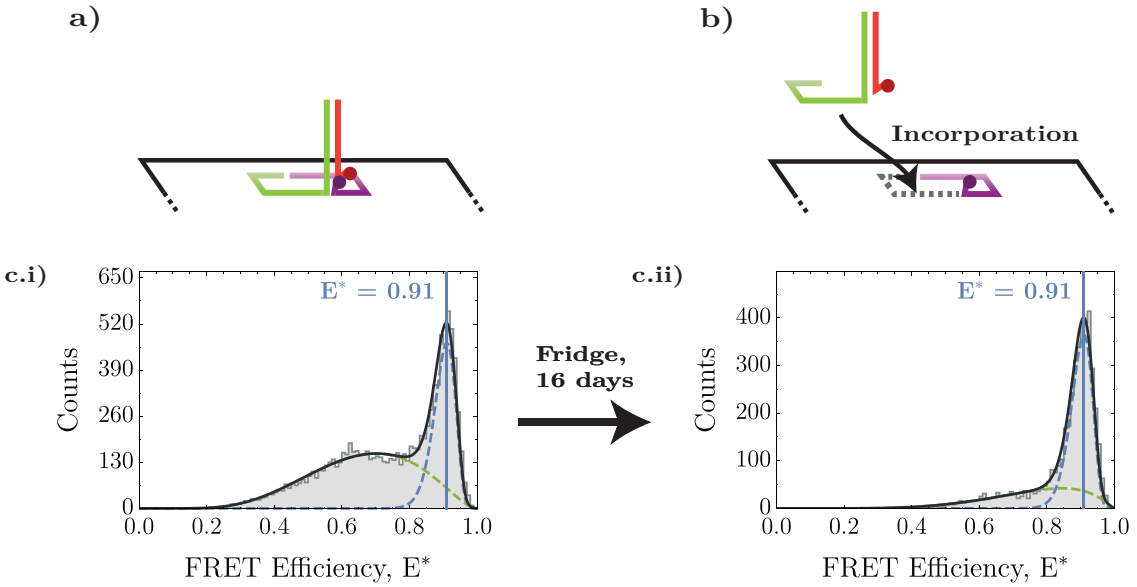


Figure 5.13: A **cargo strand** with a Cy3-modified end is complementary to the extension of an origami **staple**. The **neighbouring staple** has a Cy5-modified 5' end to provide a reference fluorophore for measuring FRET. a) A depiction of the desired structure with all the strands fully bound and both fluorophores on the same side of the origami. b) A depiction of the staple repair process: the cargo was loaded onto the origami by pre-annealing with its extended staple, the annealed duplex was then incubated with the defective origami at 37°C for 1 hr. c) The histograms of the FRET efficiency values with two fitted populations — the sample in i) was seen to converge to ii) after 16 days at 4°C.

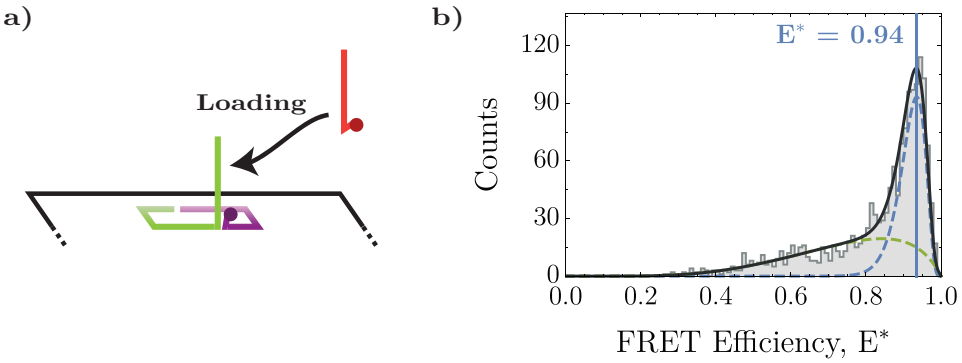


Figure 5.14: A control to compare against the staple repair process shown in Figure 5.13. a) A depiction of the process: the **extended staple** is included in the origami anneal, and the **cargo strand** is subsequently incubated at 37°C for 1 hr with it. The **neighbouring staple** has a Cy5-modified 5' end to provide a reference fluorophore for measuring FRET. b) A histogram of the FRET efficiency values with two fitted populations.

A high-FRET peak was observed at $E^* = 0.94$ along with some low-FRET values that are attributed to the threaded states. The high-FRET peak is close to that of the non-origami control (Figure 5.12a), suggesting that it arises from the desired structure, with both fluorophores close and on the same side of the origami. The peak value of the origami control is slightly higher than that of the origami after staple repair. This suggests that after staple repair the fluorophores are not as close as they are when all the staples are annealed into the origami, and hence that the repair process is not complete, even after 16 days.

Experiments with the reference dye repositioned

In order to check the peak positions for the staple repair and control more sensitively, the Cy5 reference fluorophore was moved to the 3' end of its staple, roughly $\sim 6\,\text{nm}$ away, on the same side of the origami. In this position, the donor-acceptor distance is closer to the R_0 of the pair, where the FRET efficiency is most sensitive to changes in separation. An additional control was performed with this set-up: the extended staple alone was added to the defective origami for an incubation at 37°C for 1 hr, the cargo strand was then added for an additional 10 min incubation at 37°C, and finally the sample was purified. This tests how successful staple repair is when the staple is entirely single-stranded.

Figure 5.15 compares the FRET efficiency values for the ds-extension staple repair, the ss-extension staple repair and the control with all the staples annealed into the origami. The FRET efficiencies are generally lower than in Figures 5.13 and 5.14, as expected due to the increased separation between the donor and acceptor fluorophores. The shape of the distribution is similar in that a peak is seen at higher-FRET, with an unresolved population of lower-FRET states. The exact position, width and relative percentage of the fit to the lower-FRET values is not well known as it is not easily separated from the high-FRET values. The position of the higher-FRET peak is identifiable and is used to consider differences between the samples.

The staple repair with a ss-extension has a similar higher-FRET peak value to

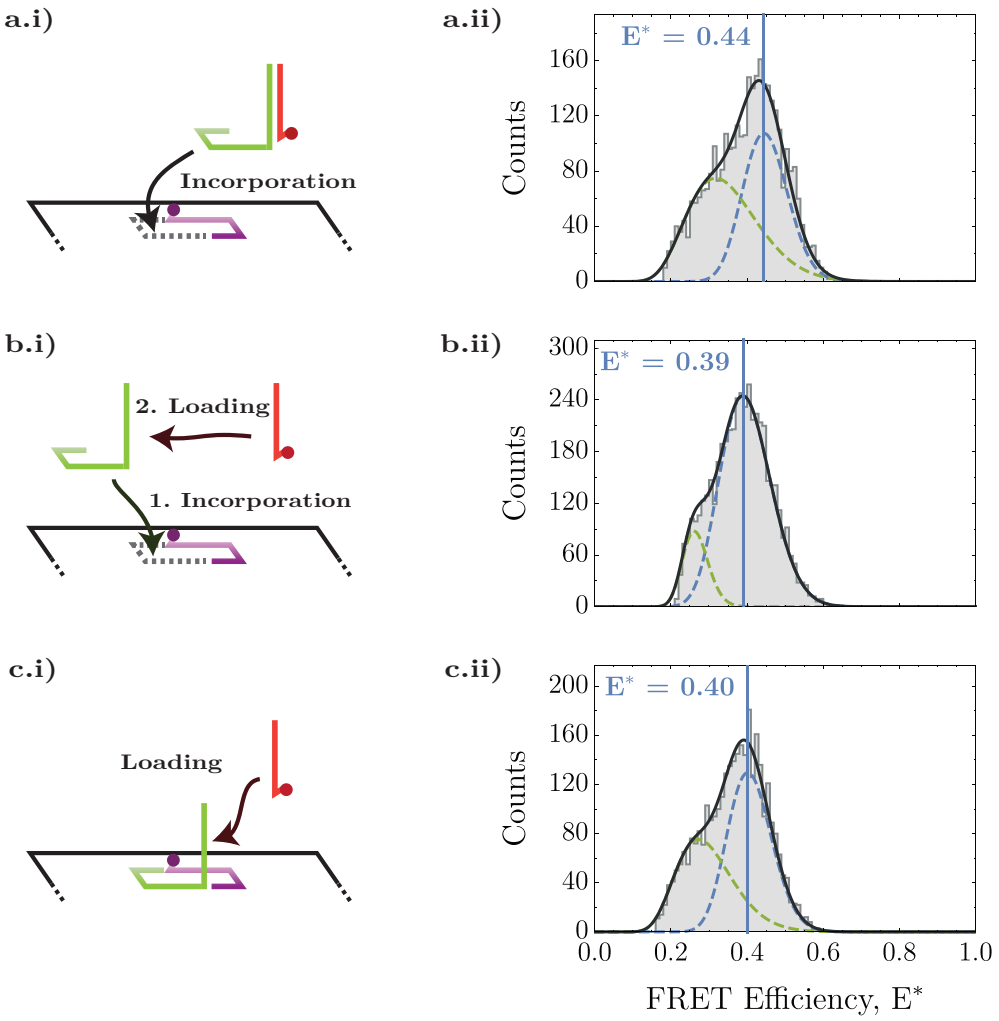


Figure 5.15: Staple repair is more sensitively investigated by moving the reference fluorophore to the 3' end of the **neighbouring staple**. a) The pre-annealed **cargo** and **extended staple** are incubated with the defective origami for at 37°C for 1 hr. b) The extended staple alone is incubated with the defective origami at 37°C for 1 hr. The cargo strand is then subsequently added for a 10 min 37°C incubation. c) The extended staple is included in the original origami anneal. The cargo strand is then loaded by incubating with the pre-formed origami at 37°C for 1 hr. i) Depictions of each process; ii) histograms of the FRET efficiency values with two fitted populations.

the control origami ($E^* = 0.39$ and $E^* = 0.40$ respectively), whilst the higher-FRET peak for the ds-extension staple repair is higher at $E^* = 0.44$. The higher peak efficiency for the ds staple repair implies that the fluorophores are closer together, which is consistent with the previous data that suggests staple repair with a ds-extension (i.e. cargo-bound) is unable to hybridise completely with the scaffold. The ss staple repair peak matches the control, suggesting that complete staple repair is possible when the staple is flexible and single-stranded.

This is supported by ensemble fluorescence measurements of the reversible motor (Section 2.3.4) which used a similar system of: a cargo (a quencher-carrying motor), extended staple (the anchorage), and a neighbouring, fluorophore-labelled staple (the F_0 staple). Instead of using FRET to determine the position of the cargo, the extent of quenching was observed. The cargo was able to quench the nearby fluorophore more (i.e. it was closer) when the extended staple had been single-stranded at some point in its past.

Testing a limited staple

It is useful to consider the arrangement of the incorporation site for the staple repair. The site for the missing staple is across the seam of the origami, where the scaffold strand loops back on itself, changing the holes in the origami weave. The holes occur when neighbouring helices separate between crossovers. The "length" of a hole can be defined as the number of bases between crossovers. Off-seam holes are normally 32 bp-long (not considering those at the edge of the origami). At the seam, there is an alternating mix of 64 bp- and 16 bp-long holes (Figure 5.16).

Adjacent to the site of the extension, the staple is complementary to an 8 nt scaffold domain. During staple repair, to completely hybridise with this scaffold domain, the staple must weave through the origami, including passing through a small 16 bp-long hole. This should be possible for flexible ss-DNA, but the rigid ds-extension will inhibit its end of the staple from passing through the small hole.

Therefore, it is possible that the staple repair is getting stuck at this final 8 nt scaffold domain. This was tested with an extended staple that has an orthogonal 8 nt

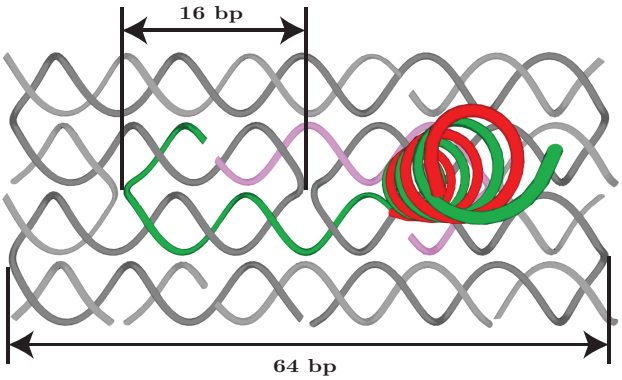


Figure 5.16: A depiction of the origami surrounding the incorporation site. The **extended staple** and **cargo** are in place, fully-bound to the **scaffold strand**. The **neighbouring staple** that is labelled with a reference dye is also highlighted amongst the other **unmodified staples**. Large (64 bp) and small (16 bp) holes are found at the seam.

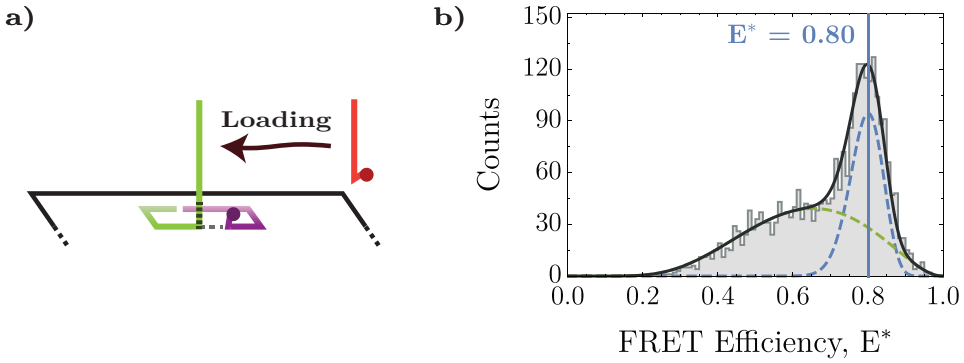


Figure 5.17: A **limited staple** is used as a control for a partially-bound conformation. The staple sequence has the last 8 nt up to the extension designed to be orthogonal to the scaffold strand that it would normally bind to. a) A depiction of the process: the extended, limited staple is included in the origami anneal, and the **cargo strand** is subsequently incubated at 37°C for 1 hr with it. The **neighbouring staple** has a Cy5-modified 5' end to provide a reference fluorophore for measuring FRET. b) A histogram of the FRET efficiency values with two fitted populations.

sequence for this domain. The limited staple was used as a control for the partially-bound structure. Figure 5.17 shows the histogram of FRET efficiency values: a high-FRET peak is seen at $E^* = 0.80$ and a broad distribution of low-FRET values. This high-FRET peak is much lower than that of the ds-extension staple repair (which was at $E^* = 0.91$), suggesting that the repair process is able to bind closer than this control, and is therefore able to bind into the last 8 nt scaffold-domain. It is possible that some base pairs are able to form without the ds-extension passing through the hole. This would draw the fluorophores closer, but not as close as the fully-bound structure.

5.4.2 Loading two cargos at one site

One extension

The same extended staple (S) was also used to load two oligonucleotide cargos (C1 and C2) at the same site on the origami (i.e. at the same nick between two staples). The three strands are pre-annealed to form a three-way junction (S.C1.C2, see Figure 5.18a) for a schematic of the structure with annotated lengths). S.C1.C2 was loaded onto the origami by incubating it with the defective origami at 37°C for 1 hr before purification.

Figure 5.18 shows the histogram of FRET efficiencies: a clear high-FRET peak at $E^* = 0.92$ and some low-FRET values are seen. This is similar to the ds-extension staple repair in Section 5.4.1 and suggests that loading a bulkier cargo does not further inhibit staple repair.

This specific structure has direct relevance to the system in Chapter 2. The same sequences were used where S, C1 and C2 correspond to the first anchor, the motor and a cut holding director (of station design 1) respectively. It was with this system that initial measurements showed additional quenching of a nearby fluorophore by the quencher-carrying motor when the first anchor was at some point single-stranded, indicating that the initial process of ds staple repair was not completely successful.

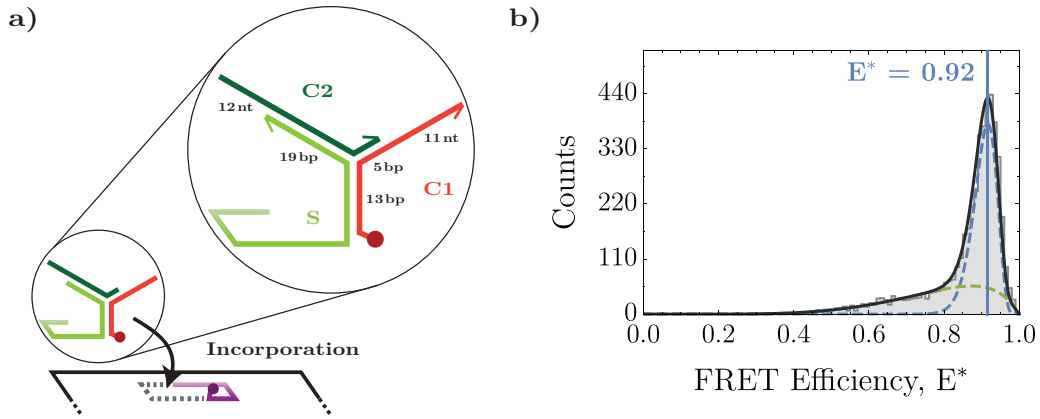


Figure 5.18: Two cargo strands (**C1** and **C2**) are loaded onto the origami by forming a three-way junction with an extended staple (**S**). The lengths of the domains are noted next to each section in the zoomed-in inset. a) A depiction of the process: both cargo strands and the extended staple are pre-annealed, and then subsequently incubation with the defective origami for 1 hr at 37°C. The **neighbouring staple** has a Cy5-modified 5' end to provide a reference fluorophore for measuring FRET. b) A histogram of the FRET efficiency values with two fitted populations.

Two extensions

Another approach to loading two oligonucleotide cargo strands is to hybridise one cargo to a 5' extension (C5 on S5) and a second cargo to a 3' extension (C3 on S3) at a nick. To investigate the structure with FRET, C3 and C5 were modified with a Cy3 on a 2 dT linker and Cy5 with no extra linker respectively. The fluorophores were attached to the ends of the cargos that are closest to the origami. As both extensions originate from the same nick, they should be close together and have a high FRET efficiency. The desired final structure is depicted in Figure 5.19a).

In this case, S5 was included in the origami anneal, while S3 was added via a staple repair incubation. S3 was pre-annealed to C3, and added to the defective origami with C5. The sample was incubated at 37°C for 1 hr before purification. The simple hybridisation of C5 to S5 is expected to have a faster rate than the incorporation of S3.C3 into the origami, as the scaffold strand will be less accesible than the extension of S5. The staple repair of S3.C3 is, therefore, likely to occur with C5 already hybridised at the site. A control origami was assembled by annealing both extended staples with the scaffold and other staples, and then incubating it

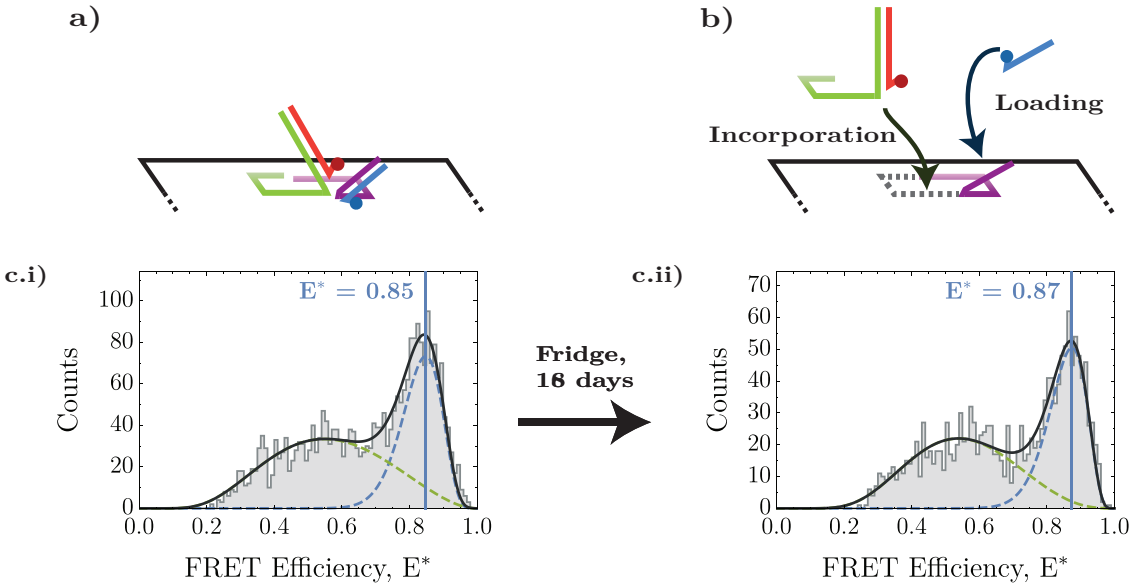


Figure 5.19: Two cargo strands (**C3** and **C5**) are loaded onto the same site. C3 has a Cy3-labelled 3' end and is complementary to a 3' extension (**S3**); C5 has a Cy5-labelled 5' end and is complementary to a 5' extension (**S5**). a) A depiction of the desired structure with all the strands fully bound and both fluorophores on the same side of the origami. b) A depiction of the loading process. The origami was annealed with S5, but not S3. C3 and S3 were pre-annealed and added to the defective origami with C5. The sample was then incubated at 37°C for 1 hr. c) Histograms of the FRET efficiency values with two fitted populations — the sample in i) was seen to converge to ii) after 18 days at 4°C.

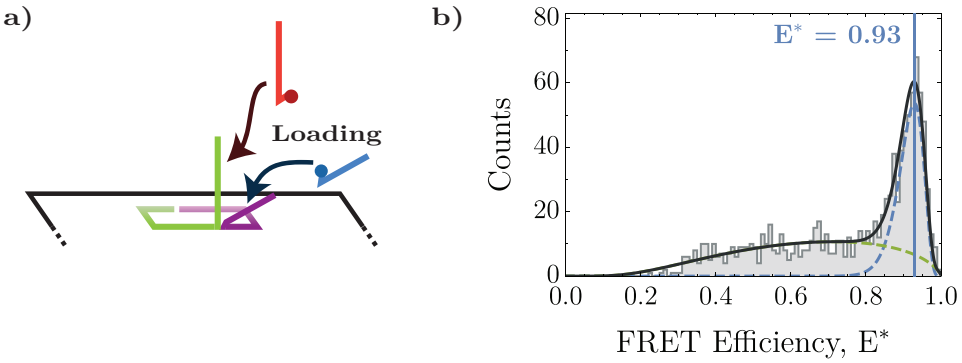


Figure 5.20: A control to compare against the cargo loading process shown in Figure 5.19. a) A depiction of the process: both extended staples (**S3** and **S5**) are included in the origami anneal, and both cargo strands (**C3** and **C5**) are then subsequently incubated at 37°C for 1 hr with it. The **neighbouring staple** has a Cy5-modified end to provide a reference fluorophore for measuring FRET. b) A histogram of the FRET efficiency values with two fitted populations.

with both cargo strands at 37° for 1 hr. As the extended staples were annealed into the origami, they should be completely bound with the scaffold.

Figure 5.19 shows the histogram of FRET efficiencies for the staple repair sample immediately after purification and also rechecked after 18 days at 4°C. In both cases, a high-FRET peak and a large distribution of low-FRET values is seen. The high-FRET peak is at $E^* = 0.85$ initially, with a minor shift to 0.87 after 18 days (it is not clear whether this shift is significant). In comparison, the control for this structure shows a high-FRET peak at $E^* = 0.93$ and a reduced percentage of low-FRET values (Figure 5.20). This control has a similar high-FRET peak to the single cargo structure in Figure 5.14 (with $E^* = 0.94$), implying a similar average separation of the fluorophores in both structures. The high-FRET peak for the staple repair sample with two cargos is appreciably lower than that of the ds-extension staple repair with one cargo in Figure 5.13 (with $E^* = 0.91$), and shows no significant decrease in the relative percentage of the low-FRET states over time. This implies that the staple repair in this case is further inhibited from binding completely by the presence of S5.C5 already in place.

This system is specifically relevant to the DNA motor and track experiments in Chapter 3. The C5 cargo strand corresponds to a fluorescently-labelled strand (the F_0 strand) that hybridises to the staple next to the first anchorage, as a cheap alternative to purchasing a directly-labelled staple. The staple repair of C3.S3 corresponds to the loading of the motor bound to the first anchorage. These results suggest that if staple repair that is as complete as possible is desired, that a directly-labelled staple should be used to provide the F_0 signal.

5.5 Discussion

This chapter has discussed various investigations into the structure of extensions to origami staples using single-molecule FRET. Modification of staple ends is often used to functionalise a specific side of an origami. If the staple end is able to pass through the origami, it can incorrectly functionalise the wrong surface. Though

threading of staple extensions has been observed when an origami is pressed against a surface[144], this has not been tested for origami floating in solution. Here, the threading of a 10 dT extension through a freely-floating origami was investigated. A clear high-FRET peak and some low FRET values indicated two populations of origami. The low FRET values were attributed to threaded systems, but additional observation techniques would be required to confirm this. The results from an origami tile with the 10 dT extension suggested that roughly 50% of the extensions were threaded. Two strategies for reducing threading were explored: by bracing the bottom of the extension at the origami surface (reducing the threaded states by approximately 40%), and by using a multi-layered origami (reducing the threaded states by approximately 80%). These offer a beneficial approach for systems that are designed to functionalise origami specifically on one surface.

It is possible that the low-FRET values that are attributed to threaded states here actually arisen from something else, though no satisfying alternative hypotheses have been found. A poorly-formed origami could separate the fluorophores, leading to a lower FRET efficiency, but it is likely that a badly-formed origami would cause greater separation between the fluorophores than the efficiency values represent. The yield of well-formed 3D origami is usually lower than 2D origami; so if the lower-FRET values arise from a poorly-formed origami, there should be even more observed for the multilayer origami, not less.

Another method of functionalising an origami is via staple repair: a pre-formed ('defective') origami missing a staple is incubated with the staple, which binds with the single-stranded scaffold to repair the defect. The repair of a staple with a single-stranded extension was found to successfully bind with the origami, whilst a staple with a ds-extension remains partially-unbound at its ds-end (but within 8 bp away).

The loading of two cargo strands via staple repair extended this study. Hybridising two cargo strands to one extended staple showed similar results to that when loading a single-cargo. Therefore, bulkier cargo hybridised to the extended staple does not seem to further inhibit the incorporation of the staple into the origami. However, loading two cargo strands onto separate extensions at the same site on the origami did further hinder staple repair.

The implications of this is that staple repair is a successful method for loading a single-stranded strand onto a pre-formed origami (if it would be degraded by the annealing temperatures, for example). However, to load a double-stranded strand (or a single-stranded strand with a bulky modification) onto a pre-formed origami so that it is completely bound at its loading site, then staple repair is not the best approach. Instead, the cargo-bound strand should be designed to hybridise to the extension to a staple, instead of to the scaffold strand directly. This way the origami can be assembled with all of the staple strands (ensuring the strands are completely bound), and the cargo can still be loaded to the specific site. This would be a useful improvement to make for the work in Chapter 2 if ensemble fluorescence measurements were used for further work.

Coarse-grained simulations are under way with collaborators in Prof. Jonathan Doye's group (Oxford Physical & Theoretical Chemistry) to simulate both the threading experiments and the process of staple repair. They should offer further insight, and other methods for improving the functionalisation of origami.

Chapter 6

Holliday Octahedron

This chapter explores a new design for a dynamic 3D DNA structure, here named a *"Holliday Octahedron"*, which uses the branch migration of Holliday junctions to cause movement within the structure. The octahedron is made up of eight strands, each one running around a face, bound to neighbouring strands so that each edge is a 20 bp (≈7 nm) double-stranded section of DNA. Carefully positioned nicks around the octahedron can be moved to the vertices, producing a different, more open structure. This could be used to encapsulate a cargo and release it.

In this chapter, the design of the *Holliday Octahedron* is described and a reference band on a polyacrylamide gel is found for a plain octahedron as the first experimental step for formation.

Experiments were undertaken in collaboration with Aiman Entwistle, due to her expertise with working with DNA tetrahedra. The modelling of the initial and final forms of the *Holliday Octahedron* was made by Flavio Romano and Petr Šulc using a coarse-grained approach[109].

6.0.1 Molecular cages

The biomedical world is constantly seeking smarter, more targeted drug delivery. Self-assembled DNA cages have great potential for the delivery of drugs. DNA (as

an inherently biological material) interacts easily with cellular components such as proteins, RNA and other DNA, giving it the potential to achieve targeted drug delivery.

Inorganic nanostructures can also be utilised for drug delivery, e.g. gold particles[166] and carbon materials (nanotubes and graphene)[167]. However, these often have toxic effects and cause safety concerns as they degrade less easily[168].

DNA cages can either be wireframe polyhedra or 3D origami, as long as they are able to carry, protect and release a cargo. Cargo can be carried in a number of ways[169]: hybridised to a DNA strand that forms the DNA cage[170–172], trapped within the enclosed space[173,174], covalently attached to the structure[23,175], non-covalently attached by DNA-protein interactions[176], by biotin-streptavidin interactions[177] or even intercalated within the DNA helix[178,179]. The type of cargo often dictates which mechanisms are appropriate. Biomedical applications have focused on delivering cancer drugs and genetic therapeutic agents, and have mostly used the first three delivery mechanisms as previously stated.

Mechanisms for the release of cargos vary, depending upon the type of DNA structure used. Some have made use of toehold-mediated strand displacement, such as Bujold *et al.* 's[35] cube that is opened in the presence of an mRNA product of a gene that is characteristic of prostate cancer cells. Others exploit the plethora of aptamers available for producing a conformational change in the DNA structure in response to certain ligands. Banerjee *et al.* 2013[174] break up two halves of an icosahedron cage using cyclic-di-GMP and aptamers that undergo a conformational change induced strand displacement. Douglas *et al.* 2012[23] go one step further and use multiple aptamers to create a logic-gated hexagonal barrel that can deliver antibody fragments.

6.0.2 Holliday junctions

Holliday junctions are branched nucleic acid structures formed of four strands that intersect and are exchanged between helices at a crossover, which is more commonly referred to as a 'vertex' in this chapter (Figure 6.1).

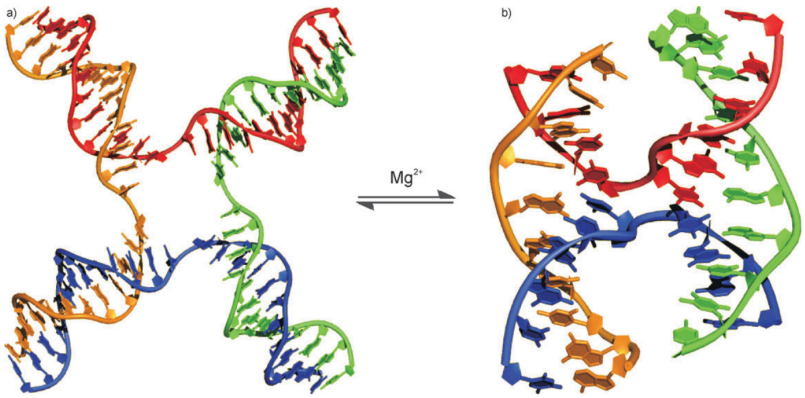


Figure 6.1: Representative structures of four DNA strands forming a Holliday junction. a) The planar, unstacked conformer formed in the absence of metal ions. b) One of two possible stacked conformers for the same strands, formed in the presence of >100 μM Mg^{2+}.
This image was reproduced from Müller 2010[180] with permission of The Royal Society of Chemistry

The structure was first proposed by Robin Holliday in 1964 when investigating meiosis in fungi[181] and is now known to be a central intermediate in genetic recombination. More recently, Holliday junctions have been used by the DNA nanotechnology community, for example as an important component of DNA origami[9].

The conformation of a Holliday junction depends upon the salt conditions, which change whether or not strands remain stacked at the junction. A strand is stabilised by base pair 'stacking', which is when the aromatic rings of the base pairs are face-to-face[182]. This is maximised when a strand is straight and reduced by bends in the strand. In the absence of metal ions, the junction forms an unstacked conformer (Figure 6.1a)[183]. The unstacked conformer is open at the vertex, approximately planar with the four ds-arms intersecting at 90° to reduce the electrostatic repulsion of the negatively-charged helical backbones. In the presence of metal ions (>100 μM Mg^{2+}[129]) the junction folds into a stacked conformer, with two strands remaining helically-stacked, and the other two crossing over at the vertex. Two stacked conformers are possible with different pairs of strands stacking or crossing over (one of which is depicted in Figure 6.1b). The stacked conformers have been found experimentally to have an intersection angle of roughly 60°[184], which is supported by models that suggest this angle is determined by the positions of the major and

minor grooves[185]. Though either stacked conformation is possible with a complete Holliday junction, if one strand has a nick at the vertex, the Holliday junction forms with the nicked strand as a crossing over strand[186]. Monovalent cations only allow the stacked conformation to partially fold, even at high concentrations[180].

If the opposite domains at the vertex are homologous, the Holliday junction is considered to be mobile, as the vertex can diffuse up and down the homologous sections by unbinding bases at the vertex and then reforming them with the other arm[187,188] (Figure 6.2). The branch migration of a Holliday junction is a random walk, with a rate dependent on the ion concentration. Panyutin *et al.* 1994[188] found step times of 270-300 ms in the presence of 10 mM Mg^{2+}, and 300-400 μs in the absence of Mg^{2+} (roughly 1000 times faster). They hypothesised that branch migration occurs via a transition to the unstacked conformer that is found in the absence of divalent cations[189].

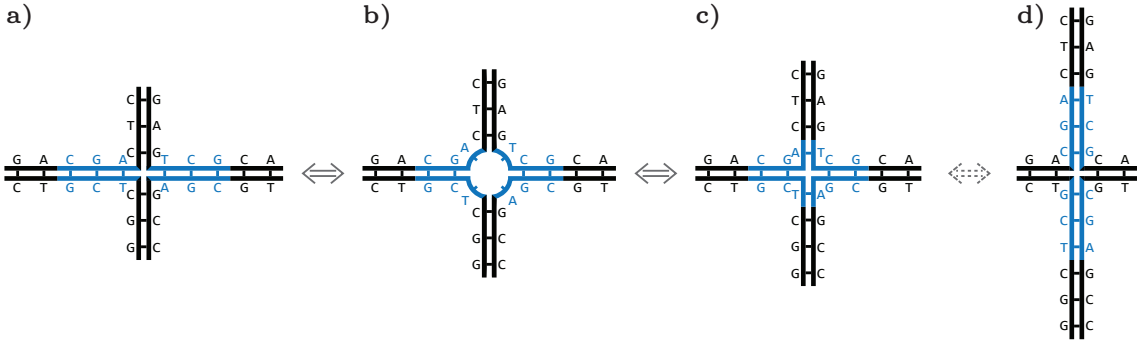


Figure 6.2: An example of the branch migration of a Holliday junction within the **homologous region**. a) The homologous segments are fully bound on opposite helices. b) The bases at the vertex unzip. c) The unbound bases are then able to rebind on the other arms. d) Branch migration can continue (reversibly) down the length of the homologous region.

The octahedra described in this chapter were formed in 100 mM NaCl. Due to the overall shape of the octahedron and assuming good formation, the Holliday junctions would have a constrained structure regardless of salt concentration. They would be expected to look like the unstacked conformer forced out of plane. We do not know how this would affect the rate of branch migration.

6.1 Design

6.1.1 Structure and movement

The simplest structure to be composed entirely of vertices of order 4 is an octahedron. Octahedra have 6 vertices of order 4, 12 edges and 8 faces. A DNA octahedron can be made in a one-pot reaction from eight strands (one per face), with each edge of the octahedron formed of double-stranded DNA (Figure 6.3). Each face is a triangle, imparting structural strength to the overall structure. If all the vertices were mobile Holliday junctions, each strand could rotate about its face, the base pairs of neighbouring strands acting like the teeth between interlocked cogs.

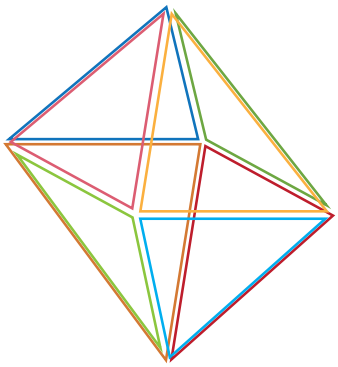


Figure 6.3: Depiction of an octahedron made from eight strands (one per face, coloured separately). The helices are omitted for clarity. An edge is formed of the double-stranded duplex between neighbouring strands. The proposed design uses 63 nt strands, giving an edge length of roughly 7 nm. In this case, the strands have been ligated so that each strand is a loop.

A simple DNA octahedron (i.e. with no branch migration) has previously been made with 20 bp edges and unbound A nucleotides from each strand at each vertex[37]. The unbound A bases are thought to help release tension in the structure. The interior volume has been modelled and the largest sphere found to fit inside has a radius of 4.1 nm[190].

The *Holliday Octahedron* was made based upon this design, using 63 nt strands. However, it cannot have unbound bases at the vertices otherwise branch migration would not take place, as it would be energetically favourable for the extra bases

to remain at the vertex as opposed to being unbound bases within a duplex (i.e. an edge). The extra bases should, therefore, be able to bind at the vertex. We hypothesise that if this causes too much tension in the structure, some of the vertex bases will unbind to reduce it.

As the double-stranded edges are stiff (the persistence length of ds-DNA is 45-47.5 nm[191], roughly 7 times the length of each edge), all the strands would need to migrate together as tension in the structure cannot be easily released if only some of the vertices migrated. For example, if a single vertex branch migrated, the two edges that extend would push away the vertex, whilst the two edges that shorten would pull the vertex towards the centre of the octahedron. Unless there was an asymmetry in the system, the vertices would branch migrate in a random walk up and down the homologous regions.

The octahedron could be ligated for extra stability, so that all the strands formed interlocking loops. If the strands were not ligated, the nicks (where the ends of each strand meet) initially need to be positioned relatively centrally in the edge for a stable octahedron structure[190]. For the *Holliday Octahedron*, branch migration would likely stop once a nick reaches the vertex as it would cause a disruption in the Holliday junction at that vertex.

If one tried to design the octahedron so that the strands could rotate continuously all the way around (with carefully chosen sequences and ligating the strands), it would need to be constructed from four copies of two complementary strands (Figure 6.4). This degeneracy would make it practically impossible to form the octahedron, as the complementary strands would prefer to bind to each other as a duplex rather than creating the entropically-lower form of the octahedron.

Therefore, we must consider a limited rotation of the octahedron. If the octahedron strands were not ligated and the nicks were carefully positioned along the edges, a rotation could bring multiple nicks to a vertex/vertices causing a conformational change to the structure. If this conformational change led to a more open, flexible structure, the starting octahedron could be used to enclose a cargo, the branch migration of the vertices could be initiated by an environmental signal, and once the rotation had taken place the cargo could be released.

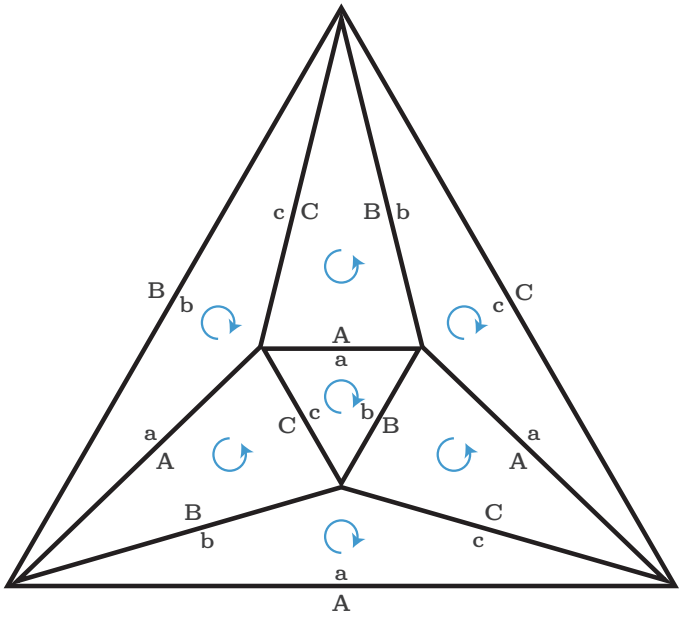


Figure 6.4: A Schlegel diagram of an octahedron. The lines depict each edge, and the crossing points between lines depict the vertices. The domains of each strand that runs around a face are labelled by letters within each face. Lower and upper-case letters reflect reverse complementary sequences. One of the faces is not represented by an enclosed triangle, but is formed by the outside edges of the diagram — the sequence for the strand that runs around this face is, therefore, noted on the outside. By considering a continuous rotation of the strand that forms the central face of the diagram, the sequence of the other strands can be determined. This would require four copies of two complementary strands.

6.1.2 Conformation change

The nicks can be placed such that, after the rotation of the strands, two nicks converge on four vertices in a ring around the octahedron (Figure 6.5). These are designated the "equatorial" vertices, whilst the other two vertices are the "polar" vertices. Once the nicks arrive at the equatorial vertices, there are no bases holding these vertices together and they will split apart. The polar vertices are expected to move further apart to allow the four duplexes that hold them together to stack.

If a cargo were trapped inside of the octahedron, the structural change into the final, extended structure could allow the cargo to be released or made accessible for interactions with reactants in solution. As the extended structure has more conformational entropy and would be less strained, it is the most energetically-favourable state, and it would not return to its initial octahedral structure.

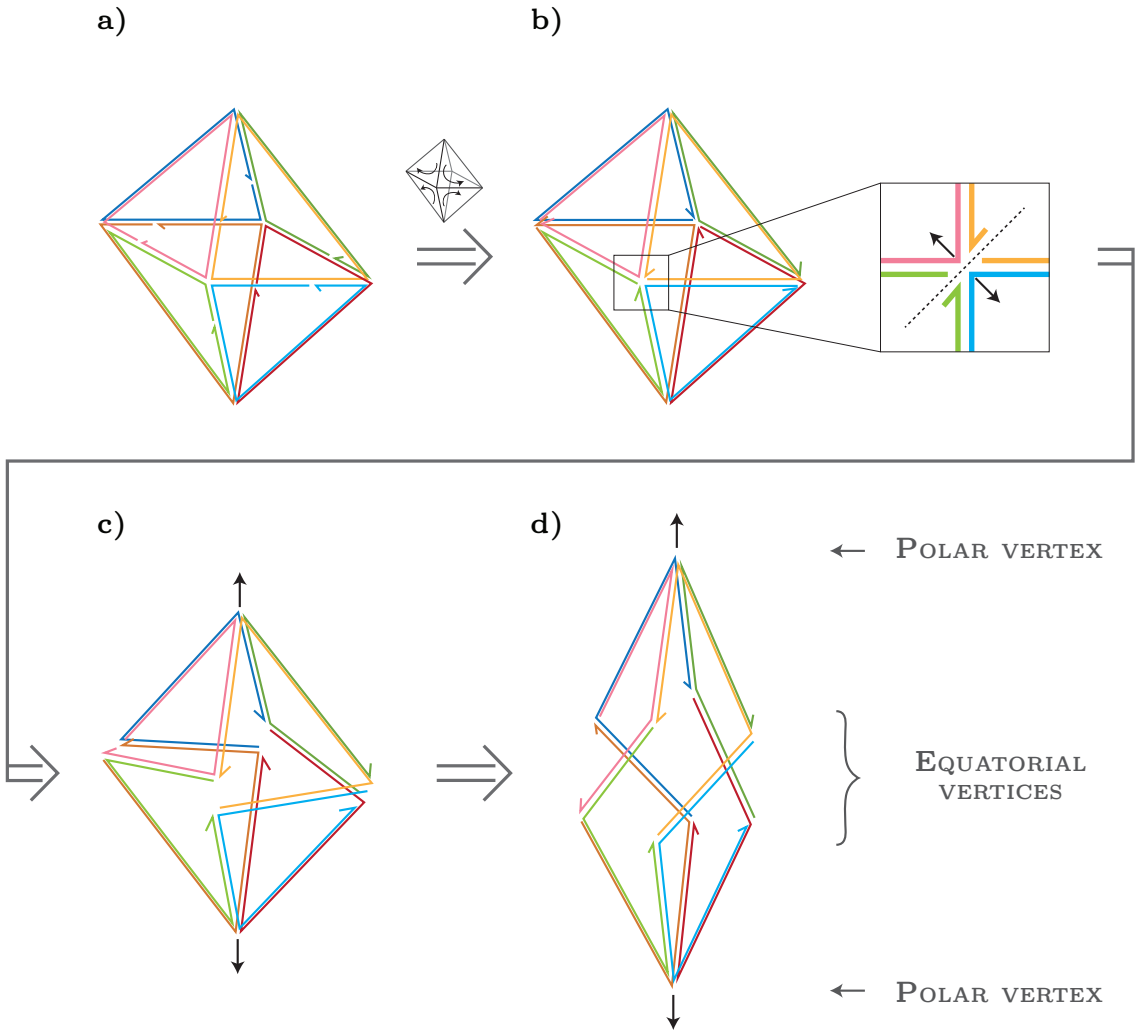


Figure 6.5: The placement of the ends of each DNA strand (the 'nicks') can produce a large conformational change once the rotation brings them to "equatorial" vertices that ring around the octahedron. a) The initial *Holliday Octahedron*, with the eight strands (one per face) coloured separately. b) The branch migration of the Holliday junctions rotates the strands, causing two nicks to converge on each equatorial vertex. The inset shows that the vertex is no longer bound together and can split apart. c) As the equatorial vertices split apart, the complete "polar" vertices move further away. d) This allows the four duplexes holding the polar vertices together to stack, producing the final, extended and more open structure.

6.1.3 Initiation and locking

As the final, extended form of the *Holliday Octahedron* would be the most stable configuration, it must originally be locked into the initial octahedral form. Branch migration would then be initiated by the release of the lock. A few different ideas are mentioned here (Figure 6.6). For example, extensions to an octahedral strand could bind with a new strand to form stiff, double-stranded "bars" coming out of an edge (Figure 6.6a). Exploiting steric hindrance, if the bars were carefully positioned so that the twist of the edge's helix projected it close to the other edges of its face, junction migration would be limited as the bar would need to twist around its edge's helix and it would hit the other edges. However, it was thought this would be hard to set up initially in the correct configuration and so was not pursued.

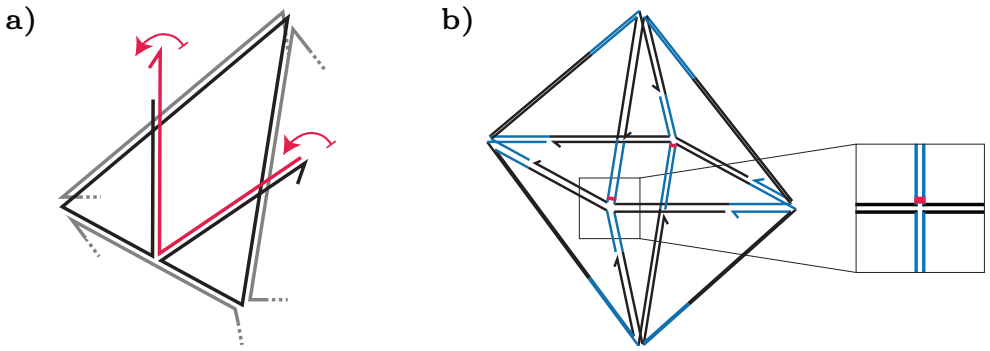


Figure 6.6: Possible locking mechanisms to stop the branch migration until a release signal is given. a) As the vertices branch migrate, the strands are expected to twist around their helices as they rotate about each face. A ds-protrusion from an edge could be used to stop the strands twisting around their helices, as it would not be able to pass through one of the other edges to do so. The **locking strand** could be removed by toehold-mediated strand displacement using a release strand, initiating the branch migration. b) Neighbouring strands could be held together at the beginning of the **homologous region** of a couple of vertices. For example, this could be done with a **disulphide bond**, which is broken in the presence of a reducing environment.

Other ideas aimed to hold neighbouring strands together at the vertex, stopping the unzipping that is required to allow bond reformation with the new strand (Figure 6.6b). A disulphide bond was considered to be the most practical, with a reducing environment providing the initiation signal. The disulphide bond would have to be attached via an amino-modified base, so as to cause minimal disruption to the base when binding within a duplex (necessary for moving the base away from

the vertex during the branch migration).

6.2 Models

Petr Šulc and Flavio Romano in Theoretical Physics used a coarse-grained model[109] to predict the structure of the *Holliday Octahedron* in its initial and final state (Figure 6.7). The model has previously shown to give a good representation[192] of a DNA tetrahedron for which there is a high resolution cryo-EM image for comparison[21].

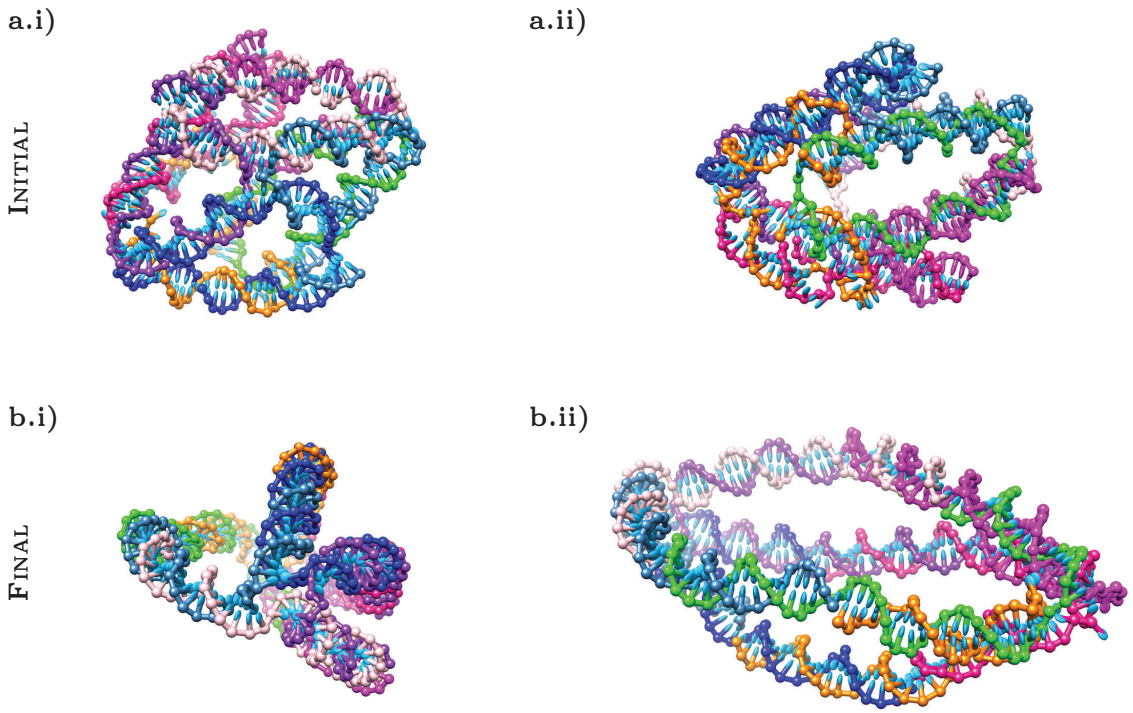


Figure 6.7: Coarse-grained models of the *Holliday Octahedron* in its a) initial and b) final state. Each strand is coloured separately. Snapshots are i) facing a polar vertex, and ii) rotated so that the polar vertices are at the left and right-hand sides of the images.

The strands were forced to bind together as expected for the initial and final structures, as the homologous Holliday regions would otherwise provide too many possible configurations. The initial structure is approximately octahedral (Figure 6.7a). On rotating the structure, each pair of faces between the polar vertices has a repeating shape: the strand with the nick at the equator has its equatorial

edge bent outwards and upwards (at a 30-60° angle), and the other strand extends down and out to match. The final structure has extended helices with large gaps (Figure 6.7b).

6.3 Formation of a plain octahedron

A plain octahedron was made with no homologous regions to provide a reference band for analysis by gel electrophoresis of the initial, closed *Holliday Octahedron*. The sequences used were based on those originally designed by Anthony Walsh, a previous lab member, who also investigated DNA octahedra[37]. Two versions of the plain octahedron were formed: one with unbound A bases on each strand at each vertex, and one with complementary bases added at each vertex. The formation of the former has previously been reported[37], with the unbound bases present to relieve tension in the structure. However, formation with no unpaired bases is required for a *Holliday Octahedron*, and hence successful formation under these conditions required testing.

Unbound A vertex bases

The plain octahedron with unbound A vertex bases was formed by annealing the eight strands at a concentration of 100 nM (Figure 6.8). Each strand provides an A base at each vertex. Some samples were ligated to investigate whether this increased the yield during PAGE analysis. For comparison, samples with only seven of the eight strands were also annealed and run on a polyacrylamide gel.

A clear single band was seen after annealing and ligation of all eight strands: this is attributed to the well-formed octahedra. DNA can still be seen in the well of the polyacrylamide gel, implying that larger structures were also forming, which did not pass into the gel. The non-ligated samples gave less clear bands on the gel, which is to be expected as ligation would stabilise the formed structure.

No unpaired vertex bases

The plain octahedron was also formed with no unpaired vertex bases (Figure 6.9). The hope was that, if release of strain at the vertices is required, a few bases would unbind. As lower concentrations should minimise aggregates and higher-order structures[6], a range of annealing concentrations was explored: 100, 200, 400 and 600 nM.

A clear band was seen at a similar level compared to the DNA ladder as the ligated octahedron with the unbound vertex bases in Figure 6.8. A stronger band was seen when the strands were annealed at lower concentrations (i.e. 100 nM). There is also a second slightly slower band that is stronger for the samples at higher concentrations. This may be from structures with an extra copy of one or more strands. As before, a significant amount of DNA has also remained in the well.

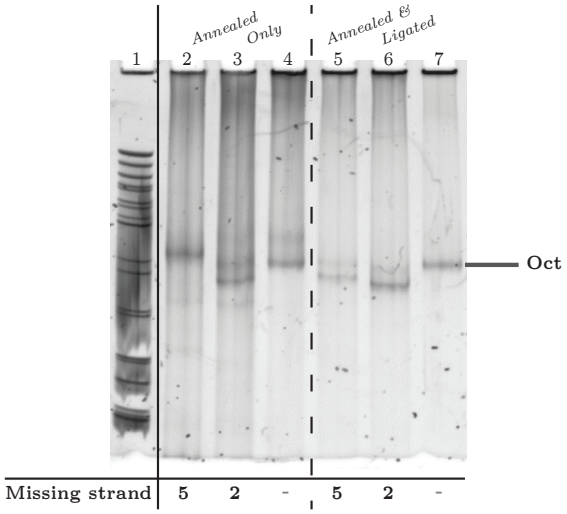


Figure 6.8: Octahedron formation with no homologous segments and unbound A bases at the vertices. Lane 1 — NEB's 50 bp DNA ladder. Lanes 2-4 — annealed only. Lanes 5-7 — annealed and ligated. Lanes 4 and 7 had a full set of octahedron strands, and hence is expected to show the formation of the complete octahedron. Samples in lanes 2 and 5 and lanes 3 and 6 had only seven strands, missing strand 5 and 2 respectively. Gel details: 6% 19:1 polyacrylamide gel, run at 170V for 120 min in an ice bath. Sample details: strands annealed at 100 nM in octahedron buffer (10 mM Tris, 100 mM NaCl, pH 8.0).

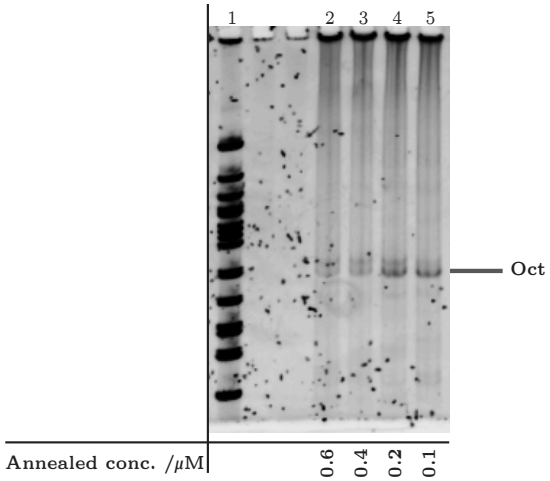


Figure 6.9: Octahedron formation with no homologous segments, but with complementary vertex bases. Lane 1 — NEB's 50 bp DNA ladder. Lanes 2-5 — all the strands were annealed together in stoichiometric amounts at varying concentrations in octahedron buffer (10 mM Tris, 100 mM NaCl, pH 8.0). Gel details: 6% 19:1 polyacrylamide gel, run at 215V for 44 min in a cold room.

6.4 Discussion & future work

In this chapter, the design for a *Holliday Octahedron* was described. Unlike other DNA octahedra that have been made, this one is designed to have mobile Holliday junctions at all the vertices, allowing each strand that runs around a face of the octahedron to rotate. A possible use of this rotation is to bring nicks in the strands to four of the vertices, inducing a conformational change to extend and open the structure.

This could be used to carry and release a cargo, and could join the DNA cages that are being considered as tools in biomedical applications. It would require a locking mechanism, so that the branch migration can be initiated on demand. Two possibilities for this were proposed.

As a first step to forming the *Holliday Octahedron*, reference structures without homologous sequences were made. Formation was successful regardless of whether the vertex bases were unbound A bases or complementary. A lower annealing concentration gave better formation (100 nM compared to a range that went up to 600 nM); higher concentrations favour aggregates or higher-order structures. Further analysis is necessary to be certain that the band represents the octahedra. This could be done using mass spectrometry to check its mass compared to that of a single component strand, or using cryo-electron microscopy. Alternatively the octahedron could be annealed with fluorophore-labelled strands to check that each strand is present. Dimers or higher-ordered structures could be checked by using a mix of two versions of a fluorophore-labelled strand (e.g. red and green), and analysing a sample from the gel-purified band with alternating-laser excitation (ALEX) to check for the presence of both fluorophores on a single structure. If some structures have both fluorophores present, this implies that there are two copies of a strand in the structure and it is not the octahedron.

Before proceeding to form an octahedron with homologous regions, further work would need to be made on an exact protocol for locking the octahedron into its starting form. This lock should encourage the correct homologous regions to initially bind, encouraging good formation of the octahedron as a whole. A consideration of

the hierarchical assembly of the octahedron may also help to form the octahedron at a higher yield[190], whereby annealing strands in a specific order inhibits the propensity to form aggregates or higher-order structures.

Once a *Holliday Octahedron* is produced with a lock and release mechanism, its mobility during gel electrophoresis could show what buffer conditions are necessary for the octahedra's vertices to be able to migrate to change it into the open conformer.

If the differing mobility of the open and closed conformers is in doubt, FRET pair fluorophores could be placed at the ends of one of the strands. Initially, in the closed form, the FRET pair would be close together bound along an edge, allowing strong transfer between the fluorophores (giving a high FRET efficiency). In the open form, once the nicks have all migrated to the equatorial vertices, the FRET pair would be separated (giving a lower FRET efficiency).

Chapter 7

Summary

The aim of this thesis was to explore novel designs and applications of DNA motors. The various designs were based on modifications to the 'burnt bridges' motor, first introduced by Bath *et al.* in 2005[1]. This work was extended by Wickham *et al.* for longer-range movement down a 100 nm track on a single origami tile[82], and for programming the motor to take a specifc path at a junction in the track[102].

Chapter 2 discussed the evolution of the basic 'burnt bridges' track into one of a replenishing track. A renewable track opens up many new applications for such motors. The desire for the replenishment process to be autonomous required intricate design of the component strands, which was described in detail. This complexity could be reduced if one wanted a resuable track that was reset through the external addition of strands. The autonomous replenishment was used to send a single motor down a 42 nm track three times, which was observed using ensemble fluorescence measurements. Though the work suffered from a couple of limitations (particularly the speed of the motor), the results were encouraging and suggested that a single-molecule approach would benefit future work on this system.

Chapter 3 outlined a design for a DNA motor and track that could perform logical computation using the ability of one motor to block another motor. Various design ideas were considered, before a specific one (the "Lollipop Track") was taken

forwards for testing. Preliminary experiments showed promise, but the system was less easy to implement on a full track on an origami tile. The main issue was that there was a low percentage of motors reaching the end of the track. A number of changes improved this percentage, such as changing the buffer and bracing the track to prevent track defects.

A new application of the 'burnt bridges' motor was then explored in Chapter 4, a project with two collaborators, Florence Benn and Natalie Haley. 100 nm origami tubes were stacked to μm lengths, and a braced track was placed down the inside of the tubes. A motor, initially located at the front of a stack of tubes, was then directed down the inside of the tube. This could be extended for future work by attaching a cargo to the motor for enclosed transportation over μm distances.

Two approaches were considered for observing the motor move down a stacked tube using TIRF-based optical microscopy. A direct method involved labelling the motor with Cy3 fluorophores. Initial microscopy experiments were able to observe these motors, but photobleaching is a problem with observation over the time-scales required for μm movement. Alternative approaches using DNA-PAINT to avoid photobleaching limitations were proposed. An indirect observation method involved labelling the track with Cy3 fluorophores. As the motor moves down the track, the labelled-tops are designed to be cut off and diffuse away: track behind the motor should therefore go dark. Preliminary microscopy experiments showed a decreased brightness of a sample when enzyme was added to initiate motor movement, as expected if the motor was successfully stepping down the track. Flashes of the diffusing Cy3-labelled tops were also observed, and analysis was performed to highlight these in a series of images from a video. Additional imaging of the labelled-track system is being carried out by the collaborators, who aim to observe movement of specific motors in real-time.

Through the process of design and experimentation of all of these systems, a number of questions arose about the exact structure of the tracks used for the experiments. The tracks are formed of origami staple extensions that are complementary to the motor strand. Chapter 5 investigated these structures using single-molecule FRET (smFRET), which is sensitive to nanoscale changes in distance within a struc-

ture. The experiments were performed with Dr Timothy Craggs, a FRET specialist. The experiments were able to show that single-stranded extensions thread through an origami tile that is freely-floating in solution (it has previously also been shown to occur when an origami was adsorbed to a surface[144]). The threading was reduced by 40% by bracing the bottom of the extension, at the surface of the origami; and was reduced by 80% by using a multi-layered origami. These methods of reducing threading may be important for the future design of origami that requires functionalisation on a specific surface.

The smFRET was also used to investigate the process of staple repair, whereby a defective origami missing a staple is incubated with the staple. This is a way of loading a cargo onto an origami after the origami has been assembled, and was used extensively in this thesis for loading motors at the beginning of tracks. The staple repair of an ds-extended staple (such as a motor-bound anchorage) was found to be incomplete; though the staple was able to hybridise to the scaffold strand, it was not fully-bound. The staple repair of a ss-extended staple, on the other hand, was able to bind completely with the origami. This suggested alternative approaches if one wanted to load a cargo onto an origami via staple repair.

Finally, Chapter 6 presented something a bit different: the idea of a *"Holliday Octahedron"*. The *Holliday Octahedron* is a dynamic octahedron formed of eight DNA strands, one strand around each face of the structure. It has mobile Holliday junctions at each vertex, allowing the strands to revolve around each face. The idea was extended to the potential use as a novel DNA cage for transporting a cargo. The rotation of the strands around each face can cause a conformational change that could release the cargo.

Appendix A

Appendix: Supplementary Results

A.1 Chapter 2 supplementary

A.1.1 Externally-reset mechanism

For completeness, Figure A.1 shows the overall mechanism for a reusable track that is externally-reset by sequential additions of removers and directors. Note that this allows the secondary design of these strands to be simplified, compared to the autonomously replenishing system in Figure 2.1.

A.1.2 A Holliday junction initiation for the remover

When the remover displaces the cut director from the anchor, it must first bind with its toehold and then undergo strand displacement whilst also opening up its hairpin. To encourage this, the anchor and remover were given a few extra nucleotides so that they could form a mobile Holliday junction with which to easily undergo strand displacement.

Removers with an extra 2 and 3 nt for a Holliday junction were tested with anchors with and without the 3 extra nt to bind to (Figure A.2). They were first

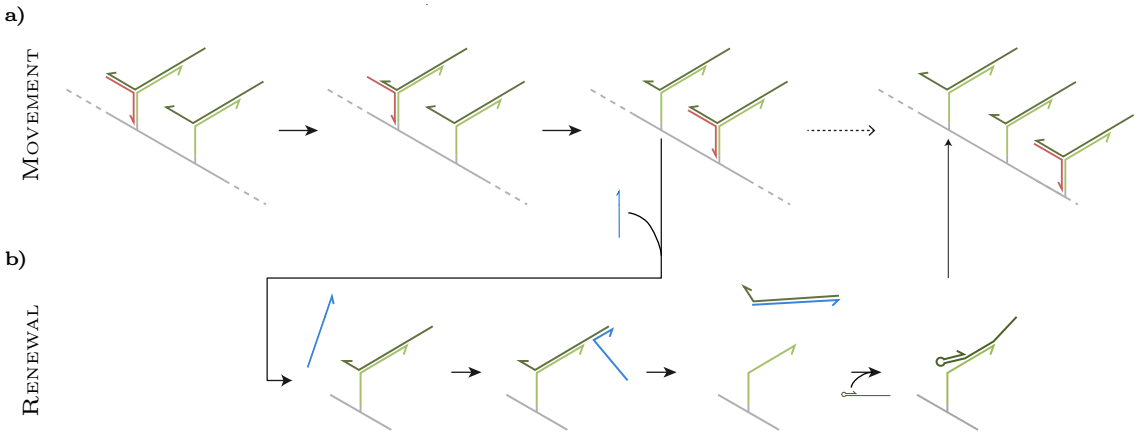


Figure A.1: The overall mechanism for the movement of a motor down a externally-reset reusable track. Compared to the autonomously regenerating track, the directors and removers here have simpler secondary structure.
a) Motor movement — the **motor** binds to an anchorage formed of an **anchor** and a **director**. The nicking enzyme cuts the director, allowing the motor to move forwards like the 'burnt bridges' motor.
b) The track renewal — a cut director is removed from its anchor by the strand displacement of an added **remover** strand. Directors are subsequently added, allowing a complete director to bind to the empty anchor, producing a complete anchorage. Until the replenishment process is completed, backwards motion of the motor is inhibited.

tested with complete directors to ensure no remover-director interaction. When the removers were incubated with the pre-annealed anchorage, there was a well maintained population when the anchor did not have the extra bases. However, when the anchor did have the extra bases, the removers displaced the complete director from the anchorage. The small toehold the removers are able to use to bind to the anchors must help them to remove the complete directors due to being so closely localised.

As the removers must not interact with complete directors, and the extra bases for a Holliday junction were found to be unnecessary for the removal of cut directors, they were not incorporated into the design.

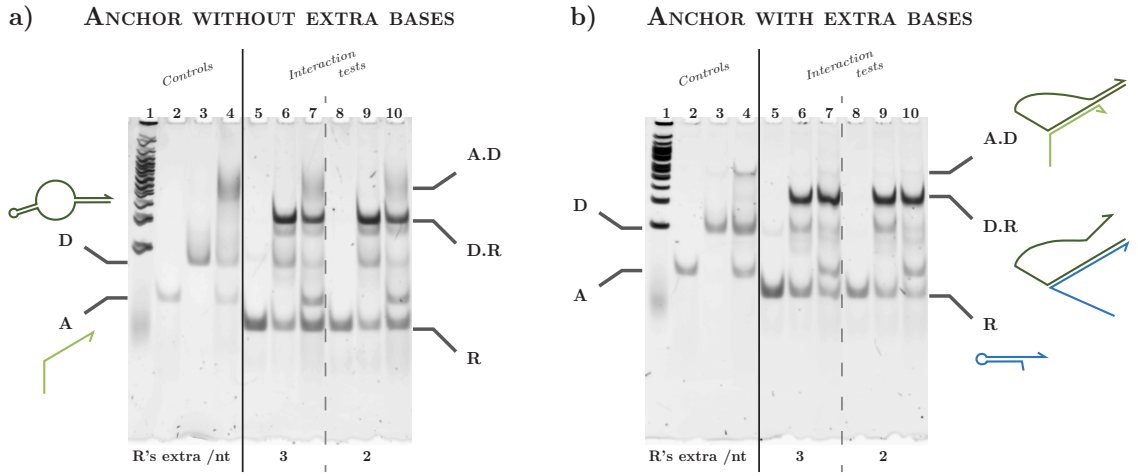


Figure A.2: Polyacrylamide gels to check for no undesired interaction between the **removers** (R) and **directors** bound to **anchors** (A.D) when the anchors a) did not have any extra bases, and b) had 3 extra nt. In both gels, lane 1 — NEB's 50 bp DNA ladder. Lanes 2-4 — control lanes containing A, D, and A and D annealed (A.D) respectively. Lanes 5-7 and lanes 8-10 use R with 3 and 2 nt extra respectively. Lanes 5 and 8 — R alone. Lanes 6 and 9 — D and R annealed (D.R). Lanes 7 and 10 — R was incubated with pre-annealed A.D for 1 hr at 37°C. Gel details: 15%, 29:1 polyacrylamide gels, run at 260V for a) 45 mins and b) 30 mins. Sample details: all strands were at 100 nM and the samples were run in 1x Origami buffer + 50 mM NaCl.

A.1.3 Enzyme cutting near a vertex

Figure A.3 shows the polyacrylamide gels used for analysing the cutting efficiency of Nt.BbvCI (summarised in Table 2.4) as the restriction site is positioned close to the vertex to a three-way junction.

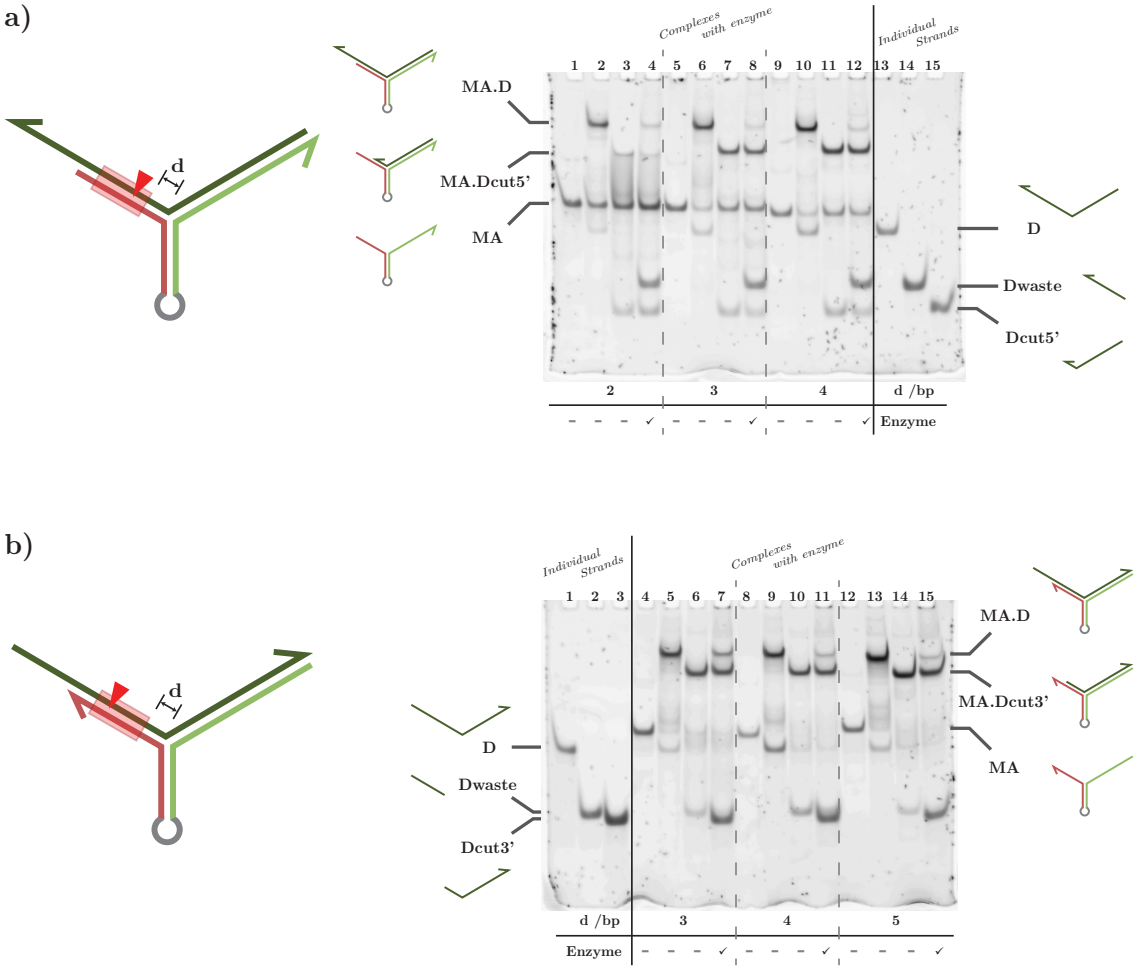


Figure A.3: PAGE analysis to check enzyme nicking efficiency as the restriction site gets moved close to the vertex of a 3-way junction. A **half director** (Dhf) was pre-annelead with a hairpin to act as the **motor**.**anchor** (MA). Different MA hairpins were used to shift the restriction site away from the vertex (a distance d /bp away). Both orientations of the restriction site are considered: with the restriction site at the a) 3' end of the motor and b) at the 5' end of the motor.
a) Lanes 1-4, 5-8 and 9-12 use MA hairpins that make d=2, 3 and 4 bp respectively. Lanes 1, 5 and 9 — MA only. Lanes 2, 6 and 10 — MA and D annealed. Lanes 3, 7, 11 — MA and Dcut5' annealed. Lanes 4, 8, 12 — MA and D pre-annealed, then incubated with Nt.BbvCI for 1 hr at 37°C. Lanes 13-15 — control samples of D, Dwaste and Dcut5' respectively.
b) Lanes 1-3 — control samples of D, Dwaste and Dcut5' respectively. Lanes 4-7, 8-11 and 12-15 use MA hairpins that make d=3, 4 and 5 bp respectively. Lanes 4, 8 and 12 — MA only. Lanes 5, 9 and 13 — MA and D annealed. Lanes 6, 10 and 14 — MA and Dcut5' annealed. Lanes 7, 11 and 15 — MA and D pre-annealed, then incubated with Nt.BbvCI for 1 hr at 37°C.
Gel details: 20%, 29:1 polyacrylamide gels, run at 260V for 80 mins. Sample details: D, Dwaste and Dcut5' were at 113 nM and the MA strands were at 125 nM. The samples were run in 1x Origami buffer + 50 mM NaCl. 0.8μl of Nt.BbvCI (10,000 units/ml) was added to 40μl samples.

A.2 Chapter 5 supplementary

A.2.1 Accuracy of low-FRET peak

As the low-FRET peaks for the FRET efficiencies in Chapter 5 are not distinct, the two-population models to the data are unable to accurately predict the low-FRET peak. A similar overall fit can be achieved by varying the ratio of the populations and the peak of the low-FRET population. This is shown in Figure A.4 where separate fits are forced to maintain a high-FRET population of 35% and 65%. A similar overall goodness of fit can be observed. Although the ratio of the populations and the low-FRET peak position is not well defined, the high-FRET peak (due to being distinct) is accurate to two significant figures.

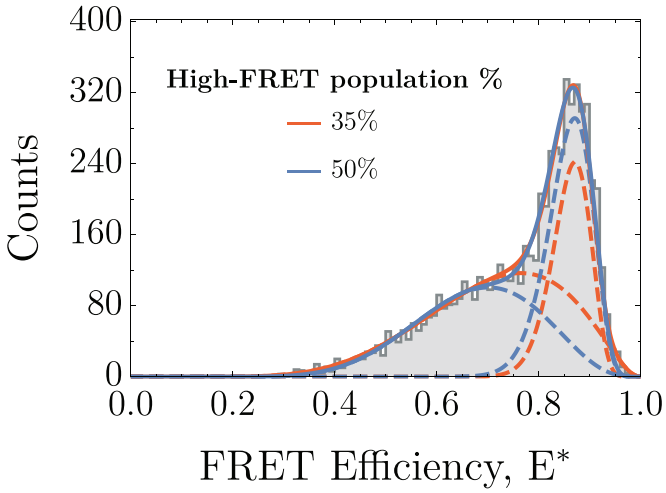


Figure A.4: The FRET histogram as in Figure 5.7 with two two-population fits that were forced to maintain a population ratio of 35:65 and 50:50 for the high-FRET peak to the low-FRET peak populations.The overall fit (solid line) and the separate populations (dashed lines) are shown.

A.3 Chapter 4 supplementary

A.3.1 Tube detection

A length distribution was found for stacked tubes in Section 4.3.2 using Wolfram Mathematica 10.2 to detect the objects in multiple microscopy images. Figure A.5 shows the example images in Figure 4.12 with the detected tubes overlaid.

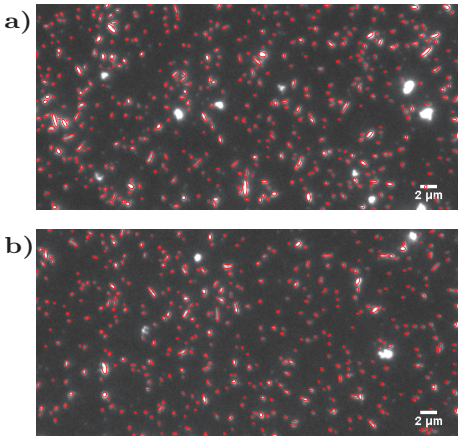


Figure A.5: Corresponding images to Figure 4.12 with the detected tubes highlighted with a fitted red ellipse for a) B-only and b) A:B of 1:20 samples. Tube detection was made in Mathematica using a Laplacian of a Gaussian filter to detect edges, and then binarisation of the image. Mathematica's inbuilt function 'ComponentMeasurements' detected each object and provided details of the best fit ellipse for each. Objects with a size below 3 and above 100 pixels, or a width above 6 pixels were ignored to filter out noise and aggregates.

Appendix B

Appendix: Methods

B.1 DNA strands

DNA strands were ordered from Integrated DNA Technologies (IDT). The strands used for the various experiments in this thesis are listed in Appendix C.

B.1.1 DNA sequence design

New DNA sequences were generated using NANEV software[7] that aims to find sequences that prevents undesired binding. All sequences — wholly-new or modified-old — were checked in NUPACK[6] for any desired or undesired interactions.

B.2 Origami synthesis

Three types of DNA origami were used in this thesis, all of which used M13mp18 as a scaffold strand. Single-stranded M13mp18 was ordered from Affymetrix at $1\,\mu g/\mu l$. Staple sequences for each origami can be found in Appendix C.1.

B.2.1 Origami tile

A minimised-twist origami tile[82] was used as a substrate for motor experiments in Chapters 2 and 3 and also in Chapter 5 for studying the threading of extensions through the tile and the repair of a missing staple.

Plain and modified staple strands were ordered from IDT and stored in MiliQ water. The origami tile was formed at 54 nM with an excess of staples in 1x Origami buffer (12.5mM MgOAc, 40mM (1x) Tris-acetate, pH 8.3). A 5x excess of staples was used in Chapter 5, elsewhere a 3x excess of staples was used. The plain and modified staples were mixed on a vortex before the addition of the M13mp18; the sample was finally mixed with a pipette. The samples were annealed from 95°C to 20°C in a PCR machine (Bio-Rad) at an average rate of 1°C/min in 0.1°C steps (a total annealing time of about 1.5 hours). The samples were held at 20°C before use or stored for up to a week in a fridge at 4°C.

B.2.2 Origami tube

The origami tubes in Chapter 4 were designed to have the staple nick position on the inside of the tube, so that modified staples would stick into the middle. The tubes can be encouraged to stack together using a 5x excess of linker staples for the ends of the tubes - these end staples were designed to force the tubes to stack at a specific rotation. To inhibit tube stacking, a 5x excess of U-shaped poly(dT)-end staples with 8dT extensions were added.

Plain and modified staple strands were ordered from IDT and stored in 1x TE. The origami buffer used in this chapter was 10 mM $MgCl_2$, 50 mM NaCl and 1x Tris-EDTA. The origami tube was formed at 54 nM for the ensemblue fluorescence measurements in Section 4.2, and 20 nM for the microscopy experiments in Section 4.3. M13mp18 was used as the scaffold strand and was annealed with a 3x excess of the plain staples (excesses are relative to the M13mp18 unless otherwise stated). For track experiments, a 5x excess of the anchorages were used and a 3x excess of their neighbouring bracing staples. $Cy5_{end}$, to provide the F_{end} signal, was added

in a 6x excess. The samples were annealed from 95°C to 20°C in a PCR machine (Bio-Rad) at an average rate of 1°C/min in 0.1°C steps (a total annealing time of about 1.5 hours). The samples were held at 20°C before use or stored in a fridge at 4°C.

B.2.3 Multi-layered origami

A multi-layered origami designed by Dr Robert Schreiber, a colleague, was used in Chapter 5 to check for threading of extensions through 3D origami. It was originally designed to carry a molecule of interest in its centre and hence has a small central region of unbound base pairs.

Plain and modified staple strands were ordered from IDT. The plain staples were stored in 1x TE, pH 8.0; the modified staples were stored in MiliQ water. The multi-layered origami was formed at 10 nM with a 10x excess of staples. The plain and modified staples were mixed on a vortex before the addition of the M13mp18; the sample was finally mixed with a pipette. The samples were annealed in a PCR machine (Bio-Rad) by heating to 65°C for 15 min, decreasing from 64°C to 60°C by 1°C every 5 mins, decreasing from 59°C to 40°C by 1°C every 40 mins, decreasing from 39°C to 20°C by 1°C every 10 mins (a total annealing time of about 16.5 hours). The samples were held at 20°C before use or stored for up to a week in a fridge at 4°C.

B.3 Origami repair

The motor was loaded at the start of its track as in Wickham *et al.* 2011[82] for all experiments in Chapters 3 and 4 by pre-annealing with the first anchorage, and then incubating with the pre-formed origami missing the staple for the first anchorage. The motor in Chapter 2 was loaded in a similar way but by pre-annealing with the first anchor and its director. This loading method was explored in Chapter 5 to determine its effectiveness.

The motor (M) and the first anchorage (A_0) (or anchor with its director (D) if appropriate, i.e. in Chapter 2) were annealed in 1x Origami buffer (12.5 mM MgOAc, 40 mM Tris-acetate, pH 8.3) by heating to 95°C and cooling to 20°C at a rate of 7.5°C/min. The strands were annealed with A_0 at 5 μM in the ratio of either a) M:A_0(:D) = 0.9:1(:3) or b) M:A_0 = 4:1. a) was used in all experiments, except those in Chapter 5 which used b) to enable complete loading of the motor.

The annealed complex was added such that A_0 was at a 0.95x excess to the origami and incubated at 37°C. Most experiments used a 1 hour loading incubation like Wickham *et al.* 2011[82]. Experiments in Chapter 2 used a 2 hour loading incubation after the motor was added to the origami, as loading during ensemble fluorescence measurements showed slower loading for this than the original 'burnt bridges' motor.

The braced tracks in Chapters 3 and 5 required the pre-formed origami to be purified (in the same way as it is normally purified after motor loading) before motor loading as well as after. This is to remove the excess neighbouring staple for the first anchorage, which can otherwise bind to the bracing region of A_0, hampering loading.

B.4 Origami purification

The origami tiles used in Chapters 2, 3 and 5 and the origami tubes used in Chapter 4 were purified with hand-packed size-exclusion columns, as used in Wickham *et al.* 2012[102]. The gel filter has an exclusion limit of 118 bp[193] — the principle is that the small staple strands get stuck inside the gel resin, whilst the larger origami cannot enter the resin and hence passes through.

The multi-layered origami used in Chapter 5 was purified from an agarose gel.

B.4.1 Size-exclusion columns

Empty chromatography columns (Micro Bio-Spin^{TM}columns, Bio-Rad) were packed with a size-exclusion resin (Sephacryl S-300 HR, GE Healthcare) to remove the staples from the origami structures.

The Sephacryl resin was resuspended into the same buffer as the origami by centrifuging 25 ml of the resin in ethanol with 25 ml of MiliQ water at 1,000g for 1 min. The solution was decanted, and refilled up to 50 ml with MiliQ water. This process was repeated 3x, and then repeated 5x with the origami's buffer. The resin was then stored in the fridge until use.

Columns placed in collection tubes were packed by adding 500 μl of the resuspended resin, centrifuging at 3.4 rpm for 1 min (using an Eppendorf Minispin centrifuge), emptying the collection tube and repeating. To ensure a dry bed of resin (to avoid diluting the sample), the columns were then spun again for 4 mins.

Sample was added to a packed column (20 μl for the samples in Chapter 5, 75 μl for the samples in Chapters 2 and 3) and spun down at 3.4 rpm for 4 mins. This was repeated with the filtered solution and new columns twice more.

The origami tubes in Chapter 4 used a similar protocol, but used a 3.8 rpm spin and prepared the columns by 4 min spins after each 500 μl of resin.

Origami loss after this purification technique is estimated as 20%. This was calculated from the band intensity on a polyacrylamid gel of the origami before and after a sample was purified (Figure B.1).

B.4.2 Gel purification

Samples of the multilayered origami were run on a 1% agarose gel at 135 mA for $\sim$ 3 hours. The band for the origami structure was detected by the Cy5 fluorescence. It was cut from the gel and squeezed by a microscope slide covered in Parafilm against another piece of Parafilm on the table. The solution that emerged was pipetteed away, avoiding any small pieces of agarose.

The solution was then spun down in 10K Amicon filters to concentrate it.

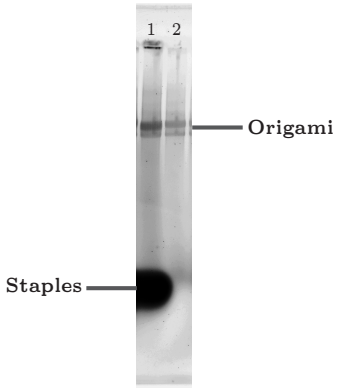


Figure B.1: Agarose gel of an origami tile sample before (lane 1) and after (lane 2) purification with 3 rounds of the Sephacryl S-300 size-exclusion resin. Gel details: 0.8% agarose gel, run at 100V for 75 min in an ice bath in the lab.

B.5 Gel electrophoresis

Polyacrylamide gel electrophoresis was used extensively in the preliminary characterisation in Chapters 2 and 3, and for minor use in Chapters 4 and 6. Gel conditions varied depending upon the required band separations. Gels were run in 1x TAE in a Bio-rad gel kit. Most of the gels were run in a cold room held at 4°C, otherwise they were run in an ice bath.

The gels were scanned using a Bio-Rad Gel Scanner. If fluorescently-labelled strands are present, the gels were first scanned for them unless otherwise stated. The gels were stained with SYBR® Gold Nucleic Acid Gel Stain (Invitrogen) before imaging with a 488 nm excitation laser and an emission filter at 530 nm. Cy3-labelled strands were imaged with a 532 nm excitation laser and an emission filter at 605 nm.

Gel band intensity was detected using the gel scanner software. The intensities stated are integrated over the area of the detected band.

B.6 Ensemble fluorescence measurements

Purified origami samples were made up to 150 μl with a final buffer of either a) 1x Ori + NaCl: 12.5 mM MgOAc, 40 mM (1x) Tris-acetate, 50 mM NaCl; b) replicate

CutSmart: 10 mM MgOAc, 20 mM Tris-acetate, 50 mM KOAc; c) NEB buffer 2.1: 10 mM $MgCl_2$, 1x Tris-EDTA, 50 mM NaCl. Samples in Chapters 2 and 3 were run in either a) or b), as stated alongside any results. Samples in Chapter 4 were run in c).

The samples were placed in 140 μl quartz cuvettes (Starna Scientific). The cuvettes were washed thoroughly with MiliQ and ethanol using a vacuum pump before use. The fluorescence was measured in a Cary Eclipse Fluorescence Spectrometer (Varian). The temperature of the samples was held at 37°C by a linked water bath. Samples were mixed with a pipette after 5 mins of acclimatising to temperature. 400 μl of mineral oil (Sigma-Aldrich) was added to stop sample evaporation (the effects of which can otherwise be seen after about 1-1.5 hours), whilst allowing other solutions to be added to the sample during the experiment.

The fluorimeter emission/excitation settings for the fluorophores used were: Cy5 645/665, TET 522/539, TEX615 596/613. For the FRET-based experiments in Section 4.2.3 the F_0 signal was recorded as the emission at 539 nm when excited at 522 nm, and the F_{end} signal was recorded as the emission at 664 nm when excited at 550 nm. The slit widths were 5 nm and 10 nm for the excitation and emission respectively.

Depending upon the experiment, different additions were made to initiate the motor movement — see individual sections for the details. All samples received 1 μl of Nt.BbvCI (10,000 units/ml, New England Biolabs). To normalise the fluorescence traces a 7x excess of motor was added, relative to the number of anchorages (assuming no loss during purification).

As some samples received a significant volume of additions, all fluorescence traces in this thesis were normalised against dilution from each addition. This was done by multiplying the signal by $\text{Volume}_{current}/\text{Volume}_{initial}$.

Some samples were affected by bubbles that formed in the cuvettes, coalesced and then moved out of the cuvette windows. This would decrease the fluorescent signals until a sudden increase, expected to coincide with when the bubble moves (see Figure B.2 for an example trace). Samples with decreasing signals can be

removed from the fluorimeter to find small bubbles in the cuvette. Mixing with a pipette can increase the signal to where it should be. Some samples were given 1x bovine serum albumin (BSA) during the initial mixing in the cuvettes in the hopes of stopping bubbles forming on the walls. This did not entirely eradicate the problem. The BSA is not expected (and was not seen to) affect the fluorescence experiments otherwise.

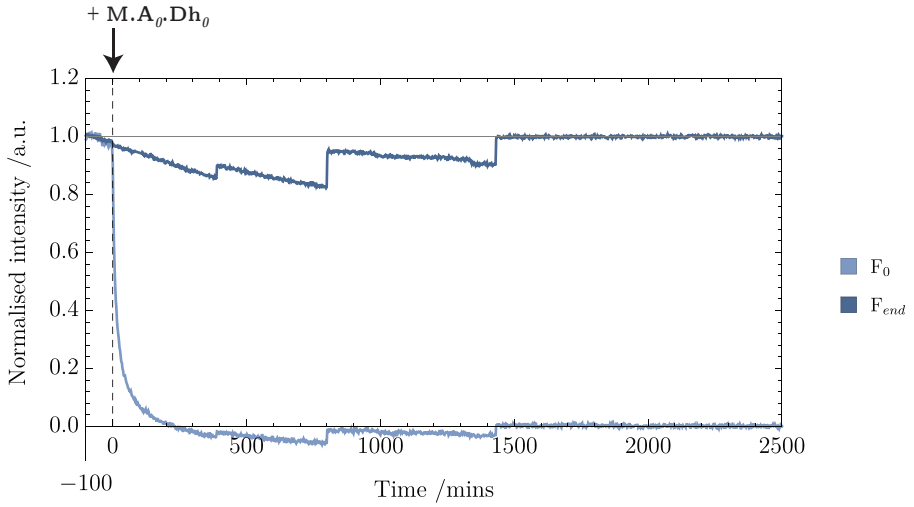


Figure B.2: An example fluorescence trace with three events causing a decrease in the fluorescence signal before a quick increase back to what is expected to be the "true" level. It is assumed that these events are bubbles growing inside the cuvette and finally releasing.

B.7 FRET measurements

The details in this section refer to the experiments in Chapter 5.

B.7.1 Sample preparation

The origami tiles were assembled with a 5x excess of staples. Cargo strands were added in a 20x excess to the tile. When annealing a cargo to an extended staple, this was done at a cargo:staple ratio of 4:1 with the staple at 5 μM. The cargo.staple complex was added to a defective origami at a 5x excess of the staple to origami.

Purified origami samples were diluted 250-fold in 1x Origami buffer and 0.1 mg/ml BSA (New England Biolabs), to around 200 pM. This was a starting point for measurement, but subject to change to ensure an appropriate rate of origami passing through the confocal volume.

Single origami samples were made for each case, except for in Figures 5.8, 5.14 and 5.20 which used data combined from two samples.

B.7.2 Microscope

The experiments were performed at room temperature (≈22°C) using a home-built confocal microscope as described in Hohlbein *et al.* 2013[150]. A 532 nm laser (operated at 240 μW) and a 638 nm laser (operated at 60 μW) were alternated at 20 kHz and focussed 20 μm into the sample solution through a x60, 1.35 NA, UPLSAPO 60XO (Olympus) objective. Fluorescence emission was collected by the same objective, and split spectrally on to two avalanche photo diodes (SPCM-AQR-14; PerkinElmer, UK) to detect the donor and acceptor fluorescence.

Slides were passivated with 1x Origami buffer (containing 0.1 mg/ml BSA) for 5 mins before being pipetted off and adding the sample. This reduces the binding of the origami to the slide surface, which decreases the concentration of origami in solution for imaging.

B.7.3 Data analysis

Multiple fluorescent bursts were identified for an individual origami as it diffused through the confocal volume. The search algorithm requires a minimum of 12 successive photons, with at least 7 neighbouring photons within a time window of 500 μs centered on their arrival time[194]. Each fluorescent burst was filtered for correct labelling stoichiometry. The apparent FRET efficiency (E^*) was then calculated for each burst according to Equation (5.3).

B.7.4 Model fitting

Initial model comparisons in Section 5.2.3 made use of a Beta distribution, defined as follows:

$$\mathcal{D}_\beta(E) = E^{(\alpha-1)}(1-E)^{(\beta-1)}, \tag{B.1}$$

where α and β are free parameters for fitting.

Through the results sections, E^* was fit with one or two populations with a distribution according to Equation (5.6) or Equation (5.7) respectively using the 'NonLinearFit' function in Wolfram Mathematica 10.2. The best fit was found by minimising the mean residuals of the fit.

B.8 Microscopy

B.8.1 Microscope details

All the microscopy experiments in Chapter 4 were performed using an Olympus IX-81 inverted microscope. An Andor iXon EMCCD camera recorded the images. An Olympus 100x, 1.4 NA magnification oil-immersion objective was used along with a 1.6x microscope internal magnification. Emission was passed through a MAG Biosystems Dual View (DV-2) device that splits the signal into two channels, which are filtered separately with a 565±20 nm and a 665±20 nm filter. The 565 nm channel was used for the sample observations — its signal was projected onto one 512 px x 256 px half of the 512 px x 512 px camera chip. The 665 nm channel was used with the Cy3/Cy5 filter to observe the beads with the mercury lamp, to compare against sample locations.

For imaging Cy3 fluorescence, the samples were illuminated with a OZ Optics 50 mW 532 nm laser fibre-coupled (single-mode, manufacturer-stated 20 mW at the fiber end) to an Olympus module for objective-based TIRF. For imaging the YOYO-1 Iodide fluorescence, the samples were illuminated with a mercury lamp (Prior Scientific, Lumen 200). Andor iQ and μManager software[195] were used as imaging and microscope control software.

B.8.2 Filter and fluorescence spectra

Figure B.3 shows the fluorescence spectra of YOYO-1 Iodide and Cy3 with the respective excitation and overall emission filters used. The filter spectra for the "WIB" filter cube is shown in Figure B.4. The filter cube details for the Cy3/Cy5 filter cube is shown in Figure B.5.

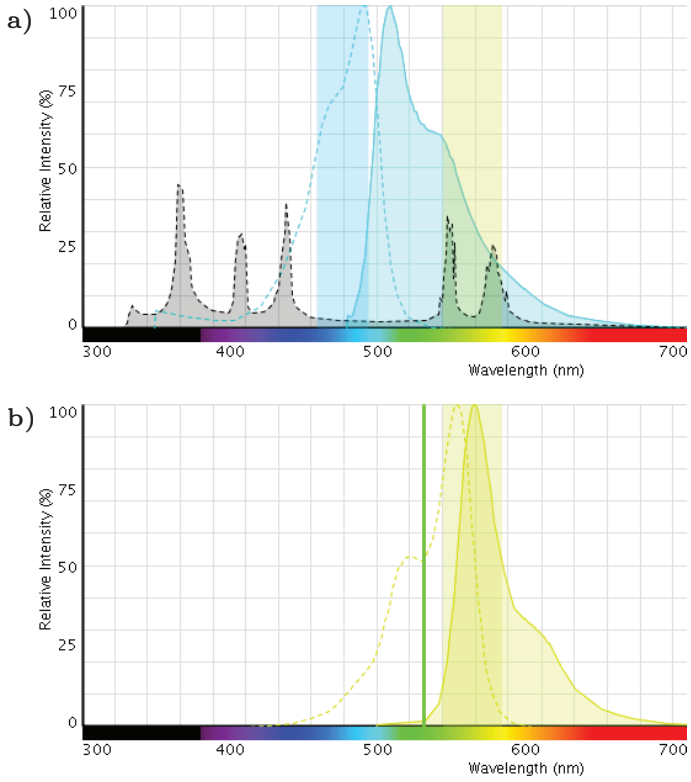


Figure B.3: The fluorescence spectra of a) YOYO-1 Iodide and b) Cy3 overlayed with the light source and excitation (low wavelength) and overall emission filter (high wavelength) for observation. a) A mercury lamp and the U-MWIB3 ("WIB") filter cube and b) a 532 nm laser and the Cy3/Cy5 filter cube were used. The emitted light from the filter cubes was finally filtered by the DV-2. The spectra were produced using Thermo Fisher's online spectra viewer.

B.8.3 Flow channel preparation

All coverslips were burned in a furnace before use by heating to over 300°C to reduce background fluorescence. Two ∼2.5 cm long, parallel strips of Parafilm are placed ∼0.5 cm apart on a 60 mm x 25 mm coverslip (Menzel Glazer No. 1.5), and a 22 mm

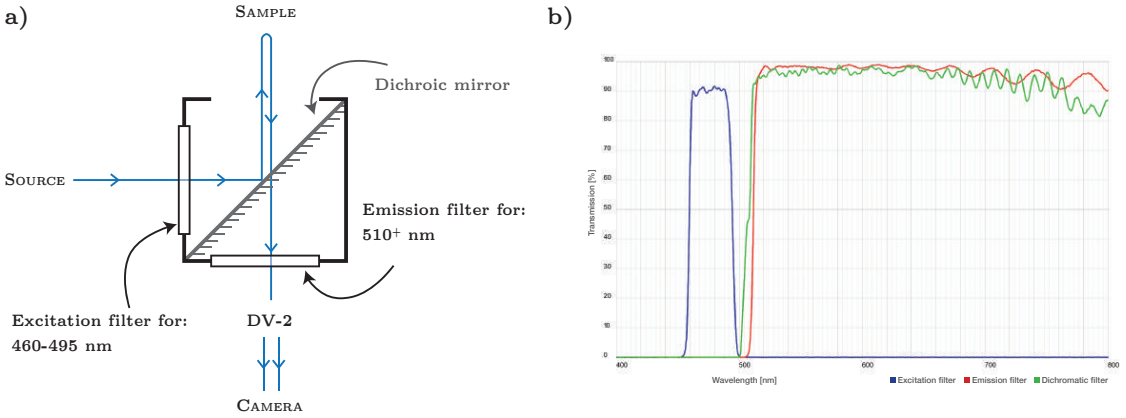


Figure B.4: The Olympus U-MWIB3 filter cube (A.K.A the "WIB" filter.) used for observing YOYO-1 Iodide. a) Schematic of the filter cube containing an excitation and emission filter. The Dual View (DV-2) separates the transmitted light with a 565±20 nm and a 665±20 nm filter and projects the two images on half of the camera chip surface. b) The filter cube spectra.

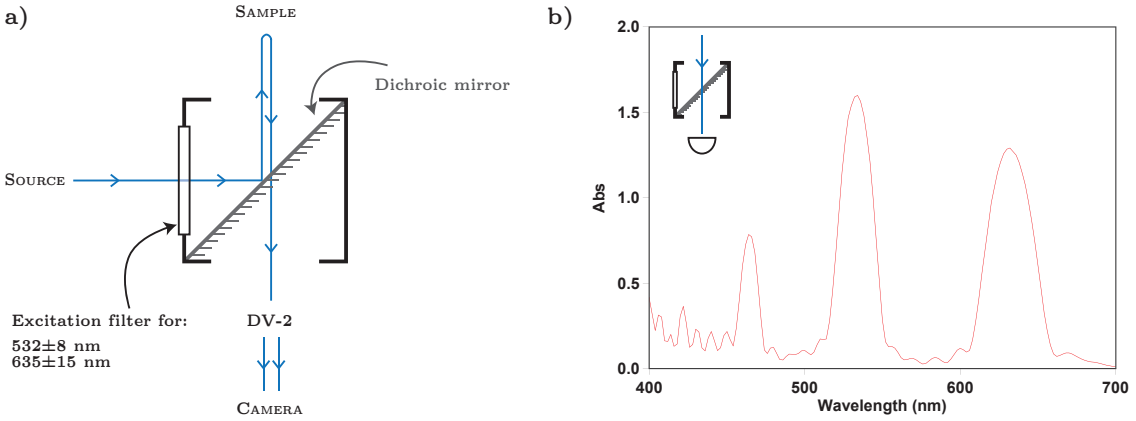


Figure B.5: a) Schematic of the Cy3/Cy5 filter cube used for detecting the Cy3 fluorescence. The excitation filter is able to select for wavelengths in two windows (for Cy3 and for Cy5). The Dual View (DV-2) separates the transmitted light with a 565±20 nm and a 665±20 nm filter and projects the two images on half of the camera chip surface. b) The tested transmission of the dichroic mirror. The absorbance of the sample denotes the reflected wavelengths. Low absorbance values are for wavelengths that are transmitted through the mirror, high values are for wavelengths that are reflected by the mirror.

x 22 mm coverslip (Menzel Glazer No. 1) is placed on top. The slide was heated on a hotplate at 80°C for ∼30 s to slightly melt the Parafilm. Gentle pressure on the coverslip then helps the Parafilm to stick to both surfaces, sealing the long edges of the channel.

Solutions were pipetted into the channel from one end, using filter paper to wick the solution out from the other. Before viewing on the microscope, the channel ends were sealed using Valap[136]. This prevented evaporation and exposure to oxygen. An advantage of Valap is that it is easily removed if subsequent additions to the sample are needed.

To prepare the surface of the slide, the channel was washed with a sequence of solutions separated by an incubation period and a wash with two channel volumes of microscopy buffer (1x TAE, 12.5 mM $MgCl_2$). Table B.1 lists the sequence and incubation timings. First, 300 nm latex beads (Interfacial Dynamics Corp.) were added to help focus on the surface of the slide – only a few beads in each field of view were necessary, and their location could be checked in Brightfield to compare against the origami signals. A bead dilution of 1-in-1,000 to 1-in-10,000 was used. A 4:1 mix of BSA: biotin-BSA was then used to coat the surface to prevent non-specific binding, followed by an incubation with streptavidin (NEB) to bind to the surface-bound biotin, and then an incubation with the sample. An anti-photobleaching buffer (see Appendix B.8 for details) was finally washed through and left in the channel before the channel ends were sealed with Valap.

The BSA and biotinylated-BSA (lyphophilised powders, Sigma Aldrich) were re-suspended to 40 mg/ml and 10 mg/ml respectively in 20 mM TrisHCl pH8.0, 10 mM KCl, 0.1 mM EDTA, 30% v/v glycerol.

B.8.4 YOYO-1 Iodide staining

YOYO-1 Iodide (1 mM stock in DMSO; Molecular Probes, Invitrogen) is a 1,271 dalton molecule. It has a 3,200-fold increase in fluorescence when bound to ds-DNA compared to ss-DNA[132]. A 1/10 dilution of the YOYO-1 was added to the DNA

Solution	Incubation time
300 nm latex beads	1 mins
Microscopy buffer	*Wash only*
4:1 BSA:biotin-BSA (2 mg/ml:0.5 mg/ml)	5 mins
Microscopy buffer	*Wash only*
1 mg/ml Streptavidin	5 mins
Microscopy buffer	*Wash only*
Sample	2 mins
Microscopy buffer	*Wash only*
Anti-photobleaching buffer (or enzyme-containing version)	Remains in the channel

Table B.1: Sequence of solutions washed through and incubated in the channel on a microscope slide. One channel volume's worth of each solution was added for an incubation, and two channel volumes of the microscopy buffer was used for washed inbetween.

tube samples in a 1:10 volume ratio. The samples were purified 10-15 mins later with Sephacryl S300 size-exclusion resin, as used for origami purification.

B.8.5 Microscopy and anti-photobleaching buffer

The microscopy buffer was 1x TAE, 12.5 mM $MgCl_2$. The anti-photobleaching buffer used in Section 4.3 was adapted by a colleague Samuel Tusk from Selvin & Ha 2008[196] and Cooper *et al.* 2013[197]. The buffer was made immediately prior to use. The recipe for it is as follows: 276 μl glucose buffer (0.8% w/v D-glucose), 2.5 μl gloxy solution, 1.25 μl Trolox (100 mg/m in DMSO), 0.78 μl NBA (100 mg/ml inDMSO), 2.25 μl COT (2% in DMSO). The final DMSO concentration is 1.5%.

Glucose buffer was made as: 1x TAE, 12.4 mM $MgCl_2$, 0.8% glucose. 100x gloxy solution was made according to: 20 μl of 0.2 mg/ml catalase, 80 μl microscopy buffer + 10 mg glucose oxidase. This was mixed by tapping, centrifuged at high speed for 1 min and the supernatant collected and stored at 4°C.

For an enzyme-containing anti-photobleaching buffer, the 276 μl glucose buffer was replaced by 273.17 μl glucose buffer and 2.83 μl KOAc or NaCl (5 M). 2.5 μl of

Nt.BbvCI (10,000 units/ml) was then added to 47.5 μl of the new anti-photobleaching buffer.

B.8.6 Leakage signals

YOYO-1 Iodide signal is not seen with the microscope settings used for observing the Cy3 fluorescence. A stained origami is observed with the YOYO-1 filter in Figure B.6a). The Cy3/Cy5 filter settings used for observing the Cy3 fluorescence is used in Figure B.6b) and shows no leakage signal. Therefore, signal seen using the Cy3/Cy5 filter cube can be assumed to be from the Cy3 fluorescence only. The signal is confirmed to not be the beads used for focusing, as the beads can be checked in Figure B.6c).

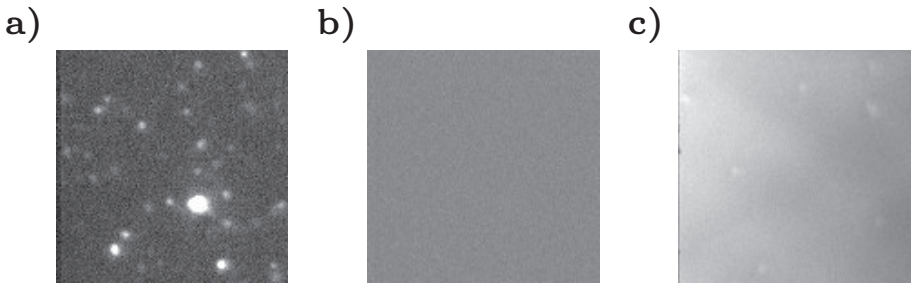


Figure B.6: The monomer origami from Dunn *et al.* 2015[27] stained with YOYO-1 Iodide is illuminated with the mercury lamp and a 532 nm laser. Leakage of the YOYO-1 signal into the image with the settings used for the Cy3 signal is tested. a) The filter cube used for the YOYO-1 signal: U-MWIB3 filter, 1s exposure, from the 565 nm channel of the DV-2. b) The filter cube used for the Cy3 signal: Cy3/Cy5 filter, 100 ms exposure, from the 565 nm channel of the DV-2. c) Cy3/Cy5 filter, 100 ms exposure, from the 665 nm channel of the DV-2 — this shows the beads used for focusing.

B.9 Image analysis

ImageJ[198] software was used for viewing the microscopy images and setting constant brightness/contrast settings across a sample.

B.9.1 Detecting spots

Spot detection was required for the image analysis in Sections 4.3.2 and 4.3.4. This was not meant to be a perfect method, but to provide a useful tool for highlighting tubes and differences between video snapshots in order to aid discussion. The analysis was done in Wolfram Mathematica 10.2 using the Laplacian of the Gaussian for edge detection[140,141], normalising and then binarising the images. Spots were detected in the binarised images using the 'ComponentMeasurements' function. This is then able to provide values for a fitted ellipse to each spot, which was used to highlight the detected spots on comparison images for visual inspection. The spot size was measured as the number of pixels forming the spot. Very small or large spots were filtered out with respect to minimum and maximum sizes or widths, to avoid noise and aggregates.

The Laplacian of the Gaussian

The Laplacian of the Gaussian is a tool used for edge detection in images[140,141]. Intensity changes at edges are characterised by a peak in the first derivative and hence a zero-crossing in the second derivative. This was implemented using the 'LaplacianGaussianFilter' function in Mathematica. The process is that an input image ($I(x, y)$) is first convolved with a Gaussian kernel ($G(x, y, r)$) to smooth out noise, according to:

$$G(x, y; r) = \frac{1}{2\pi r^2} e^{-\frac{x^2+y^2}{2r^2}} \tag{B.2}$$

The Laplacian of the Gaussian is then found according to Equation (B.3). The choice of r depends upon the sizes of the objects you are trying to detect — too small and it won't smooth out the noise, too big and it will smooth out the objects.

$$f(x, y) = \nabla^2[I(x, y) * G(x, y; r)] \tag{B.3}$$

Gamma correction

In some (stated) cases the images were transformed with a gamma correction to better highlight the spots to be detected. This was used during the spot detection, but not on the displayed microscopy images. The transformations were made according to Equation (B.4) where p_{old} and p_{new} refer to a single pixel value before and after the correction, Min and Max are the minimum and maximum values for normalising the image, and γ is the gamma correction parameter.

$$p_{new} = \left(\frac{p_{old} - \text{Min}}{\text{Max} - \text{Min}} \right)^{\gamma} \tag{B.4}$$

Tube detection

Section 4.3.2 required the detection of tubes. The images were initially transformed with a gamma correction with γ=0.6 to better highlight the spots for the detection process. Images from each sample were normalised between the minimum and maximum value across the sample. A Laplacian of the Gaussian filter was used with r=2. Each image was normalised individually and binarised with Mathematica's chosen cut-off value. Only spots with sizes between 3 and 100 pixels, and with widths below 6 pixels were considered.

Flashes in the videos

The median subtracted image were created by applying Equation (B.5) to each pixel of the image, where p is the original pixel value, p_{median} is the median original pixel value for that pixel over the entire video, and p_{ms} is the new median subtracted pixel.

$$P_{ms} = \frac{p - p_{median}}{p_{median}} \tag{B.5}$$

Section 4.3.4 required the detection of the bright spots in the median subtracted images that correspond to flashes in the videos. All the median subtracted images

for all 3 samples were normalised together with respect to the 0.001th and 0.999th quantile value (as the minimum and maximum are too sensitive to outliers). A Laplacian of the Gaussian filter was used with r=3. The output images were then normalised between the minimum and maximum value of all the images. The images were then binarised with a set cut-off of 0.42. Only spots with sizes between 5 and 70 pixels were considered.

B.10 Octahedron protocol

The strands for the octahedra were annealed in a stoichiometric ratio. The annealing protocol involved heating the strands up to 95°C and cooling to 20°C at a rate of 7.5°C in a PCR machine. This was done in a buffer of 10 mM Tris, 100 mM NaCl, pH 8.0.

Phosphorylation of the strands was made by adding T4 PNK (New England Biolab) according to the New England Biolab protocol. Ligation of the strands was made by adding 1 μl of T4 DNA Ligase (New England Biolab) to each 19 μl sample, and leaving at 16°C in a PCR machine for 7.5 hrs.

Appendix C

Appendix: DNA Sequences

Strands were ordered from Integrated DNA Technologies (IDT). Unmodified strands were ordered unpurified or PAGE purified, at IDT's recommendation based on the length of the strands. Modified strands were ordered HPLC purified; the modifications are stated with IDT nomenclature.

Strands are listed in tables from their 5' to 3' end. Some domains are highlighted by colour to match figures in the main text that they correspond to. Tables in Appendix C.1 list the basic staple mixes for the three origamis used. The following sections list the strands used in each results chapter, as stated in the table captions.

C.1 Origami staple sequences

C.1.1 Minimised-twist tile

The staples for the minimised-twist origami tile were used as published in Wickham 2011[128]. Replaced staples are referred to by their original name.

C.1.2 Multi-layered origami

Name	Sequence	Name	Sequence
MuSt1	ATGCAGAGAGAATTAGAAACGATTTTTTGTGCTATTTTGGCTTAT	MuSt100	AATTTACGGCGAGGCGTGAAGCCT
MuSt2	CAGACGACAGGGTAATAACAGCCAGGCATGATGTGGCAAC	MuSt101	GAAAAAGCAGAATCGCAAAACTTTTATGTAAACGATAGCT
MuSt3	AGAATATAAAGTACCACCTTTTTGACCTAAATTAGAGTG	MuSt102	TAAGAATAGAATTACCAATTAATTATAACGGAGTCAGATGATT GTTTG
MuSt4	AAAGCCAATCTTCTAACCTCCGAATAGTGAATTTATCAACAGAAA	MuSt103	ACCGAAGCTTTGCCTTTGAAACCACACCAGAGCTGGTAATGTG CCCGT
MuSt5	CCGGTATTCTAAGAACAGCATGTAAAAAATGAAAACAGGGGCTATCTT	MuSt104	CAAAATTACCTTTGCCTATCAGATACAGTTGACTCAAATAAGC AGAAG
MuSt6	ATAGCAAGCAAATCAGCTTTCCTTCCAAATAAACTGAACAAATAAGAG	MuSt105	GAGCCACCTACCGCCATAAGTATATTCCAGACTCGGTTTAGCT TGATA
MuSt7	TCGTAGGACCAAGTACACAAAATATGAGCGCTAATATTCT	MuSt106	TTACAAACCAACAGAGAAACATCGAGAACAATTGCCTGAGTCT TTGAT
MuSt8	GCGTTATACAAATTCTTACCCAAGGTTTGAA	MuSt107	ATAGTTAGACGGAGATTCATCTTTAAGAGTAATTTTAAGAAGA AAAAT
MuSt9	TAAATCAAAATCAATAAGTTACCAGTCACCAATAGCGTCACACCCTCA	MuSt108	CACGACCAAGCTAAACGTCCATCACGAACGTGTTAGAGCTACT ACGTG
MuSt10	TGCCAGTTCGCACTCAGTAAAGTAATTCTGTC	MuSt109	ACAGACCAACCAAAATTAAGAGCAAAAAAGATGGATGGCTTCA ACATG
MuSt11	TAGACGGACGCGCCTTCAATAATCGGCTGTATATAGAAGCACCCA	MuSt110	TGCTTTGATTTGATGGAAGGGCGATTTGCGTACGTGCCAGGTG TAAAG
MuSt12	AAAGTCAGGACAATAAAAGAACGGGTATTAAAATCATTACCCAACGCT	MuSt111	GACTATTAAGGCAAGGATCAATTCGTCAAATCGAAAAGCCTAA ATTGT
MuSt13	GAGAGACTGACAAAAGTCGAGAACAAGAGTAT	MuSt112	AGCAAGCGTCTAGAGGCAATTCCAGATGTGCTCGATCGGT
MuSt14	TTGGGTTATCGAGCCACAGTAGGGCTTAATTGCTGTTTAGGCGTTAAA	MuSt113	TAAAGATTGCCAGTTTGGATAGGT
MuSt15	CAAGAAATCATCGGCTTACCATTTGAGGCACATACATGATTTCGG	MuSt114	TCCGCTCAATCCCCGGCGACGGCCAGTGCCAA
MuSt16	TTGAGTTAAAAGAACTTATTATTTGAATCTTACGCGCCCA	MuSt115	CACAAGAAAGCGTTTGCCATCTTTAATCACCG
MuSt17	TAGATTAAGGTTTAACTTCGCCTGTTCCTGATCGAACGTTATTAGACT	MuSt116	TATCACCGTCACCGACTGGAAAGC
MuSt18	AATACCCAAGCCCAATCCCTGAAC	MuSt117	GAACCAGACAGGGATAGCAAGCCC
MuSt19	TCGCTATTTTTTTTAACAAGAAAA	MuSt118	CCGTTCCATTCATTAAAGGTGAATATATAAAA
MuSt20	TTTGTCACGATTAGTTTTAACGTCGAAACCAAGTTTATCAACAATAGA	MuSt119	GCAGTCTCGTATTAAGAGGCTGAGACTAGATT
MuSt21	GAAACGCATTTATCCTATCCCAATATCATTCCACAACATGTTCAGCTA	MuSt120	AGAGCCGTTTTTGCGGAGCCAGAATTGTTCATTTCAATTAAAC GTAGA
MuSt22	AAATACATTCTTTCCAGAGCCAATGCCGTTTTTATTTTCA	MuSt121	CTCATTTTGCCACCACCGGAACCGTCATAGCCCCCTTATT
MuSt23	GTACATAACCGTGTGATTAATTTCACGCTCAAGTAATAAG	MuSt122	AATAGCGCTGAGAGCCTATCAAAATTAATCAATCATA
MuSt24	ACCGATTGGGAGTGTACCGCCGCCGGTTGATACCCTCAGACAGCCCTC	MuSt123	GTAACACTGAGTTTCGTCACCAGTCCACCACC
MuSt25	GAAATTAGTAAGCGTGGTCAGACTCAGTACCCCTCAGAGACAAACTA	MuSt124	ATAATTTTTTCACGTTGAAAAATTCTGAAACATGAAATGAATTTA
MuSt26	AATTAAGCCTTATTACAGGCAGAGAGATAACC	MuSt125	GGACTAAGTAAAGCACTAAATCGTGGGGTC
MuSt27	TCGGCCTCCCTCAGAGCCGACCGCCACAGGCGGAT	MuSt126	GTAGTAAACAGTTGAGACGCTGCGTTGGCAAA
MuSt28	TTTGCACGTAAAAAATCATGCAGTATGTTTTAATT	MuSt127	TTATTACAGGTAGAAAGATTCATTTGGGCTTGAGATGGT
MuSt29	GATTTTCAGACGCTGAGTAAATCGTATTTTAGTAAATAAGTATCATAT	MuSt128	GCCGCGCTTAATGCGCCGCTACAAGAAAGCG
MuSt30	GATTATACTGCTGAACAAGGAATTTAGCCCTAATAGAACCACCAGTCA	MuSt129	AAATGTTTAGACTGGATAGCGTCCATCCCCCT
MuSt31	ATGATACAAGGGAGGGCCGGAAACGAAGGAAATAGCAATAAAGCGCAT	MuSt130	CTCCAACAGGTCAGGATTAGAGAG
MuSt32	TAAAAGTTATGATGAAGAATACCATTGCTTCTGAAGAGTCGCTTAGG	MuSt131	AGATAGGGCGTAACCACCACACCC
MuSt33	ATAAACAGTAATTGTAGTTAGTAATAAAACACTTGTATCAAACGGTGT	MuSt132	AATCGGTTTTAAACAGTTCAGAAATAATAGTA
MuSt34	AACCTATTTCTCCAAAGCTAAACAAACCTAAA	MuSt133	AATACTTTCATAAATATTCATTGAAATACTGC
MuSt35	CCTCAGACCACCCTCCAGGAGGTAGCAAGGAAGGTAAAAGTTTAT	MuSt134	CCGCCTGCAACAGTGCCAGAACCCATGTACC
MuSt36	CATCACCTTTCTGAATTCATCATAATTGCTTTACAAACATTGGAAACA	MuSt135	TGACGCTCAATCG ACAGACAAACTAAAGGAATTGCGAATA
MuSt37	CAACGCCTGTCGAAAACGAAAG	MuSt136	CGCCAGAATCAGAAACACCAGAACGA
MuSt38	ATAAAACAACATCACTATTACCGCAAGAGTCTAGGAGGCCACTATGGT	MuSt137	GGAATCGTAGACTTTTTCATGAGGAAGTTGGCGCA
MuSt39	GGATTTTAAAAAGGCACAACCATCGC	MuSt138	ACCTACCAAGCAGCAAATGAAAAATATTAACA
MuSt40	GGAGCCTTTTAATGCCGTCGAGAGAGCATTGAAGAACCGCGACTGTAG	MuSt139	TTAGGAGCAATGGCTATTAGTCTAAAAACGGAAAGACAGGCTTTGA
MuSt41	CTGAAAGCTTGAGGATTTATCTAACGGAATTAAATGGAAGTTGCGTA	MuSt140	GACGGTCAATCATAAGGGAACCTGCTCCATGTTACTTAGCC
MuSt42	CCGATAGTTTATGCGATCTTGACAAGGCATAGAGCGAGAGTTTACCCT	MuSt141	TAACATTATCACAATAGATAATACATGTAAGAATACGT
MuSt43	CCACGCATAACCAAGGCACCACTTTCAA	MuSt142	GGCTCTGAAATGGATTATGACAGGAACGGTA
MuSt44	TAAATTGTGTAGCATTCTGTATGAAGTGCCCCCTGCCTGCTTTTG	MuSt143	AACTAAACAAAGCTGCTCATTCCACTACGGATATATTCGG TCGCTGA
MuSt45	TCCGCGACCGAACTGACCAACTTGTTTTGCCACATAACG	MuSt144	GCTACAATAAGACACCAATAACGGTAGCACCAATTT
MuSt46	AACGAGGGGAGGTGAGCGAACTGAGAGGAAGGTTAGAAGTATTAATTT	MuSt145	AATAACCAGTTACATAAAGAAAGGTTAGA
MuSt47	TAGTAATACCCCCGATGCGAGAAACAACGTCATGGTTCCGAGAGTTGC	MuSt146	TTAATTTCATCAACGTATGCAGATAGAGGGGGACGAGAAT
MuSt48	TGAGGCCAGCTACAGAGCATCGG	MuSt147	CTCGAATTACCGCCTGTTTTTCTTTAAAGAACAAGTTTTT GAACCCT
MuSt49	GAATTACCTGCGCCGAGAATACACATGAATTTTCCACAGAACCGCCAC	MuSt148	ATACCGAATCAATATATGTGCACCTGAGCAAAAGAAGTGAG
MuSt50	GGATTTTATTACATTGGCAACAGGTTAATGCGGCGGTCAGTCTAAAG	MuSt149	CGCGTTTCAATGAAACCGAGGAAACGCAATACGGAATATA TTGACG
MuSt51	CTACGTTAATTTTTGCTAAGAGGAAAGGTGGCCAAAGAATTGTGTAGG	MuSt150	TACCCAAAACTTTAAGAACAACA
MuSt52	AAAAGAATGAAAGAGATATTCATAGGCAAAACAATGACATCCAAAA	MuSt151	CAGGGTGGGCCCTGAGAAATCGGCAAAATCCCTTAT
MuSt53	AAAGGGAGTAGCAACGCCGAGTAACAGCCATTGCAGATTCCTTCTGAC	MuSt152	CTGCCAACATGTAAT
MuSt54	GACCATAATAAAGCCTTTCATTTTCTAGCTTGTCAATCCGCATTA	MuSt153	CTAATATCCCATCCT
MuSt55	CAAATGCTGTACCAAATCGCAAATGCTATTTTAGAATCGATTTAACCA	MuSt154	CTCCCATAATTACTA
MuSt56	GAGGTGCCCGTTGCGCGTGAGACGGTCCATAG	MuSt155	CTGACTTGCGGGAGGTTTTTTTAGCGAACCTCCCTC
MuSt57	AACCATCAAAACCTGTTTGGGCGC	MuSt156	CTGCAAGACAAAGAACGCGAGCATATTTAACAACTC
MuSt58	AATATCGATTGCTCCGTGTCTG	MuSt157	CTAGAGAGAAGAACAAGAAAAATTC
MuSt59	ACCGGAAAGTGATACATTAACATTATATTTCAACG	MuSt158	CTCTTGAAAACATAGTGCTGATGCAAATCCAATCTC
MuSt60	AAGAGGTCATAAAACGGAATTACGAGAACCGGGACAGATGTCGCCTGA	MuSt159	CTAGTAAGCAGATAGGCCTTTACTC
MuSt61	TACCTTTACGTTTTAAAGCTATATTCAGAGCACTCATATA	MuSt160	CTCAATTTCATTTAACACCGGAATTC
MuSt62	AAATCAAAAGAAGCTGATTGCCCTTCCGTAATC	MuSt161	CTCCAAAGACAAAAGGGCATATGGTTTACCAGCGTC
MuSt63	TTTTAAATGATAATCAACCATCAACCGTAATGGAGGGGACGACGACAG	MuSt162	CCTTTTACATCGGGAGAAACATTCCCTTAGAATCTC
MuSt64	GAAGTTTCAACTAGCAGATAAATTGGATTCTCGATCGCACTCCAGCCA	MuSt163	CTCAGTAGCGACAGAATCAAGCCTTTTTAAGAAATC
MuSt65	ATTCTGCGCAAACAAGTGAGAGATCAACATTATCTGGTGCCGGA	MuSt164	CTCAATATAATCCTGAATATACAGTAACAGTACCTC
MuSt66	TTAAGCAAATCAAAAAGACTTCACCAAAAGAACTAACGTCATTGT	MuSt165	CTCCACCAGAACCACTCGATAGCAGCACCGTAATTC
MuSt67	CAGTCGGGCCCAAATCGTGGACTCGGAAGGGAGGGCGCGTGATTAAAG	MuSt166	CTTCGTATTAAATATTACATTTAATC
MuSt68	TTTTAAACTCAGGAACGTGGGAACAAACGGTTAAAATTATATGTA	MuSt167	CTAGTGCCTTGAGTAACAAAGTTTTAACGGGGTCTC
MuSt69	CAAGGATGCACCGCTAATGTGAGCGAGTAACGCTCATTTTGAACGGTAA	MuSt168	CTCTGGTCAGTTGGCAAATCAGATGGCAATTCATTC
MuSt70	ATTAATTGCGCCATTCGCCTTCCTGTAGCCA	MuSt169	CTCCGTACTCAGGAGGTTTAGACCCTCAGAGCCGTC
MuSt71	CCTGGGGTGGGAAGGGGCAAGGCGATTAAGTTTTGTAAAAGTACCGAG	MuSt170	CTCGAACGAACCACCTCAAACCCTCAATCAATATTC
MuSt72	CTGTTTCCCAGGGTTGCCATTCAGGCTGCG	MuSt171	CTAGTTTTGTCGTCTGCCCGGAATAGGTGTATCATC

Table C.1: (continued)

Name	Sequence	Name	Sequence
MuSt73	CCCCGGTTATGCAACTGAGCTGAAAGCCCGAAATCAGGTCGCTTTTGC	MuSt172	CTGACATTCTGGCAATTCGACAACTC
MuSt74	GTCTGGAGAACGAGTAGATTTAACATAGCCCG	MuSt173	CTGTGAATTTCTTAAACATCAGCTTGCTTTCGAGTC
MuSt75	ATGGTATTCGCGTCTGTTCCCAG	MuSt174	GGCTTGCAGGGAGTTAAAGGCCGCTTTTGCGGGATCGTCA CCCTCAGCAGCCTCA
MuSt76	AAACGTTAATATTTTGCGGATTGATATGATATCTGAGTAATAGCAAAA	MuSt175	CTGGCCTTGCTGGTAATATCCCCATTAAAAATACTC
MuSt77	AATTTTTGTTAAATCAAACCCGTCAATGCCGGTTAGAACCTAAAGCTA	MuSt176	CTAAGCGCGAAACAAAGTACACGTAACGATCTAATC
MuSt78	ATAGGAACGCCATCAAAAATAATTGCCTGAGA	MuSt177	CCTTGTAGCAATACTTAGAAGAACTCAAACTATCTC
MuSt79	TCACGACGGGGTAACGCTGTGTGAAGTGAGCTCGCTTTC	MuSt178	CTGCTGACCTTCATCGACCCCCAGCGATTATACCTC
MuSt80	GCTTTCATCTACAAAGAAGCCTTTGACCCTGT	MuSt179	CTCCTCGTTAGAATCAGAGCGGGGTAATAAAAGGTC
MuSt81	TATCGGCTGCAATGCTCAACCGTGGGGCGCAAAGTACGTTTTGAT	MuSt180	CTAGTCAGGACGTTGGGAACTGGCTCATTATACCTC
MuSt82	GCTTTCCGAAAAATTTAGAGGGTAGGTCAATATAACAGTTGATTCCCA	MuSt181	CGAGCACGTATAACGTGCTTTCC
MuSt83	AACCAGGCAAAGTGCGGGAGGCTATCAGGGCAGTTT	MuSt182	CTAAAGCCGGCGCAAATTAACCGTC
MuSt84	CAACTGTTGCCTAATGAATTGTTA	MuSt183	CCTTACCAGACGACGATAAAAGGCGCATAGGCTGTC
MuSt85	AACGAGCGACATAAAGTAAGACTCCATTTGGGAATTAGAGCACAAACA	MuSt184	CTGGGCGATGGCCCTGACGGGGTC
MuSt86	AAATCGCGAACCACCAGAAGGAGAATATCT	MuSt185	CTAGCGGATTGCATCACACTATCATAACCCTCGTTC
MuSt87	TTGATATTCCAGCAAAATCACCAG	MuSt186	CCTTTGCCCCAGCAGGCGAAAATCCTG
MuSt88	AATAAATCCAAGAGAAGGATTAGGGCGGAGTG	MuSt187	CTAATATAATGCTGTAGCTAGAGCTTAATTGCTGTC
MuSt89	ACTAACAACTAATCCTCTCATTAAAACAAAGACAGAGGCG	MuSt188	CTAACGCGCGGGGAGAGGCGGAAAACCGTCTATCATC
MuSt90	CAGTTTCAATTAGCGGGGTTTTGCGATTGGCC	MuSt189	CTAACATCCAATAAATCATACTAGTCAGAAGCAATC
MuSt91	AGAATAGAAAGGAACATATTTTTG	MuSt190	CTCCGGAAGCATAAACTGCATTAATGAATCGGCCTC
MuSt92	ACGTAATGCAGTGAATAAGGCTTGTAGCGGTCATTTAGGAAACCAG	MuSt191	CTAAGGCCGGAGACATACTAATAGTAGTAGCATTCC
MuSt93	TGGATGTTTTTATAATCAGAAAGGAG	MuSt192	CTTGCAGGTCGACGTCCACGCTGGTC
MuSt94	GGCAAGTGCCCTGACGCTGAGAAGAATACCTA	MuSt193	CTTGTATAAGCAAATATTCCAAAAACAGGAAGATTC
MuSt95	CGGGCGCTACAAGAGTCCACTATTTCACCATCACTGCCAACTCAC	MuSt194	GCTTGCATGCCTCTC
MuSt96	GACCATTAGTTGTTCCAGTTTGGAAGGGCGCT	MuSt195	CACGTTGGTGTAGATGGGCTC
MuSt97	TCGTAAATTCCATAACCTGTTTTTCGAGCTTCAAAGCGATACCACATTC	MuSt196	CTCGCCAGCTGGCGAAAGGGGCACAACATACGAGTC
MuSt98	TAAGTCCTTAACATAAAAATAGCACCGAACAAGAAAATTCGACATTCA	MuSt197	CTGCATCGTAACCGTGCATCTCAAAAGGGTGAGATC
MuSt99	TTAGGCAGAGGCATTTATAACTATTCAAATA		

Table C.1: Staple strands for the 3-layered origami used in Chapter 5.

C.1.3 Origami tube

Name	Sequence	Name	Sequence
TuSt1	TGCTTTCGCAAAAAAAAGGCTCCACAAATAAA	TuSt108	ATCAGAAAGGCCTCAGGAAGATCGCCTAATG
TuSt2	AAAATCTAAACGAGTAGTAAATTGAACAGCTTG	TuSt109	TGAGCGAGATAATTCGCGTCTGGTTTAGTTT
TuSt3	TCTGAATTCACCACCAGAGCCGCCGGAAACCG	TuSt110	AACACTGACCATTAAACGGGTAAAACGAGGC
TuSt4	ACCAGAACTACCGTTCCAGTAACAACTAAA	TuSt111	CACCCTCAAAGAATACACTAAAATTTGTAT
TuSt5	GAACTGGCAATATCAGAGAGATAATAAGTCCT	TuSt112	AAACCAAGTCATAATTACTAGAAAACATAAATC
TuSt6	TGAGCGCTATGATTAAGACTCCAGAACCGC	TuSt113	TGGCCCTGTTTTCTTTTCACCAGCATTAAATG
TuSt7	CGAGCATGAGCCAACGCTCAACAGAAGAAAACA	TuSt114	GTACTCAGCACCAGTAGCACCATTCACCGACT
TuSt8	CAGTATAATAGAAACCAATCAAAGAATTAA	TuSt115	GCTTTGAATAACAGTACCTTTTACAAGCGTAAG
TuSt9	TACCTTTTTTGTTTGGATTATACTAGGTGAGG	TuSt116	ATCCTTGAATCATTTTGCGGAACAAAATATCA
TuSt10	AATCCTGATTAATGGAAACAGTAAGCCTGT	TuSt117	TAAAACATCAATCGTCTGAAATGGTTTTTGGG
TuSt11	ACGCTGAGCAAACTATCGGCCTTGAGAAAGGA	TuSt118	GCCAGCTTCAATCATATGTACCCCATTAAGCAA
TuSt12	GAAGAACTAGCCAGCAGCAAATCATATTCC	TuSt119	GAAGGCTTTATTTTAGTTAATTTCCTTAGATTA
TuSt13	CGCTGGCATTCCACACAACATACGGTGCCGGA	TuSt120	GAGAGGCTGTCAATCATAAGGGAATTTCATGAG
TuSt14	GCTCACAAAGTGTAGCGGTCACATACTTCT	TuSt121	AGAGCGGGTAAAACGACGGCCAGTAAGTTGGGT
TuSt15	TGCGCAACATTGCCTGAGAGTCTTAATACTTT	TuSt122	CCTGAATCGTGAATTATCACCGTACCATTAG
TuSt16	ATCAGGTCTGTTGGGAAGGGCGAATCATGGT	TuSt123	TTTTGAAGTATGTAAATGCTGATTACCTTTTT
TuSt17	TAAAAATTGCAAAGCGGATTGCATTGCCAGAG	TuSt124	AATCAGCTACGGCGGATTGACCGGCCAACGC
TuSt18	AGTCAGAATTTAGAACCCTCATACCGGAGAG	TuSt125	TTAGTATCTTATCATTCCAAGAAAACATAAA
TuSt19	CGTCCAATGATAAATTGTGTCGATAAAACGAA	TuSt126	CATAGCTCACCCGCCGCGCTTACTGTCCAT
TuSt20	CATCGCCTACTGCGGAATCGTCAACCATAAA	TuSt127	ACCGGAATACCGCACTCATCGAAAAATGAA
TuSt21	TTTGACCCAGAACCGCCACCCTCTGTATCACC	TuSt128	AGTAGTAGTTTGCGGATGGCTTAGATTCATCAG
TuSt22	CTCATTATATTTCAACTTTAATCTTATCAGCT	TuSt129	GATAGCAGGATAAGTGCCGTCGATTTCAGGG
TuSt23	TGACAGGAAAGCCAGAATGGAATCACGTTG	TuSt130	AATAGCAGGAATAAGTTTATTTTAGCCCCC
TuSt24	ATACCGATCGAATAATAATTTTTAGCGCAGTC	TuSt131	TGTGATAATTATTTTCATCGTACAAATAAG
TuSt25	AATTGAGCAATAATAACGGAATGAGCCGCC	TuSt132	AGTGAGGCTGAAAGGAATTGAGAAATCCTT
TuSt26	ATGGCTTTGAGCCACCACCCTCAACCCAAAA	TuSt133	GCCTATTTGTTTGCCATCTTTTCAACGCAAAG
TuSt27	TAATTGAAAAATAATATCCCATAGGGTAAT	TuSt134	CACCCTCATGATGATACAGGAGTACAGTTTC
TuSt28	AGTATGTTCCTGAACAAAGTCAGCCTAATTTA	TuSt135	AGAGGCAAGAGCCACCACCCTCATGAGGGTTG
TuSt29	ATGGAAGTACATTTAACAATTTATTCTTAC	TuSt136	ATAAGCAATCTGCCAGTTTGAGCGTTGCGC
TuSt30	GTCTTTCCATATGCGTTATACAACATTTGAAT	TuSt137	AGGCTTTGTAGCATTCCACAGACATGAAACAT
TuSt31	ATCCAGAATTAACACCGCCTGCATCAATAT	TuSt138	CTACAGGGCGAGCTCGAATTCGTATCGGTGCG
TuSt32	AATATATGAGATGATGGCAATTCAACAGTGCC	TuSt139	CAAGGCCATAGCCCGGAATAGGAGAACCGC
TuSt33	AGCATAAAAAGCGAAAGGAGCGGCCTGAGTA	TuSt140	TTGACGCTCGCCATTAAAAATATATCAAAA
TuSt34	AAAGCATCTAATAACATCACTTGGCGCTAGGG	TuSt141	ACCTAAATCAATAGCAAGCAAATAAAATAAA
TuSt35	CAAGAGAAAAAGCGCCATTCGCTGTTATCC	TuSt142	AATCCTGTTTGATGGTTGCCCCAGCAGGCGAA
TuSt36	AACCACCAGTTTCCTGTGTGAAATCATTCAGGC	TuSt143	CGTTTTAGGACAAAGAACGCGAGATGAATTTA
TuSt37	ATTAAGAGAAGCCTTTATTTCACAAAGGCT	TuSt144	TCAAAAACCTGAGTAATGTGTAGATATTCA
TuSt38	GGCCTCTTATTTTTGAGAGATCTAACGCAAGGA	TuSt145	AGGAAACGTTAAGCCCAATAATAAAATGCAGAA
TuSt39	ACCTGCTCAGTAAAATGTTTAGACTATTAT	TuSt146	TAAAGCCTCAAACTCCAACAGGTATTACGAGG

Table C.2: (continued)

Name	Sequence	Name	Sequence
TuSt40	ATGCAATGTCAGGTCTTTACCCTGACTGGATAG	TuSt147	GAAGTTTGTTTCGTCACCAGTACCTCAAGAG
TuSt41	TCTGAATTCACCACCAGAGCCGCCGGAAACCG	TuSt148	AAAGGGCGAAAAACCGAAAAGAATAGCCCGAG
TuSt42	CATTGAATACAAAGTACAACGGAGACACTCATC	TuSt149	TTGCGGGACGTTAGTAAATGAATCCTTGAGTA
TuSt43	ATGGTTTAACCAGTCAGGACGTGTCTGGAA	TuSt150	GTTTTCATAAGAGGCTGAGACTCAAACTAC
TuSt44	ACACCAGCGTTAATAAAACGAAAACATGTT	TuSt151	AGCATGTTCCGGCACCGCTTCTGAGCCGGA
TuSt45	CATTCAGTTTACAGGTAGAAAGAGCTTAAT	TuSt152	ACCGTTCTGCTGCAAGGCGATTGCCAAGCT
TuSt46	TCATTACCTAGGAATACCACATTTGATAAGA	TuSt153	CCTAAAGGCGCTTTCCAGTCGGGCGCATCGTA
TuSt47	ATCAAGAATAACGCCAAAAGGACAGGATTA	TuSt154	AAGGATTAGCCTTTAGCGTCAGACCCAGCGCC
TuSt48	AACCAGGCTCGATGAACGGTAATCAATCGGTT	TuSt155	TACAGACCGAGCAACACTATCACGAACCAG
TuSt49	AACGCCAGAATCACCATCAATATGGTAAAGAT	TuSt156	GTCGAGGTCTGCATTAATGAATCGTAATGGGA
TuSt50	GTTTCATGATACATTTCGCAAAAGGAACGC	TuSt157	TAGGTCACAAAATTCGCATTAAATTTGGGGCGC
TuSt51	TTAAATATAGCTATATTTTCATTTTTGTTA	TuSt158	GAGCTGAAATAATGCTGTAGCTCCTAACGGAA
TuSt52	TGCTGAATAAGGTGGCATCAATTCGTTAATA	TuSt159	TCAAGTTTGGATTAGCGGGGTTTGTACCGT
TuSt53	GGTCATTCATTAACATCCAATAAAGATTGT	TuSt160	ACCGTGCAATATTTAAATTGTAAACTACTAAT
TuSt54	GAGAGTACAAAGAATTAGCAAAGGTTGATA	TuSt161	AGTGAGCCCGGCGAACGTGGCGCTGGTAAT
TuSt55	GTACCAAAAATTCGAGCTTCAAAGTAACCCTCG	TuSt162	GAACAAGAGAATCGCCATATTTAACCTGAGCAA
TuSt56	TCAAAAGGTCAGAAAACGAGAATGTAAATATT	TuSt163	CATTGGCCTTTAATGCGCGAACAAAGAAAT
TuSt57	TGGGATTTTTGCAGGGAGTTAACCGGATAT	TuSt164	CAATAGAATTTTGTTTAACGTCAGAACAAGCA
TuSt58	TTTCCAGATCGTCACCCTCAGCATGACCTTC	TuSt165	CAAACAAATAGGTCTGAGAGACGCAAATCC
TuSt59	AGTTAGCGAACGAGGGTAGCAAGAACGGTG	TuSt166	AGCGGAGCACGCATAACCGATAAAGCTGCT
TuSt60	GGGGATGTAGCTGATAAATTAATGTATTTTAA	TuSt167	TAAAGGTGAAGCGCATTAGACGGGTAATCGGCT
TuSt61	TGCGGGAGGAAGCCCGAAAGACTTAAAATAGC	TuSt168	ACCAGGCGCACCGTAATCAGTAGCCGATTGAG
TuSt62	AAATTAATGGTTAGAACCTACCACCGAACGAA	TuSt169	GGGAACAACATTTTTTAACCAATTGGTCAATA
TuSt63	CTAAAATATCCTGAGAAGTGTTTCTTTGACGA	TuSt170	GCGGGGATCACCCAAATCAAGTATTATTTA
TuSt64	TCCTCATTAGGTTGAGGCAGGTCAAGTAAGCAG	TuSt171	TGAGCCATTTTTGCACCCAGCTACTGCGGGAGG
TuSt65	TCAAAATCTTCGACAACTCGTATTGAAGGTTAT	TuSt172	GTAACATTAAACATAGCGATAGATCTTCTG
TuSt66	AACAATGACAAAGTTACCAGAAGCCAGCAT	TuSt173	AAAGACAAATTATTTATCCCAATCGGAATCATT
TuSt67	CGTGCCAGGCCGTAAAGCACTAACCTACATT	TuSt174	GAAAGTATTCGGCATTTTCGGTCATGTCACAAT
TuSt68	TTTTGTTGTTGGTGTAGATGGGAAACCTGT	TuSt175	ACCAACTTACGACGATAAAAACCCAAATATC
TuSt69	GTCCACTATTAAAGAATTCCAGTTTGGAACAA	TuSt176	TTGATTAGACCTTGCTGAACCTCAAGAAACC
TuSt70	ACAGTATCAGCCCCAAAAACAGGAATCATACA	TuSt177	TGCCCGAAAGAAGAGTCAATAGAAACTTTT
TuSt71	TCAACAGTCACCGAGTAAAAGAGTATGCGCCG	TuSt178	GGCGAATTTTTTCAGGTTTAACGTTTGAATGG
TuSt72	CATCAAAATAACAACCCGTCGGTGGGCGCC	TuSt179	ATGCCACTGCCCAATAGGAACCCATTGCTCAGT
TuSt73	ACAGGAAACAGAAGATAAAACAGTCTGAATA	TuSt180	AATACGTGGGACATTCTGGCCAATTCACCGCC
TuSt74	GGTAGCTCGCTATTACGCCAGCGAGGATCC	TuSt181	TGCATGCCAACGTGCTTTCCTCGAACGGTA
TuSt75	ACAGTGCCGAACCAGAGCCACCACTACATACA	TuSt182	AACCTCCGAGGATTTAGAAGTATTACAACTAAT
TuSt76	CACGCAAATCAATATCTGGTCAAAGTTTGA	TuSt183	CAGTAATACAACATGTTCAGCTGAGCAAGA
TuSt77	AGATTAGAAGGGATTTTAGACAGGTTAGAATC	TuSt184	CTATTAGTAGATTCACCAGTCACAGCCCACTAC
TuSt78	GGTTCCGAAATCGGCAGCGGTCCACGCTGGTT	TuSt185	CAGCCATAAGGGCGACATTCAACGACAGAA
TuSt79	AACAGGGGCAACATATAAAAGAATAATCAA	TuSt186	CTGAACACAGCAAACGTAGAAAACGGAACCG
TuSt80	AGGGAAGAGTGTAAAGCCTGGGGTGCACTCCA	TuSt187	GCAGACGTTTGCAAAAGAAGTTTCAAAAAG
TuSt81	AAGAAGATACGTAAAACAGAAATTGATAGCCC	TuSt188	TGCGTAGAATTCATTTCAATTACAACGCCA
TuSt82	TCACTGCCGAGCCCCCGATTTACCATTGCA	TuSt189	TATACAGTACCAAGTTACAAAATTTCGAGC
TuSt83	TCAAATAATCCGGTATTCTAAGAGCGTCTT	TuSt190	GGAGGGAACTAATTTGCCAGTTACCAGATATA
TuSt84	TCCAGAGCGGTAAATATTGACGAAACCATC	TuSt191	TTTACCAGTGAAAGAGGACAGATCGGCTACAG
TuSt85	TTGAGATTCAAATCAACGTAACATATTCGGTC	TuSt192	AAACGATTAATTCATATGGTTTATGTAGCGC
TuSt86	AACGCCTGAGGACTAAAGACTTCCGAACTG	TuSt193	CCATCGCCTGAGAATAGAAAGGAAGCGTCATAC
TuSt87	GCGTTTTAACATTATGACCCTGGGAGCAAA	TuSt194	CCACCAGAACGCTCATGGAAATAATCGGAAC
TuSt88	GGGGTAATCATGTTACTTAGCCGGAATACGTA	TuSt195	AAATCGTCGGAGCGGAATTATCATGAAAAATCT
TuSt89	GTGAACCAGAGGCGGTTTGCGTATATTCTCCGT	TuSt196	CCGGGTACCGCGTACTATGGTTGTTATAATC
TuSt90	AAATCCCTTATAAATCTCTATCATTGCAGCAA	TuSt197	ATAGCAAACGAAGGCACCAACCAATCCGCG
TuSt91	ACCGCGCCTTAATGGTTTGAAATTCCCTTAGA	TuSt198	AGCCGTTTATAAGGCGTTAAATAAGCTTCTGT
TuSt92	ATATAAGTGGAAACGTCACCAATGGAAATTATT	TuSt199	CAGCATCGGTAACGATCTAAAGTTATGCCCCCT
TuSt93	CGTGGACTCCAACGTCATAGGGTTGAGTGTTG	TuSt200	GCACGTATTGCAGGTCGACTCTATGGCGAAAG
TuSt94	ACCAGAAGCTATTAATTAATTTACCGACCG	TuSt201	ACCGGAAGCAGAGCATAAAGCTAGTAAAACT
TuSt95	CATTAAAGTTACCAACGCTAACGAACGCGAGG	TuSt202	ACACCACGCCTTTACAGAGAGAATCGGGTATT
TuSt96	CAACATTAGAATAAGGCTTGCCCTGACAACAA	TuSt203	ACAATAAAAGAGAATATAAAGTACGCCTGATT
TuSt97	TGATTATCTGAGTGAATAACCTTGAATAAAC	TuSt204	ACATGTAATTTATCAACAATAGACCCACAAG
TuSt98	TTATTTGCGATGAAACAAACATCTAGGGCT	TuSt205	AATAAGTTCAGAGCCGCCACCCTCTTATTACGC
TuSt99	GGAATTGAGTTGCGCCGACAATGACGAGAA	TuSt206	CGCCAGAATCTTTAGGAGCACTAAGACTTTA
TuSt100	CGGTCAGTACAATATTACCGCCAGGAGCTTGAC	TuSt207	AAAATCTCAGGTGAATTTCTTAGGCTTGAG
TuSt101	AGACGCTGCGTTATTAATTTTAAGTTGGCAAA	TuSt208	GGGGAAAGTAACTCACATTAATTGGGGACGACG
TuSt102	AATCGCAACGAACCTCCCGACTAATTTTAT	TuSt209	AACCCTCAATTAACCGTTGTAGCAGCTGCGCGT
TuSt103	AATAAAAGGCACAGACAATATTTCAGATGAA	TuSt210	ACCTGTTTGCAACTAAAGTACGGTTGGGAAGA
TuSt104	GCTGAGGCTGCTAAACAACTTTCAGTACTGGT	TuSt211	CGCGCCTGTTTAGGCAGAGGCATTCGCGCAGA
TuSt105	AGGGTGGTAGAGAGGGGCGATGCGACCAGT	TuSt212	GACCATTATCCATATAACAGTTGAAAGAACTGG
TuSt106	GGCAAGGCCTTTAATTGCTCCTTTCAACTAAT	TuSt213	CATAGTAAAGGCGCATAGGCTGGCGCGAAAGA
TuSt107	GCAGATACGTAATCTTGACAAGAAAGGCCGCTT		

Table C.2: Staple strands for the origami tube used in Chapter 3.

Strand Name	Sequence	Strand Name	Sequence
Poly(dT)-end staples for suppressing stacking		**Linker end staples for promoting stacking**	
Tu_polydTend1	TTTTTTTT AGCTTTCATCAATGAGACGGGCAAC TTTTTTTT	Tu_Linker1	TGAGACGGGCAAC TCACGACGTTG
Tu_polydTend2	TTTTTTTT CGAACGAGTAGACCTTCCTGTAGCC TTTTTTTT	Tu_Linker2	GGTTTTCCCAG AGCTTTCATCAA
Tu_polydTend3	TTTTTTTT TTATGCGATTTTTTCCCAATTCTG TTTTTTTT	Tu_Linker3	CCTTCCTGTAGCC CGGAGACAGTCA
Tu_polydTend4	TTTTTTTT AATTGTATCGGTATTGTGAATTACC TTTTTTTT	Tu_Linker4	GTGAGAAAGGC CGAACGAGTAGA
Tu_polydTend5	TTTTTTTT GATATTCACAAAAAAGGAGCCTTT TTTTTTTT	Tu_Linker5	TTCCCAATTCTG GCTTTAAACAGT
Tu_polydTend6	TTTTTTTT CTTTTTAAGAAAGACGATTGGCCTT TTTTTTTT	Tu_Linker6	CCCCCTCAAAT TTATGCGATTTT
Tu_polydTend7	TTTTTTTT AGTAATTCTGTCTCTTACCGAAGCC TTTTTTTT	Tu_Linker7	ATTGTGAATTACC ACCAAGCGCGAA
Tu_polydTend8	TTTTTTTT ATAACGGATTCCGACAAAAGGTAA TTTTTTTT	Tu_Linker8	CCAGCGATTAT AATTGTATCGGT
Tu_polydTend9	TTTTTTTT CTTCTGACCTGAATCGGGAGAAACA TTTTTTTT	Tu_Linker9	AAAGGAGCCTTT ACCGCCACCCTC
Tu_polydTend10	TTTTTTTT AGCTGATTGCCCCAGAGATAGAACC TTTTTTTT	Tu_Linker10	GAGGTTTAG GATATTCACAAA
Tu_polydTend11	TTTTTTTT TCACGACGTTGAGCTAAACAGG TTTTTTTT	Tu_Linker11	GACGATTGGCCTT AGCCAGCAAAAT
Tu_polydTend12	TTTTTTTT CGGAGACAGTCAGGTTTTCCCAG TTTTTTTT	Tu_Linker12	TTGGGAATTAG CTTTTTAAGAAA
Tu_polydTend13	TTTTTTTT GCTTTAAACAGTGTGAGAAAGGC TTTTTTTT	Tu_Linker13	TCTTACCGAAGCC GATTAGTTGCTA
Tu_polydTend14	TTTTTTTT ACCAAGCGCGAACCCCCTCAAAT TTTTTTTT	Tu_Linker14	CCTTAAATCAA AGTAATTCTGTC
Tu_polydTend15	TTTTTTTT ACCGCCACCCTCCCAGCGATTAT TTTTTTTT	Tu_Linker15	CGACAAAAGGTAA GTTATATAACTA
Tu_polydTend16	TTTTTTTT AGCCAGCAAAATGAGGTTTAGT TTTTTTTT	Tu_Linker16	GCTTAGGTTGG ATAACGGATTC
Tu_polydTend17	TTTTTTTT GATTAGTTGCTATTGGGAATTAG TTTTTTTT	Tu_Linker17	ATCGGGAGAAACA ATAATACATTTG
Tu_polydTend18	TTTTTTTT GTTATATAACTACCTTAAATCAA TTTTTTTT	Tu_Linker18	GCCGTCAATAG CTTCTGACCTGA
Tu_polydTend19	TTTTTTTT ATAATACATTTGGCTTAGGTTGG TTTTTTTT	Tu_Linker19	CAGAGATAGAACC AGGCCGATTAA
Tu_polydTend20	TTTTTTTT AGGCCGATTAAGCCGTCAATAG TTTTTTTT	Tu_Linker20	AGCTAAACAGG AGCTGATTGCCC

Table C.3: Poly(dT) and linker end staples used for controlling stacking of the tubes in Chapter 4.

C.2 Strands for Chapter 2

Strand Name	Sequence
Enzyme cutting near a vertex - 5' end of motor: used in Section 2.2.1	
Rev_D5'	CTGAGACTCTTGG CCCCTCAGCACGATGACGGTAACCC
Rev_D5'_cut3	TCAGCACGATGACGGTAACCC
Rev_D5'_cut5	CTGAGACTCTTGG CCCC
Rev_MA_d2	TGCTGAGGGG TTGATTGTAGC GAAAGTAGG GCTACAATCAA CCAAGAGTCTCAG
Rev_MA_d3	TGCTGAGGGGC TTGATTGTAGC GAAAGTAGG GCTACAATCAA CAAGAGTCTCAG
Rev_MA_d4	TGCTGAGGGGCC TTGATTGTAGC GAAAGTAGG GCTACAATCAA AAGAGTCTCAG
Enzyme cutting near a vertex - 3' end of motor: used in Section 2.2.1	
Rev_D3'	CCCAATGGCAGTAGCGGAACCTCAGCCC GGTTCTCAGAGTC
Rev_D3'_cut3	TCAGCCC GGTTCTCAGAGTC
Rev_D3'_cut5	CCCAATGGCAGTAGCGGAACC
Rev_AM_d3	GACTCTGAGAAC AACTAACATCG GGATGAAAG CGATGTTAGTT CGGGCTGAGGTTCC
Rev_AM_d4	GACTCTGAGAA AACTAACATCG GGATGAAAG CGATGTTAGTT CCGGGCTGAGGTTCC
Rev_AM_d5	GACTCTGAGA AACTAACATCG GGATGAAAG CGATGTTAGTT ACCGGGCTGAGGTTCC
Holliday junction initiation: used in Figure A.2	
Rev_A_8a	/56-FAMN/ TTT GCTACAATCAA CAGCA TA GTTCCGTG
Rev_A_8a_HJ	/56-FAMN/ TTT GCTACAATCAA CAGCA TA GTTCCGTG GCG
Rev_D_8a9si_15T_v2	AGGCACATT CACGGAAC TA TGCTG GGCCCCT CAGCA TA TTTTTTTTTTTTTTT AATGTGCCT
Rev_R_8a8_3HJ	CGC CACGGAAC CAGCA TA GTTCCGTG AATGTGCCT
Rev_R_8a8_2HJ	GC CACGGAAC CAGCA TA GTTCCGTG AATGTGCCT
Rev_R_8a5_3HJ	CGC CACGG CAGCA TA GTTCCGTG AATGTGCCT
Optimising lengths: used in Figure 2.7	
Rev_A_8a_HJ	/56-FAMN/ TTT GCTACAATCAA CAGCA TA GTTCCGTG GCG
Rev_A_12a	TTT GCTACAATCAA CAGCA TA ACGTTACGATAG
Rev_A_15a	TTT GCTACAATCAA CAGCA TA ACGTTACGATAGGCG
Rev_D_8a9si_15T	CCTGTAGAC CACGGAAC TA TGCTG GGCCCCT CAGCA TA TTTTTTTTTTTTTTT GTCTACAGG
Rev_D_8a12si_15T	CTTCTAATGGAC CACGGAAC TA TGCTG GGCCCCT CAGCA TA TTTTTTTTTTTTTTT GTCCATTAGAAG
Rev_D_12a9si_15T	CCTGTAGAC CTATCGTAACGT TA TGCTG GGCCCCT CAGCA TA TTTTTTTTTTTTTTT GTCTACAGG
Rev_D_12a12si_15T	CTTCTAATGGAC CTATCGTAACGT TA TGCTG GGCCCCT CAGCA TA TTTTTTTTTTTTTTT GTCCATTAGAAG
Rev_D_15a9si_15T	CCTGTAGAC CGCCTATCGTAACGT TA TGCTG GGCCCCT CAGCA TA TTTTTTTTTTTTTTT GTCTACAGG
Rev_D_15a12si_15T	CTTCTAATGGAC CGCCTATCGTAACGT TA TGCTG GGCCCCT CAGCA TA TTTTTTTTTTTTTTT GTCCATTAGAAG
Rev_R_8a8_9si	CACGGAAC CAGCA TA GTTCCGTG GTCTACAGG
Rev_R_8a8_12si	CACGGAAC CAGCA TA GTTCCGTG GTCCATTAGAAG
Rev_R_12a12_9si	CTATCGTAACGT CAGCA TA ACGTTACGATAG GTCTACAGG
Rev_R_12a12_12si	CTATCGTAACGT CAGCA TA ACGTTACGATAG GTCCATTAGAAG
Rev_R_15a15_9si	CGCCTATCGTAACGT CAGCA TA ACGTTACGATAGGCG GTCTACAGG
Rev_R_15a15_12si	CGCCTATCGTAACGT CAGCA TA ACGTTACGATAGGCG GTCCATTAGAAG
Rev_R_8a8_9si2co	AC CACGGAAC CAGCA TA GTTCCGTG GTCTACAGG
Rev_R_8a8_12si2co	AC CACGGAAC CAGCA TA GTTCCGTG GTCCATTAGAAG
Rev_R_12a12_9si2co	AC CTATCGTAACGT CAGCA TA ACGTTACGATAG GTCTACAGG
Rev_R_12a12_12si2co	AC CTATCGTAACGT CAGCA TA ACGTTACGATAG GTCCATTAGAAG
Rev_R_15a15_9si2co	AC CGCCTATCGTAACGT CAGCA TA ACGTTACGATAGGCG GTCTACAGG
Rev_R_15a15_12si2co	AC CGCCTATCGTAACGT CAGCA TA ACGTTACGATAGGCG GTCCATTAGAAG
Rev_R_8a8_9si3co	GAC CACGGAAC CAGCA TA GTTCCGTG GTCTACAGG
Rev_R_8a8_12si3co	GAC CACGGAAC CAGCA TA GTTCCGTG GTCCATTAGAAG
Rev_R_12a12_9si3co	GAC CTATCGTAACGT CAGCA TA ACGTTACGATAG GTCTACAGG
Rev_R_12a12_12si3co	GAC CTATCGTAACGT CAGCA TA ACGTTACGATAG GTCCATTAGAAG
Rev_R_15a15_9si3co	GAC CGCCTATCGTAACGT CAGCA TA ACGTTACGATAGGCG GTCTACAGG
Rev_R_15a15_12si3co	GAC CGCCTATCGTAACGT CAGCA TA ACGTTACGATAGGCG GTCCATTAGAAG
Final sequences — basic interactions: used in Figure 2.8a)	
Rev_A_12a	TTT GCTACAATCAA CAGCA TA ACGTTACGATAG
Rev_D_12a12si_15T	CTTCTAATGGAC CTATCGTAACGT TA TGCTG GGCCCCT CAGCA TA TTTTTTTTTTTTTTT GTCCATTAGAAG
Rev_D_12a12si_cut5	CTTCTAATGGAC CTATCGTAACGT TA TGCTG GGCCCC
Rev_R_12a8_12si4co	GGAC CTATCGTA CAGCA TA ACGTTACGATAG GTCCATTAGAAG
Final sequences — cutting: used in Figure 2.8b)	
Rev_M	TA TGCTG AGGGGCC TTGATTGTAGC
Rev_A_12a	TTT GCTACAATCAA CAGCA TA ACGTTACGATAG
Rev_D_12a1_12si	CTTCTAATGGAC CTATCGTAACGT TA TGCTG GGCCCCT CAGCA TA TTTTTTTTTTTTTTTTTTTT GTCCATTAGAAG
Rev_D_12a12si_cut5	CTTCTAATGGAC CTATCGTAACGT TA TGCTG GGCCCC

Table C.4: Strands used for preliminary testing in Section 2.2. Sequences that are part of each enzyme's restriction site are highlighted by underlining.

Strand Name	Sequence	Used in Section	Replaced staple
Track			
Rev_A0_a1	GGATTAGGAGAGGCTGAGACTCCTGCATAACC TTT CG GCTACAATCAA CAGCA TA ACGTTACGATAG	2.3.2	M1t2f
Rev_A0_a2	GGATTAGGAGAGGCTGAGACTCCTGCATAACC TTT CG GCTACAATCAA ACACTTATCCTTCTGTTTT	2.3.3 to 2.3.6	M1t2f
Rev_A1_a1	GCATTGACGAACCACCACCAGAGCGGAGATTT TTT GCTACAATCAA CAGCA TA ACGTTACGATAG	2.3.2 to 2.3.6	M1t4f
Rev_A2_a1	TTAGCAAGAATCACCAGTAGCACATTGGGCT TTT GCTACAATCAA CAGCA TA ACGTTACGATAG	2.3.2 to 2.3.6	M1t6f
Rev_A3_a1	TCCTTATTAAAAGAACTGGCATGATAGCGAG TTT GCTACAATCAA CAGCA TA ACGTTACGATAG	2.3.2 to 2.3.6	M1t8f
Rev_A4L_a1	ACCAGACGGCAAAAGAAGTTTTGTTTTAATT TTT GCTACAATCAA CAGCA TA ACGTTACGATAG	2.3.2	M-1t8f
Rev_A5L_a1	CAATAAATTCAATAACCTGTTTAAGTACCTT TTT GCTACAATCAA CAGCA TA ACGTTACGATAG	2.3.2	M-3t12e
Rev_A6L_a1	CCCGAAAGCCTTTTGATAAGAGGTACATTTC TTT GCTACAATCAA CAGCA TA ACGTTACGATAG	2.3.2	M-3t10f
Rev_A7L_x	AAGGCTATTTTAAATGCAATGCCTAGAATTAG TTT GCTACAATCAA GGCCCTT CAGCA TA	2.3.2	M-5t14e
Rev_A4_a1	TACAGAGAGTCAAAAATGAAAATAGGAAGCAA TTT GCTACAATCAA CAGCA TA ACGTTACGATAG	2.3.3 to 2.3.6	M1t10f
Rev_A5_a1	GCGCCCAATTTTCATCGTAGGAAAGGTGGCA TTT GCTACAATCAA CAGCA TA ACGTTACGATAG	2.3.3 to 2.3.6	M1t12f
Rev_A6_a1	CCAGTAATATTTAGGCAGAGGCAAATATGAT TTT GCTACAATCAA CAGCA TA ACGTTACGATAG	2.3.3 to 2.3.6	M1t14f
Rev_A7_a3	CCAATCGCTATATGTAAATGCTGCCAATAGG TTT CG GCTACAATCAA GAGAGGTATCCTGAGGAGC	2.3.3	M1t16f
Rev_A7_a4	CCAATCGCTATATGTAAATGCTGCCAATAGG TTT CG GCTACAATCAA GAGACGTATCCTTACGAGC	2.3.4 to 2.3.6	M1t16f
Fluorophores			
Rev_F0_TET	/5TET/ GATATATTAACAACCATCGCCCACCAAGAGAA	2.3.2 and 2.3.4 to 2.3.6	M-1t2e
Rev_F8L_Cy5	/5Cy5/ CAAAATTAAGTTTGACCATTAGATCATTTTT	2.3.2	M-5t12e
Rev_F8_Cy5	/5Cy5/ AACGCCATTCAGCTCATTTTTTAAATGCAAAT	2.3.4 to 2.3.6	M-1t16e
Rev_F0_cCy5	CCTTTTACTTCCACTACCCA TT GATATATTAACAACCATCGCCCACCAAGAGAA	2.3.3	M-1t2e
Cy5_5'	/5Cy5/ TGGGTAGTGGAAGTAAAAGG	2.3.3	-
Rev_F7_cTET	ATCCCACTCCCTACACTTCG TT AACGCCATTCAGCTCATTTTTTAAATGCAAAT	2.3.3	M-1t16e
TET	/5TET/ CGAAGTGTAGGGAGTGGGAT	2.3.3	-
Motors			
Rev_M_Q	TA TGCTG AGGGGCC TTGATTGTAGC CG /3IAbRQSp/	2.3.2 and 2.3.3	-
Rev_M_ext4_Q	GAGG TA TGCTG AGGGGCC TTGATTGTAGC CG /3IAbRQSp/	2.3.4 to 2.3.6	-
Rev_M_ext9_Q	CGGGAGAGG TA TGCTG AGGGGCC TTGATTGTAGC CG /3IAbRQSp/	2.3.3	-
Directors & removers			
Rev_D_12a1_12si	CTTCTAATGGAC CTATCGTAACGT TA TGCTG GGCCCCT CAGCA TA TTTTTTTTTTTTTTTTTTTT GTCCATTAGAAG	2.3.2 to 2.3.6	-
Rev_D_12a1_12hf	CTTCTAATGGAC CTATCGTAACGT TA TGCTG GGCCCCT CAGCA TA	2.3.2	-
Rev_R_12a8_a1_12si_4co	GGAC CTATCGTA CAGCA TA ACGTTACGATAG GTCCATTAGAAG	2.3.4 to 2.3.6	-

Strand Name	Sequence
Station design 1: used in Section 2.3.3	
Rev_M_ext9_Q	CGGGAGAGG TA TGCTG AGGGGCC TTGATTGTAGC CG /3IAbRQSp/
Rev_Dhold_a2	ACATTACTTGCG AAAACAGAAGGATAAGTGT GGCCCCT CAGCA TA CCTCTCCCG CACGAGTAAAGT
Rev_Rl1_hold	ACTTTACTCGTG CGGGAGAGG TA TGCTG A
Rev_Dhold2_a3	ATAGTTAGTGAC GCTCCTCAGGATACCTCTC GGCCCCT CAGCA TA CCTCTCCCG CCTGGATTCGAA
Station design 2: used in Section 2.3.3	
Rev_M_Q	TA TGCTG AGGGGCC TTGATTGTAGC CG /3IAbRQSp/
Rev_D_hold3x_a2	ACATAACTTCCG AAAACAGAAGGATAAGTGT GGCCCTT CAGCA TA CACGAGTAAAGT
Rev_Rl1_hold3	ACTTTACTCGTG TA TGCTG A
Rev_D_hold4x_a3	ATAGTTAGTGAC GCTCCTCAGGATACCTCTC GGCCCTT CAGCA TA CCTGGATTCGAA
Station design 3: used in Section 2.3.3	
Rev_M_ext9_Q	CGGGAGAGG TA TGCTG AGGGGCC TTGATTGTAGC CG /3IAbRQSp/
Rev_D_hold5x_a2	ACATAACTTCCG AAAACAGAAGGATAAGTGT GGCCCTT CAGCA TA CCTCTCCCG CACGAGTAAAGT
Rev_Rl1_hold	ACTTTACTCGTG CGGGAGAGG TA TGCTG A
Rev_D_hold6x_a3	ATAGTTAGTGAC GCTCCTCAGGATACCTCTC GGCCCTT CAGCA TA CCTCTCCCG CCTGGATTCGAA
Station design 4: used in Sections 2.3.4 to 2.3.6	
Rev_M_ext4_Q	GAGG TA TGCTG AGGGGCC TTGATTGTAGC CG /3IAbRQSp/
Rev_D_hold7x_a2	ACATAACTTCCG AAAACAGAAGGATAAGTGT GGCCCTT CAGCA TA CCTC CACGAGTAAAGT
Rev_Rl1_hold7	ACTTTACTCGTG GAGG TA TGCTG A TA CCTC
Rev_Rl2_hold7	ACACTTATCCTTCTGTTTT CGGAAGTTATGT
Rev_D_hold8x_a4	ATAGTTAGTGAC GCTCGTAAGGATACGTCTC GGCCCTT CAGCA TA CCTC CCTGGATTCGAA
Rev_Rl1_hold8	TTCGAATCCAGG GAGG TA TGCTG A TA CCTC
Rev_Rl2_hold8	GAGACGTATCCTTACGAGC GTCACTAACTAT

Table C.5: Strands used for ensemble fluorescence measurements in Section 2.3. Sequences that are part of each enzyme's restriction site are highlighted by underlining.

C.3 Strands for Chapter 3

Strand Name	Sequence
Enzyme choice - Nt.AlwI: used in Figure 3.8	
Lpop_NtAlwI_AI	TTT GGATCGCAATGTAGTTATCTGTAAA TTTTTTTTTTT
Lpop_NtAlwI_M_t4	CG TTTACAGATAACTACATTGC
Lpop_NtAlwI_M_t5	CG TTTACAGATAACTACATTGCG
Lpop_NtAlwI_M_t6	CG TTTACAGATAACTACATTGCGA
Lpop_NtAlwI_M_t7	CG TTTACAGATAACTACATTGCGAT
Enzyme choice - Nt.BbvCI: used in Figure 3.8	
Lpop_NtBbvCI_AI	TTTTTTTTT TTTACAGATAACTACCTCAGC ATTTTT
Lpop_NtBbvCI_M_t4	CTGAGGTAGTTATCTGTAAA GC
Lpop_NtBbvCI_M_t5	GCTGAGGTAGTTATCTGTAAA GC
Lpop_NtBbvCI_M_t6	T GCTGAGGTAGTTATCTGTAAA GC
Enzyme choice - Nt.BsmAI: used in Figure 3.8	
Lpop_NtBsmAI_AI	TTTTTT GTCTCGAGTAGTTATCTGTAAA TTTTTTTTTTT
Lpop_NtBsmAI_M_t5	CG TTTACAGATAACTACTCGAGA
Lpop_NtBsmAI_M_t6	CG TTTACAGATAACTACTCGAGAC
Lpop_NtBsmAI_M_t7	CG TTTACAGATAACTACTCGAGAC A
Enzyme choice - Buffers: used in Figure 3.9	
Lpop_NtBbvCI_M1	GCTGAGGTTCTTGTAGCTATG GC
Lpop_NtBbvCI_A1v2	TTT CATAGCTACAAGAACCTCAGC GAAGGCG TTTT CGCCTTC
Lpop_NtBbvCI_A1v2_c5	TTT CATAGCTACAAGAACC
Plain track: used in Figure 3.10	
Lpop_NtBbvCI_M1	GCTGAGGTTCTTGTAGCTATG GC
Lpop_NtBbvCI_M2	GCTGAGGTAGTTATCTGTAAA GC
Lpop_NtBbvCI_A1	TTT CATAGCTACAAGAACCTCAGC ACGATCC TTTT GGATCGT
Lpop_NtBbvCI_A2	TTT TTTACAGATAACTACCTCAGC GGATCGT TTTT ACGATCC
Interaction site: used in Figure 3.11	
Lpop_NtBbvCI_M2	GCTGAGGTAGTTATCTGTAAA GC
Lpop_NtBbvCI_A1I	TCGGTGCTCCGCTTAC TTTTTTTTTTT CATAGCTACAAGAACCTCAGC ACGATCC
Lpop_NtBbvCI_A2I	GTAAGCGGAGCACCGA TTTTTTTTTTT TTTACAGATAACTACCTCAGC GGATCGT
Lpop_NtBbvCI_A2I_c5	GTAAGCGGAGCACCGA TTTTTTTTTTT TTTACAGATAACTACC
Interaction site - not forming dimers: used in Figure 3.12	
Lpop_NtBbvCI_M1	GCTGAGGTTCTTGTAGCTATG GC
Lpop_NtBbvCI_A1I	TCGGTGCTCCGCTTAC TTTTTTTTTTT CATAGCTACAAGAACCTCAGC ACGATCC
Lpop_NtBbvCI_A2I	GTAAGCGGAGCACCGA TTTTTTTTTTT TTTACAGATAACTACCTCAGC GGATCGT
Lpop_NtBbvCI_A2I_ext	CACTGCCAGGCGACCC GTAAGCGGAGCACCGA TTTTTTTTTTT TTTACAGATAACTACCTCAGC GGATCGT
Lpop_NtBbvCI_A2I_extCOMP	GGGTCGCCTGGCAGTG
Interaction site - intra-molecular cutting: used in Figure 3.13	
Lpop_NtBbvCI_M2	GCTGAGGTAGTTATCTGTAAA GC
Lpop_NtBbvCI_A2I	GTAAGCGGAGCACCGA TTTTTTTTTTT TTTACAGATAACTACCTCAGC GGATCGT
Lpop_NtBbvCI_A2I_c5	GTAAGCGGAGCACCGA TTTTTTTTTTT TTTACAGATAACTACC
Lpop_NtBbvCI_mock_A1I	TT CATAGCTACAAGAACCTGCAC ACGATCC
Interaction site - cutting with flexi linker length: used in Table 3.2	
Lpop_NtBbvCI_M1	GCTGAGGTTCTTGTAGCTATG GC
Lpop_NtBbvCI_M2	GCTGAGGTAGTTATCTGTAAA GC
Lpop_NtBbvCI_A1I_3T	TCGGTGCTCCGCTTAC TTT CATAGCTACAAGAACCTCAGC ACGATCC
Lpop_NtBbvCI_A2I_3T	GTAAGCGGAGCACCGA TTT TTTACAGATAACTACCTCAGC GGATCGT
Lpop_NtBbvCI_A1I_6T	TCGGTGCTCCGCTTAC TTTTTT CATAGCTACAAGAACCTCAGC ACGATCC
Lpop_NtBbvCI_A2I_6T	GTAAGCGGAGCACCGA TTTTTT TTTACAGATAACTACCTCAGC GGATCGT
Lpop_NtBbvCI_A1I_9T	TCGGTGCTCCGCTTAC TTTTTTTTT CATAGCTACAAGAACCTCAGC ACGATCC
Lpop_NtBbvCI_A2I_9T	GTAAGCGGAGCACCGA TTTTTTTTT TTTACAGATAACTACCTCAGC GGATCGT
Lpop_NtBbvCI_A1I	TCGGTGCTCCGCTTAC TTTTTTTTTTT CATAGCTACAAGAACCTCAGC ACGATCC
Lpop_NtBbvCI_A2I	GTAAGCGGAGCACCGA TTTTTTTTTTT TTTACAGATAACTACCTCAGC GGATCGT

Table C.6: Strands used for preliminary testing in Section 3.4. Sequences that are part of each enzyme's restriction site are highlighted by underlining.

Strand Name	Sequence	Replaced staple
Unbraced track		
Lpg_M1_Q	GCTGAGGTTCTTGTAGCTATG GCATG /3IAbRQSp/	-
Lpg_tr1_A0b3	TGACCTAAATCAAAATCATAGGTTGGAAACA TTT TGC CATAGCTACAAGAACCTCAGC ACGATCC TTTT GGATCGT	M5t16f
Lpg_tr1_A1	ATCGCGCAAATTACCTTTTTTAACTGAGAGA TTT CATAGCTACAAGAACCTCAGC ACGATCC TTTT GGATCGT	M3t18e
Lpg_tr1_A2	AGGTAAAGGAATCGCCATATTTAAGAAAACT TTT CATAGCTACAAGAACCTCAGC ACGATCC TTTT GGATCGT	M3t14f
Lpg_tr1_A3	TATATAACAAGACAAAGAACGCGACAACGCC TTT CATAGCTACAAGAACCTCAGC ACGATCC TTTT GGATCGT	M1t16e
Lpg_tr1_A4	ATTCAACCAGTCAAATCACCATCTTTTCGAG TTT CATAGCTACAAGAACCTCAGC ACGATCC TTTT GGATCGT	M-1t14e
Lpg_tr1_A5	GCGCCCAATTTTCATCGTAGGAAAGGTGGCA TTT CATAGCTACAAGAACCTCAGC ACGATCC TTTT GGATCGT	M1t12f
Lpg_tr1_A6	CGAGCTTCAGGTCAGGATTAGAGGCTATATT TTT CATAGCTACAAGAACCTCAGC ACGATCC TTTT GGATCGT	M-1t10f
Lpg_tr1_A6I	CGAGCTTCAGGTCAGGATTAGAGGCTATATT TTTTTTTTT CATAGCTACAAGAACCTCAGC ACGATCC	M-1t10f
Lpg_tr1_A7e_nx	CAATAAATTCAATAACCTGTTTAAGTACCTT TTT CATAGCTACAAGAACCTCAGC	M-3t12e
Lpg_tr2_A2I	GGAGAGGGAAGATTCAAAAGGGTTTAACATC TTTTTTTTT TTTACAGATAACTACCTCAGC GGATCGT	M-3t14e
Lpg_tr2_A2I_cut	GGAGAGGGAAGATTCAAAAGGGTTTAACATC TTTTTTTTT TTTACAGATAACTACC	M-3t14e
Lpg_tr1_F0_cTET	ATCCCACTCCCTACACTTCG TT GTACATAATTGCTTTGAATACCAAAAGGGTTA	M5t18f
TET	/5TET/ CGAAGTGTAGGGAGTGGGAT	-
Lpg_tr1_F0_cTEX	CTCTATCTCACTCAACCCTC TT GTACATAATTGCTTTGAATACCAAAAGGGTTA	M5t18f
TEX615	/5TEX615/ GAGGGTTGAGTGAGATAGAG	-
Lpg_tr1_F7_cCy5	CCTTTTACTTCCACTACCCA TT TAATTGCTACTTCAAATATCGCGCCAGAGGG	M-3t10e
Cy5_5'	/5Cy5/ TGGGTAGTGGAAGTAAAAGG	-
Braced track		
Lpg_M1_Q	GCTGAGGTTCTTGTAGCTATG GCATG /3IAbRQSp/	-
Lpg_tr1_A0b3_br	TGACCTAAATCAAAATCATAGGTTGGAAACA AA CTCAGTCAGGGC TTT TGC CATAGCTACAAGAACCTCAGC GAAGGCG TTTT CGCCTTC	M5t16f
Lpg_tr1_A1_br	ATCGCGCAAATTACCTTTTTTAACTGAGAGA AA CCCCAGACCGAC TTT CATAGCTACAAGAACCTCAGC GAAGGCG TTTT CGCCTTC	M3t18e
Lpg_tr1_A2_br	AGGTAAAGGAATCGCCATATTTAAGAAAACT AA CCACAGACTGCG TTT CATAGCTACAAGAACCTCAGC GAAGGCG TTTT CGCCTTC	M3t14f
Lpg_tr1_A3_br	TATATAACAAGACAAAGAACGCGACAACGCC AA GCCCGCATCCGA TTT CATAGCTACAAGAACCTCAGC GAAGGCG TTTT CGCCTTC	M1t16e
Lpg_tr1_A4_br	ATTCAACCAGTCAAATCACCATCTTTTCGAG AA CCCGACACTCCG TTT CATAGCTACAAGAACCTCAGC GAAGGCG TTTT CGCCTTC	M-1t14e
Lpg_tr1_A5_br	GCGCCCAATTTTCATCGTAGGAAAGGTGGCA AA GTTATCCCTCCG TTT CATAGCTACAAGAACCTCAGC GAAGGCG TTTT CGCCTTC	M1t12f
Lpg_tr1_A6_br	CGAGCTTCAGGTCAGGATTAGAGGCTATATT AA GTGGGGAACGAT TTT CATAGCTACAAGAACCTCAGC GAAGGCG TTTT CGCCTTC	M-1t10f
Lpg_tr1_A7e_nx_br	CAATAAATTCAATAACCTGTTTAAGTACCTT AA GCTCGTCGGGTA TTT CATAGCTACAAGAACCTCAGC	M-3t12e
Lpg_tr1_N1_br	GTCGGTCTGGGG AA CTACCTTTTATATTTTAGTTAATTAGTAGGGC	M3t16e
Lpg_tr1_N2_br	CGCAGTCTGTGG AA TTTTCAAATTAACCTCCGGCTTATTAACAAT	M3t16f
Lpg_tr1_N3_br	TCGGATGCGGGC AA AACATGTAAAGAGAATATAAAGTAAAGCAAGC	M1t14e
Lpg_tr1_N4_br	CGGAGTGTCGGG AA CCAGTAATATTTAGGCAGAGGCAAATATGAT	M1t14f
Lpg_tr1_N5_br	CGGAGGGATAAC AA TCAATTCTGGGCGCGAGCTGAAATCATTACC	M-1t12e
Lpg_tr1_N6_br	ATCGTTCCCCAC AA TTCATTTGACTAATAGTAGTAGCAGAGAAAGG	M-1t12f
Lpg_tr1_F0_cTET_br	ATCCCACTCCCTACACTTCG TT GCCCTGACTGAG AA GTACATAATTGCTTTGAATACCAAAAGGGTTA	M5t18f
TET	/5TET/ CGAAGTGTAGGGAGTGGGAT	-
Lpg_tr1_F0_cTEX_br	CTCTATCTCACTCAACCCTC TT GCCCTGACTGAG AA GTACATAATTGCTTTGAATACCAAAAGGGTTA	M5t18f
TEX615	/5TEX615/ GAGGGTTGAGTGAGATAGAG	-
Lpg_tr1_F7_cCy5_br	CCTTTTACTTCCACTACCCA TT TACCCGACGAGC AA TAATTGCTACTTCAAATATCGCGCCAGAGGG	M-3t10e
Cy5_5'	/5Cy5/ TGGGTAGTGGAAGTAAAAGG	-

Table C.7: Strands used for the ensemble fluorescence measurements in Section 3.5. The unbraced track used two versions of the strands for the F_0 signal: the TEX strands in the experiments run in CutSmart buffer, the TET strands were used in the other experiments. Sequences that are part of each enzyme's restriction site are highlighted by underlining. The braced track also used two versions of the strands for the F_0 were used: the TET strands were used for one experiment, the TEX strands in another. These gave similar fluorescence traces and were averaged over. Sequences that are part of each enzyme's restriction site are highlighted by underlining.

C.4 Strands for Chapter 4

Strand Name	Sequence	Replaced staple
Motors		
Tu_M	CG ATGTTAGTTGGGCTGAGGTTCC	-
Tu_M_Q	CG ATGTTAGTTGGGCTGAGGTTCC TTT /3IAbRQSp/	-
Tu_Cy3M	/5Cy3/ TT TCATCACACTC TT /3Cy3Sp/	-
Tu_M_11	GAGTGTGATGA TT GC ATGTTAGTTGGGCTGAGGTTCC TT GAGTGTGATGA	-
Tu_M_02	GC ATGTTAGTTGGGCTGAGGTTCC TT GAGTGTGATGA TTT GAGTGTGATGA	-
Track		
Tu_A0_br	AGGTTCCGATCTACAT T GGAACCTCAGCCCAACTAACAT CG T CACTCCAC AA TGCTTTCGCAAAAAAAAGGCTCCACAAATAAA	TuSt1
Tu_A0_cTET_br	ATCCCACTCCCTACACTTCG T GGAACCTCAGCCCAACTAACAT CG T CACTCCAC AA TGCTTTCGCAAAAAAAAGGCTCCACAAATAAA	TuSt1
Tu_tr0_br	AGGTTCCGATCTACAT T GGAACCTCAGCCCAACTAACAT T CACTCCAC AA TGCTTTCGCAAAAAAAAGGCTCCACAAATAAA	TuSt1
Tu_tr1_br	AGGTTCCGATCTACAT T GGAACCTCAGCCCAACTAACAT T CACTCCAC AA AAAATCTAAACGAGTAGTAAATTGAACAGCTTG	TuSt2
Tu_tr2_br	AGGTTCCGATCTACAT T GGAACCTCAGCCCAACTAACAT T CACTCCAC AA TCTGAATTCACCACCAGAGCCGCCGGAAACCG	TuSt3
Tu_tr3_br	AGGTTCCGATCTACAT T GGAACCTCAGCCCAACTAACAT T CACTCCAC AA ACCAGAACTACCGTTCCAGTAACAACTAAA	TuSt4
Tu_tr4_br	AGGTTCCGATCTACAT T GGAACCTCAGCCCAACTAACAT T CACTCCAC AA GAACTGGCAATATCAGAGAGATAATAAGTCCT	TuSt5
Tu_tr4_cCy5_br	CCTTTTACTTCCACTACCCA T GGAACTTCAGCCCAACTAACAT T CACTCCAC AA GAACTGGCAATATCAGAGAGATAATAAGTCCT	TuSt5
Tu_tr5_br	AGGTTCCGATCTACAT T GGAACCTCAGCCCAACTAACAT T CACTCCAC AA TGAGCGCTATGATTAAGACTCCAGAACCGC	TuSt6
Tu_tr6_br	AGGTTCCGATCTACAT T GGAACCTCAGCCCAACTAACAT T CACTCCAC AA CGAGCATGAGCCAACGCTCAACAGAAGAAAACA	TuSt7
Tu_tr7_br	AGGTTCCGATCTACAT T GGAACCTCAGCCCAACTAACAT T CACTCCAC AA CAGTATAATAGAAACCAATCAAAGAATTAA	TuSt8
Tu_tr8_br	AGGTTCCGATCTACAT T GGAACCTCAGCCCAACTAACAT T CACTCCAC AA TACCTTTTTTGTTTGGATTATACTAGGTGAGG	TuSt9
Tu_tr9_br	AGGTTCCGATCTACAT T GGAACCTCAGCCCAACTAACAT T CACTCCAC AA AATCCTGATTAATGGAAACAGTAAGCCTGT	TuSt10
Tu_tr10_br	AGGTTCCGATCTACAT T GGAACCTCAGCCCAACTAACAT T CACTCCAC AA ACGCTGAGCAAACTATCGGCCTTGAGAAAGGA	TuSt11
Tu_tr11_br	AGGTTCCGATCTACAT T GGAACCTCAGCCCAACTAACAT T CACTCCAC AA GAAGAACTAGCCAGCAGCAAATCATATTCC	TuSt12
Tu_tr12_br	AGGTTCCGATCTACAT T GGAACCTCAGCCCAACTAACAT T CACTCCAC AA CGCTGGCATTCCACACAACATACGGTGCCGGA	TuSt13
Tu_tr13_br	AGGTTCCGATCTACAT T GGAACCTCAGCCCAACTAACAT T CACTCCAC AA GCTCACAAAGTGTAGCGGTCACATACTTCT	TuSt14
Tu_tr14_br	AGGTTCCGATCTACAT T GGAACCTCAGCCCAACTAACAT T CACTCCAC AA TGCGCAACATTGCCTGAGAGTCTTAATACTTT	TuSt15
Tu_tr15_br	AGGTTCCGATCTACAT T GGAACCTCAGCCCAACTAACAT T CACTCCAC AA ATCAGGTCTGTTGGGAAGGGCGAATCATGGT	TuSt16
Tu_tr16_br	AGGTTCCGATCTACAT T GGAACCTCAGCCCAACTAACAT T CACTCCAC AA TAAAAATTGCAAAGCGGATTGCATTGCCAGAG	TuSt17
Tu_tr17_br	AGGTTCCGATCTACAT T GGAACCTCAGCCCAACTAACAT T CACTCCAC AA AGTCAGAATTTAGAACCCTCATACCGGAGAG	TuSt18
Tu_tr18_br	AGGTTCCGATCTACAT T GGAACCTCAGCCCAACTAACAT T CACTCCAC AA CGTCCAATGATAAATTGTGTCGATAAAACGAA	TuSt19
Tu_tr19_br	AGGTTCCGATCTACAT T GGAACCTCAGCCCAACTAACAT T CACTCCAC AA CATCGCCTACTGCGGAATCGTCAACCATAAA	TuSt20
Tu_tr20_br	AGGTTCCGATCTACAT T GGAACCTCAGCCCAACTAACAT T CACTCCAC AA TTTGACCCAGAACCGCCACCCTCTGTATCACC	TuSt21
Tu_N0_br	CTCATTATATTTCAACTTTAATCTTATCAGCT AA GTGGAGTG	TuSt22
Tu_N1_br	TGACAGGAAAGCCAGAATGGAATCACGTTG AA GTGGAGTG	TuSt23
Tu_N2_br	ATACCGATCGAATAATAATTTTTAGCGCAGTC AA GTGGAGTG	TuSt24
Tu_N3_br	AATTGAGCAATAATAACGGAATGAGCCGCC AA GTGGAGTG	TuSt25
Tu_N4_br	ATGGCTTTGAGCCACCACCCTCAACCCAAAA AA GTGGAGTG	TuSt26
Tu_N5_br	TAATTGAAAAATAATATCCCATAGGGTAAT AA GTGGAGTG	TuSt27
Tu_N6_br	AGTATGTTCCTGAACAAAGTCAGCCTAATTTA AA GTGGAGTG	TuSt28
Tu_N7_br	ATGGAAGTACATTTAACAATTTATTCTTAC AA GTGGAGTG	TuSt29
Tu_N8_br	GTCTTTCCATATGCGTTATACAACATTTGAAT AA GTGGAGTG	TuSt30
Tu_N9_br	ATCCAGAATTAACACCGCCTGCATCAATAT AA GTGGAGTG	TuSt31
Tu_N10_br	AATATATGAGATGATGGCAATTCAACAGTGCC AA GTGGAGTG	TuSt32
Tu_N11_br	AGCATAAAAAGCGAAAGGAGCGGCCTGAGTA AA GTGGAGTG	TuSt33
Tu_N12_br	AAAGCATCTAATAACATCACTTGGCGCTAGGG AA GTGGAGTG	TuSt34
Tu_N13_br	CAAGAGAAAAAGCGCCATTCGCTGTTATCC AA GTGGAGTG	TuSt35
Tu_N14_br	AACCACCAGTTTCCTGTGTGAAATCATTCAGGC AA GTGGAGTG	TuSt36
Tu_N15_br	ATTAAGAGAAGCCTTTATTTCACAAAGGCT AA GTGGAGTG	TuSt37
Tu_N16_br	GGCCTCTTATTTTTGAGAGATCTAACGCAAGGA AA GTGGAGTG	TuSt38
Tu_N17_br	ACCTGCTCAGTAAAATGTTTAGACTATTAT AA GTGGAGTG	TuSt39
Tu_N18_br	ATGCAATGTCAGGTCTTTACCCTGACTGGATAG AA GTGGAGTG	TuSt40
Tu_N19_br	CACCCTCAAAGAATACACTAAAATTTGTAT AA GTGGAGTG	TuSt41
Tu_N20_br	CATTGAATACAAAGTACAACGGAGACACTCATC AA GTGGAGTG	TuSt42
Tu_TET_0	/5TET/ CGAAGTGTAGGGAGTGGGAT	-
Tu_Cy5_end	TGGGTAGTGGAAGTAAAAGG /3Cy5Sp/	-
Tu_Cy3A	/5Cy3/ T ATGTAGATCGGAACCT	-
Tu_Cy3A_unmod	T ATGTAGATCGGAACCT	-

Table C.8: Strands used in Chapter 4.

Strand Name	Sequence	Replaced staple
Biotin strands for surface immobilisation during microscopy experiments: used in Section 4.3		
Tu_BioTether1	ATGGTTTAACCAGTCAGGACGTGTCTGGAA GTT CTCCTCTCCACCACCT	TuSt43
Tu_BioTether2	ACACCAGCGTTAATAAAACGAAAACATGTT TTAA CTCCTCTCCACCACCT	TuSt44
Tu_BioTether3	CATTCAGTTTACAGGTAGAAAGAGCTTAAT TGCT CTCCTCTCCACCACCT	TuSt45
Tu_BioTether4	TCATTACCTAGGAATACCACATTTGATAAGA GGT CTCCTCTCCACCACCT	TuSt46
Tu_BioTether5	ATCAAGAATAACGCCAAAAGGACAGGATTA GAGA CTCCTCTCCACCACCT	TuSt47
Tu_BioTether6	AACCAGGCTCGATGAACGGTAATCAATCGGTT GTAC CTCCTCTCCACCACCT	TuSt48
Tu_BioTether7	AACGCCAGAATCACCATCAATATGGTAAAGAT TCAA CTCCTCTCCACCACCT	TuSt49
Tu_BioAnchor	/5Biosg/ GGGTAGGGAAGATA AGGTGGTGGAGAGGAG	-
Tu_BioN1	TCATGATACATTTCGCAAAAGGAACGC	TuSt50
Tu_BioN2	ATATAGCTATATTTTCATTTTTGTTA	TuSt51
Tu_BioN3	GAATAAGGTGGCATCAATTCGTTAATA	TuSt52
Tu_BioN4	CATTCATTAACATCCAATAAAGATTGT	TuSt53
Tu_BioN5	GTACAAAGAATTAGCAAAGGTTGATA	TuSt54
Tu_BioN6	CAAAAATTCGAGCTTCAAAGTAACCCTCG	TuSt55
Tu_BioN7	AAGGTCAGAAAACGAGAATGTAAATATT	TuSt56

Table C.9: Strands used for surface immobilisation within the flow chambers during the microscopy experiments in Chapter 4.

C.5 Strands for Chapter 5

Strand Name	Sequence	Replaced staple
Threading - unbraced tile: used in Figure 5.8		
FRET_S_10dT_Cy3	GGATTAGGAGAGGCTGAGACTCCTGCATAACC TTTTTTTTTT /3Cy3Sp/	M1t2f
FRET_F_2dT_5'Cy5	/5Cy5/ TT GATATATTAACAACCATCGCCCACCAAGAGAA	M-1t2e
Threading - braced tile: used in Figure 5.9		
FRET_Sbr_10dT_Cy3	GGATTAGGAGAGGCTGAGACTCCTGCATAACC AA CCGC TTTTTTTTTT /3Cy3Sp/	M1t2f
FRET_Fbr_2dT_5'Cy5	/5Cy5/ TT GCGG AA GATATATTAACAACCATCGCCCACCAAGAGAA	M-1t2e
Threading - multilayer: used in Figure 5.10		
FRETmulti_S_10dT_Cy3	CCTCAGACCACCCTCCAGGAGGTAGCAAGGAAGGTAAAAGTTTAT TTTTTTTTTT /3Cy3Sp/	MuSt35
FRETmulti_F_2dT_5'Cy5	/5Cy5/ TT TTTGTCACGATTAGTTTTAACGTCGAAACCAAGTTTATCAACAATAGA	MuSt20
Non-origami controls: used in Figure 5.12		
FRET_FS_base	TTCTCTTGGTGGGCGATGGTTGTTAATATATC GGTTATGCAGGAGTCTCAGCCTCTCCTAATCC	-
FRET_C3_Cy3	AAAACAGAAGGATAAGTGTTTGATTGTAGCCG TT /3Cy3Sp/	-
FRET_S	GGATTAGGAGAGGCTGAGACTCCTGCATAACC TTT CGGCTACAATCAAACACTTATCCTTCTGTTTT	-
FRET_S-5	GGATTAGGAGAGGCTGAGACTCCTGCA**GTCCA** TTT CGGCTACAATCAAACACTTATCCTTCTGTTTT	-
FRET_S-10	GGATTAGGAGAGGCTGAGACTC**GGAGACCCAT** TTT CGGCTACAATCAAACACTTATCCTTCTGTTTT	-
FRET_S-10replace	**CTGCATAACC**	-
FRET_S-16	GGATTAGGAGAGGCTG**GGCGATGCTTTAGACA** TTT CGGCTACAATCAAACACTTATCCTTCTGTTTT	-
FRET_S-16replace	**AGACTCCTGCATAACC**	-
FRET_F_2dT_5'Cy5	/5Cy5/ TT GATATATTAACAACCATCGCCCACCAAGAGAA	-
Repair - single cargo: used in Figures 5.13 to 5.15 and 5.17		
FRET_C3_Cy3	AAAACAGAAGGATAAGTGTTTGATTGTAGCCG TT /3Cy3Sp/	-
FRET_S	GGATTAGGAGAGGCTGAGACTCCTGCATAACC TTT CGGCTACAATCAAACACTTATCCTTCTGTTTT	r1t2f
FRET_S-8	GGATTAGGAGAGGCTGAGACTCCT**AGACCCAT** TTT CGGCTACAATCAAACACTTATCCTTCTGTTTT	r1t2f
FRET_F_2dT_5'Cy5	/5Cy5/ TT GATATATTAACAACCATCGCCCACCAAGAGAA	r-1t2e
FRET_F_2dT_3'Cy5	GATATATTAACAACCATCGCCCACCAAGAGAA TT /3Cy5Sp/	r-1t2e
Repair - two cargos, one extension: used in Figure 5.18		
FRET_C1_Cy3	CGGGAGAGGTATGCTGAGGGGCCTTGATTGTAGCCG TT /3Cy3Sp/	-
FRET_C2	ACATTACTTGCGAAAACAGAAGGATAAGTGTGGCCCC	-
FRET_S	GGATTAGGAGAGGCTGAGACTCCTGCATAACC TTT CGGCTACAATCAAACACTTATCCTTCTGTTTT	r1t2f
FRET_F_2dT_5'Cy5	/5Cy5/ TT GATATATTAACAACCATCGCCCACCAAGAGAA	r-1t2e
Repair - two cargos, two extensions: used in Figures 5.19 and 5.20		
FRET_C3_Cy3	AAAACAGAAGGATAAGTGTTTGATTGTAGCCG TT /3Cy3Sp/	-
FRET_S3 (A.K.A. FRET_S)	GGATTAGGAGAGGCTGAGACTCCTGCATAACC TTT CGGCTACAATCAAACACTTATCCTTCTGTTTT	r1t2f
FRET_S5	CCTTTTACTTCCACTACCCA TT GATATATTAACAACCATCGCCCACCAAGAGAA	r-1t2e
FRET_C5 (A.K.A. Cy5_5')	/5Cy5/ TGGGTAGTGGAAGTAAAAGG	-

Table C.10: Strands used for experiments in Chapter 5.

C.6 Strands for Chapter 6

Strand Name	Sequence
Oct1_S1	CGCGGATG A CTCAACTGCCTGGTGATACG A TCTAGTCTCTACGTCAAGTA A GAACCTTAGCTG
Oct1_S2	CTCGCATG A CATCCGCGCAGCTAAGGTTC A AAGTTCCTGCCGCTTCACGG A CGGTATTGGACC
Oct1_S3	CGAAGCCT A CTTGCATACCCCTCTATCCG A CCGTGAAGCGGCAGGAACTT A ATTACGCTGGCT
Oct1_S4	TCGTACTC A AGGCTTCGAGCCAGCGTAAT A TACTTGACGTAGAGACTAGA A AGGCCAGTCCTG
Oct1_S5	GTGATAAA A TGGGATGGAACTTTCCGCTA A GAGTACGACAGGACTGGCCT A CTACTATGGCGG
Oct1_S6	TATGCAAG A TAGCGGAAAGTTCCATCCCA A CGTGTAGCAAGCTGTAATCG A CGGATAGAGGGG
Oct1_S7	GCTACACG A TTCAGACTTAGGAATGTTCG A CATGCGAGGGTCCAATACCG A CGATTACAGCTT
Oct1_S8	CAGTTGAG A CGAACATTCCTAAGTCTGAA A TTTATCACCCGCCATAGTAG A CGTATCACCAGG

Table C.11: Octahedron strands for formation with unbound A bases at the vertices, used in Figure 6.8. Ordered from IDT with 5' phosphates.

Strand Name	Sequence
Oct2_S1	CGCGGATG T CTCAACTGCCTGGTGATACG T TCTAGTCTCTACGTCAAGTA C GAACCTTAGCTG
Oct2_S2	CTCGCATG T CATCCGCGCAGCTAAGGTTC G AAGTTCCTGCCGCTTCACGG A CGGTATTGGACC
Oct2_S3	CGAAGCCT G CTTGCATACCCCTCTATCCG T CCGTGAAGCGGCAGGAACTT G ATTACGCTGGCT
Oct2_S4	TCGTACTC A AGGCTTCGAGCCAGCGTAAT C TACTTGACGTAGAGACTAGA A AGGCCAGTCCTG
Oct2_S5	GTGATAAA T TGGGATGGAACTTTCCGCTA T GAGTACGACAGGACTGGCCT A CTACTATGGCGG
Oct2_S6	TATGCAAG C TAGCGGAAAGTTCCATCCCA A CGTGTAGCAAGCTGTAATCG T CGGATAGAGGGG
Oct2_S7	GCTACACG C TTCAGACTTAGGAATGTTCG A CATGCGAGGGTCCAATACCG A CGATTACAGCTT
Oct2_S8	CAGTTGAG A CGAACATTCCTAAGTCTGAA G TTTATCACCCGCCATAGTAG T CGTATCACCAGG

Table C.12: Octahedron strands for formation with complementary vertex bases, used in Figure 6.9.

Bibliography

[1] J. Bath, S. J. Green, and A. J. Turberfield. "A free-running DNA motor powered by a nicking enzyme". *Angewandte Chemie (International ed. in English)* 44.28 (2005), pp. 4358–61.

[2] H. R. Drew et al. "Structure of a B-DNA dodecamer: conformation and dynamics". *Proceedings of the National Academy of Sciences of the United States of America* 78.4 (1981), pp. 2179–83.

[3] J. D. Watson and F. H. C. Crick. "Molecular structure of nucleic acids". *Nature* 171.4356 (1953), pp. 737–738.

[4] B. Alberts et al. *Molecular Biology of the Cell*. Fifth edit. Garland Science, 2008.

[5] S. B. Smith, L. Finzi, and Bust. "Direct mechnical measurements of the elasticity of single DNA molecules by using magnetic beads". *Science* 258.5085 (1992), pp. 1122–1126.

[6] J. N. Zadeh et al. "NUPACK : analysis and design of nucleic acid systems". *Journal of computational chemistry* 32 (2011), pp. 170–173.

[7] R. P. Goodman. "NANEV: a program employing evolutionary methods for the design of nucleic acid nanostructures." *BioTechniques* 38.4 (2005), pp. 548, 550.

[8] N. C. Seeman. "Nucleic acid junctions and lattices". *Journal of Theoretical Biology* 99.2 (1982), pp. 237–247.

[9] P. W. K. Rothemund. "Folding DNA to create nanoscale shapes and patterns". *Nature* 440.7082 (2006), pp. 297–302.

[10] H. Dietz, S. M. Douglas, and W. M. Shih. "Folding DNA into twisted and curved nanoscale shapes." *Science (New York, N.Y.)* 325.5941 (2009), pp. 725–30.

[11] S. M. Douglas et al. "Self-assembly of DNA into nanoscale three-dimensional shapes". *Nature* 459.7245 (2009), pp. 414–418.

[12] X.-c. Bai et al. "Cryo-EM structure of a 3D DNA-origami object". *PNAS* 109.49 (2012), pp. 0–5.

[13] R. P. Goodman, R. M. Berry, and A. J. Turberfield. "The single-step synthesis of a DNA tetrahedron". *Society* 44.12 (2004), pp. 1372–1373.

[14] J. B. Lee et al. "A mechanical metamaterial made from a DNA hydrogel". *Nature Nanotechnology* 7.December (2012), pp. 3–7.

[15] H. Qi et al. "DNA-directed self-assembly of shape-controlled hydrogels". *Nature Communications* 4 (2013), pp. 1–10.

[16] J. Zheng et al. "From molecular to macroscopic via the rational design of a self-assembled 3D DNA crystal". *Nature* 461.7260 (2009), pp. 74–77.

[17] A. Rajendran et al. "Programmed two-dimensional self-assembled assembly of multiple DNA origami jigsaw pieces". *ACS Nano* 5.1 (2011), pp. 665–671.

[18] Z. Zhao, Y. Liu, and H. Yan. "Organizing DNA origami tiles into larger structures using preformed scaffold frames". *Nano Letters* 11.7 (2011), pp. 2997–3002.

[19] Z. Li et al. "Molecular behavior of DNA origami in higher-order self-assembly". *Journal of the American Chemical Society* 132.38 (2010), pp. 13545–13552.

[20] S. M. Douglas et al. "Rapid prototyping of 3D DNA-origami shapes with caDNAno". *Nucleic Acids Research* 37.15 (2009), pp. 5001–5006.

[21] T. Kato et al. "High-resolution structural analysis of a DNA nanostructure by cryoEM". *Nano Letters* 9.7 (2009), pp. 2747–2750.

[22] N. A. W. Bell et al. "DNA origami nanopores". *Nano letters* 12.1 (2012), pp. 512–7.

[23] S. M. Douglas, I. Bachelet, and G. M. Church. "A logic-gated nanorobot for targeted transport of molecular payloads". *Science* 335.6070 (2012), pp. 831–834.

[24] Y. Fu et al. "Single-step rapid assembly of DNA origami nanostructures for addressable nanoscale bioreactors." *Journal of the American Chemical Society* 135.2 (2013), pp. 696–702.

[25] G. P. Acuna et al. "Distance dependence of single-fluorophore quenching by gold nanoparticles studied on DNA origami." *ACS nano* 6.4 (2012), pp. 3189–95.

[26] S. Pal et al. "DNA-origami-directed self-assembly of discrete silver-nanoparticle architectures". *Angewandte Chemie - International Edition* 49.15 (2010), pp. 2700–2704.

[27] K. E. Dunn et al. "Guiding the folding pathway of DNA origami". *Nature* 525.7567 (2015), pp. 82–86.

[28] J.-P. J. Sobczak et al. "Rapid folding of DNA into nanoscale shapes at constant temperature". *Science* 338.6113 (2012), pp. 1458–1461.

[29] T. G. Martin and H. Dietz. "Magnesium-free self-assembly of multi-layer DNA objects". *Nature Communications* 3 (2012), p. 1103.

[30] A. A. Greschner, K. E. Bujold, and H. F. Sleiman. "Intercalators as molecular chaperones in DNA self-assembly". *Journal of the American Chemical Society* (2013), pp. 3–8.

[31] B. Wei, M. Dai, and P. Yin. "Complex shapes self-assembled from single-stranded DNA tiles". *Nature* 485.7400 (2012), pp. 623–626.

[32] Y. Ke et al. "Three-dimensional structures self-assembled from DNA bricks". *Science* 338.6111 (2012), pp. 1177–1183.

[33] E. Benson et al. "DNA rendering of polyhedral meshes at the nanoscale". *Nature* 523.7561 (2015), pp. 441–444.

[34] J. Chen and N. C. Seeman. "Synthesis from DNA of a molecule with the connectivity of a cube". *Nature* 350 (1991), pp. 6310–0633.

[35] K. E. Bujold et al. "Sequence-responsive unzipping DNA cubes with tunable cellular uptake profiles". *Chemical Science* 5.6 (2014), pp. 2449–2455.

[36] C. M. Erben, R. P. Goodman, and A. J. Turberfield. "A self-assembled DNA bipyramid." *Journal of the American Chemical Society* 129.22 (2007), pp. 6992–6993.

[37] A. S. Walsh. "Biological Applications of DNA Cages Biological Applications of DNA Cages". PhD thesis. 2011.

[38] Y. Zhang and N. C. Seeman. "Construction of a DNA-truncated octahedron". *Journal of the American Chemical Society* 116.13 (1994), pp. 1661–1669.

[39] Y. He et al. "Hierarchical self-assembly of DNA into symmetric supramolecular polyhedra". *Nature* 452.7184 (2008), pp. 198–201.

[40] W. M. Shih, J. D. Quispe, and G. F. Joyce. "A 1.7-kilobase single-stranded DNA that folds into a nanoscale octahedron". *Nature* 427.February (2004), pp. 618–621.

[41] R. M. Zadegan et al. "Construction of a 4 zeptoliters switchable 3D DNA box origami". *ACS nano* 6.11 (2012), pp. 10050–3.

[42] E. S. Andersen et al. "Self-assembly of a nanoscale DNA box with a controllable lid". *Nature* 459.7243 (2009), pp. 73–6.

[43] Y. Ke et al. "Scaffolded DNA origami of a DNA tetrahedron molecular container". *Nano Letters* 9.6 (2009), pp. 2445–2447.

[44] A. J. M. Wollman et al. "Transport and self-organization across different length scales powered by motor proteins and programmed by DNA." *Nature nanotechnology* 9.1 (2014), pp. 44–7.

[45] P. Lally. "Construction of a Synthetic Ribosome using DNA as the Building Material". PhD thesis. University of Oxford, 2010.

[46] S. Venkataraman et al. "An autonomous polymerization motor powered by DNA hybridization." *Nature nanotechnology* 2.8 (2007), pp. 490–494.

[47] A. E. Marras et al. "Programmable motion of DNA origami mechanisms". *Proceedings of the National Academy of Sciences* 112.3 (2015), pp. 713–718.

[48] Y. Tian and C. Mao. "Molecular gears: a pair of DNA circles continuously rolls against each other." *Journal of the American Chemical Society* 126.37 (2004), pp. 11410–1.

[49] B. Yurke et al. "A DNA-fuelled molecular machine made of DNA". *Nature* 406.6796 (2000), pp. 605–8.

[50] W. U. Dittmer et al. "Using gene regulation to program DNA-based molecular devices". *Small* 1.7 (2005), pp. 709–712.

[51] N. Srinivas et al. "On the biophysics and kinetics of toehold-mediated DNA strand displacement". *Nucleic Acids Research* 41.22 (2013), pp. 10641–10658.

[52] B. Yurke and A. P. Mills. "Using DNA to power nanostructures". In: *Genetic Programming and Evolvable Machines*. Springer, 2003, pp. 111–122.

[53] D. Y. Zhang and G. Seelig. "Dynamic DNA nanotechnology using strand-displacement reactions". *Nature chemistry* 3.2 (2011), pp. 103–13.

[54] R. R. F. Machinek et al. "Programmable energy landscapes for kinetic control of DNA strand displacement". *Nature Communications* 5 (2014), p. 5324.

[55] A. J. Genot et al. "Remote toehold: a mechanism for flexible control of DNA hybridization kinetics". *Journal of the American Chemical Society* 133.7 (2011), pp. 2177–82.

[56] A. J. Turberfield et al. "DNA fuel for free-running nanomachines". *Physical Review Letters* 90.11 (2003), p. 118102.

[57] P. Yin et al. "Programming biomolecular self-assembly pathways". *Nature* 451.7176 (2008), pp. 318–22.

[58] G. Seelig et al. "Enzyme-free nucleic acid logic circuits." *Science (New York, N.Y.)* 314.5805 (2006), pp. 1585–8.

[59] X. Liang et al. "A DNA nanomachine powered by light irradiation". *ChemBioChem* 9.5 (2008), pp. 702–705.

[60] M. Zhou et al. "A light-driven DNA nanomachine for the efficient photoswitching of RNA digestion." *Angewandte Chemie (International ed. in English)* 49.12 (2010), pp. 2167–70.

[61] T. E. Ouldridge, A. A. Louis, and J. P. K. Doye. "DNA nanotweezers studied with a coarse-grained model of DNA". *Physical Review Letters* 104.17 (2010), pp. 1–4.

[62] S. Modi et al. "A DNA nanomachine that maps spatial and temporal pH changes inside living cells". *Nature nanotechnology* 4.5 (2009), pp. 325–330.

[63] W. Shen et al. "A protein-driven DNA device that measures the excess binding energy of proteins that distort DNA". *Angewandte Chemie - International Edition* 43.36 (2004), pp. 4750–4752.

[64] C. M. Niemeyer et al. "Nucleic acid supercoiling as a means for ionic switching of DNA–nanoparticle networks." *Chembiochem* 2.4 (2001), pp. 260–4.

[65] V. Viasnoff, A. Meller, and H. Isambert. "DNA nanomechanical switches under folding kinetics control". *Nano Letters* 6.1 (2006), pp. 101–104.

[66] D. Liu and S. Balasubramanian. "A proton-fuelled DNA nanomachine." *Angewandte Chemie (International ed. in English)* 42.46 (2003), pp. 5734–6.

[67] S. Surana et al. "An autonomous DNA nanomachine maps spatiotemporal pH changes in a multicellular living organism." *Nature communications* 2.May (2011), p. 340.

[68] A. Idili, A. Vallée-Bélisle, and F. Ricci. "Programmable pH-triggered DNA nanoswitches". *Journal of the American Chemical Society* 136.16 (2014), pp. 5836–5839.

[69] S. Modi et al. "Two DNA nanomachines map pH changes along intersecting endocytic pathways inside the same cell." *Nature nanotechnology* 8.6 (2013), pp. 459–67.

[70] H. Gu, W. Yang, and N. C. Seeman. "A DNA scissors device used to measure MutS binding to DNA mis-pairs". *Journal of the American Chemical Society* 132.12 (2010), pp. 4352–4357.

[71] C. Liu et al. "A DNA-based nanomechanical device used to characterize the distortion of DNA by Apo-SoxR protein". *Biochemistry* 51 (2012), pp. 937–943.

[72] L. Zhou et al. "DNA origami compliant nanostructures with tunable mechanical properties". *ACS Nano* 8.1 (2014), pp. 27–34.

[73] R. Galletto, M. J. Jezewska, and W. Bujalowski. "Unzipping mechanism of the double-stranded DNA unwinding by a hexameric helicase: quantitative analysis of the rate of the dsDNA unwinding, processivity and kinetic step-size of the Escherichia coli DnaB helicase using rapid quench-flow method". *Journal of Molecular Biology* 343.1 (2004), pp. 83–99.

[74] H. C. Berg. "The rotary motor of bacterial flagella". *Annual Review of Biochemistry* 72 (2003), pp. 19–54.

[75] S. Higashi-Fujime et al. "The fastest-actin-based motor protein from the green algae, Chara, and its distinct mode of interaction with actin". *FEBS Letters* 375.1-2 (1995), pp. 151–154.

[76] K. Svoboda et al. "Direct observation of kinesin stepping by optical trapping interferometry." *Nature* 365 (1993), pp. 721–727.

[77] J. Howard, A. J. Hudspeth, and R. D. Vale. "Movement of microtubules by single kinesin molecules". *Nature* 342 (1989), pp. 154–8.

[78] T. Watanabe, H. Hosoya, and S. Yonemura. "Regulation of myosin II dynamics by phosphorylation and dephosphorylation of its light chain in epithelial cells". *Molecular biology of the cell* 18.February (2007), pp. 605–616.

[79] H. M. J. Carstairs. "A DNA-Kinesin Based Molecular Shuttle & Studies of DNA Kagome Arrays". PhD thesis. University of Oxford, 2008.

[80] A. J. M. Wollman. "DNA Motor-Protein Hybrids for Molecular Transport and Self-Organisation". PhD thesis. University of Oxford, 2013.

[81] C. Jung, P. B. Allen, and A. D. Ellington. "A stochastic DNA walker that traverses a microparticle surface". *Nature Nanotechnology* 11.November (2015), pp. 1–8.

[82] S. F. J. Wickham et al. "Direct observation of stepwise movement of a synthetic molecular transporter". *Nature Nanotechnology* 6.3 (2011), pp. 166–9.

[83] R. Masoud et al. "Studying the structural dynamics of bipedal DNA motors with single-molecule fluorescence spectroscopy". *ACS nano* 6.7 (2012), pp. 6272–6283.

[84] C. Zhou, X. Duan, and N. Liu. "A plasmonic nanorod that walks on DNA origami." *Nature communications* 6 (2015), p. 8102.

[85] Y. Yang et al. "Direct visualization of walking motions of photocontrolled nanomachine on the DNA nanostructure". *Nano Letters* 15.10 (2015), pp. 6672–6676.

[86] M. Liber et al. "A bipedal DNA motor that travels back and forth between two DNA origami tiles". *Small* 11.5 (2015), pp. 568–575.

[87] T. E. Tomov et al. "Rational design of DNA motors: fuel optimization through single-molecule fluorescence". *Journal of the American Chemical Society* 135 (2013), pp. 11935–11941.

[88] P. Yin et al. "A unidirectional DNA walker that moves autonomously along a track". *Angewandte Chemie International Edition* 43.37 (2004), pp. 4906–11.

[89] J.-S. Shin and N. A. Pierce. "A synthetic DNA walker for molecular transport". *Journal of the American Chemical Society* 126.35 (2004), pp. 10834–5.

[90] S. J. Green, J. Bath, and A. J. Turberfield. "Coordinated chemomechanical cycles: a mechanism for autonomous molecular motion". *Physical Review Letters* 101.23 (2008), pp. 20–23.

[91] R. A. Muscat, J. Bath, and A. J. Turberfield. "A programmable molecular robot". *Nano letters* 11.3 (2011), pp. 982–7.

[92] Y. Tian et al. "A DNAzyme that walks processively and autonomously along a one-dimensional track." *Angewandte Chemie (International ed. in English)* 44.28 (2005), pp. 4355–8.

[93] J. Bath et al. "Mechanism for a directional, processive, and reversible DNA motor". *Small (Weinheim an der Bergstrasse, Germany)* 5.13 (2009), pp. 1513–6.

[94] R. Pei et al. "Behavior of polycatalytic assemblies in a substrate-displaying matrix". *Interface* 24 (2006), pp. 12693–12699.

[95] K. Yehl et al. "High-speed DNA-based rolling motors powered by RNase H". *Nature nanotechnology* 11.November (2015), pp. 184–190.

[96] H. Gu et al. "A proximity-based programmable DNA nanoscale assembly line". *Nature* 465.7295 (2010), pp. 202–5.

[97] K. Lund et al. "Molecular robots guided by prescriptive landscapes". *Nature* 465.7295 (2010), pp. 206–10.

[98] R. A. Muscat, J. Bath, and A. J. Turberfield. "Small molecule signals that direct the route of a molecular cargo". *Small* 8.23 (2012), pp. 3593–3597.

[99] M. L. McKee et al. "Multistep DNA-templated reactions for the synthesis of functional sequence controlled oligomers". *Angewandte Chemie - International Edition* 49.43 (2010), pp. 7948–7951.

[100] M. L. McKee et al. "Programmable one-pot multistep organic synthesis using DNA junctions". *Journal of the American Chemical Society* 134 (2012), pp. 1446–1449.

[101] J. Bath and A. J. Turberfield. "DNA nanomachines". *Nature nanotechnology* 2.May (2007), pp. 275–284.

[102] S. F. J. Wickham et al. "A DNA-based molecular motor that can navigate a network of tracks". *Nature Nanotechnology* 7.January (2012), pp. 1–5.

[103] D.-N. Kim et al. "Quantitative prediction of 3D solution shape and flexibility of nucleic acid nanostructures." *Nucleic acids research* 40.7 (2011), pp. 2862–2868.

[104] C. E. Castro et al. "A primer to scaffolded DNA origami." *Nature methods* 8.3 (2011), pp. 221–229.

[105] J. R. Lakowicz. *Principles of Fluorescence Spectroscopy*. Third edit. Springer, 2006, p. 362.

[106] R. Jungmann et al. "Single-molecule kinetics and super-resolution microscopy by fluorescence imaging of transient binding on DNA origami". *Nano Letters* 10.11 (2010), pp. 4756–4761.

[107] R. Jungmann et al. "Multiplexed 3D cellular super-resolution imaging with DNA- PAINT and exchange-PAINT". *Nature Methods* 11.3 (2015), pp. 313–318.

[108] M. A. Behlke et al. "Fluorescence quenching by proximal G-bases". *Integrated DNA Technologies (IDT)* (2005), pp. 2–4.

[109] T. E. Ouldridge, A. A. Louis, and J. P. K. Doye. "Structural, mechanical, and thermodynamic properties of a coarse-grained DNA model". *Journal of Chemical Physics* 134.8 (2011), pp. 0–22.

[110] P. Šulc et al. "Sequence-dependent thermodynamics of a coarse-grained DNA model." *The Journal of chemical physics* 137.13 (2012), p. 135101.

[111] L. M. Adleman. "Molecular computation of solutions to combinatorial problems". *Science* 266 (1994), pp. 1021–1024.

[112] L. Qian and E. Winfree. "Scaling up digital circuit computation with DNA strand displacement cascades." *Science (New York, N.Y.)* 332.6034 (2011), pp. 1196–201.

[113] M. N. Stojanovic and D. Stefanovic. "A deoxyribozyme-based molecular automaton." *Nature biotechnology* 21.9 (2003), pp. 1069–74.

[114] Y. Benenson et al. "An autonomous molecular computer for logical control of gene expression." *Nature* 429.6990 (2004), pp. 423–9.

[115] K. Montagne et al. "Programming an in vitro DNA oscillator using a molecular networking strategy." *Molecular systems biology* 7.466 (2011), p. 466.

[116] Y. Benenson et al. "Programmable and autonomous computing machine made of biomolecules". *Nature* 414.6862 (2001), pp. 430–4.

[117] T. Fujii and Y. Rondelez. "Predator-prey molecular ecosystems". *ACS nano* 7.1 (2013), pp. 27–34.

[118] D. Soloveichik, G. Seelig, and E. Winfree. "DNA as a universal substrate for chemical kinetics." *Proceedings of the National Academy of Sciences of the United States of America* 107.12 (2010), pp. 5393–8.

[119] L. Qian, D. Soloveichik, and E. Winfree. "Efficient Turing-universal computation with DNA polymers". In: *Lecture Notes in Computer Science: DNA computing and molecular programming*. 6518/2011. Springer, 2011, pp. 123–140.

[120] M. R. Lakin et al. "Abstractions for DNA circuit design". *Journal of the Royal Society, Interface / the Royal Society* July 2011 (2011), pp. 1–17.

[121] A. Phillips and L. Cardelli. "A programming language for composable DNA circuits". *Journal of the Royal Society, Interface* 6.Suppl 4 (2009).

[122] R. A. Muscat et al. "DNA-based molecular architecture with spatially localized components". *ACM SIGARCH Computer Architecture News* 41.3 (2013), p. 177.

[123] F. Dannenberg et al. "DNA walker circuits: computational potential, design, and verification". *Natural Computing* 14.2 (2014), pp. 195–211.

[124] M. A. Boemo, A. J. Turberfield, and L. Cardelli. "Automated design and verification of localized DNA computation circuits". *Lecture Notes in Computer Science* 9211 (2015), pp. 168–180.

[125] M. A. Boemo et al. "The formal language and design principles of autonomous DNA walker circuits (in press)". *Acs Synth. Bio.* (2016).

[126] New England Biolabs. "Cleavage close to the end of DNA fragments (oligonucleotides)" (2011), pp. 1–3.

[127] S.-H. Chan, B. L. Stoddard, and S.-Y. Xu. "Natural and engineered nicking endonucleases–from cleavage mechanism to engineering of strand-specificity". *Nucleic acids research* 39.1 (2011), pp. 1–18.

[128] S. F. J. Wickham. "DNA Origami: A Substrate for the Study of Molecular Motors". PhD thesis. University of Oxford, 2011, pp. 1–246.

[129] D. M. J. Lilley. "Structures of helical junctions in nucleic acids." *Quarterly reviews of biophysics* 33.2 (2000), pp. 109–59.

[130] N. A. Licata. "Theory and modeling of particles with DNA-mediated interactions" (2008).

[131] A. L. Benvin et al. "Fluorescent DNA nanotags: supramolecular fluorescent labels based on intercalating dye arrays assembled on nanostructured DNA templates". *Journal of the American Chemical Society* 129.7 (2007), pp. 2025–2034.

[132] H. S. Rye et al. "Stable fluorescent complexes of double-stranded DNA with bis-intercalating asymmetric cyanine dyes: properties and applications." *Nucleic acids research* 20.11 (1992), pp. 2803–2812.

[133] E. Ambrose. *A Surface Contact Microscope for the study of Cell Movements*. 1956.

[134] A. L. Stout and D. Axelrod. "Evanescent field excitation of fluorescence by epi-illumination microscopy". *Applied optics* 28.24 (1989), pp. 5237–5242.

[135] R. R. F. Machinek. "Control and Observation of DNA Nanodevices". PhD thesis. University of Oxford, 2014.

[136] "Valap protocol". *Cold Spring Harbor Protocols* (2007).

[137] T. Zal and N. R. J. Gascoigne. "Photobleaching-corrected FRET efficiency imaging of live cells". *Biophysical journal* 86.6 (2004), pp. 3923–39.

[138] B. Kundukad, J. Yan, and P. S. Doyle. "Effect of YOYO-1 on the mechanical properties of DNA". *Soft matter* (2014), pp. 9721–9728.

[139] W. C. Lo. "Ring Polymers as Topological Glass, a New Phase of Matter?" PhD thesis. The University of Warwick, 2012.

[140] D. Marr and E. Hildreth. "Theory of edge detection". *Proceedings of the Royal Society of London* 207 (1980), pp. 187–217.

[141] R. Jain, R. Kasturi, and B. G. Schunck. "Machine Vision, Ch.5". In: *Machine Vision*. 1995. Chap. 5, pp. 149–161.

[142] M. H. Ulbrich and E. Y. Isacoff. "Subunit counting in membrane-bound proteins". *Nature methods* 4.4 (2007), pp. 319–21.

[143] L. S. B. Goldstein and Z. Yang. "Microtubule-based transport systems: the roles of kinesins and dyneins". *Annual review of neuroscience* 23 (2000), pp. 39–71.

[144] N. Wu et al. "Molecular threading and tunable molecular recognition on DNA origami nanostructures". *Journal of the American Chemical Society* 135 (2013), pp. 12172–12175.

[145] v. T. Förster. "Energiewanderung und Fluoreszenz". *Annalen der Physik* 437.2 (1948), pp. 55–75.

[146] R. M. Clegg. "Fluorescence resonance energy transfer and nucleic acids". *Methods in Enzymology* 211.1971 (1992), pp. 353–388.

[147] M. C. Murphy et al. "Probing single-stranded DNA conformational flexibility using fluorescence spectroscopy". *Biophysical journal* 86.4 (2004), pp. 2530–7.

[148] J. Hohlbein, T. D. Craggs, and T. Cordes. "Alternating-laser excitation: single-molecule FRET and beyond". *Chemical Society reviews* 43.4 (2014), pp. 1156–71.

[149] L. Stryer and R. P. Haugland. "Energy transfer: a spectroscopic ruler". *Proceedings of the National Academy of Sciences of the United States of America* 58.2 (1967), pp. 719–726.

[150] J. Hohlbein et al. "Conformational landscapes of DNA polymerase I and mutator derivatives establish fidelity checkpoints for nucleotide insertion". *Nature Communications* 4 (2013), pp. 1–11.

[151] G. W. Gordon et al. "Quantitative fluorescence resonance energy transfer measurements using fluorescence microscopy". *Biophysical Journal* 74.5 (1998), pp. 2702–2713.

[152] F. Stühmeier et al. "Global structure of three-way DNA junctions with and without additional unpaired bases: a fluorescence resonance energy transfer analysis". *Biochemistry* 36.44 (1997), pp. 13530–8.

[153] P. J. Santangelo et al. "Dual FRET molecular beacons for mRNA detection in living cells". *Nucleic acids research* 32.6 (2004), e57.

[154] T. Ha et al. "Probing the interaction between two single molecules: fluorescence resonance energy transfer between a single donor and a single acceptor". *Proceedings of the National Academy of Sciences* 93.13 (1996), pp. 6264–6268.

[155] A. N. Kapanidis et al. "Fluorescence-aided molecule sorting: analysis of structure and interactions by alternating-laser excitation of single molecules." *Proceedings of the National Academy of Sciences of the United States of America* 101.24 (2004), pp. 8936–8941.

[156] M. Sustarsic. "In Vitro , In Silico and In Vivo Studies of the Structure and Conformational Dynamics of DNA Polymerase I". PhD thesis. University of Oxford, 2015.

[157] I. Gopich and A. Szabo. "Theory of photon statistics in single-molecule Forster resonance energy transfer". *Journal of Chemical Physics* 122.1 (2005).

[158] Y. Liu et al. "Time-Binned Single-Molecule FRET Data Analysis". *The Journal of Physical Chemistry B* 114.16 (2010), pp. 5386–5403.

[159] Q. Chi, G. Wang, and J. Jiang. "The persistence length and length per base of single-stranded DNA obtained from fluorescence correlation spectroscopy measurements using mean field theory". *Physica A: Statistical Mechanics and its Applications* 392.5 (2013), pp. 1072–1079.

[160] K. Rechendorff et al. "Persistence length and scaling properties of single-stranded DNA adsorbed on modified graphite." *The Journal of chemical physics* 131.9 (2009), p. 095103.

[161] N. B. Leontis, W. Kwok, and J. S. Newman. "Stability and structure of three-way DNA junctions containing unpaired nucleotides". *Nucleic acids research* 19.4 (1991), pp. 759–66.

[162] J. B. Welch, D. R. Duckett, and D. M. J. Lilley. "Structures of bulged three-way DNA junctions". *Nucleic acids research* 21.19 (1993), pp. 4548–55.

[163] B. N. van Buuren et al. "Solution structure of a DNA three-way junction containing two unpaired thymidine bases. Identification of sequence features that decide conformer selection." *Journal of molecular biology* 304.3 (2000), pp. 371–83.

[164] J. B. Welch, F. Walter, and D. M. J. Lilley. "Two inequivalent folding isomers of the three-way DNA junction with unpaired bases: sequence-dependence of the folded conformation". *Journal of molecular biology* 251.4 (1995), pp. 507–19.

[165] J. L. Kadrmas, A. J. Ravin, and N. B. Leontis. "Relative stabilities of DNA three-way, four-way and five-way junctions (multi-helix junction loops): unpaired nucleotides can be stabilizing or destabilizing." *Nucleic acids research* 23.12 (1995), pp. 2212–22.

[166] B. Duncan, C. Kim, and V. M. Rotello. "Gold nanoparticle plateforms as drug and biomolecule delivery systems". *Journal of Control release* 148.1 (2010), pp. 122–127.

[167] Z. Liu et al. "Carbon materials for drug delivery & cancer therapy". *Materials Today* 14.7-8 (2011), pp. 316–323.

[168] Y. Liu et al. "Understanding the toxicity of carbon nanotubes". *Accounts of Chemical Research* 46.3 (2013), pp. 702–713.

[169] J. Li et al. "Smart drug delivery nanocarriers with self-assembled DNA nanostructures". *Advanced materials (Deerfield Beach, Fla.)* (2013), pp. 4386–4396.

[170] H. Lee et al. "Molecularly self-assembled nucleic acid nanoparticles for targeted in vivo siRNA delivery". *Nature Nanotechnology* 7.June (2012), pp. 389–393.

[171] J. Li et al. "Self-assembled multivalent DNA nanostructures for noninvasive intracellular delivery of immunostimulatory CpG oligonucleotides". *ACS Nano* 5.11 (2011), pp. 8783–8789.

[172] V. J. Schüller et al. "Cellular immunostimulation by CpG sequence-coated DNA origami structures". *ACS Nano* 5.12 (2011), pp. 9696–9702.

[173] S. Juul et al. "Release of an active enzyme in the cavity of a self-assembled DNA nanocage". *ACS Nano* 7.11 (2013), pp. 9724–9734.

[174] A. Banerjee et al. "Controlled release of encapsulated cargo from a DNA icosahedron using a chemical trigger". *Angewandte Chemie - International Edition* 52.27 (2013), pp. 6854–6857.

[175] C. M. Erben, R. P. Goodman, and A. J. Turberfield. "Single-molecule protein encapsulation in a rigid DNA cage." *Angewandte Chemie International Edition* 45.44 (2006), pp. 7414–7.

[176] R. Crawford et al. "Non-covalent single transcription factor encapsulation inside a DNA cage". *Angewandte Chemie - International Edition* 52.8 (2013), pp. 2284–2288.

[177] X. Liu et al. "A DNA nanostructure platform for directed assembly of synthetic vaccines". *Nano Letters* 12.8 (2012), pp. 4254–4259.

[178] Y.-x. Zhao et al. "DNA origami delivery system for cancer therapy with tunable release properties". *ACS nano* 6.10 (2012), pp. 8684–8691.

[179] Q. Jiang et al. "DNA origami as a carrier for circumvention of drug resistance". *Journal of the American Chemical Society* 134.32 (2012), pp. 13396–13403.

[180] J. Müller. "Functional metal ions in nucleic acids." *Metallomics : integrated biometal science* 2.5 (2010), pp. 318–327.

[181] R. Holliday. "A mechanism for gene conversion in fungi." *Genetical research* 89.5-6 (1964), pp. 285–307.

[182] E. T. Kool. "Hydrogen bonding, base stacking, and steric effects in dna replication". *Annual review of biophysics and biomolecular structure* 30 (2001), pp. 1–22.

[183] D. R. Duckett et al. "The structure of the holliday junction, and its resolution". *Cell* 55.1 (1988), pp. 79–89.

[184] A. I. H. Murchie et al. "Fluorescence energy transfer shows that the four-way DNA junction is a right-handed cross of antiparallel molecules". *Nature* 341 (1989), pp. 763–766.

[185] E. von Kitzing, D. M. J. Lilley, and S. Diekmann. "The stereochemistry of a four-way DNA junction: a theoretical study". *Nucleic acids research* 18.9 (1990), pp. 2671–2683.

[186] J. R. G. Pohler, D. R. Duckett, and D. M. J. Lilley. "Structure of four-way DNA junctions containing a nick in one strand". *Journal of molecular biology* 238 (1994), pp. 62–74.

[187] R. Holliday. "Molecular aspects of genetic exchange and gene conversion". *Genetics* 78.1 (1974), pp. 273–287.

[188] I. G. Panyutin and P. Hsieh. "The kinetics of spontaneous DNA branch migration." *Proceedings of the National Academy of Sciences of the United States of America* 91.6 (1994), pp. 2021–2025.

[189] I. G. Panyutin, I. Biswas, and P. Hsieh. "A pivotal role for the structure of the Holliday junction in DNA branch migration". *The EMBO journal* 14.8 (1995), pp. 1819–26.

[190] C. M. Erben. "Self-Assembled DNA Cages". PhD thesis. 2007.

[191] P. J. Hagerman. "Flexibility of DNA". *Annual review of biophysics and biophysical chemistry* 17 (1988), pp. 265–286.

[192] J. P. K. Doye et al. "Coarse-graining DNA for simulations of DNA nanotechnology". *Physical Chemistry Chemical Physics* 15.47 (2013), p. 20395.

[193] GE Healthcare. "Sephacryl high resolution media HiPrep Sephacryl HR columns" (2008).

[194] E. Nir et al. "Shot-noise limited single-molecule FRET histograms: comparison between theory and experiments". *The journal of physical chemistry B* 110.44 (2006), pp. 22103–22124.

[195] A. Edelstein et al. "Computer control of microscopes using Micro- manager". *Current Protocols in Molecular Biology* SUPPL. 92 (2010), pp. 1–22.

[196] P. R. Selvin and T. Ha. *Single-molecule Techniques: A Laboratory Manual*. 2008, p. 507.

[197] D. Cooper et al. "Photobleaching Lifetimes of Cyanine Fluorophores Used for Single Molecule Förster Resonance Energy Transfer in the Presence of Various Photoprotection Systems". *ChemBioChem* 14.9 (2013).

[198] M. D. Abràmoff, P. J. Magalhães, and S. J. Ram. "Image processing with imageJ". *Biophotonics International* 11.7 (2004), pp. 36–41.